Biologically Motivated Neuro-Mechanical Stepping Model in the Frontal Plane with Integration of Sensor-Driven Balance Control

Sonja Andrea Karg

TECHNISCHE UNIVERSITÄT MÜNCHEN

Lehrstuhl für Realzeit-Computersysteme

Biologically Motivated Neuro-Mechanical Stepping Model in the Frontal Plane with Integration of Sensor-Driven Balance Control

Sonja Andrea Karg

Vollständiger Abdruck der von der Fakultät für Elektrotechnik und Informationstechnik der Technischen Universität München zur Erlangung des akademischen Grades eines

Doktor-Ingenieurs (Dr.-Ing.)

genehmigten Dissertation.

Vorsitzender:	Univ.- Prof. Dr. rer. nat. habil. B. Wolf
Prüfer der Dissertation:	1. Univ.- Prof. Dr.-Ing. G. Färber
	2. Priv.-Doz. Dr.-Ing. St. Glasauer Ludwig-Maximilians-Universität München

Die Dissertation wurde am **23.06.2008** bei der Technischen Universität München eingereicht und durch die Fakultät für Elektrotechnik und Informationstechnik am **24.11.2008** angenommen.

Acknowledgements

First of all, I want to thank my advisor Prof. Dr. Georg Färber who gave me the opportunity for this very interesting and thrilling work. With his manner of giving me plenty of space to develop own ideas he enabled me to find my own way and to learn from many valuable experiences which finally lead to this work.

I also want to thank PD.Dr. Stefan Glasauer with whom I had some very helpful and informative discussions. With his experience on both sides of the topic, the technical and the biological/medical side, he supported me to accomplish the split between the different disciplines.

At the Neurological Clinic of Grosshadern I want to thank my colleagues for the good co-operation, especially my medical colleague PD.Dr. Klaus Jahn, who joined me for many experiments and for the lively discussions about new ideas and concepts. Thanks so much to Dr. Erich Schneider who helped me with many technical details for experimental setups and had always good advise for my questions. Also I want to thank Markus Huber who gave me a helpful hand for my experiments.

One important part in doing my project, not to forget, is the contribution of all the students who did a really good job in their bachelor and master thesis as there are Herrmann Seuschek, Shen Zhang, Thomas Villgrattner, Lukas Diduch, Giatwan Kosumo, Roland Zibi and Alexander Kronthaler. It is inspiring to work with motivated students with fresh ideas and I am really glad I made this experience.

I also want to thank all my colleagues at the RCS, Institute for Real-Time Computer Systems, which accompanied me on my way. It was a great time and the atmosphere at the RCS is really a welcoming one. I will miss the lunch-times and coffee breaks (IGKK) which have always been a place for open feedback and a source of new ideas and *'procrastination'*. Special thanks go to my office-mate Philipp for the fact that he made me always feel like my problem was better than his and hence not the worst.

Last but not least I want to thank my husband Stefan for his never ending patience and encouragement during all the time. And thanks a lot to all of my big family for supporting me during this *'large something at university'*.

München, 2008 Sonja Karg

"Jeder dumme Junge kann einen Käfer zertreten. Aber alle Professoren der Welt können keinen herstellen." Das schrieb der Philosoph Arthur Schopenhauer vor ca. 150 Jahren.

Contents

Contents

List of Symbols

CNS	central nervous system
COM	center of mass
COP	center of pressure
CPG	central pattern generator
DOF	degree(s) of freedom
g	gravitational force
GVS	galvanic vestibular stimulus
FFT	fast Fourier transformation
fps	frames per second
LQR	linear quadratic regulator
MSE	mean square error
ode	ordinary differential equation
RMS	root mean square
ZMP	zero moment point

Symbols of Equations

A	system state matrix in discrete state space description
$a_{i,j}$	weight of inhibiting synaptic input between neuron i and j
α	angle of stance leg in frontal-plane model
$\dot{\alpha}$	angular velocity of stance leg in frontal-plane model
B	system input matrix in discrete state space description
β	angle of hip in frontal-plane model
$\dot{\beta}$	angular velocity of hip in frontal-plane model
C	measurement matrix in discrete state space description
D	measurement input matrix in discrete state space description
$G(q)$	matrix of gravitational forces
γ	angle of swing leg in frontal-plane model
$\dot{\gamma}$	angular velocity of swing leg in frontal-plane model
f_i	firing rate of neuron i
f_d	feedback gain for position
f_{dv}	feedback gain for velocity
H, h	hip width

$H(jw)$	transfer function in the frequency range
L, l	leg length
m	leg mass
M	body mass
$M(q)$	matrix of mass or inertia
$N(q, \dot{q})$	matrix of centrifugal and Coriolis terms
n_i	neuron activation which is the membrane potential of the i-th neuron
Φ	angle of stance leg in stance model
$\dot{\Phi}$	angular velocity of stance leg in stance model
Φ_{com}	angle of the COM position in relation to stance foot position
$\dot{\Phi}_{com}$	angular velocity of COM
$\mathbf{P}_i$	network number i of oscillators for the frontal-plane model
q	general vector of system states
Q	noise covariance matrix of the system
R	noise covariance matrix of the measurements
s	external input to a neuron
θ	angle of stance leg in sagittal-plane model
$\dot{\theta}$	angular velocity of stance leg in sagittal-plane model
T_a, T_b	constants for oscillator time constraints
u	general vector of inputs
$u_a ct$	input vector of oscillator generated joint torques
$u_c = (u_a, u_b, 0)$	vector of superposition control input for joint torques
v_k	statistic noise of measurements
w_k	statistic noise of the system
w_{ij}	weight of neuron activation for torque generation
x	applied vector of system states
y	vector of system outputs

List of Symbols

Abstract

A new model for frontal-plane stepping movements is developed in order to evaluate medio-lateral gait movements. Using this model it is possible to study individual stepping parameters, stability of movements and various stepping patterns. Gait research to date has mainly focused on forward locomotion, but as maintaining lateral balance is critical for stable gait, the proposed model concentrates on stepping in the frontal plane. The modeling is carried out on the basis of biological principles and using a bottom-up approach. The model is accordingly split into a low-level and a high-level component in line with biological processes, where low-level tasks are chiefly automatic and high-level tasks are primarily directive. The actuation of the passive mechanical model is achieved by creating a neuronal oscillator structure with muscular feedback and antagonistic joint torque generation. Characteristic parameters of this low-level model are identified for functions such as step frequency or stepping patterns. Various movements are presented for stable stepping in place with dropping or lifting hip, stepping to the side, and stepping upwards. The simulated stepping is compared with real video tracking data and found to be very similar. The stepping is also tested under disturbing influences such as slipping or getting stuck; the model shows robust reactions and returns to a stable solution within a few steps. The stability and performance of the low-level stepping model have their limitations as this system lacks "perception" of the overall context.

A high-level model is therefore developed to represent perception of the whole body position and the environment to accomplish posture control tasks. The basis for this model is model knowledge in the form of statistical estimation and sensory models derived from biology. This is integrated in a feedback loop where the two main optimization criteria are upright posture and low actuation input. To evaluate the performance of the sensor-driven posture control model, two experiments with real subjects are performed, one for vestibular stimulation and another for visual pursuit stimulation. The experimental data for posture response are reproduced and verified by the high-level model.

To enhance the performance and abilities of the low-level model, the two models are integrated by a superposition control concept. Superpositioning does not influence the low-level actuation directly, but the two levels are superimposed wherever the whole body balance is considered to be at risk. This integration leads to improved stability of the stepping movements without reducing low-level autonomy. Stability of movement is no longer mainly dependent on the initial values and this leads to an increased range of stable solutions and the possibility of influencing stepping movements by sensory cues.

This relatively simple framework integrates the main low-level and high-level mechanisms of stepping movements in one model. It is used to simulate autonomous stepping movements under the aspect of sensor-driven posture control, with the possibility of analyzing medio-lateral stepping characteristics, and of influencing them.

1 Introduction

Human stance and gait mechanisms are a complex interaction of extremely diverse processes enabling the body to perform locomotion, to maintain balance and to react to environmental influences. These processes relate to the mechanics, the muscles, the neuronal structures, sensory cues and the brain, to name only the most obvious. This complex scenario and the variety of integration mechanisms required to achieve the walking task are still not well understood and research into them covers a very wide field ranging from biology and medicine to engineering and natural sciences.

1.1 Motivation

The work presented in the following evolved from a joint project with a neurological medical research unit. The key ideas were triggered by several studies of sensory influence on locomotion in a lateral direction. Hence, a model to evaluate sidewards movements of stance and gait is of special interest. For clinical purposes this could lead to a better understanding of locomotion behaviors of patients with a variety of defects, knowledge which can subsequently be used to change and improve therapy. To this end a frontal plane posture model for stepping movements was needed.

This thesis presents and analyzes a mathematical model originated in the engineering environment and based on known and accepted biological structures, in order to analyze postural stance and stepping tasks.

A biological model such as this stands in contrast to today's robotic stance and gait realizations because the concept is different and because the performance is often worse at first sight. The reason for creating such biologically motivated models is the realization that robotics has its limits and that conventional solutions can push those limits but not overcome them entirely. It is not well known how human beings solve movement tasks and the classic robotic approach brings us no nearer to an explanation. Biologically motivated models are often used to obtain further understanding and insight into common complex movement actions and interactions.

Especially the medio-lateral stepping movements (stepping in the frontal plane) are not a well explored aspect of movement in gait research. This thesis studies several aspects of medio-lateral stepping movements and introduces a general model with the possibilities of researching this stepping plane depending on the individual components and on sensory influences. If locomotion is considered as a task of human survival, the stability of this

task is the most essential property, followed by robustness and flexibility. This requires an intensive study of influence parameters on stepping movements, always under the aspect of stability and robustness. The flexibility and variety of the stepping movements is so important because the stepping task is adapted to suit every real life situation. This leads to the creation of variations of the stepping movement in the frontal plane - stepping in place, stepping to the side and stepping up or down under different stepping strategies - and to systematic analysis of the influencing factors. To study how the vestibular or visual sensors influence posture control, those influences have to be verified experimentally and explained by mathematical relations. This work focuses particularly on vestibular and visual influences (through eye movements) as the subject of experiments and model evaluation because these are two important sensory cues influencing stepping task and performance. The extend to which sensor-driven posture control influences the task of stepping is not clear from a biological point of view. For this reason general posture tasks and environmental influences are considered separately and jointly.

The general principle followed for creating the model presented in this work is to look for the abilities of the most simple model and extend them where biological constraints and facts found experimentally require it. The strategy is to build the model bottom up, starting low-level and extending it by a high-level control. The model considers medio-lateral stepping movements as there are no other models known to the author which analyze lateral steps in more detail.

1.2 State of the Art Context

Either walking and Gait or the operation of posture control are generally studied under different aspects in literature: on the one hand from the technical angle, which is the application of locomotion mechanisms in robotics, and on the other hand from the biological or medical angle, which focuses on understanding locomotion mechanisms for therapy purposes or to explain biological structures. These two approaches differ both as regards the methods used, as well as the requirement to find a working technical solution on the one hand, and to explain the biological reality on the other hand. Two examples can be given to demonstrate the differences between technical systems and the human being. Firstly, the energy consumption of a walking robot is much higher than that of a human being. In [23] it is determined at 0.2 [cet] for humans and 3.2 [cet] for Honda's ASIMO robot, where [cet] is defined as the specific cost of transport, which is the energy used per weight and distance moved. Because of this, many new robotic approaches try to compensate this energy waste as shown in [182]. In [20] a robot realized by passive mechanics is actuated at the ankles for push-off with a very energy-efficient gait. This can be seen in the graphics published by Collins [22].

The second example is the natural appearance of a stepping movement. A characteristic of human steps is that the steps are often similar but never identical; the variability of step trajectories is large [175, 56]. An approach often used in robotics is control by predefined desired trajectories [16, 102, 11, 17]. This approach does not resemble the
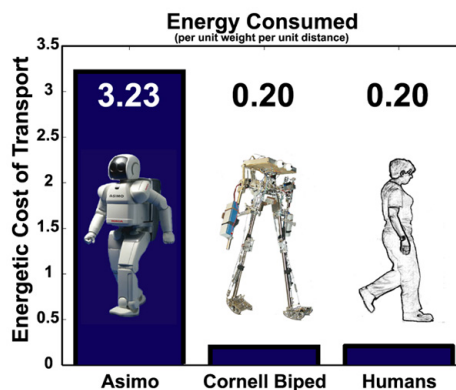
Figure 1.1: Energy comparison between human being, the Cornell nearly passive robot and the Honda ASIMO robot taken from [22]

natural variability. It is also not very flexible about adapting to changing conditions and requires a good a priori knowledge of the movement or a large memory for saved possible trajectories [103]. None of these 3 points are present in natural systems, which nevertheless produce robust walking and posture movements.

On the other hand there are technical approaches which try to exploit the natural resources for their ability to generate walking movements. There are the dynamics of mechanics which are able to use gravity as their only actuation [125, 113, 21] to produce realistic gaits. Ground reaction forces or trajectories which are characteristic for humans are analyzed and applied to technical systems to evaluate their efficiency [101]. Additionally there are several parameters of the human walking movement which can be measured and used to explain and reconstruct the walking movement and its properties. Muscle activation patterns are used to evaluate muscle speed, propulsive energy and the development of forward dynamical models [198, 134, 194]. Spinal cord injuries are studied to obtain more knowledge about the influence of spinal neuron circuits on walking [57, 110]. As it is very difficult to extract information about these complex and internal neuronal structures, simpler animals are studied and described mathematically [73]. These findings are assigned to human locomotion characteristics and adapted [10, 151]. Another, even more complex, component which constitutes an integral part of the walking task is the aspect of perception and central processing and the control tasks of the brain. The range of experiments which investigate the influence of perception on posture or balance-maintenance is wide. Often these experiments are done in stance [65, 15, 170], or during walking [77, 193]. From these experiments mathematical functions of perception posture relations are derived and approximated to describe possible interrelations [79, 6, 89].

1.3 Outline

The model in this work is structured bottom up, starting with the lowest constraints and extending the model further for enhanced capabilities. The most basic requirement for a

standing and stepping model is the mechanics. The simplest and most effective mechanics are the ballistic gait models driven only by gravity and these form the basis for the model developed here. This is elaborated in chapter 2 where the sagittal (section 2.2) and frontal (section 2.3) plane models are presented. Further movement generation can be divided into subsystems. Such subsystems were found experimentally, as it was ascertained that movements of certain animals could still be achieved if those animals were decerebrated, meaning that the brain no longer played any active role in the locomotion tasks. In line with these findings the model is divided into a high-level and a low-level component.

The low-level model is extended in chapter 3 with a simple actuation. According to biological findings it can generate autonomous basic rhythmic movements such as stepping. In this work the oscillator-driven movements, such as those found in simple life forms as well as in more complex life forms such as the cat (section 3.2), are used to generate stepping patterns. The actuation itself is correlated to the antagonistic actuation of muscles in order to stay close to biology presented in 3.3 and 3.4. The comparison to human stepping patterns shows many similarities but of course also differences. For the desired lateral component for stepping movements several stepping patterns are possible and should be generated. This includes stepping in place with different patterns and lateral sway as well as other possible movements in this plane as stepping up/down (e.g. a ladder) and stepping to the side. So different and robust stepping patterns can be produced by relatively simple mechanisms which is shown in section 3.6, 3.7 and 3.8.

By analyzing these stepping patterns and finding out the limits, such as no integration of any sensory information and therefore no influence by the environment, this low-level stepping model is extended further. The extension is a posture control model which integrates the sensory modalities with a central processing procedure. This model is presented in chapter 4. Stance and gait are not locally optimized tasks but are optimized by statistical means to ensure good balance and robust locomotion. To keep the model simple, a well-known engineering approach, the Kalman filter (section 4.3), was chosen. This model integrates mechanics and sensory cues (section 4.2) to achieve a stable but sensitive posture control. Experimental studies in section 4.4 evaluate posture control characteristics that can be seen again in the model. The simulation results are detailed in section 4.5.

Finally in chapter 5, this posture control, which means keeping balance while sensing the environment, is applied to the moving (stepping) model, which till then had no ability to sense the environment or global body positions. The aim of this integration is to control the general whole body upright position in the frontal plane. Again a simple approach is chosen to show how a complete model of a biologically motivated structure can be realized.

Such a realization never replicates reality exactly or completely but is a model of some aspects of reality that are known. However, it can be used to explain results found experimentally and to succeed in understanding complex movement responses in stance and stepping. The work presented is summed up in chapter 6. Further possibilities for the use of this medio-lateral stepping model and some possible extensions for future research are outlined in section 6.1.

2 Passive Mechanical Models

One possible manner of examining walking is to determine it first from its most obvious aspect, from the mechanics. Walking does of course involve mechanisms such as muscles, neuronal activation and complex ligament constructions, but the ability of the actual mechanics to enable walking can best be examined if this aspect is investigated separately. It is a fact that e.g. the body masses, the leg length or different lengths of legs influence the walking task profoundly. For this reason there have been many approaches to observe the mechanics as they are only influenced by gravitational forces, the so-called ballistic walkers.

These are the most simple walking models but they nevertheless reveal a close similarity to natural human walking. Typical characteristics of these models are the reduction of energetic cost due to the fact that actuation is exclusively gravitational and the ballistic swing movement they have during walking. To show the abilities of movement produced by ballistic models, a frontal-plane model is developed and introduced which follows the style of an established sagittal-plane model.

In the following section 2.1 the wide range of state-of-the-art ballistic models is presented. In section 2.2.2 a 2D model for ballistic walking will be presented. This model uses [38, 111] as a starting point as these integrate much of the state-of-the-art knowledge about ballistic sagittal walking models. This 2D model is used in this thesis as a reference for the developed frontal-plane model, to show that the introduced actuation mechanisms can be applied to a sagittal-plane model without further specifications. The ballistic models are implemented in MATLAB. They are evaluated with respect to their ability to provide stable walking solutions for walking down a slope and other parameter influences. The resulting movements will be shown in section 2.4. The ballistic model for frontal stepping movements, which is newly developed in this thesis, will be shown in 2.3. As there are no stable solutions for the medio-lateral movement according to [94] and as there is no slope scenario comparable to that for the sagittal walker, no periodic movements will be produced and shown. Stepping movements will be presented later in section 3.4 of chapter 3 on actuated models.

2.1 State of the Art of Passive Mechanical Models

A first ballistic walker was evaluated by Mochon and McMahon in the 80's [115, 114, 124]. They observed the swing phase of a step and from their ballistic model were able to derive characteristic data which correlated with experimental data, such as swing phase length

to step length relation. They also found correlations between the step length and step frequency and their interdependence with knee and hip flexion. Later, in the early 90's, McGeer initiated a new series of ballistic walkers [111, 112]. From a rimless wheel he derived the ballistic walker that walks down a shallow slope. This was the most simple form of a walker with two stiff legs which are the master for the models presented in the following. Another model created by McGeer was a model with knees, and McGeer was also the first to develop a 3D ballistic walker [113]. Coleman [19] and Garcia [38, 39] also took the McGeer model as their template. Coleman devoted particularly attention to investigating the movement of the rimless wheel and from this research derived his ballistic walker [18]. Garcia focused particularly on the influence of model parameters on stabilization and walking characteristics [37]. Goswami conducted detailed research into the stability of ballistic walking models, as stability is not a self-evident property of these models. 3D walkers that can run down a slope without falling have also been developed. Quite early on McGeer came to the conclusion that lateral stabilization is needed for stable 3D walking. This means that the 3D walkers are either not completely 3D or not completely passive. To be not completely 3D means that they are bound to certain mechanical constraints in order to achieve lateral stabilization; in particular they feature parallel legs in the frontal plane and no hip movement relative to the stance leg in the frontal or sagittal plane. All this is explained in detail in [19] (page 135/136). Another possible solution for a 3D ballistic walking model is given by Kuo [94]. This assumes that the lateral stabilization cannot be achieved by a passive model itself, but has to be achieved by additional medio-lateral activation of the model as a form of active stabilization. The model which was used for the active stabilization still retains much of the model's passivity [92].

The use of ballistic walking models or passive dynamic models, as they are alternatively called, is interesting as these provide an opportunity to use walking models which combine relatively low complexity with natural behavior. As mentioned in [94, 54, 181] a ballistic model can be taken as the basis for analyzing to comprehend bipedal walking and the role of additional actuation for enhancing walking abilities.

As mentioned in chapter 1, walking has important characteristics which have been taken into account: (a) stability of walking movements, (b) the energy consumption of the system and (c) the appearance of a walking movement. To get an idea of the influence, walking mechanics have on these three features, ballistic models are used to determine characteristics. The stability (a) of a movement, which is the most indispensable factor for survival, can be achieved by these ballistic models as shown in [49, 48, 50, 37, 18, 38]. However, the parametrization of the model has a big influence on the system and external disturbances cannot be handled well. Furthermore the stability range is narrow.

The energy consumption (b) of ballistic systems is ideal, as only the energy of gravitation is added to the system to make it walk and no additional activation is needed. However, the ground contact model also determines the energy characteristics, e.g. the rigid ground contact model presented in section 2.2.3 can lose energy during contact as it is not possible to preserve contact impulses for completely non-elastic contacts. As Kuo [93] and researchers before him [111, 39] found out, the additional energy that is fed into the system is an impulsive torque added just before heel strike. This is discussed in more
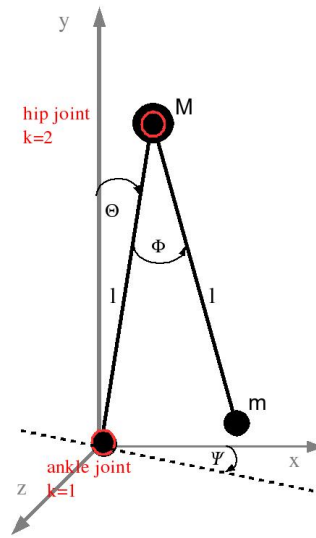
Figure 2.1: A double pendulum with Cartesian and Polar coordinates, two sticks of length l with point masses m and M and angles Θ and Φ.

detail together with energy conservation of the system in sections 2.3.2 and 2.3.3. The third point, the appearance of the movement (c), is not so easily determined, but relations such as step length to step frequency are found to be adequate and walking velocity can be modified [29]. It is also mentioned in literature that the ballistic gait, which is a pendulum style of walking, resembles the natural appearance of walking [37, 132].

2.2 Stepping Model in the Sagittal Plane

Ballistic walking is a pendulum style of walking. During the swing phase, with only one support leg, a straight-legged ballistic walker is a double pendulum. Therefore, the general equation of a pendulum 2.2 is used and presented here. This will be used later in sections 2.2.2 and 2.3 for the passive dynamic equations which represent the ballistic mechanics of the sagittal-plane and the frontal-plane walkers.

2.2.1 Lagrangian Principle of a Pendulum

The coordinates of the used double pendulum are x and y in the Cartesian coordinate system and l, Θ, Φ in a polar coordinate system. This is seen in figure 2.1. The Euler-Lagrange differential equations are derived for the system. The Lagrangian L is:
$L = (T_1 + T_2) - (L_1 + L_2)$ where T is the kinetic energy for the two pendulum parts and L is the potential energy for both parts. The Euler-Lagrangian differential equation with

a state vector $q = \begin{pmatrix} \Theta \\ \Phi \end{pmatrix}$ is as follows:

$$\frac{\mathrm{d}}{\mathrm{d}t}\frac{\partial L}{\partial \dot{q}} - \frac{\partial L}{\partial q} = 0 \tag{2.1}$$

which results in the pendulum equation:

$$M(q) * \ddot{q} + N(q, \dot{q}) + G(q) = 0 \tag{2.2}$$

where $M(q)$ is the mass matrix or inertial matrix, $N(q, \dot{q})$ is the matrix of centrifugal and Coriolis terms, $G(q)$ is the matrix of gravitational forces and q describes the state of the passive mechanics. The form of this equation is independent of how many segments the pendulum has, the matrices and state vector are adapted to it. As this is a common model in literature the detailed derivation can be found in [4, 122].

Inverse Pendulum Mechanics for Stance

The inverse pendulum which is used to represent a standing body or the stance leg movement during walking is briefly derived in the following. The coordinates of the pendulum mass M are given in x and y coordinates or by the angle Φ and the pendulum length l. The Lagrangian for the pendulum is derived with:

$$L = \frac{1}{2}M * v^2 - M * g * \ell * \cos \Phi \tag{2.3}$$

where v is the velocity of the point mass M.

$$v^2 = \ell^2 * \dot{\Phi}^2$$

The Lagrangian is now given by:

$$L = \frac{1}{2}M * l^2 * \dot{\Phi}^2 - M * g * l * \cos \Phi$$

and the Euler-Lagrangian equation of motion with substituted L and after simplification leads to:

$$\frac{\mathrm{d}}{\mathrm{d}t}\frac{\partial L}{\partial \dot{\Phi}} - \frac{\partial L}{\partial \Phi} = M * l^2 * \ddot{\Phi} - M * g * l * \sin \Phi = 0 \tag{2.4}$$

which describes the motion of the inverted pendulum. With matrix $M(q) = M * l^2$, matrix $N(q, \dot{q}) = 0$ and matrix $G(q) = M * g * l * sin(\Phi)$ the pendulum equation 2.2 is obtained in the form of:

$$M(q) * \ddot{q} + N(q, \dot{q}) + G(q) = 0$$
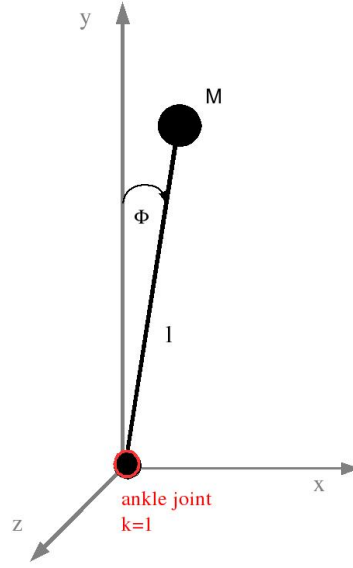
Figure 2.2: Inverse pendulum with a single mass representing the body mass.

2.2.2 Mechanics of the 2D Stepping Model in the Sagittal Plane

The most simple walking model is a ballistic model consisting of two knee-less legs with point masses and a third point mass, the hip, which joins the two legs [111, 49, 38]. So this model has the form of a double pendulum. The ballistic model is driven by the gravitational force by walking down a slope. The energy gained by the change of potential energy into downward movement is dissipated at the ground contact at the end of each step. The appearance of the gait is determined by the mechanical parameters such as the masses and leg length, the slope gradient and the initial values to start the model. These initial values have to be chosen carefully so that the energy gained and dissipated compensate each other, leading to a stable walking cycle. The passive dynamics of the mechanics are derived from the double pendulum equations. The detailed equations are taken from [38], where the leg masses are situated at the end of the legs whereas with [49] the masses are situated in the middle of the legs. The general basic equation for passive dynamics 2.2 is rewritten:

$$M(q) * \ddot{q} + N(q, \dot{q}) + G(q) = 0$$

As the gradient of the slope influences the gravitational forces, the value ψ gives the slope gradient. The detailed matrices $M(q), N(q, \dot{q}), G(q)$ according to the mechanical model of [38] are:

$$M(q) = \begin{pmatrix} \Big(M + 2 * m * (1 - \cos\phi)\Big) & \Big(- m * (1 - \cos\phi)\Big) \\ \Big(m * (1 - \cos\phi)\Big) & -m \end{pmatrix} \tag{2.5}$$
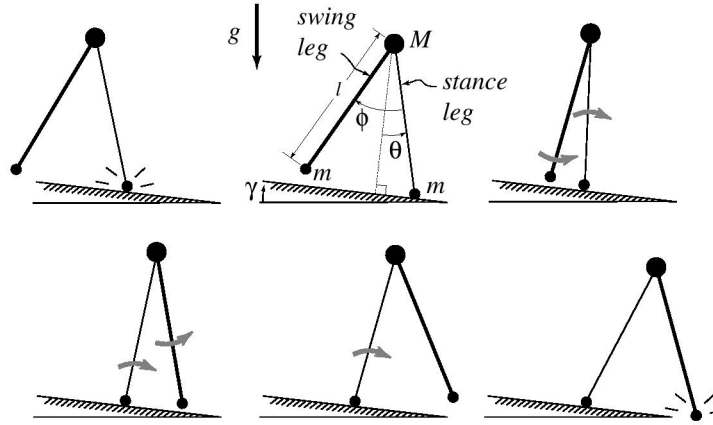
Figure 2.3: The 2-D ballistic walker, also called the "simplest walking model", showing one step; taken from [38] (heavier line = swing leg, lighter line = stance leg).

and

$$N(q, \dot{q}) = \begin{pmatrix} \left(-m * \sin\phi * (\dot{\phi}^2 - 2 * \dot{\phi} * \dot{\theta}) \right) \\ \left(m * \dot{\theta}^2 * \sin\phi \right) \end{pmatrix} \tag{2.6}$$

and

$$G(q) = \begin{pmatrix} \left(\frac{m*g}{l} * (\sin(\theta - \phi - \psi) - \sin(\theta - \psi)) - \frac{M*g}{l} * \sin(\theta - \psi) \right) \\ \left(\frac{m*g}{l} * \sin(\theta - \phi - \psi) \right) \end{pmatrix} \tag{2.7}$$

This equation now gives the body mechanics of a ballistic walker which is shown in figure 2.3 and 2.1 with leg masses m and body mass M and leg length l.

The walking cycle can be divided into two phases: (a) the single support phase or swing phase and (b) the double support or stance phase. In the swing phase (a), the swing leg swings forward according to gravitation. This can also be seen in figure 2.6. The step is finished and the transition between the two phases (a) and (b) takes place at the moment when the swing leg just gets ground contact. This is the moment of heel strike, which terminates the swing phase (a) and starts the double support phase (b). The swing phase is completely determined by equation 2.2. The double support phase starts when the heel strike of the swing leg occurs and ends when the former stance leg toes off the ground and initiates the new swing phase. This transition from (a) to (b) to (a) again is integrated in the ground contact model. The ground contact model used for the sagittal-plane ballistic walker is described in section 2.2.3.

2.2.3 Ground Contact Model

As in many walking models, the ground contact is modeled as an inelastic impact of two rigid bodies that is instantaneous [38, 54, 49, 93, 111].

If equation 2.2 is simulated for the swing phase (a), it is observed whether ground contact occurs. This ground contact occurs if the body has a certain angular position. For the sagittal-plane ballistic walker this occurs if :

$$\phi(t) - 2 * \theta(t) = 0 \qquad (2.8)$$

When this angular condition is attained, the heel just strikes the ground and the transition from swing phase (a) to double support phase (b) takes place. There is also another constellation when a straight-legged walker, in a mathematical meaning, touches the ground with both legs. This is the case when $\phi(t) = \theta(t) = 0$ where the swing leg just swings past the stance leg. For a straight-legged walker this case is simply handled as swing and not as ground contact. As the ground contact is instantaneous it is calculated as a discrete transition of the form:

$$q(t + \tau) = H * q(t - \tau) \qquad (2.9)$$

where q is the vector of system states, H is the transition matrix of the ground contact, τ is a very small amount of time and q is the vector of state angles and angular velocities $q = (\Theta, \Phi, \dot{\Theta}, \dot{\Phi})$. So the state of the system just after the heel strike depends on the transition matrix H and the state of the system just before the heel strike. The matrix H is defined according to [38, 18], with the conservation of torsional moment and the model of an inelastic impact of two rigid bodies:

$$H = \begin{pmatrix} -1 & 0 & 0 & 0 \\ 0 & \frac{cos(2*\theta)}{1+m/M*sin(2*\theta)^2} & 0 & 0 \\ -2 & 0 & 0 & 0 \\ 0 & -(1 + cos(2 * \dot{\theta})) & 0 & 0 \end{pmatrix} \qquad (2.10)$$

After the collision, the stance leg becomes the swing leg and vice versa. The angles of the stance and swing leg simply interchange as in equation 2.10 and the initial velocities for the next step are calculated anew. As the ground contact is modeled as a complete nonelastic impact of two rigid bodies, the system loses energy with the ground contact as there is no conservation of momentum. If this loss of energy is compensated by the gravitational energy added by the slope to the system, the system walks down the slope at a steady pace.

2.3 Stepping Model in the Frontal Plane

In the previous section the forward movement of stepping was described. In this section the movement to the side or the lateral movement will be considered explicitly. Walking is a complex 3-D task where the interaction between the forward movement and the lateral movement is not jet known. To analyze the effect of the lateral stability of walking, one possibility is that the lateral and sagittal stabilizing effects are only slightly interconnected

which was shown by Kuo [92, 94]. In this research the medio-lateral walking movements and balance task are of special interest which lead, together with Kuo's assumption, to a stepping model in the frontal plane. In the following this 2-D frontal model is described and derived, which moves only in a medio-lateral direction with no forward movement. This type of movement includes such movements such as stepping in place or stepping to the side.

In this section the mechanical principles of the presented model are described and the formulas used are derived. The basic mechanics are a chain of rigid links, which are two legs joined by two joints at the hip as is shown in figure 2.4. This mechanical system has 1 or 3 DOF. If the body is standing without lifting a leg, the so-called double support phase, the system has only one DOF: the lateral angle of sway in the frontal plane described by the angle α. If one leg leaves the ground, the so-called single support phase, the system has 3 DOF: the lateral sway in the ankle of the stance leg (angle α), the up and down movement of the hip (angle β) and the lateral movement of the swing leg (angle γ), see figure 2.5. To simplify the mechanics, the masses are all point masses positioned in the center of each link, see also figure 2.4.
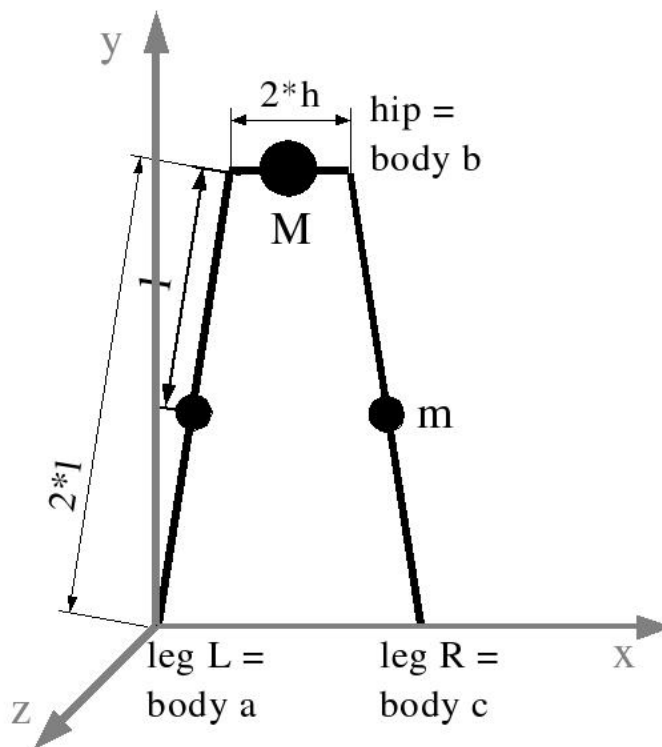
Figure 2.4: The 2-D walking model for medio-lateral movements in the frontal plane, consisting of two legs and a hip with point masses.

The mechanical system of the frontal plane is a pendulum of three segments whereas the sagittal plane system is a double pendulum. This means that the general equation for the single support phase of the frontal-plane mechanics is a pendulum equation as described

in equation 2.2. To derive the formulas of this mechanical constellation the Lagrangian formalism is used. The following symbols are used:

g : gravitational force with $9.8[N/s^2]$

m : mass of a leg with $11[kg]$

M : body mass represented as hip mass $49[kg]$

α, γ : angles of the left and right leg see figure 2.5

β : angle of the hip see figure 2.5

l, h : length of body segments legs and hip see figure 2.4

$\mathbf{q} = (\alpha, \beta, \gamma)^T$ which is as before the state vector of the system.

The central formula expressing the equation of motion for joints and segments due to gravitation and mechanical constraints is taken from section 2.2.1, equation 2.2. The system is conservative with time-invariant constraints. The equation used here has the state vector $q = (\alpha, \beta, \gamma)^T$, this equation takes the form of pendulum equation:

$$M(q) * \ddot{q} + N(q, \dot{q}) + G(q) + u_{corrective} = 0$$

with an extension $u_{corrective}$ which is the corrective torque. It is a torque applied to the system that will be generated by the actuation and therefore is actively applied to the mechanical system. Here, the torque is produced by muscular forces that are determined by a neural oscillator system which will be described in detail in section 3.3. In the following the equation for the frontal-plane mechanics is derived which results in a pendulum style description, given in the equation above. The system seen in figures 2.4 and 2.5 is used as generalized coordinate system . The Lagrangian formalism is used to derive the equation. Shortly described the procedure is as follows: determination of the Cartesian coordinates by polar coordinates of each segment, calculation of the kinetic and potential energy of each segment, computation of the Lagrangian L and finally derivation of the Euler-Lagrange differential equation, see also equation 2.2. These steps of derivation are detailed in the following.

2.3.1 Mechanics of the 2D Stepping Model in the Frontal Plane

Coordinates

Here the Cartesian coordinates of each segment are determined. The Cartesian coordinates are described by polar coordinates, see also figure 2.5. Coordinates $r = (xyz)^T$ of the center of mass of body segment a:

$$\mathbf{r_a} = \begin{pmatrix} l \sin \alpha \\ l \cos \alpha \\ 0 \end{pmatrix} \qquad \dot{\mathbf{r}}_\mathbf{a} = \begin{pmatrix} l\dot{\alpha} \cos \alpha \\ -l\dot{\alpha} \sin \alpha \\ 0 \end{pmatrix}$$
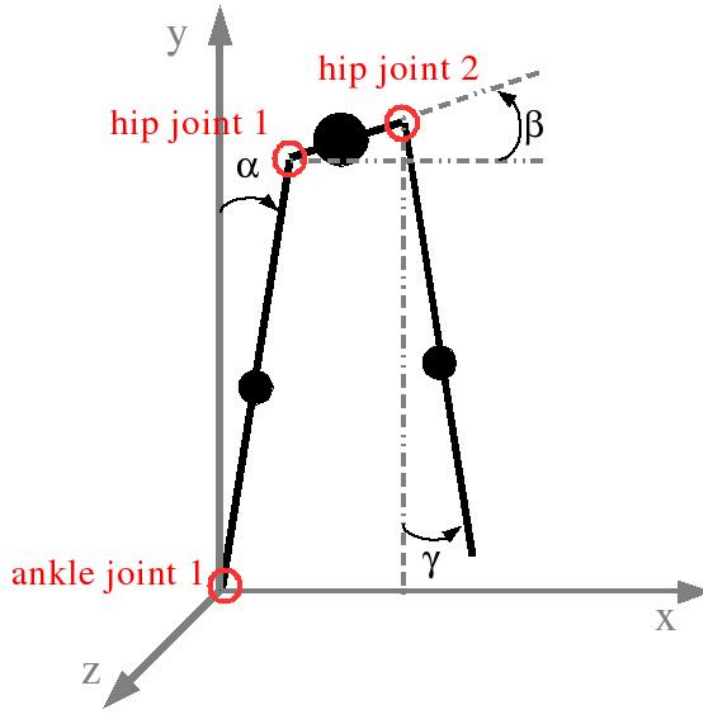
Figure 2.5: The 2-D walking model in the frontal plane with the angles α, β, γ as angular joint positions for the three joints.

Coordinates r of the center of mass of body segment b:

$$\mathbf{r_b} = \begin{pmatrix} 2l\sin\alpha + h\cos\beta \\ 2l\cos\alpha + h\sin\beta \\ 0 \end{pmatrix} \qquad \dot{\mathbf{r}}_{\mathbf{b}} = \begin{pmatrix} 2l\dot{\alpha}\cos\alpha - h\dot{\beta}\sin\beta \\ -2l\dot{\alpha}\sin\alpha + h\dot{\beta}\cos\beta \\ 0 \end{pmatrix}$$

Coordinates r of the center of mass of body segment c:

$$\mathbf{r_c} = \begin{pmatrix} 2l\sin\alpha + 2h\cos\beta + l\sin\gamma \\ 2l\cos\alpha + 2h\sin\beta - l\cos\gamma \\ 0 \end{pmatrix} \qquad \dot{\mathbf{r}}_{\mathbf{c}} = \begin{pmatrix} 2l\dot{\alpha}\cos\alpha - 2h\dot{\beta}\sin\beta + l\dot{\gamma}\cos\gamma \\ -2l\dot{\alpha}\sin\alpha + 2h\dot{\beta}\cos\beta + l\dot{\gamma}\sin\gamma \\ 0 \end{pmatrix}$$

Euler-Lagrange differential equation

The Lagrangian L is the difference between kinetic energy T and potential energy V: $L = T - V$. And the Euler-Lagrange equation is the sum of derivatives of it. The Euler-Lagrange equation 2.1 can also be transformed into the derivatives of the individual

energies, which is:

$$\frac{d}{dt}\left(\frac{\partial L}{\partial \dot{q}}\right) - \left(\frac{\partial L}{\partial q}\right) =$$

$$= \frac{\mathbf{d}}{\mathbf{dt}}\left(\frac{\partial \mathbf{T_a}}{\partial \dot{\mathbf{q}}}\right) - \frac{\partial \mathbf{T_a}}{\partial \mathbf{q}} + \frac{\partial \mathbf{V_a}}{\partial \mathbf{q}} + \frac{\mathbf{d}}{\mathbf{dt}}\left(\frac{\partial \mathbf{T_b}}{\partial \dot{\mathbf{q}}}\right) - \frac{\partial \mathbf{T_b}}{\partial \mathbf{q}} + \frac{\partial \mathbf{V_b}}{\partial \mathbf{q}} + \frac{\mathbf{d}}{\mathbf{dt}}\left(\frac{\partial \mathbf{T_c}}{\partial \dot{\mathbf{q}}}\right) - \frac{\partial \mathbf{T_c}}{\partial \mathbf{q}} + \frac{\partial \mathbf{V_c}}{\partial \mathbf{q}}$$

$$(2.11)$$

Derivation of the Lagrangian Equation

The kinetic energy T and the potential energy V are calculated for each segment. The kinetic energy T of body segment a is:

$$\mathbf{T_a} = \tfrac{1}{2}m\dot{r}_a^2 = \tfrac{1}{2}m[(l\dot{\alpha}\cos\alpha)^2 + (-l\dot{\alpha}\sin\alpha)^2] = \tfrac{1}{2}ml^2\dot{\alpha}^2$$

The potential energy V of body segment a is:

$$\mathbf{V_a} = mgl\cos\alpha$$

The kinetic energy T of body segment b is:

$$\mathbf{T_b} = \frac{1}{2}\mathbf{M}\dot{\mathbf{r}}_{\mathbf{b}}^2$$

$$= \frac{1}{2}M[(2l\dot{\alpha}\cos\alpha - h\dot{\beta}\sin\beta)^2 + (-2l\dot{\alpha}\sin\alpha + h\dot{\beta}\cos\beta)^2]$$

$$= \frac{1}{2}M[4l^2\dot{\alpha}^2\cos^2\alpha + h^2\dot{\beta}^2\sin^2\beta - 4lh\dot{\alpha}\dot{\beta}\cos\alpha\sin\beta + 4l^2\dot{\alpha}^2\sin^2\alpha +$$

$$+ h^2\dot{\beta}^2\cos^2\beta - 4lh\dot{\alpha}\dot{\beta}\sin\alpha\cos\beta]$$

$$= \frac{1}{2}M[4l^2\dot{\alpha}^2 + h^2\dot{\beta}^2 - 4lh\dot{\alpha}\dot{\beta}\sin(\alpha + \beta)]$$

The potential energy V of body segment b is:

$$\mathbf{V_b} = Mg(2l\cos\alpha + h\sin\beta)$$

The kinetic energy T of body segment c is:

$$\mathbf{T_c} = \frac{1}{2}m\dot{\mathbf{r}}_c^2$$

$$= \frac{1}{2}m[(2l\dot{\alpha}\cos\alpha - 2h\dot{\beta}\sin\beta + l\dot{\gamma}\cos\gamma)^2 + (-2l\dot{\alpha}\sin\alpha + 2h\dot{\beta}\cos\beta + l\dot{\gamma}\sin\gamma)^2]$$

$$= \frac{1}{2}m[4l^2\dot{\alpha}^2\cos^2\alpha + 4h^2\dot{\beta}^2\sin^2\beta + l^2\dot{\gamma}^2\cos^2\gamma - 8lh\dot{\alpha}\dot{\beta}\cos\alpha\sin\beta$$
$$+ 4l^2\dot{\alpha}\dot{\gamma}\cos\alpha\cos\gamma - 4hl\dot{\beta}\dot{\gamma}\sin\beta\cos\gamma + 4l^2\dot{\alpha}^2\sin^2\alpha + 4h^2\dot{\beta}^2\cos^2\beta$$
$$+ l^2\dot{\gamma}^2\sin^2\gamma - 8lh\dot{\alpha}\dot{\beta}\sin\alpha\cos\beta - 4l^2\dot{\alpha}\dot{\gamma}\sin\alpha\sin\gamma + 4hl\dot{\beta}\dot{\gamma}\cos\beta\sin\gamma]$$

$$= \frac{1}{2}m[4l^2\dot{\alpha}^2 + 4h^2\dot{\beta}^2 + l^2\dot{\gamma}^2 - 8lh\dot{\alpha}\dot{\beta}\sin(\alpha+\beta) + 4l^2\dot{\alpha}\dot{\gamma}\cos(\alpha+\gamma) - 4hl\dot{\beta}\dot{\gamma}\sin(\beta-\gamma)]$$

The potential energy V of body segment c is:

$$\mathbf{V_c} = mg(2l\cos\alpha + 2h\sin\beta - l\cos\gamma)$$

Calculation of the Derivatives

Now the derivative of L after q and $\dot{q}$ will be determined. This is achieved not by adding all the individual potential and kinetic energies and then derivating the total, but as in equation 2.11 by deriving the individual energies and adding them afterwards.
Derivatives of kinetic and potential energy after q and $\dot{q}$ of the body segment a:

$$\frac{\partial \mathbf{T_a}}{\partial \dot{\mathbf{q}}} = \begin{pmatrix} ml^2\dot{\alpha} \\ 0 \\ 0 \end{pmatrix} \qquad\qquad \frac{\mathbf{d}}{\mathbf{dt}}\frac{\partial \mathbf{T_a}}{\partial \dot{\mathbf{q}}} = \begin{pmatrix} ml^2\ddot{\alpha} \\ 0 \\ 0 \end{pmatrix}$$

$$\frac{\partial \mathbf{T_a}}{\partial \mathbf{q}} = 0 \qquad\qquad \frac{\partial \mathbf{V_a}}{\partial \mathbf{q}} = \begin{pmatrix} -mgl\sin\alpha \\ 0 \\ 0 \end{pmatrix}$$

Derivative of kinetic and potential energy after q and $\dot{q}$ of the body segment b:

$$\frac{\partial \mathbf{T_b}}{\partial \dot{\mathbf{q}}} = \begin{pmatrix} 4Ml^2\dot{\alpha} - 2Mlh\dot{\beta}\sin(\alpha+\beta) \\ Mh^2\dot{\beta} - 2Mlh\dot{\alpha}\sin(\alpha+\beta) \\ 0 \end{pmatrix}$$

$$\frac{\mathbf{d}}{\mathbf{dt}}\frac{\partial \mathbf{T_b}}{\partial \dot{\mathbf{q}}} = \begin{pmatrix} 4Ml^2\ddot{\alpha} - 2Mlh\ddot{\beta}\sin(\alpha+\beta) - 2Mlh\dot{\beta}(\dot{\alpha}+\dot{\beta})\cos(\alpha+\beta) \\ Mh^2\ddot{\beta} - 2Mlh\ddot{\alpha}\sin(\alpha+\beta) - 2Mlh\dot{\alpha}(\dot{\alpha}+\dot{\beta})\cos(\alpha+\beta) \\ 0 \end{pmatrix}$$

$$\frac{\partial \mathbf{T_b}}{\partial \mathbf{q}} = \begin{pmatrix} -2Mlh\dot{\alpha}\dot{\beta}\cos(\alpha+\beta) \\ -2Mlh\dot{\alpha}\dot{\beta}\cos(\alpha+\beta) \\ 0 \end{pmatrix} \qquad \frac{\partial \mathbf{V_b}}{\partial \mathbf{q}} = \begin{pmatrix} -2Mgl\sin\alpha \\ Mgh\cos\beta \\ 0 \end{pmatrix}$$

Derivative of kinetic and potential energy after q and $\dot{q}$ of the body segment c:

$$\frac{\partial \mathbf{T_c}}{\partial \dot{\mathbf{q}}} = \begin{pmatrix} 4ml^2\dot{\alpha} - 4mlh\dot{\beta}\sin(\alpha+\beta) + 2ml^2\dot{\gamma}\cos(\alpha+\gamma) \\ 4mh^2\dot{\beta} - 4mlh\dot{\alpha}\sin(\alpha+\beta) - 2mhl\dot{\gamma}\sin(\beta-\gamma) \\ ml^2\dot{\gamma} + 2ml^2\dot{\alpha}\cos(\alpha+\gamma) - 2mhl\dot{\beta}sin(\beta-\gamma) \end{pmatrix}$$

$$\frac{\mathbf{d}}{\mathbf{dt}}\frac{\partial \mathbf{T_c}}{\partial \dot{\mathbf{q}}} = \begin{pmatrix} 4ml^2\ddot{\alpha} - 4mlh\ddot{\beta}\sin(\alpha+\beta) - 4mlh\dot{\beta}(\dot{\alpha}+\dot{\beta})\cos(\alpha+\beta) \\ 4mh^2\ddot{\beta} - 4mlh\ddot{\alpha}\sin(\alpha+\beta) - 4mlh\dot{\alpha}(\dot{\alpha}+\dot{\beta})\cos(\alpha+\beta) \\ ml^2\ddot{\gamma} + 2ml^2\ddot{\alpha}\cos(\alpha+\gamma) - 2ml^2\dot{\alpha}(\dot{\alpha}+\dot{\gamma})\sin(\alpha+\gamma) \end{pmatrix}$$

$$\begin{pmatrix} +2ml^2\ddot{\gamma}\cos(\alpha+\gamma) - 2ml^2\dot{\gamma}(\dot{\alpha}+\dot{\gamma})\sin(\alpha+\gamma) \\ -2mhl\ddot{\gamma}\sin(\beta-\gamma) - 2mhl\dot{\gamma}(\dot{\beta}-\dot{\gamma})\cos(\beta-\gamma) \\ -2mhl\ddot{\beta}\sin(\beta-\gamma) - 2mhl\dot{\beta}(\dot{\beta}-\dot{\gamma})\cos(\beta-\gamma) \end{pmatrix}$$

$$\frac{\partial \mathbf{T_c}}{\mathbf{q}} = \begin{pmatrix} -4mlh\dot{\alpha}\dot{\beta}\cos(\alpha+\beta) - 2ml^2\dot{\alpha}\dot{\gamma}\sin(\alpha+\gamma) \\ -4mlh\dot{\alpha}\dot{\beta}\cos(\alpha+\beta) - 2mhl\dot{\beta}\dot{\gamma}\cos(\beta-\gamma) \\ -2l^2\dot{\alpha}\dot{\gamma}\sin(\alpha+\gamma) + 2mhl\dot{\beta}\dot{\gamma}\cos(\beta-\gamma) \end{pmatrix} \qquad \frac{\partial \mathbf{V_c}}{\mathbf{q}} = \begin{pmatrix} -2mgl\sin\alpha \\ 2mgh\cos\beta \\ mgl\sin\gamma \end{pmatrix}$$

The energies of all body segments have now been derived after q and $\dot{q}$, so that equation 2.11 can now be calculated. After the simplification of this formula the system can be written in the form of equation 2.2 which was:

$$M(q) * \ddot{q} + N(q, \dot{q}) + G(q) = 0$$

In the following the values calculated for the matrices M, N and G are given:

$$M(q) = \begin{pmatrix} \left(ml^2 + 4Ml^2 + 4ml^2\right) & \left(-2Mlh\sin(\alpha+\beta) - 4mlh\sin(\alpha+\beta)\right) & \left(2ml^2\cos(\alpha+\gamma)\right) \\ \left(-2Mlh\sin(\alpha+\beta) - 4mlh\sin(\alpha+\beta)\right) & \left(Mh^2 + 4mh^2\right) & \left(-2mlh\sin(\beta-\gamma)\right) \\ \left(2ml^2\cos(\alpha+\gamma)\right) & \left(-2mhl\sin(\beta-\gamma)\right) & \left(ml^2\right) \end{pmatrix} \quad (2.12)$$

17

$$N(q,\dot{q}) = \left(\begin{array}{c} -2Mlh\dot{\alpha}\dot{\beta}\cos(\alpha+\beta) - 2Mlh\dot{\beta}(\dot{\alpha}+\dot{\beta})\cos(\alpha+\beta) - 4mlh\dot{\beta}(\dot{\alpha}+\dot{\beta})\cos(\alpha+\beta)- \\ -2Mlh\dot{\alpha}\dot{\beta}\cos(\alpha+\beta) - 2Mlh\dot{\alpha}(\dot{\alpha}+\dot{\beta})\cos(\alpha+\beta) - 4mlh\dot{\alpha}(\dot{\alpha}+\dot{\beta})\cos(\alpha+\beta)- \\ -2ml^2\dot{\alpha}(\dot{\alpha}+\dot{\gamma})\sin(\alpha+\gamma) - 2mhl\dot{\beta}(\dot{\beta}-\dot{\gamma})\cos(\beta-\gamma)- \end{array} \right.$$

$$\left. \begin{array}{c} -2ml^2\dot{\gamma}(\dot{\alpha}+\dot{\gamma})\sin(\alpha+\gamma) - 4mlh\dot{\alpha}\dot{\beta}\cos(\alpha+\beta) - 2ml^2\dot{\alpha}\dot{\gamma}\sin(\alpha+\gamma) \\ -2mlh\dot{\gamma}(\dot{\beta}-\dot{\gamma})\cos(\beta-\gamma) - 4mlh\dot{\alpha}\dot{\beta}\cos(\alpha+\beta) - 2mlh\dot{\beta}\dot{\gamma}\cos(\beta-\gamma) \\ -2ml^2\dot{\alpha}\dot{\gamma}\sin(\alpha+\gamma) + 2mhl\dot{\beta}\dot{\gamma}\cos(\beta-\gamma) \end{array} \right) \quad (2.13)$$

$$G(q) = \left(\begin{array}{c} -mgl\sin\alpha - 2Mgl\sin\alpha - 2mgl\sin\alpha \\ Mgh\cos\beta + 2mgh\cos\beta \\ mgl\sin\gamma \end{array} \right) \quad (2.14)$$

Equation 2.2 is the final formula expressing the equation of motion of joints and segments under gravitation and mechanical constraints. The system is conservative with time-invariant constraints. This is only the differential equation for the single support phase. When the swing leg hits the ground, ground contact occurs. This equation determines the mechanics of ground contact, presented in the next section 2.3.2. The $u_{corrective}$ which was mentioned above in the pendulum equation is an activation of the passive system and this will be introduced and explained in chapter 3 section 3.3.

2.3.2 Ground Contact

Stepping is, as mentioned before, a movement consisting of two phases: the swing phase and the support phase of a leg. This means, if walking is characterized by a sequential rhythmic movement, it is a sequence of one leg supporting and one leg swinging, followed by a short phase where both legs have ground contact and are therefore support legs. In this research the double support phase is constrained to be very short, so that the transition from swing to support leg is modeled infinitesimally short. The state transition can be seen in figure 2.6 for one complete step cycle.

The impact is a contact between two rigid bodies. It takes place without any slipping and rebounding of the leg. This impact happens when the swing leg touches the ground. The continuous part of the movement, the swing phase, is followed by the state transition when the discrete impact between the ground and the swing leg is transferred from the swing leg to the support leg and vice versa. This is a hybrid nonlinear system. A model without knees requires an explicitly defined ground contact to get similar movements as with knees. In the literature various possibilities for ground contact are described such as in [111] or in [54], where the impact moment is defined by the angular position. In the case of mechanics moving in the frontal plane, this is similar. The ground contact is defined by the angular position just when the swing leg is crossing the zero ground
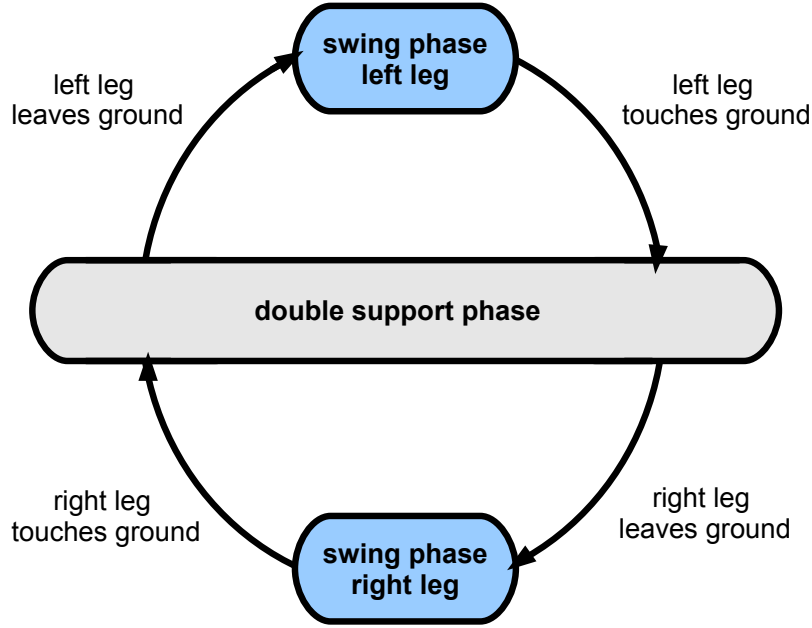
Figure 2.6: State transition diagram for one complete step cycle: the state change between double support phase, where both legs have ground contact, and single support or swing phase, where only one leg has ground contact.

line (surface). It is possible for the swing leg to dip beneath the ground surface and to get ground contact later at the moment when the swing leg crosses the zero ground line again. This is important because normal stepping in place where the hip drops while the knee bends. The ground contact is avoided till the hip rises again and the knee stretches. Without knees this can theoretically be achieved by dipping the leg into the ground and coming up again to have an impact for a new step. This is the case for level ground when:

$$l * cos(\alpha) - h * sin(\beta) - l * cos(\gamma) = 0 \qquad (2.15)$$

where l is the leg length, h is the hip width and the angles are as defined in figure 2.5. If ground contact occurs, the position and angle of the leg do not change, only their angular velocity changes instantaneously. There are many ground contact models in literature. Here the model of [54] described earlier in [68] is used. The new angular velocity is determined by the following equation:

$$M(q) * \ddot{q} + N(q, \dot{q}) * \dot{q} + G(q) = u_{corrective} + \delta F_{ext} \qquad (2.16)$$

with M, N, G matrices (mass, centrifugal forces, gravitation) of the mechanical system as determined earlier in sections 2.2.2 and 2.3 and F_{ext} is the external force applied to the contact point during ground contact. The constraints are, that these external forces are (1) instantaneous, (2) impulsional but that (3) the position remains continuous and (4) $u_{corrective}$ (the joint torque applied by the actuators) is not impulsional. This leads to the

fact that the integration of equation 2.16 results in:

$$M(q) * (\dot{q}^+ - \dot{q}^-) = F_{ext} = E(q)^T * \begin{pmatrix} F_T \\ F_N \end{pmatrix} \tag{2.17}$$

with $\dot{q}^+$ angular velocity right after the contact and $\dot{q}^-$ before contact where the position stays the same $q^+ = q^-$.

$F_{ext} = \int_{t^-}^{t^+} \delta F_{ext}(\tau)d\tau$ are the external applied forces consisting of F_T and F_N which are the tangent and normal forces. As the difference of position $q^+ - q^- = 0$ and the $torque_{corrective}$ does not change in the infinitesimal length of time of contact, the terms of $N, G, torque_{corrective}$ become zero with integration. The matrix $E(q) = \frac{\partial J}{\partial q}$ is determined where J is the final position of the swing leg in Cartesian coordinates:

$$E(q) = \frac{\partial J}{\partial q} = \begin{pmatrix} 2 * l * cos(\alpha) & -2 * h * sin(\beta) & 2 * l * cos(\gamma) \\ -2 * l * sin(\alpha) & 2 * h * cos(\beta) & 2 * l * sin(\gamma) \end{pmatrix} \tag{2.18}$$

The condition that the swing leg does not slip and the impact is completely inelastic leads to equation:

$$E(q) * \dot{q}^+ = 0 \tag{2.19}$$

With equations 2.17 and 2.19 there are 5 equations to solve for 5 unknowns q^+, F_T, F_N which are:

$$\begin{pmatrix} \dot{q}^+ \\ F_T \\ F_N \end{pmatrix} = \begin{pmatrix} M(q) & -E(q)^T \\ E & 0 \end{pmatrix}^{-1} * \begin{pmatrix} M(q) * \dot{q}^- \\ 0 \end{pmatrix} \tag{2.20}$$

The invertible of the first matrix on the right hand side is defined because the matrices $E(q)$ and $M(q)$ have full rank and are nonsingular. This means that equations:

$$\dot{q}^+ = \frac{1}{det()} * M(q) * M(q) * \dot{q}^-$$

determines the new velocity and equation:

$$\begin{pmatrix} F_T \\ F_N \end{pmatrix} = \frac{1}{det()} * -E(q)^T * M(q) * \dot{q}^-$$

determines the ground contact forces; here $det()$ is the determinant of the first matrix of equation 2.20 to calculate the inverse of this nonsingular matrix. In other words these equations lead to the transformation of the angular velocities just before the ground contact $\dot{q}^-$ to the angular velocities just after the ground contact $\dot{q}^+$ by equation:

$$\dot{q}^+ = T * \dot{q}^- \tag{2.21}$$

where T is the transformation matrix for the state transition between steps.

2.3.3 Extended Ground Contact Model for Actuated Mechanics

In the next chapter the system consists of both the mechanics for stepping and the actor component, the oscillator network which applies a corrective torque to joints during the swing phase. If the swing leg touches the ground again, ground contact takes place. The position during ground contact does not vary because there is no impulsive corrective torque applied to the system. The stability of the whole system depends on the energy kept in the system from step to step. If the energy decreases with each step, the step movement decreases as well. This decrease can lead to instabilities of the stepping movements which should be corrected by the actuation. The actuation can not compensate this energy loss in all cases because the oscillator state is not necessarily synchronized with the point of time when the swing leg touches the ground. This leads to the fact that when the leg touches the ground the state of the oscillator network can be different for each step. This synchronization problem leads to a variation of how much corrective torque was already applied to the system. An appropriate measure for the synchronization and the oscillator state is the energy state of the system. Over several steps the energy should be about the same at the beginning of each step in oder to enable steady periodic stepping. To ensure this energy constancy over several steps an energy control can be integrated, which will be explained in the following.

During the swing phase the system is continuous and the corrective torque is generated and applied to the mechanics in a continuous way. Where there is instantaneous ground contact occurs it is not clear what happens to the activation level of the individual neurons. The ankle actuation of the former support leg is no longer used after the ground contact when it becomes the swing leg, because the ankle of the swing leg does not receive any corrective torques. In this research the neuronal activation stays constant during the ground contact. If the overlaid frequencies of the mechanical dynamics and the oscillator actuation is not synchronous this leads to a shift between the two systems which finally leads to instable movement solutions. To enlarge the range of stability the lack of synchronization can be compensated additionally. This leads to an extension of the ground contact model. An energy transition rule is introduced to ensure that the energy at the beginning of the step is the same as it was at the beginning of the last step by a push-off. The system energy which is lost or added to the system as a result of lacking synchronization between the neuron activation and ground contact model is compensated by the energy transition rule with the push-off. This can be imagined as a recovery of system energy E during impact, which results in corrective torques applied during push-off. This leads to velocities of the push-off leg being adapted immediately after the impact. The equation for this is:

$$E(step_i(1)) - E_{pot}(step_{i+1}(1)) = E_{kin}(step_{i+1}(\dot{\alpha}(1), \dot{\beta}(1), \dot{\gamma}(1))) \qquad (2.22)$$

where E is the complete potential and kinetic amount of energy of the system. E_{pot} and E_{kin} are the potential and kinetic energies of the system respectively. There are several succeeding steps with $i = 1 \ldots number \ \ of \ \ steps$. $Step_i(1)$ stands for the first state values of $step_i$ wherever there are state values for each time step. The initial values

for the new step $i + 1$ (angular velocities $\dot{\alpha}^{++}, \dot{\beta}^{++}$ and $\dot{\gamma}^{++}$) are calculated by solving the equation 2.22 for these three values by the Powell dogleg trust region algorithm [145], which solves a nonlinear minimization problem. The initial values for solving the equation are therefore the outputs of equation 2.20 q^+. This gives the new values q^{++}, which are the initial angular velocities $\dot{\alpha}^{++}, \dot{\beta}^{++}$ and $\dot{\gamma}^{++}$. This energy transition rule is an alternative to synchronizing the two systems mechanics and actuation as proposed in the section about stability in 3.5 and enlarges therefore the possible working range of the stepping model.

2.4 Simulation Results

The ballistic walkers step down a slope by gravitational forces. It can be objected that for natural walking many more factors influence and control the system. Nevertheless with this ballistic walker a quite natural-looking type of walk can be generated which is extremely energy-efficient and stable solutions for walking movements can be found. Stability is crucial, for if the system falls down, neither natural appearance nor energy balance can be optimized. In human surviving strategies stability of walking has always been an important factor as the ability to walk stably is essential for hunting and collecting food. The stability of a periodic movement, such as walking, is not easily derived. An extra section 3.5 is required therefore which defines the term stability and the mathematical proof. The stability is verified for the fully actuated frontal-plane model in section 3.5.3. According to the literature [49, 48, 50, 126, 111, 112, 92], the sagittal-plane model of the ballistic walker achieves stable solutions for certain parameter constellations. In the following the simulated periodic movements produced with the model introduced in 2.2 are analyzed and the characteristics of these ballistic periodic movements are detailed.

The characteristics of a downhill ballistic walker are a stance leg acting as a pivot and a swing leg swinging like a pendulum. This continuous movement is interrupted when the swing leg strikes the ground. Then the discrete ground model transforms the model state before the strike into the model state after the strike, and the next step starts with the former swing leg as new stance leg and vice versa. Then when the swing leg strikes the ground again, this step is finished and so on. The result is a rhythmic movement which is repeated step by step periodically. Ground contact occurs at the precise moment when the system has a special angular constellation. In a system with no knees, the swing leg also naturally scuffs the ground during the steps e.g. when the two legs are in equal positions, which means that θ and ϕ are both zero. These situations are not taken into consideration for ground contact. There are several possibilities for avoiding such situations such as shortening the swing leg [48, 29] or causing the swing leg to move to the side (laterally) [111].
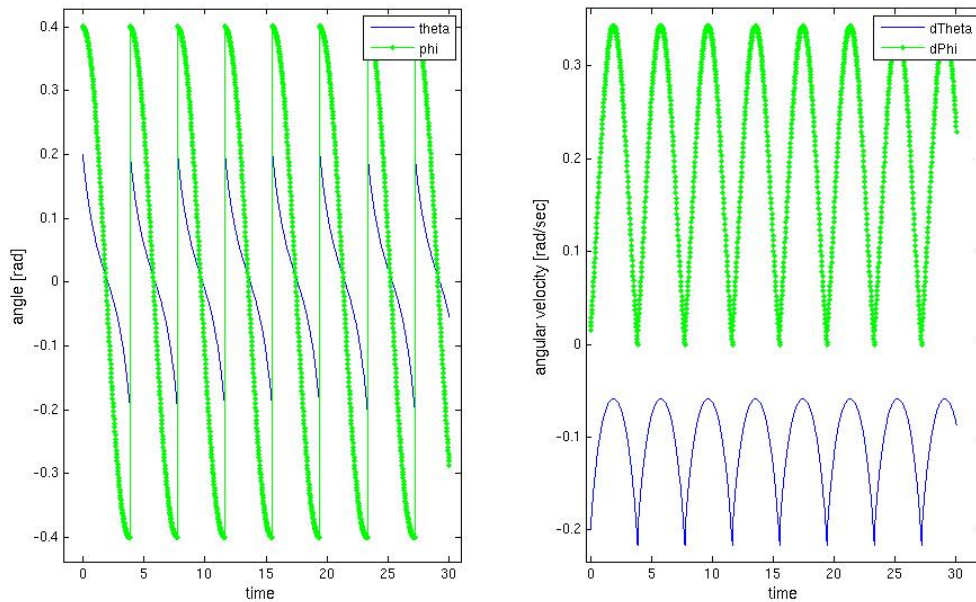
Figure 2.7: Simulation of the angles (left) and angular velocities (right) of a stable ballistic walker, taking 8 steps down a very shallow slope with 0.009 [rad] gradient.
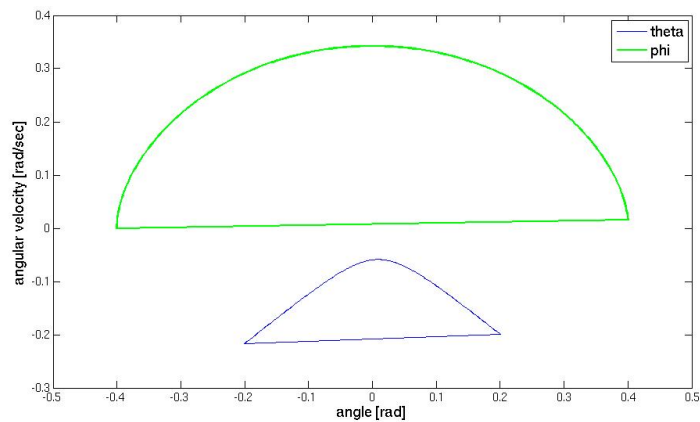
Figure 2.8: Phase plot for the same simulation of 8 steps down a very shallow slope with 0.009 [rad] gradient.

2.4.1 Ballistic Periodic Movements in the Sagittal Plane

Using equations 2.5, 2.6, 2.7 from section 2.2.2 and ground contact equations 2.8 and 2.9 from section 2.2.3 the following results have been calculated and are shown in figures 2.7 to 2.14. In Figure 2.7 the angle and angular velocity for 8 steps are shown. In Figure 2.8 the related phase plot of the system is shown. It can be seen that the phase plot is a cyclic solution of a one-periodic system as all the periodic solutions are identical

repetitions and each step looks the same as the last. A stable solution such as this can be found experimentally or, as Garcia [38] mentions, by a multi-variable Newton Raphson or gradient search method to find a local minimal solution for an unconstrained nonlinear function (MATLAB function fminunc). This does however mean that the initial values for the search have to be already close to the solution as this is a local minima search.

Slope Angle

One important parameter of the model is the slope angle, which determines the gravitational forces affecting the ballistic walker. As studied in [38, 48] the slope angle influences not only the stability of the system and the periodicity, but also the step length and frequency. In figures 2.9 and 2.10 results can be seen for a changed slope angle to 0.01 $[rad]$ and the resulting variations in step length and step frequency. A bigger angle produces longer steps and a slower step frequency. As can be seen in figure 2.11 and figure 2.12 the walking becomes unstable if the slope angle is enlarged further to 0.015 $[rad]$. In figures 2.11 and 2.12 this finally leads to the ballistic walker falling.

Variation of initial values

For the slope angle variation it is shown that the ballistic walker quickly becomes unstable. Other important parameters which are interesting to vary are the initial values for the model, which are the angles and angular velocities. As the model is a system which is in general unstable and only has very small parameter ranges to produce stable solutions, it is clear that the initial conditions of such a system have a large influence on its stability. The results in this subsection are produced with a slope value of $slope \quad angle = 0.009 \quad [rad]$. Figures 2.13 and 2.14 show how a change in the initial velocity of the stance foot $\dot{\theta}$ about 0.004 $[rad]$ alters the movement of the ballistic walker with the third step. The result is falling at the third step. The original value of $\dot{\theta}$ was 0.199 $[rad]$, which is seen in figures 2.7 and 2.8.
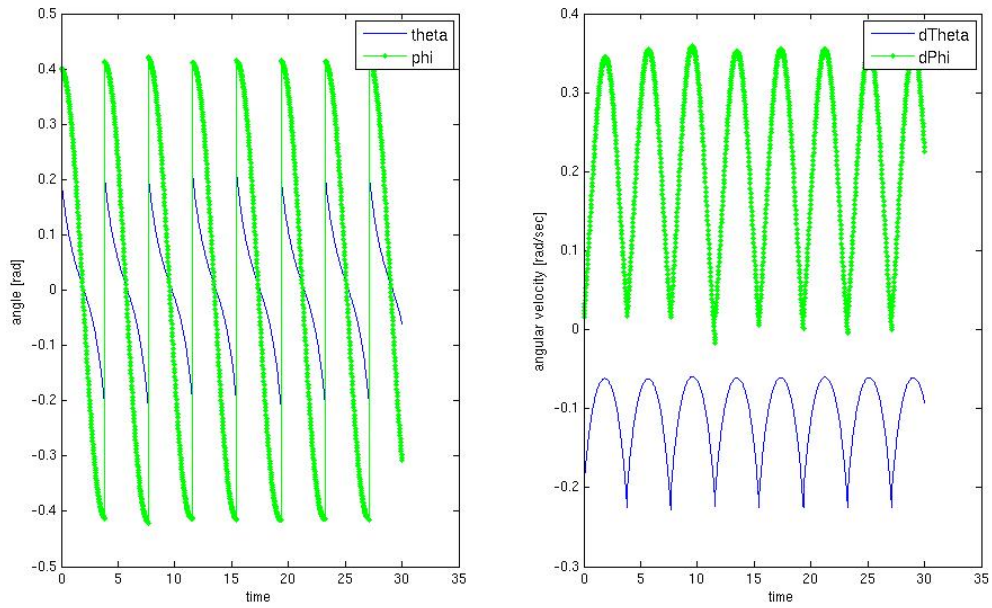
Figure 2.9: Changing the slope angle to 0.01 [rad] gradient, leads to slightly larger angles and angular velocities for 8 steps of walking but is still stable.
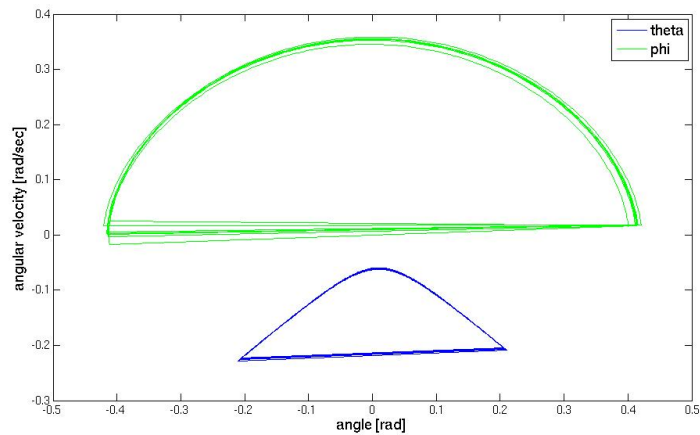
Figure 2.10: Phase plot of a ballistic walker with changed slope angle to 0.01 [rad] gradient. This leads to slightly larger angles and angular velocities for 8 steps of walking but is still stable.
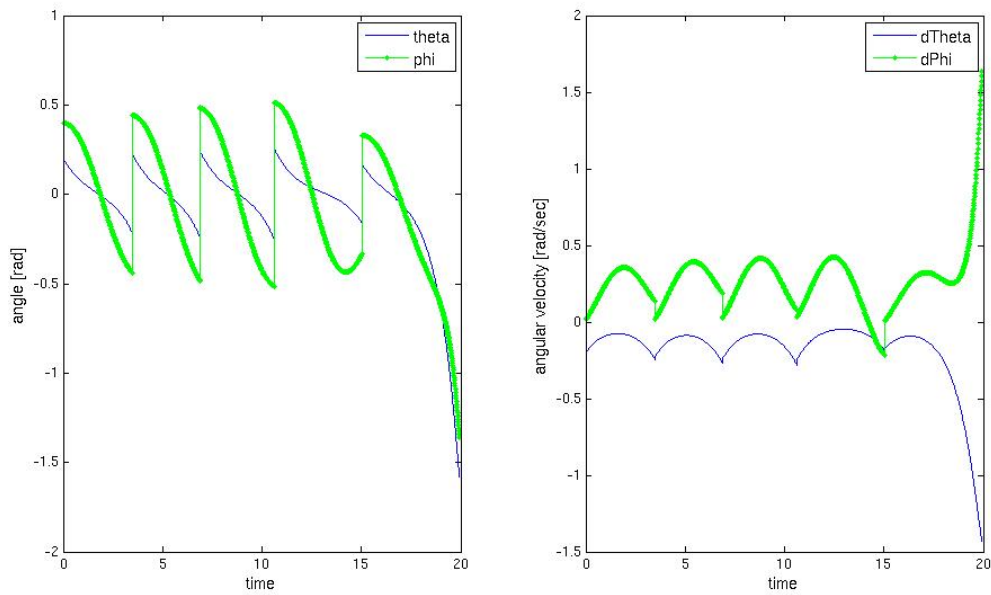
Figure 2.11: Simulation of the angles and angular velocities of a ballistic walker, taking 5 steps. Changing the slope to 0.015 [rad] gradient leads to an instability which results in a fall at the 5th step.
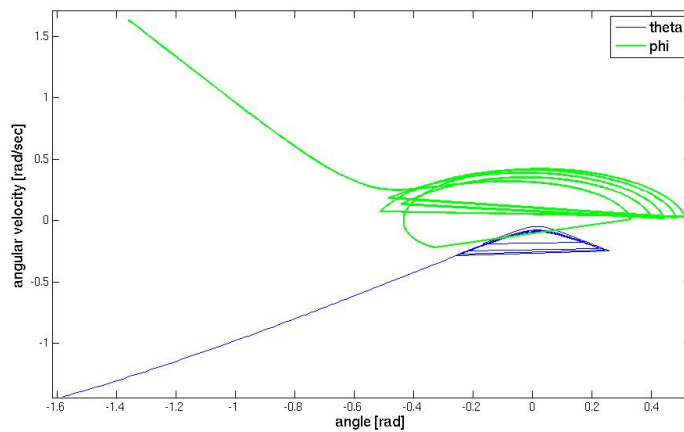
Figure 2.12: Phase plot of a ballistic walker. The changed slope with 0.015 [rad] gradient leads to an instability which results in a large increase in the angles and angular velocities at the 5th step.
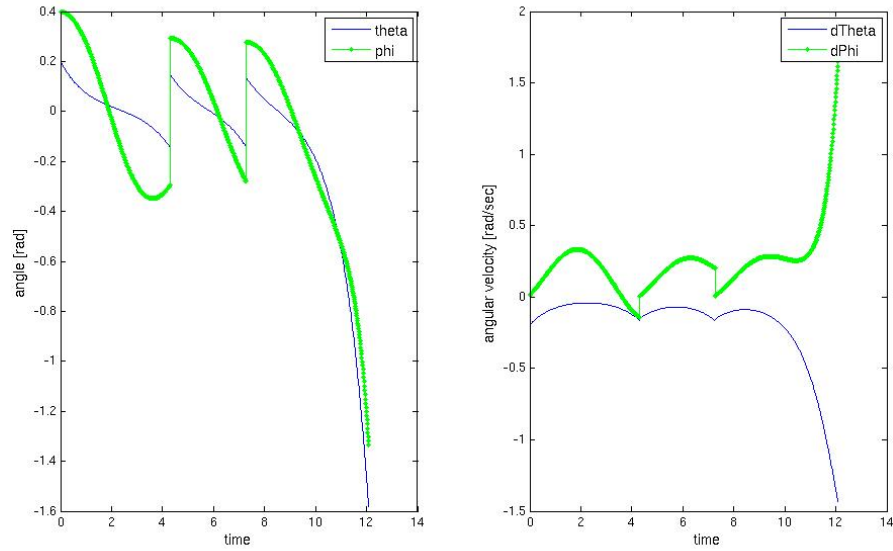
Figure 2.13: Simulation of the angles and angular velocities of a ballistic walker with a varied initial condition for angular velocity $\dot{\theta} = 0.195$. This leads to unstable walking and a fall at step 3.
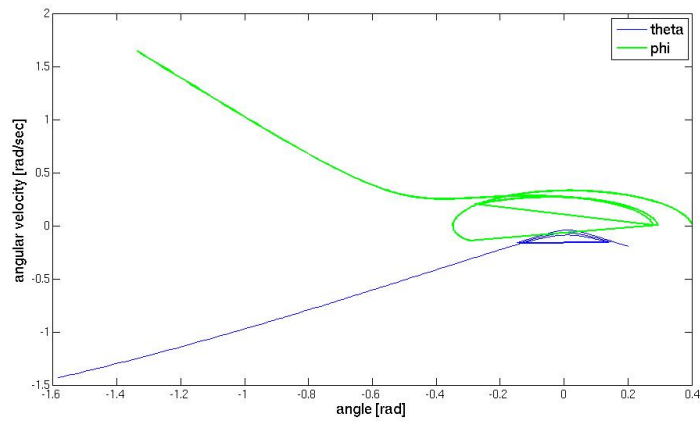
Figure 2.14: Phase plot of a ballistic walker with varied initial condition of initial angular velocity $\dot{\theta} = 0.195$.

2.5 Conclusion

The mechanical model presented in this chapter was designed on ballistic principles. In general the aim was to develop the simplest model which is able to achieve the desired mechanical abilities. The ballistic mechanics for the sagittal plane can produce stepping movements on a slope. To show how the developed structures could be applied to the sagittal-plane mechanics an established model was used for reference. The stability range of those stepping movements is narrow and depends on the mechanics, the initial values and the slope gradient. The influence of initial conditions and slope gradient were simulated to demonstrate their relevance for stability. Challenges which the actuation presented in the following chapter will have to meet are to improve stability, to expand the possible parameter range, to enable different stepping patterns, and to vary the stepping movement strategies. Another task will be for the actuation to attenuate the influence of disturbances applied to the system.

The mechanics introduced for the frontal plane do not offer a suitable driving mechanism such as a slope. In addition to this, as was earlier mentioned by Kuo [94], the medio-lateral walking movement needs an additional actuation to achieve stability and is mainly independent of the sagittal-plane walking movements. This leads to the separate evaluation of frontal-plane stepping movements. The requisite actuation and the abilities it provides for this new model will be detailed in the next chapter 3.

3 Actuation of Passive Mechanical Models

In the previous chapter two ballistic models were presented, one for the sagittal plane and one for the frontal plane. The sagittal plane model achieved stable walking on a slope. With the frontal-plane model no stable walking was possible. The sagittal walker required a shallow slope to power it, but stable solutions of walking movements were found to be very sensitive to changes in the slope gradient and to initial conditions.

Actuation of a passive model enables powering and control of the model, which means that it no longer needs a slope to produce walking steps. Furthermore, actuation is a possible way to stabilize the dynamics of mechanics [87, 85, 92, 41, 123] and to enhance their robustness with respect to initial conditions, slope gradients, external disturbances etc., to name only a few influences. For the research described in this thesis an oscillator network was selected for actuation because it represents real biological neuronal structures which produce rhythmic movements like stepping. A new frontal-plane stepping model is introduced incorporating antagonistic application of the actuation to the joints and a feedback mechanism which is based on the muscular receptor feedback. The selected mechanisms are applied in identical fashion to the sagittal-plane model to prove that they are also practicable for stepping movements in the sagittal plane. Both models will be evaluated, with respect to their stability and to parameter influences on the stepping movement. In addition, possible stepping patterns and strategies are studied for the frontal-plane stepping model introduced, together with their resemblance to real human stepping movements.

A selection of state-of-the art actuation methods for walking models is presented in the next section 3.1. The neuronal structure which is taken as the basis for the chosen actuation, is detailed further in section 3.3. The actuation is coupled with the mechanics presented in chapter 2 as antagonistic muscle forces applied to the joints; this is described in section 3.4. The controllability of the system by actuation and the gain in stability are mentioned above. The term walking stability is defined in section 3.5 and the used proof for stable stepping patterns is introduced. The actuation is applied the mechanics of both the sagittal and frontal-plane model, and the simulation results for stepping movements are shown in sections 3.7 and 3.8.

3.1 State of the Art of Actuation Mechanisms for Walking Models

There are several possible actuation types, for instance, actuation by joint torques that follow a precalculated trajectory or a fixed control law [11, 102, 17]. This type is very commonly used in robotics. Another method of actuation is the modeling of spring and damper elements to influence the movement. In [195] this was realized for a sagittal model by following two simple rules: first, that the swing leg moves quickly enough for the model not to fall forward, and second, that the swing leg is not placed too far in front, so that the next step can still be stabilized. In [29] another approach is demonstrated with the leg length and step length being varied to obtain the desired walking result. A further possible mechanism is to store energy in the ankle to give and release this energy in a controlled manner to the system via a push-off during the stance phase [23]. The addition of any kind of actuation means that the passivity of the walking system is lost, but controllability, stability and robustness are gained. As found by [194], the muscles of human beings are of course active, but the level of activation during walking is much less than during other movements; especially the swing leg muscles are little activated. This indicates that actuation during walking is reduced to a minimum to keep the energy cost low, but nevertheless provides additional stability and robustness.

For the present research, actuation by neural networks was chosen. This actuation bases on the physiological structures found in the central nervous system (CNS). These are networks of neurons that generate so called "central patterns". Neuronal cell structures that can produce oscillations without sensory input are called central pattern generators CPGs according to [30]. These CPGs activate neuronal structures and finally the muscles, where they produce rhythmic movements. These movements can be e.g. swimming [51], flying [153] or walking [156]. In section 3.2 the basic structures of such neuronal oscillators are explained in more detail. The actuation of leg movements by CPG structures has been the subject of various researches, such as [40, 172, 100, 152, 129, 183]. In [172] bipedal locomotion driven by neural oscillators is used to achieve stable walking patterns. The forward movement can be varied by model parameters. [152] and [40] build their neuronally driven bipedal walking models on biological paradigms and provide an adaptive structure to adapt locomotion to environmental changes. However they both concentrate on walking in the sagittal plane. Genetic algorithms can be used as in [70], to optimize the parameters for the neuronal network.

3.2 Examples of Oscillator-Driven Movements in Biology

The setup and functioning of the Matsuoka oscillator network to represent the neuronal structures, used in the following, are derived here. Hence, a short overview of biological prototypes in animals is given. There are no experiments about oscillator structures and their detailed mode of operation in the CNS of humans [53]. But there are experiments and
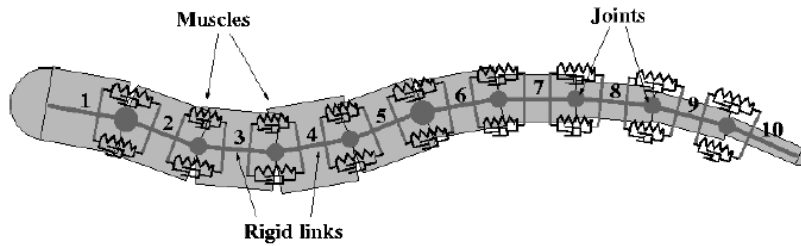
Figure 3.1: Mechanics of the lamprey consist of rigid segments in a line from [55].

results about the neuronal structures of oscillators and their functionality in animals. In the following the two examples 'lamprey' and 'cat' are presented to give an idea about the functionality of such neuronal structures which work like mutually inhibiting oscillators. The animals' movement is a rhythmic one and this can be directly correlated with the neuronal structure.

3.2.1 Lamprey

The lamprey is an eel-like fish, which has very ancient and therefore simple and large neuronal structures. In the lamprey it was first found and proven that neural oscillators can produce a rhythmic pattern, and that this pattern produces the swimming movement of this fish [51]. These neuronal cells were found in the CNS of the fish and it was proven that no brain was necessary to instigate the rhythmic movement, only an initial impulse to the neuronal oscillators. This impulse prompts the neurons to autonomously produce a rhythmic activation pattern for swimming. Additionally, this motor pattern is reproduced in the isolated brainstem cord [53]. These neuronal structures are interconnected and mutually inhibitory so that they are able to produce oscillations. Such a neuron network is connected to the muscles of the lamprey fish, so that the motoneurons of the muscles are activated. The activation pattern always leads to a contraction of the muscles on one side of the fish, while the muscles on the opposite side just relax.

This can be seen in figure 3.1 where the individual joint mechanics are interconnected with the antagonistic muscle pairs. In figure 3.2.1 the corresponding neuronal structures consisting of four neurons connected to the muscles are shown as well as the resulting movement of the lamprey. Inhibitory neurons (I), excitatory neurons (E) and interneurons (L) are associated with an oscillator which is connected to the muscles via motoneurons (MN). While the motoneuron of one side is excited the motoneuron on the other side is inhibited. On one side the muscles are contracted, while on the other side the muscles are not contracted and therefore can be stretched. As the individual oscillators are consecutive from head to tail of the fish, one oscillator subsequently triggers the next oscillator with a short latency in between and so on. This leads to a phase shift between the segments. So the movement of sequential contraction and relaxation results in a serpentine movement for swimming.
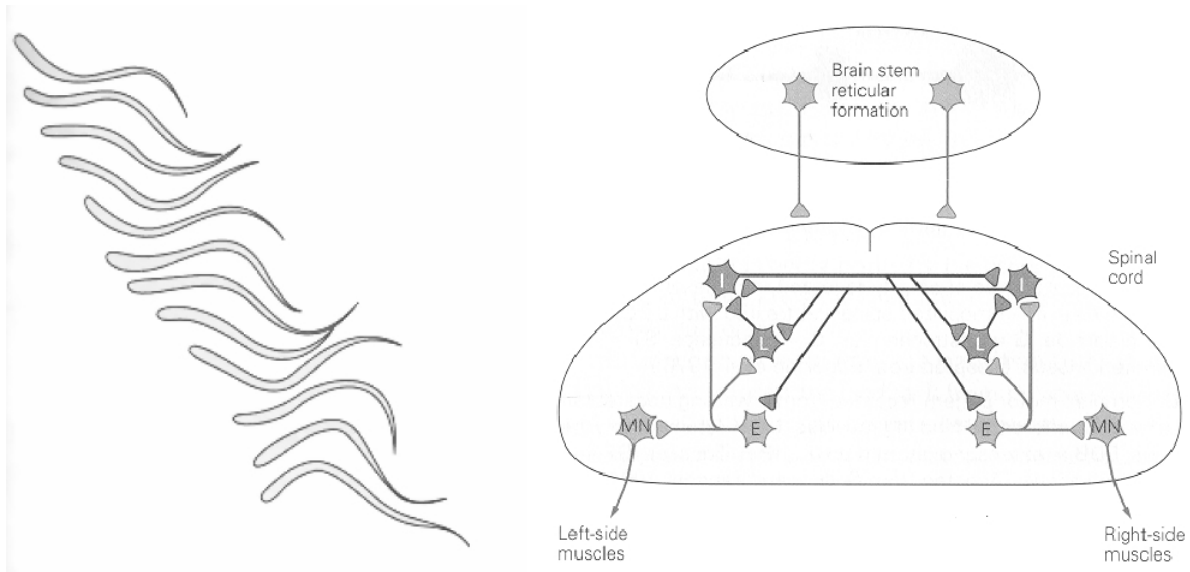
Figure 3.2: Neuronal interconnection of one segment (oscillator) of the lamprey with the muscles via the motoneurons.

3.2.2 Cat

There are some interesting experiments with cats that give an insight into how locomotion functions in the cat. It has been proven that rhythmical motor patterns according to a CPG in the CNS produce rhythmic movements [53, 51, 161]. In [45] it is shown that in decerebrated cats activation patterns can still be found that induce walking movements. Such cats are furthermore able to do walking movements on a treadmill. This finding has proven that the basic motor pattern is generated by the CNS without any high-level sensory input such as vision, sense of equilibrium or overall proprioception, but that additional high-level sensory input influences this setting. The concept of an autonomous rhythmic movement generator is not an organ but more or less a principle of functioning.

These autonomous patterns are a "substrate of locomotion" [147]. According to [110] the muscular flexions and extensions during locomotion in mammalian are produced by a CPG structure. The neuronal outputs of the CPG, in the form of neuron spiking activity, can be determined during locomotion but the structure of the CPG and its neuronal interactions are not known [53].
It is also clear that this CPG has its limits. Nevertheless, the cat is a good example of how rhythmic movements, especially walking, are produced in lower level control circuits than the brain, even in higher vertebrates. The CPG is only a possible representation of these control circuits, as no complete structure but the functioning of this system has been proven in the cat [73].

It is not known what a CPG structure looks like in human beings, but as vertebrates as highly developed as cats have such neuronal functionalities, this is an indication that evolution is more likely to advance this established structure than to discard it. Therefore
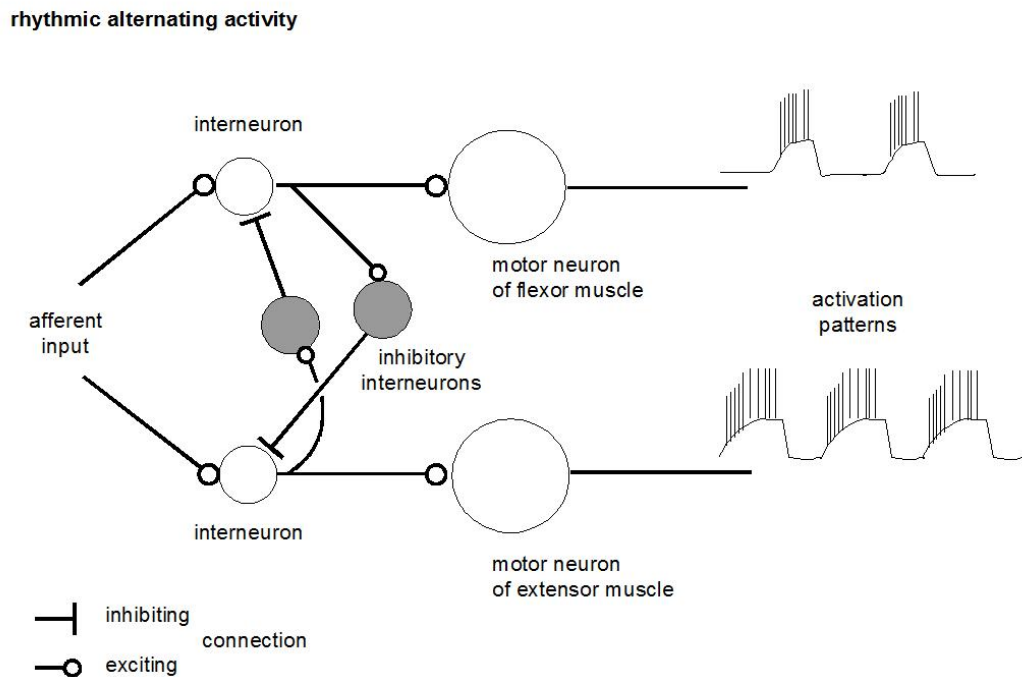
Figure 3.3: Activation pattern generated by mutually inhibiting neurons with antagonistic activation of flexor and extensor muscles.

this idea of a CPG structure is adopted to create a biped stepping model for rhythmic leg movements.

3.3 Neural Oscillator Model

The actuation of the passive mechanical system is realized by neuronal oscillators which generate antagonistic joint torques resembling to muscle activation. The functioning of muscles is only based on contraction of the muscles and its fibers. This requires an antagonistic composition of the muscles. For example a simple hinge joint requires two muscles at minimum: an extensor and a flexor. If one muscle contracts then the other is extended and vice versa. This principle of flexor and extensor is transferred to the neural activation. Each muscle is controlled by motoneurons and the feedback of muscular stretch sensors. Figure 3.3 shows a pair of flexor and extensor muscles which are activated by a mutually inhibiting pair of neuron compounds. Each neuron compound consists of excitatory, inhibitory and motor- neurons. The excitatory neuron of one pair activates the motoneuron, e.g. of the flexor muscle, and the inhibitory neuron inhibits the other pair, e.g. of the extensor. The two motoneuron activations, and consequently the muscles, are activated antagonistically therefore and show alternating activity which is seen on the right in figure 3.3. Here the natural spiking rate of an active neuron is shown.
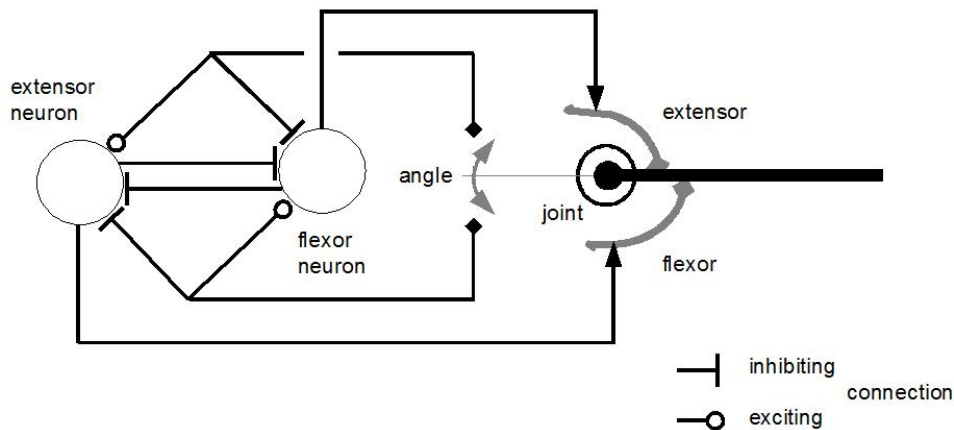
Figure 3.4: Schematic representation of neuron interconnections with the muscular system which contracts the joint muscles.

A simple model of this functionality has one motoneuron for one flexor and one for one extensor. This pair of flexor extensor motoneurons is represented by a mutually inhibiting oscillator consisting of two neurons, each integrating the inhibitory and excitatory component. This is visualized in figure 3.4.

This principle of mutually inhibiting neural networks was introduced by Matsuoka [107, 108] the so-called Matsuoka oscillator. With different combinations of oscillators a network is built which generates an activation pattern. If this pattern is coupled with muscle activation then a movement pattern of the musculo-skeletal system can be generated. This integration of oscillator network and muscle activation which leads to actuated movements of the mechanical system will be described in section 3.4.

3.3.1 The Matsuoka Oscillator

The neuron model used in the present study is a continuous-time neuron model as described in [131]. The model represents the firing rate of a neuron by means of a continuous variable of time which corresponds to the activation of the muscles. The Matsuoka oscillator model integrates mutual inhibition, excitation and external input e.g. from higher control levels such as sensors and the brain. This integration of natural neuron properties in a time-continuous relatively simple mathematical model represents an advantage over other neurons such as the Hodgkin-Huxley model [3]. Furthermore the Matsuoka oscillator applies these properties to interconnected neuron groups, which is useful for direct antagonistic actuation.
Mutual inhibition is realized by weighting the synaptic conjunctions, which are positive if they are excitatory and negative if they are inhibitory. The present neuron model includes an adaption over time. This means that constant excitation does not lead to a constant output by the neurons, but decreases over time. The extended equation for an inhibiting
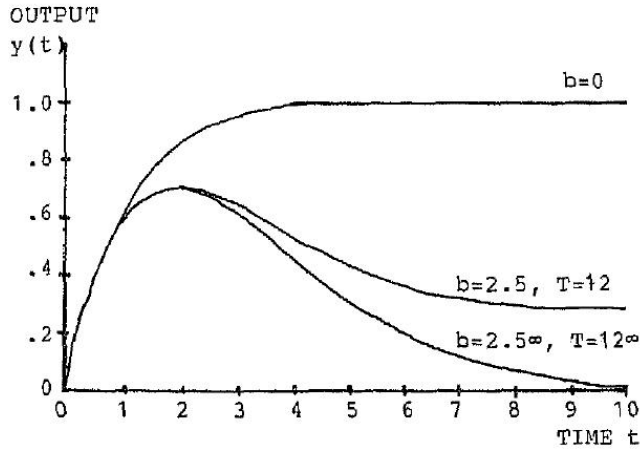
Figure 3.5: Adaptive neuron characteristics visible for a step response, taken from [107].

neuron model as proposed in [107, 108] is:

$$
\begin{aligned}
\dot{n}_i &= \frac{1}{T_a} * \left(-n_i - \sum_{j=1}^{k} a_{ij} * f_j - b * y_i + c_i * s_i + ext_i\right) \\
\dot{y}_i &= \frac{1}{T_b} * (f_i - y_i)
\end{aligned}
\tag{3.1}
$$
$$
\text{with } f_i = max(0, n_i - \Delta)
$$

where:

i	:	the number of the actual neuron
j	:	a selected number of the $1 \ldots k$ neurons in the network
n	:	the membrane potential of the neuron i (internal state of the neuron)
T_a, T_b	:	the time constants of the oscillator
Δ	:	the threshold value under which the neuron does not fire
f	:	the firing rate of the output of neuron j
a_{ij}	:	weight of inhibitory synaptic connection to a neuron j in the network
s	:	the impulse rate of an external input signal
c	:	weight of the synaptic conjunctions
y	:	adaptation or fatigue variable
b	:	the adaptation rate for steady-state firing
ext_i	:	external inputs from higher levels such as the brain or sensors, which also can directly influence the neuron activity

Table 3.1: Parameters of the neuron model.

This model takes the adaptation of a neuron into account. If the neuron receives a step input, the output firing rate initially increases but then decreases to a lower level, which is the adaptation level. This is shown in figure 3.5.
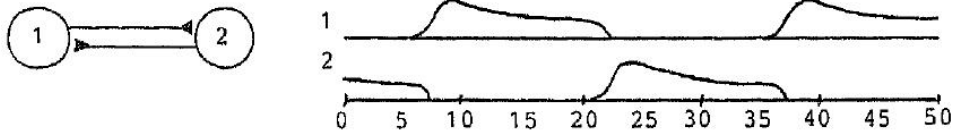
Figure 3.6: A simple 2-neuron oscillator network and its rhythmic activity from [107]

For example, two neurons are connected (j=1,2) and one is firing, which means a high n_1 value, the adaptation rate leads to a decrease in this value and therefore the influence of the other neuron increases as $a_{12} * f_2$ rises. Therefore the second neuron inhibits the first and after a while the second is firing at $n_2 > 0$. This is seen in figure 3.6. In the following the value Δ is set at zero. This definition means no limitation of generality to the system.

3.3.2 Constraints for Oscillation

There are some mathematically defined constraints to guarantee an oscillation mode for the neurons of a neuronal network with a special parameter configuration. A stable rhythmic solution can be achieved for the oscillator network in equation 3.1 if the following two constraints according to [107] are fulfilled:

$$\frac{a_{ij}}{1+b} < \frac{s_i}{s_j} \quad for \quad i,j = 1....n \tag{3.2}$$

where n is the number of neurons in the network and

$$\sqrt{a_{ij} * a_{ji}} > 1 + \frac{T_b}{T_a} \tag{3.3}$$

The oscillator networks presented in the following are all parametrized to meet these criteria for achieving a stable oscillation solution.

3.3.3 Basic Network Types

In the following the properties of some different basic oscillator networks are described as they are used for movement pattern generation: type A) the 2-neuron network, which is an oscillator and type B) the 4-neuron networks with different interconnections between the two oscillators. The first basic network A) is the 2-neuron network seen in figure 3.6. Each neuron suppresses and stimulates the activity of the other neuron. This oscillator has the characteristic that only one neuron fires at a time. The oscillator correlates to movements such as simple rhythms e.g, fluttering, chewing, moving one leg which, as mentioned above, is a simple antagonistic movement by flexor and extensor.

The type B) network with two oscillators can have different interconnections between the neurons or the oscillators. In this study three kinds of interconnections and the related
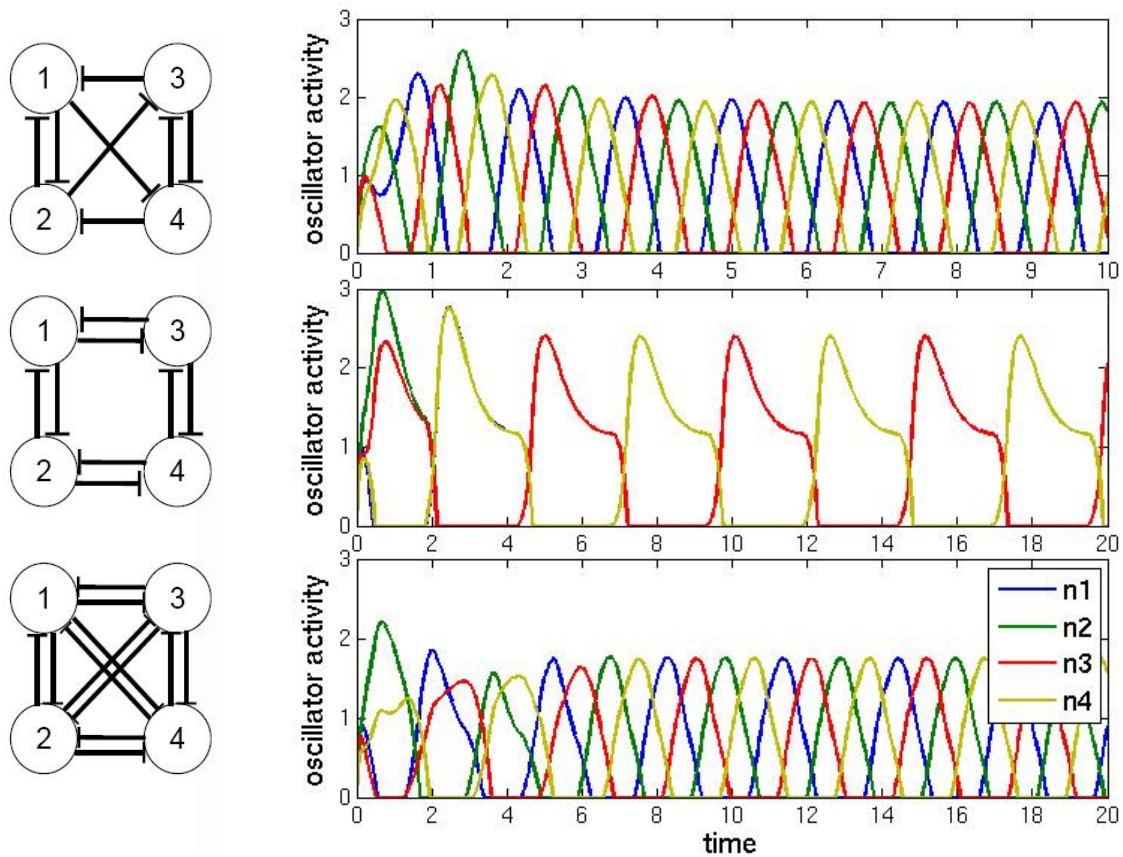
Figure 3.7: Three 4-neuron networks with different interconnections produce different activation patterns.

activation pattern according to [85, 107] are shown. If each joint requires an antagonistic oscillator (= pair of neurons), a symmetric network, there are three possible basic 4-neuron networks, which are shown in figure 3.7.

In the first example in figure 3.7 the interconnections are anti-clockwise with inhibitory synapses and crosswise between the two corners. This leads to a sequence of activation from neuron 1, 3, 2, 4. In the second example in figure 3.7 the interconnections are between the oscillator pair on each side and between the congenerous neurons on each side. The resulting activation is oscillation for the neurons on each side 1,2 and 3,4 with 3 identical to 2 and 4 to 1. In the third example in figure 3.7 the interconnections are as in the second example but also include additional crosswise interconnection as in the first line plot. This leads to a third activation pattern. It is a sequence of shorter activations as in the first network and with lower amplitude. The basic activation patterns described will be used in the oscillator networks for the stepping model presented in the next section.
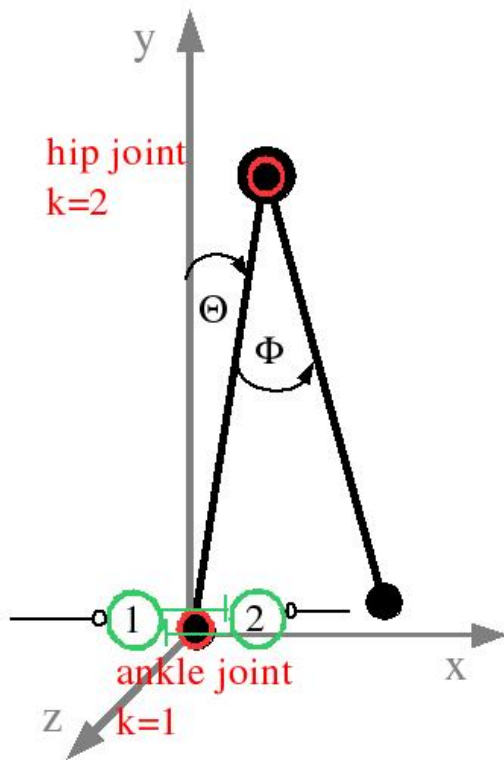
Figure 3.8: Interconnection of the oscillator with the mechanics. Actuation of the ankle joint of the stance leg.

3.3.4 Neuronal Oscillator Networks for Walking

First, one oscillator pattern for the sagittal-plane mechanics is shown. As this is a simple model of a double pendulum, only one network to actuate and stabilize this model is presented. Second, for the main subject of this research, the frontal-plane model, there are more variations of interconnections which are suitable, so 4 different networks are introduced.
An oscillating 2-neuron model is called an oscillator. All oscillator networks which are used in this work always consist of several 2-neuron networks. A joint is always antagonistically actuated which means that a joint is actuated by one 2-neuron oscillator which oscillates and reacts therefore antagonistically on the joint. The 2-neuron oscillators are interconnected to networks to interrelate the individual joint movements.

Networks for the Sagittal-Plane Model

The mechanics used for the passive walking on a slope shown in figure 2.3 are the structure used to interconnect with the oscillator network. As the sagittal plane is not the main topic of this thesis but is presented to round off the modeling of walking movements, only

one possibility for an actuation network for the mechanics is given. In the model seen in figure 3.8 only the ankle joint is actuated in this case by one oscillator. The swing leg is still unactuated so there is no oscillator for the hip joint movement. This is related to the fact that the swing leg reacts mainly ballistic during the swing phase [114].

This simple network relates also to the fact that the main metabolic cost is the step-to-step transition according to [28, 95]. The actuation of the ankle joint enables the system to compensate the energy lost during the step-to-step transition in the push-off phase and afterwards. All other movements result from gravitational forces. This is moreover one of the simplest actuations possible. Nevertheless it shows a strong influence on the movement without eliminating the ballistic principle completely. The results show that movement variability and an increase in robustness are achieved by this actuation. Another possible actuation would have been actuation of the hip joint, which relates to the hip strategy to balance forward walking according to [193]. Another possibility would have been the actuation with a 4-neuron network type of any kind which activates ankle and hip in combination. The results presented in section 3.7 are all generated with the ankle network shown in figure 3.8.

As the networks are used for all models in stance and walking or walking in place, the activation and the influence of the ankle neurons depend on the other oscillators but also on the ground reaction. If there is no ground reaction, there can be no force transmission to the ground and therefore the ankle oscillator does not have any influence on the system. This means that the activation for the neurons of the leg with no ground contact has no effect and they are therefore not shown in the figures. In the sagittal-plane model this always refers to neurons 5 and 6 and in the frontal-plane model these are always neurons 7 and 8 (see figure 3.9).

Networks for the Frontal-Plane Model

Four different configurations of a neuronal oscillator network are used with the frontal-plane model. The 4 networks are visualized in figures 3.10 to 3.13 and are denoted by (a); in addition the simulated neuronal activation patterns for the stand-alone case of neuronal activity are visualized in the subfigures denoted by (b). Stand-alone means without any coupling or interaction with the mechanics although the location of the neurons is shown in relation to the later position for coupling with the mechanics. The basis for these different neuronal networks is always the constellation of joints and oscillators shown in figure 3.9. In this figure the relation of neuron to joint is visualized. For each joint two neurons are applied as an oscillator, which operates in an antagonistic way like the extensors and flexors of the muscular system. All joints are hinge joints, which means that one flexor extensor pair is sufficient to realize the full spectrum of joint movement. The different neuron constellations and their activation patterns are denoted **P1** ... **P4**.

Figure 3.10(a) shows the first neuronal network **P1** with respect to the related mechanics. Here the hip is interconnected like the second 4-neuron network outlined in section 3.3.3, which is shown in figure 3.7. The ankles are connected to the hip with the same type
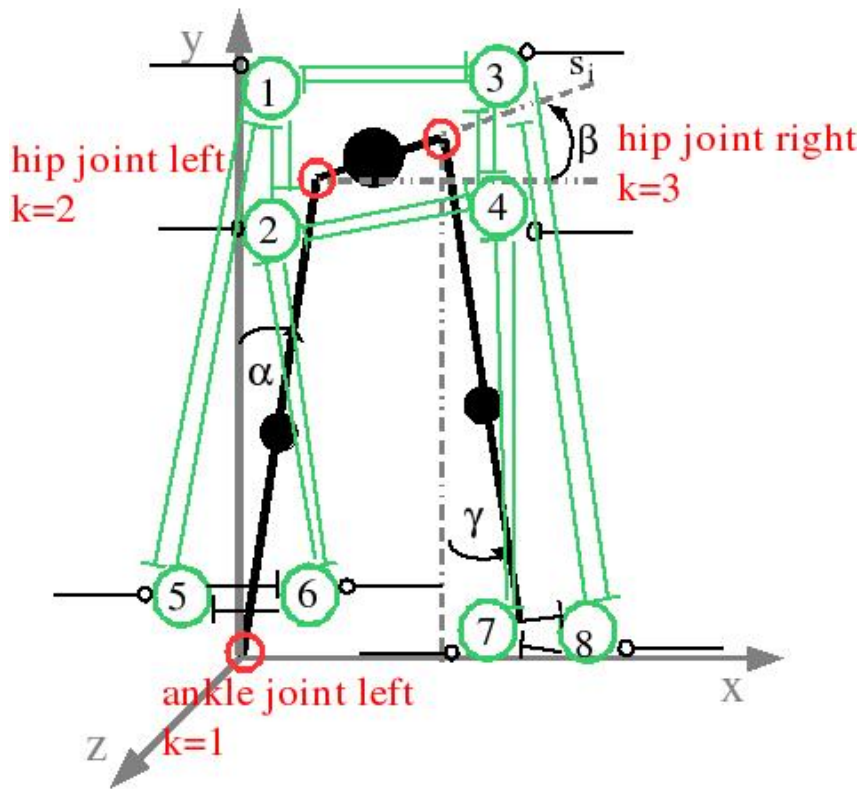
Figure 3.9: Frontal-plane mechanics linked with the actuating neurons at each joint.

of network, which leads to a synchronization of activation of the hip and ankle. The activation is in antagonistic rhythm. At any given time one neuron of an oscillator is active and the other is inactive and all the neurons are synchronized. This is shown for the neuronal activation pattern of neuronal network **P1** in figure 3.10(b). When neuron $n1$ is active, neurons $n2$ and $n3$ are inhibited and therefore not active, but neuron $n4$ is active at the same time. The ankle joint neurons are coupled, which means that neuron $n6$ is active when neuron $n4$ is activated. The activation is synchronous for hip and ankle neurons, except that the ankle is activated slightly earlier but continues till the activated hip neurons become inactive again.

The second oscillator network **P2** is also structured in line with the second example network type outlined in section 3.3.3, which is shown in figure 3.7. The hip and the ankles are connected as in the first network type but with the hip connection changed crosswise. This can be seen in figure 3.11(a). The resulting activation pattern is the same and is synchronized for the whole network in active and inactive neurons, but there is a change in the neurons which are activated at the same time. The hip activation is still pairwise, but now active with neurons $n1$ and $n3$ at the same time and ankle neuron $n5$ activated just before the hip reacts. This is the same characteristic as in pattern **P1**. This means for later movements an earlier, longer but lower ankle activation. This can be seen in figure 3.11(b).
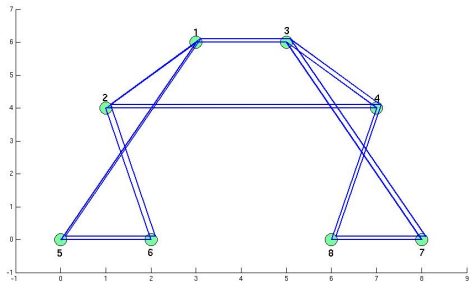
(a) Neuronal network pattern 1 **P1**
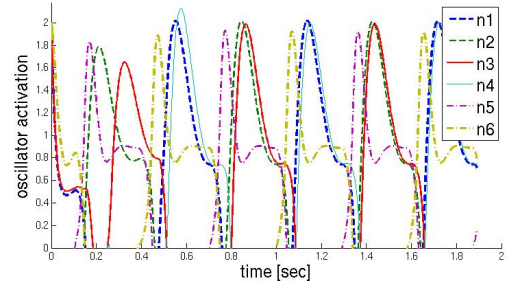
(b) Neuronal network **P1** activity pattern.

Figure 3.10: Neuronal oscillator pattern **P1**
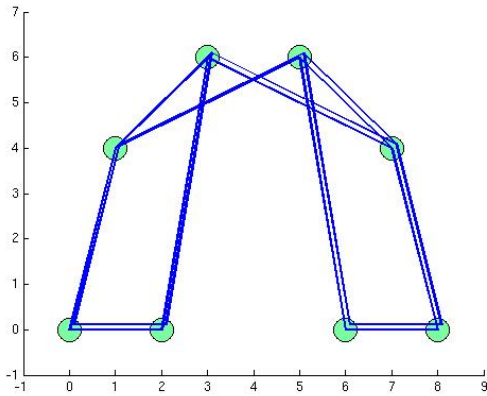
(a) Neuronal network pattern 2 **P2**.
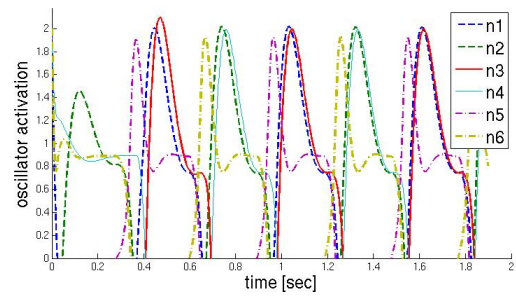
(b) Neuronal network **P2** activity pattern.

Figure 3.11: Neuronal oscillator pattern **P2**

(a) Neuronal network pattern 3 **P3**.

(b) Neuronal network **P3** activity pattern.
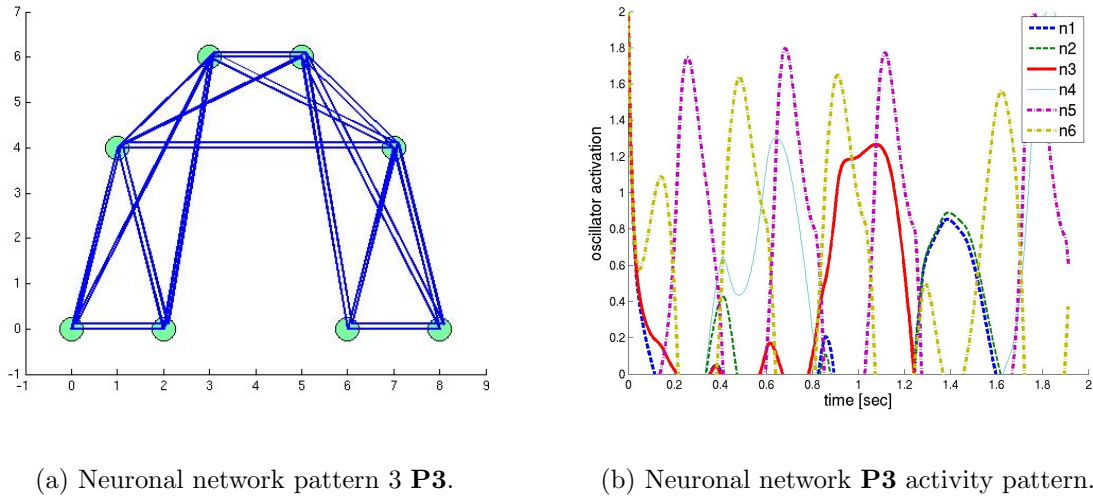
Figure 3.12: Neuronal oscillator pattern **P3**

The third network type **P3** is derived from the third example network type outlined in section 3.3.3, which is shown in figure 3.7. The 4-neuron networks are additionally crosswise interconnected which can be seen in figure 3.12(a). The resulting oscillator activation pattern is a hip activation, which is of double time duration as the ankle activation. This signifies that neurons $n1$ and $n2$ are active during both active phase plus inactive phase of the ankle neurons $n5$ and $n6$, which are mutually activated respectively. This is seen in figure 3.12(b).

(a) Neuronal network pattern 4 **P4**.

(b) Neuronal network **P4** activity pattern.
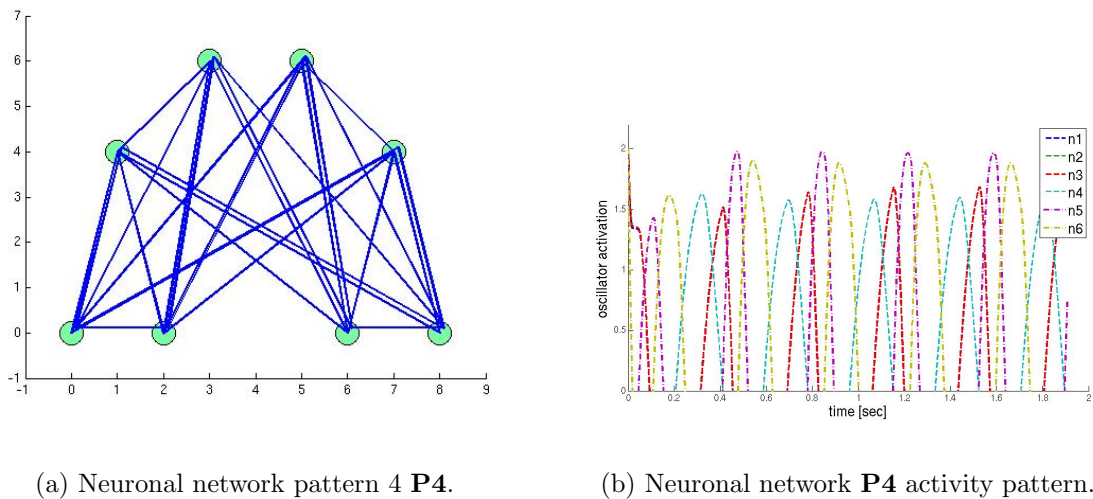
Figure 3.13: Neuronal oscillator pattern **P4**

The fourth and last network type **P4** for the frontal walking mechanics is derived from the first basic 4-neuron network type outlined in section 3.3.3 in figure 3.7. Here the

idea is that each side of the hip is interconnected with both ankle sides, so that the hip interconnection is directly influenced by the ankle connection. Figure 3.13(a) shows all connections. The resulting activation pattern is a crosswise active hip where both sides are synchronized but the ankle activation is phase shifted as shown in figure 3.13(b).

3.4 Activation of Mechanics with Oscillators

In this section the coupling of the passive dynamics of the mechanical model with the oscillator network is proposed. The following subsection 3.4.1 and 3.4.2 introduce (I) the generation of torques applied to the mechanics and (II) feedback from the mechanics to the oscillator. (I) force generation is a simple weighted additive mechanism which adds up the combination of activations. The (II) feedback is a combination signal of joint position and velocity. With (I) and (II), the mechanics and the oscillator network, a complete system is presented which performs rhythmic movements. In figure 3.14 an overview of the system with the interconnections between mechanics and neural oscillators is shown.
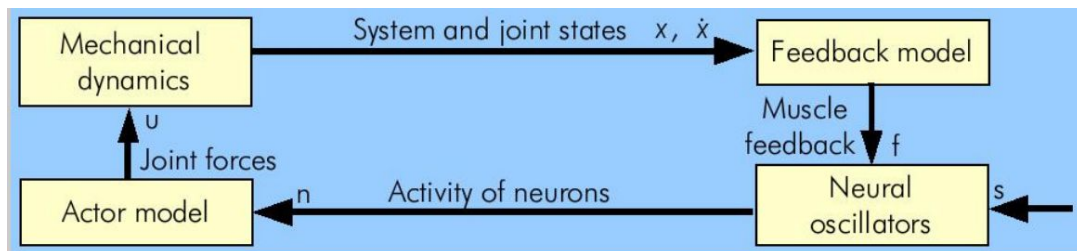
Figure 3.14: System overview of the actuation of the passive mechanics by neuronal oscillators with proprioceptive feedback.

3.4.1 Joint Torque Generation

The activity generated by the oscillator network is transformed to a torque which is applied to the mechanics. In formula 2.3 the torque applied directly to the joints in addition to the gravitational forces is the $u_{corrective}$. In section 3.3 the antagonistic structure of the muscular system was described. Put simply, muscular innervation includes motoneurons which contract the corresponding muscle fibers if they are activated. The muscle cannot do the contrary movement, the stretching. This stretching has to be performed by its antagonist, which in its turn is contracted by motoneuron activation. The contraction strength depends on the motoneuron activation level and therefore on the quantity of muscle fibers which are activated. The activation of the oscillator neurons is proportional. The activation of the oscillator network induces the motoneuron activation and this generates the muscle contraction which in turn applies a torque to the attached joint. The different activation patterns P_i lead to a different muscle contraction and therefore to a different torque being applied to the joints. If there are 4 oscillator pairs as in figure

3.9 the force generation for the four joints $u_{corrective} = u_k$, where $k = 1 \ldots 4$ number of joints, is:

$$u_k = \sum_{j=1}^{8} w_{jk} * n_j \qquad (3.4)$$

where w is the weight with which the oscillator neuron n_j influences the corresponding joint k.

In the case of the sagittal model the torque generation is identical. Only the number of generated joint torques and neurons is less with $k = 1, 2$. The joint torque of the ankle is generated with two neurons as seen in figure 3.8. This is the torque u_1 for the stance ankle, which is generated by the weighted sum of the two neurons $n1$ and $n2$ at the ankle joint. The torque applied to the ankle is: $u_1 = w_{11} * n_1 + w_{21} * n_2$. The hip joint is not actuated. Therefore the applied joint torque $u_2 = 0$.

Now the joint torques are determined in the same way for the frontal-plane model. A torque is applied to each joint k. This torque is computed according to equation 3.4. The computed torques depend directly on the neuron activation level n_j and the weighting. In the presented model it is always the directly connected neurons which combine their activation levels to generate one joint torque. Like a pair of flexor and extensor muscles, the torque applied to a joint is generated by the combined sum of applied torques. For example for joint $k = 1$ for the frontal-plane model, these are the neurons n_1 and n_2 as can be seen in figure 3.9. Therefore most of the weights are zero as there is no interconnection between e.g., the foot neurons and the hip actuation. The weight values which are not zero and therefore active are $w_{12}, w_{22}, w_{33}, w_{43}, w_{51}, w_{61}$. The joint $k = 4$ is not actuated as this is the joint which has no ground contact but is the swing leg ankle. The torque $u_4 = 0$. The other torques $u_1 \ldots u_3$ are as follows:

$$u_1 = w_{51} * n_5 + w_{61} * n_6$$
$$u_2 = w_{12} * n_1 + w_{22} * n_2$$
$$u_3 = w_{33} * n_3 + w_{43} * n_4$$

Table 3.2: The corrective torques applied to the three joints.

There are different strategies in human beings determining which muscle groups are activated during stance and walking. The joint torques can therefore vary in the weighting which depends on the strategy used. If the hip is actuated more than the ankle, the weights for the hip joints are larger than the weights for the ankle joints. In section 3.8.2 the variation of the weights according to different strategies is investigated in more detail and the resulting movement patterns are shown.

3.4.2 Muscle Feedback Applied to the Oscillator

Feedback is the information which is transmitted from the mechanical system to the oscillators. It is dependent on how the oscillator network reacts to changes of the me-

chanics. The feedback is combined with joint actuation which leads to a feedback signal corresponding to the individual joint movements. In section 3.3 the oscillator activation represents the neuron activation which directly induces muscle contraction in line with an antagonistic flexor and extensor pair.

According to [178, 159] muscular feedback is represented by two different feedback loops. First, the muscle length and velocity feedback of the muscle spindle afferents, which is a proprioceptive feedback. This feedback directly influences the motoneurons. The second feedback is the force feedback from the tendon organs and influences the interneurons. These two mechanisms are beside other reflexes the main mechanisms for muscular feedback and stabilization [9]. These proprioceptive feedback loops allow a stable posture control if the frequencies are not too high [178]. The advantage is that this kind of proprioceptive feedback does not cost extra energy, unlike other mechanisms such as co-contraction of muscles in order to increase the intrinsic muscle visco-elasticity [178].

The present model represents the proprioceptive muscle spindle length feedback which corresponds directly to the angular joint position. The spindle velocity feedback is also used and this is proportional to the angular joint velocity. The force feedback is omitted in order to simplify the model; it is not needed because it improves the impedance characteristic of the muscle system [178], which is not a critical factor for the proposed model.

In the model presented a simple structure is used based on the following principle: If a muscle is contracted its antagonist is stretched. This stretching or extension is sensed by proprioceptive sensors which are represented as inhibitory synapses of the neurons in the neuron oscillator itself. Proprioceptive information, given by the muscles and the joints, can be used for external sensory information to adapt the oscillator network to achieve a stable oscillating movement. This sensory information is the feedback signal given to the oscillators as external excitatory input s_i introduced in equation 3.1. As this feedback depends on proprioceptive information, the feedback signal is chosen to be a combination of joint position and angular velocity of the joints as proposed in [52, 172]. The feedback signal s_i for each oscillator neuron $i = 1 \ldots 8$, as is shown in figure 3.9, is a weighted sum of the angular positions and velocities. The following equations are the feedback signal for a pair of antagonistic oscillator neurons i and $i + 1$:

$$
\begin{aligned}
s_i &= \pm f_d * x \pm f_{dv} * \dot{x} \\
s_{i+1} &= \mp f_d * x \mp f_{dv} * \dot{x}
\end{aligned}
\tag{3.5}
$$

where f_d and fdv are the weighting gains of the angular joint position and angular joint velocity. The *angle* is one of the three angles of the mechanical system α, β, γ according to the influence of the oscillator neurons on the muscles and the joint. See figure 3.9 for the numbers of oscillators related to each joint and angle for the frontal-plane model. So neurons $n1$ and $n2$ are influenced by the difference between angles α and β, neurons $n3$ and $n4$ are influenced by the difference between angles β and γ, neurons $n5$ and $n6$ by angle α and neurons $n7$ and $n8$ by angle γ, but only if the relevant leg has contact with the ground.

For the sagittal-plane model neurons $n1$ and $n2$ are influenced by angle Θ as shown in

figure 3.8.

The feedback completes the loop of activated mechanics according to figure 3.14. According to the transition chart of figure 2.6 in section 2.3.2 the whole process for one stepping phase is as follows: the mechanical dynamics react to the gravitational forces plus the joint torques added additionally. These joint torques are produced by the oscillator network, which represents the activation level of the muscles. The activation of the oscillator network is influenced by the proprioceptive muscle feedback, which represents the muscle length and contraction velocity. A stepping phase is terminated if ground contact occurs. In the model proposed here this ground contact is modeled as an instantaneous event. So the next stepping phase is the next swing phase of the other leg. In the following section 3.5 these stepping movements are commented in more detail with especial reference to the stability of such stepping movements.

3.5 Stability

Stability is a very important characteristic of walking and stepping in general. As mentioned in section 2.4 the walking stability was and is crucial for human survival. Besides other important characteristics of walking this is the most important characteristic. In the following, the term stability is detailed further in a mathematical way and applied to stepping movements. Further a numerical proof of stability is shown which is applied to walking movements in this work.

3.5.1 Poincaré Sections

The differential equations for mechanics and oscillators are nonlinear. So the walking system is a nonlinear dynamic system in continuous time. With each step ground contact occurs which makes the system discontinuous. So the stability and therefore the attractor properties of this hybrid system can not be determined by eigenvalues of a simple Jacobian matrix as for continuous nonlinear differential equations. Walking is a periodic movement with subsequent continuous periods which are the swing phases. This movement has to be presented as a periodic solution. A periodic solution is searched which is stable. This means that all movement trajectories stay in the neighborhood of one cyclic movement trajectory, the periodic orbit, if they started in the close neighborhood of the periodic orbit. It is an attracting orbit if all solutions converge to this orbit for time $\rightarrow \infty$. The periodic solution is asymptotically stable if it is stable and an attracting orbit. This is also called a limit cycle. To determine the stability of such a periodic orbit the Poincaré map can be applied [91, 5].

The Poincaré Map considers an autonomous or non-autonomous system of the form:

$$\dot{x} = f(x) \quad or \quad \dot{x} = f(x,t) \quad with \quad x(t_0) = x_0 \tag{3.6}$$

The Poincaré Map P is defined by:

$$x_{k+1} = P(x_k) \tag{3.7}$$

where P is the mapping from solution x_k of the system onto solution x_{k+1} where k and $k+1$ denote the time. If a time-periodic system is divided into n sections of period T the system can be written as:

$$x(T) = f(x, T) \quad with \quad x(t = t_0 + n * T) = x_{k+n}$$

where the duration of one section is the time T between two points in time k and $k+1$. These sections of the orbit of the motion from time k to $k+1$ can be described by the Poincaré sections. For a periodic solution which starts at x_k at time k and returns to the same state in space x_{k+1} at time $k+1$ this is a fixed point of the the Poincaré Map P with $x_k = x_{k+1}$. This implies that the stepping system returns after a certain time to a solution where it can be mapped to an earlier solution. A Poincaré section is a plane because it has one dimension less than the original phase space and intersects with the orbits. For stepping this means that e.g. at double support phase which is one instant in time, the system state of the last double support phase or the before last can be mapped to the actual. The system is discretely divided into continuous-time parts, the single steps.

For a periodic orbit the Poincaré sections intersect with the orbit in the fixed point x^* for each period. In general the intersection points can be mapped by the Poincaré map onto each other. The Poincaré map turns a continuous dynamical system into a discrete one. Therefore the Poincaré map reduces the search for a stable periodic solution to the linearization of the Poincaré map around the fixed point x^* with $x^* = P(x^*)$. An equilibrium point x^* is Lyapunov stable in case that:

$$\|x(t_0) - x^*\| < \delta \implies \|x(t) - x^*\| < \epsilon \quad \forall \quad t \quad \geq t_0 \tag{3.8}$$

The equilibrium point x^* is said to be locally asymptotically stable if x^* is stable and, furthermore is locally attractive and there exists a $\delta(t_0)$ which means that all solutions starting near x^* tend towards x^* as $t \to \infty$. Mathematically speaking there exists $\delta(t_0, \epsilon) > 0$ so that:

$$\|x(t_0) - x^*\| < \delta \implies \lim_{t \to \infty} x(t) = x^* \tag{3.9}$$

This can be transfered to the Poincare map according to [91] equation 3.8 and 3.9 are:

$$\|x_0 - x^*\| < \delta \implies \|P^{\circ n}(x_0) - x^*\| < \epsilon \quad \forall \quad n \geq 0 \tag{3.10}$$

and

$$\|x_0 - x^*\| < \delta \implies \lim_{n \to \infty} P^{\circ n}(x_0) = x^* \tag{3.11}$$

where $^{\circ n}$ means the repeated application of P, i.e. $P^{\circ n}(x) = \underbrace{P \circ P \circ \ldots \circ P}_{n \quad times}(x)$.

The linearization of the Poincaré map in the stable solution and fixed point x^* is used to

prove the stability of the fixed point with equation:

$$P(x_0) - x^* \approx \frac{\partial P}{\partial x_0}(x^*)(x_0 - x^*) \tag{3.12}$$

If the eigenvalues λ_i of this linearized map are in the range for all i: $|\lambda_i| < 1$, the periodic solutions are stable. If there is at least one with $|\lambda_i| > 1$, then the periodic solution is unstable.

3.5.2 Stability Proof Applied to Periodic Walking

In the following the stability theory is applied to a stability proof for periodic walking movements. There are several ways of proving walking stability in literature [126, 18, 37, 48, 67]. They all handle walking as a periodic movement with periodic recurring phases which can be analyzed as continuous systems over time. To analyze the stability properties a discrete mapping method as a Poincaré map is applied. The presented stability proof is numeric and was used for all identified stable stepping movements presented in this work. As described cited by [48] from [69] *a gait is stable if starting from a steady closed phase trajectory, any finite disturbance leads to another nearby trajectory of similar shape.* This means that the phase plane of the movement attracts the trajectories in a certain area to one *stable* trajectory (orbit), which is called limit cycle of the system. To analyze the orbital stability of a limit walking cycle, the whole hybrid system is mapped by determining the Poincaré map and analyzing whether the fixed point is stable or not. If the fixed point x^* is stable then the complete step cycle is also taken to be stable. The procedure for a periodic gait is as follows: The map of the hybrid cycle is one step which starts with the initial condition for take off of the swing leg right after the double support phase and ends again with the new initial values right after the double support phase. For this also see figure 2.6. So the system divided into steps can be written according to equation 3.7 as $x(step_{k+1}) = P(x(step_k))$ where x is the state vector of the system, $x = [\alpha, \quad \beta, \quad \gamma, \quad \dot{\alpha}, \quad \dot{\beta}, \quad \dot{\gamma}]^T$. If the trajectory is periodic it is valid to say $x_k = x_{k+1}$. So it follows according to equation 3.7 $x^* = P(x^*)$. To state that the fixed point is really stable the following derivation is made according to [48]. The nonlinear Poincaré mapping function P is linearized by writing it as Taylor series which is:

$$P(x^* + \delta x) \approx P(x^*) + \frac{\partial P}{\partial x} * \delta x \tag{3.13}$$

where $\frac{\partial P}{\partial x}$ is the gradient of P according to the states and δx is a small perturbation δx_i applied to each state of the cyclic solution of x^*. The gradient of P can be calculated by:

$$\frac{\partial P}{\partial x} = \Lambda * \Gamma^{-1} \tag{3.14}$$

with

$$\Gamma = \begin{bmatrix} \delta x_1 & 0 & 0 & \dots & 0 \\ 0 & \delta x_2 & 0 & \dots & 0 \\ \vdots & \ddots & & \dots & \vdots \\ 0 & \dots & & \dots & \delta x_i \end{bmatrix} \quad \text{and} \quad \Lambda = \begin{bmatrix} (x_1^p - x^*) & (x_2^p - x^*) & \dots & (x_i^p - x^*) \end{bmatrix}$$

where i is the number of system states and $x_i^p = P(x^* + \delta x_i)$ are the solutions for each disturbed state i. The distance between the fixed point solution x^* and each perturbed state solution x_i^p at the end of a period is also called monodromy matrix [1].
Now the eigenvalues of matrix gradient $\frac{\partial P}{\partial x}$ are determined. If the eigenvalues are within the unit circle the configuration is stable.

This stability also means that if a step is perturbed in some way and this perturbation does not push the system out of the basin of attraction the system will be attracted to the stable solution. So in this step cycle and the following cycles the system will return to the same gait pattern or to a similar stable pattern.

3.5.3 Finding Configurations for Stable Periodic Movements

As the whole system has 22 states which depend on about 40 parameters it is no easy task to find a stable configuration. The last subsections 3.5.1 and 3.5.2 described how the term *stable* or *stability* is defined by mathematical means and what this means for stepping and walking. In general it can be said that a gait is stable if it is stable with respect to the corresponding fixed point of the Poincaré Map. This means that a solution of the system exists: $F(x_k) = x_{k+n}$, where k is the time where the system periodically returns to e.g. the ground contact of a step and n is the n-periodicity of the system. But a stepping system can also be non-falling if it is not stable as this could be a chaotic solution which is still an attractor. Such a solution is not stable in a mathematical sense but there are also no falls during stepping.

First, a short overview will be given of the whole procedure to find a configuration for the stepping system which appears to be stable and which then can be proven to be stable or not stable. The procedure is as follows: At the beginning a desired frequency or the approximate resonance frequency of the pendulum mechanical system is determined $\omega_0 = \sqrt{\frac{g}{l}}$ where g is the gravity and l is the length of the pendulum. In the mechanical system this resonance frequency is taken for the eigenfrequency of the swing leg.

The frequency of the isolated oscillator system is directly determined by the time parameters and the coupling of the oscillators. This system can be adapted to the required frequency characteristics before it is combined with the mechanical system.

Next, the complete system is observed for changing parameters, and the parameters are

---

[1] Additionally also the Fundamental matrix of a system can be determined as linearization of the system around the periodic orbit which is $\dot{\Phi} = Df(\bar{x}) * \Phi$ where Φ is the periodic solution of the system $f(x, t)$.

generally adapted to ensure a desired or correct performance of the system. This observation is performed experimentally in order to establish the full range of obviously possible solutions. The performance of the system is observed according to the following criteria. Is the activation series for the neurons in the intended order? Do the levels of activation exist for all neurons, in other words are the activation levels all positive? And are the activation levels of the same dimension, in other words the activation level of one oscillator is not a 100 times higher than that of the neighboring oscillator. This leads to all oscillators having a comparable influence on the actuation of the mechanics. Last but not least the signs are checked to ensure that the first determination of the body angles takes the right direction and the right order.

Two methods have been applied to find an initial fixed point: (1) the Newton-Raphson method and (2) the secant method. The Newton-Raphson method only works if the initial guess is close enough to the later fixed point, otherwise the method does not converge. The result of these methods is an initial state vector x_0, the fixed point, which gives a good approximation of a stable solution for a periodic gait. This means that $F(x_0) \approx x_0$.

Then the system is then processed with x_0 as the initial guess and refined to a stable solution by iterative approximation to the limit cycle solution of the system. The method to check for stability presented in section 3.5.2 is used by other studies of gait in the sagittal plane such as [48, 49, 38] which corresponds to the local stability of limit cycles.

In section 3.8 below, the simulated stepping movements with the proposed actuated models are presented. If a movement is denoted stable this always refers to the stability proof introduced here. Amongst other things the subsequent simulation results regard the influence of parameter variations or external perturbations on the stability of periodic stepping movements.

3.6 Simulation of Stepping Movements and Visualization

The simulations are all implemented in MATLAB. For the following results, all the integrations are done by the MATLAB solver ode45 with the setting: variable step size, absolute tolerance $'AbsTol' = 1e - 5$ and the relative tolerance $'RelTol' = 1e - 7$, the other integration values are set to default MATLAB values.

The plots presented to visualize the results are of the same type for all sections below. Here the individual plot types are briefly commented to give a better overview. Important parameters of the system are the positions of the hinges, which are represented by Φ and θ for the sagittal model and with the three angles $\alpha, \beta \quad and \quad \gamma$ for the frontal model. These positions are equal to the angles shown in figures 2.3 and 2.4. The phase plot is a visualization of these positions against the related angular velocities $\dot{\Phi}, \dot{\theta}$ for the sagittal model and against $\dot{\alpha}, \dot{\beta} \quad and \quad \dot{\gamma}$ for the frontal model. This plot is a common form of visualizing the stability of limit cycles. If a system is stable, the shown cycle takes the form of one line and not multiple lines. The attraction of a solution to the limit cycle can be seen as convergence with this limit cycle trajectory. In addition the velocity

discontinuities can be seen as discrete velocity changes when ground contact occurs.

A further plot is the plot against time of the activation levels of the oscillator network. As the swing leg has no ground contact, the swing leg ankle is not active and this activation level is omitted in the plot. For the sagittal model there is only the two neurons at the ankle of the stance leg which are shown. And for the frontal model only the six neurons, two for the stance ankle, two for the stance hip hinge and two for the swing leg hip hinge are shown. Finally, the movement plot draws a stick figure for different time steps in the same plot to visualize the movement. Here the discretization of the stick figure movement is performed with a much lower sampling rate than the original integration time steps used by the MATLAB ode solvers. This is because single lines have to be seen to imagine the movements, so this plot has no definite time baseline but shows a motion sequence.The whole system consists of the four components: mechanics, oscillator network, torque generation and feedback from the mechanics to the oscillators. In the following some movement results for this system will be shown. The movement of the mechanical system, angles and or angular velocities, the oscillation pattern of the neuron network activation and the reaction of the system to parameter changes such as frequency and disturbances applied to the mechanical system like foot sliding. In the following all simulation results presented are calculated for the sagittal and frontal mechanics, each with a constant setting for mechanical parameters and most of the oscillator parameters. Any variation in the parameters is always indicated separately for each result.

3.7 Simulated Stepping Movements in the Sagittal Plane

In literature there are several examples of actuated walking models in the sagittal plane as mentioned at the beginning of chapter 3. Models with an actuated hip joint are e.g. as proposed in [127, 158, 157]. Biped walking models with actuated ankles are proposed by e.g. [12, 93]. In robotics normally all joints are actuated e.g. as presented in [174, 11]. The stability of unactuated and actuated sagittal plane models was proven for many models. Stability analysis examples of passive models can be found amongst others in [111, 112, 113, 38, 18, 49, 48] and for actuated passive models in [67, 126, 174]. There are therefore various possible actuations with stable solutions and this opens up a wide range of actuation possibilities for the simple ballistic model of a walking pendulum presented here. One of those possibilities is shown with some parameter variations. The stability analysis is always carried out with the method and limit cycle solutions presented in section 3.5.

3.7.1 Walking Movements

Continuous ankle actuation of the passive walker in the sagittal plane leads to a walking movement on level ground without the gradient of a slope. The pattern of the movement is influenced by the activation pattern of the ankle oscillator. The ground contact and transition that occurs in the double support phase are factors that also influence the

system significantly. The direction of ground reaction forces influences the initial velocity values for the next step and therefore the gait pattern. The initial values determine whether a movement solution is attracted to a stable solution and where the fixed point of this solution is. Stability is also affected by the parameters of feedback values f_d and f_{dv} as well as the external inputs s_i or ext_i to the oscillator; these parameters have a principal influence on the walking pattern. In the following a general set of parameters is used for each simulation equivalently. The parameters and their values can be seen in table 3.3 and table 3.4.

parameter	value	unit
M	70	$[kg]$
m	0	$[kg]$
l	1	$[m]$
g	9.8	$[kg * m/sec^2]$

Table 3.3: Parameters of the mechanics.

Other parameters are varied and those variations influence the walking pattern. The parameters of table 3.3 are as used in equation 2.2.2 for the mechanics. The equation is normalized.

The constant parameters for the oscillator network are the same for all neurons. The names of the parameters correlate with equation 3.1 of the Matsuoka oscillator:

parameter	value
a_{12}, a_{21}	1.5
b	2.5
s	8
T_a	1 [sec]
T_b	2 [sec]
f_d	1.5
f_{dv}	-1.5

Table 3.4: Parameters of the neuronal oscillator.

A walking movement generated with the above values is a simple forward walking movement on level ground which is shown in figure 3.15. The subplots (a), (b), (c) and (d) show the angular positions and angular velocities of the two angles θ, ϕ, the neuron activation, the phase plot and the movement of the mechanics of figure 2.3. The result which can be seen is the superimposing of the neuron oscillations with the mechanical oscillations and therefore a new oscillation. Only the ground contact produces discontinuities in the velocities. The angles are symmetric. The trajectory is attracted to the cyclic solution after a few steps. This is seen in figure 3.15(c) where the single trajectories converge to a stable limit cycle after the initial transient time where the lines are separate and distinct. The discrete event of ground contact is visualized by a break in the lines, which would be a vertical connection line if represented by a solid line. In the plotted movement in figure 3.15(d) the 1-periodicity can be seen. Every step resembles the previous one.
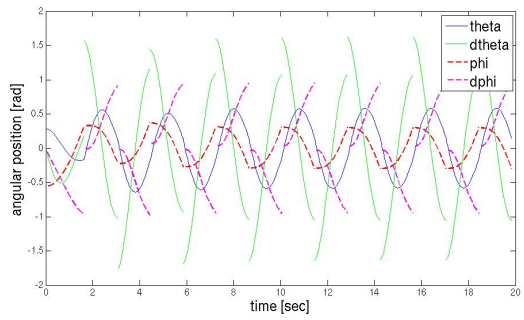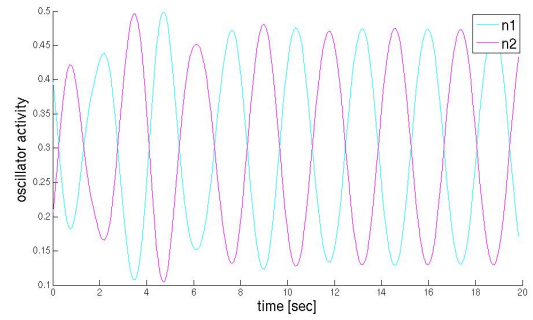
(a) Angular position

(b) Oscillator activation
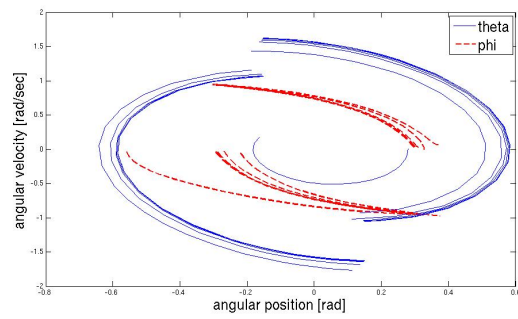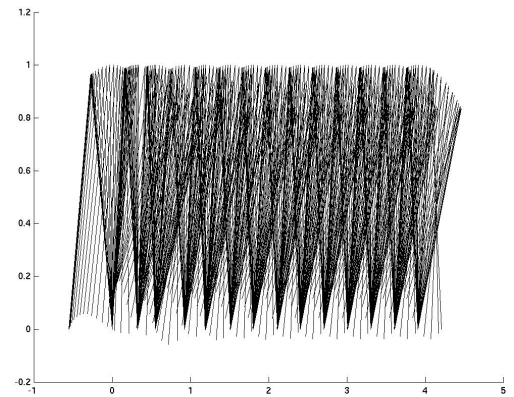
(c) Phase plot

(d) Movement

Figure 3.15: 1-periodic stable solution for walking movement in the sagittal plane on level ground.
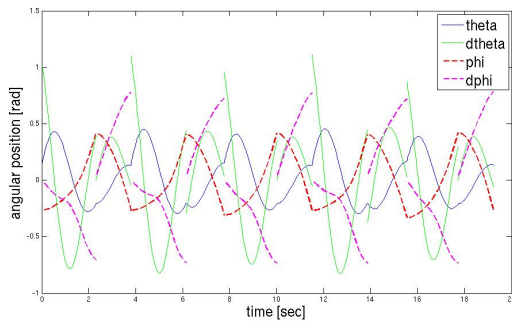
(a) Angular position
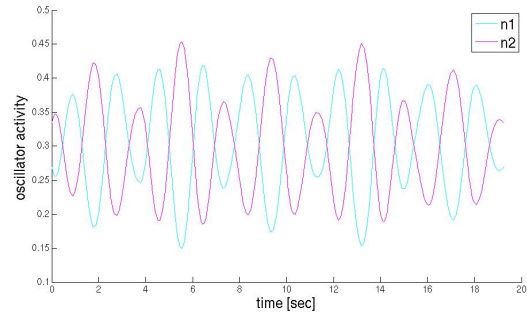
(b) Oscillator activation
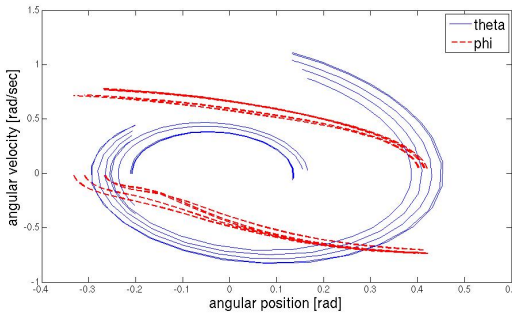
(c) Phase plot
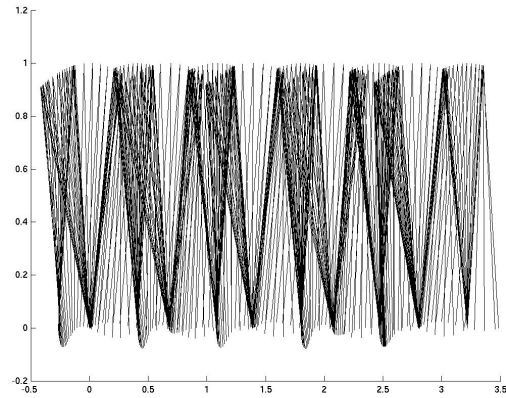
(d) Movement

Figure 3.16: 2-periodic walking movement with a modulated ground contact direction vector.

Another possible solution is a 2-periodic solution as shown in figure 3.16. Here the periodic patterns are repeated every second step. The discontinuous state transition can be seen in the velocities and the angles are no longer symmetric. This solution differs from the first solution with respect to the ground contact condition. The direction of the vector for the initial velocity of the stance leg is exactly inverted for every second step. This is like a clubfoot movement. With each step the stance leg starts in the other direction but due to the actuation it is forced into the same direction, which is like an initial tension of the ankle for each step.
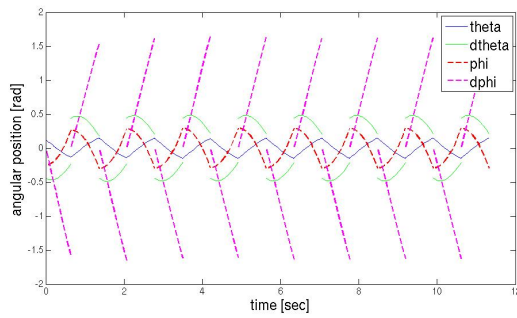
(a) Angular position
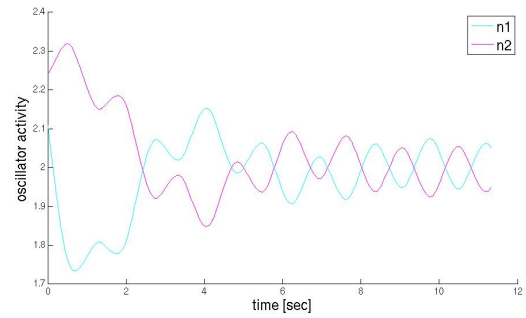
(b) Oscillator activation
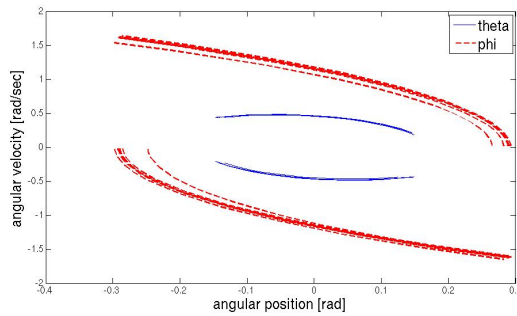
(c) Phase plot
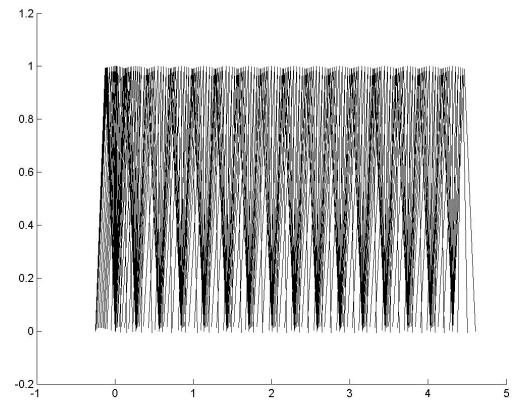
(d) Movement

Figure 3.17: Variation of neuron parameter $s = 10$ results in a higher step frequency. Stable 1-periodic walking movement with parameter $f_{dv} = 3.5, T_b = 1.5$.

3.7.2 Variation of Parameter s

Another possible stable 1-periodic walking solution is taken and the parameter variation examined. The variation of the external input s of the oscillator system represents a variation of external influences such as sensory input or other high-level commands. This variation influences the step frequency. In figures 3.17 and 3.18 two examples with s-values of 10 and 2 respectively are shown. Figure 3.19 visualizes the variation in step frequency resulting from variations in parameter s.
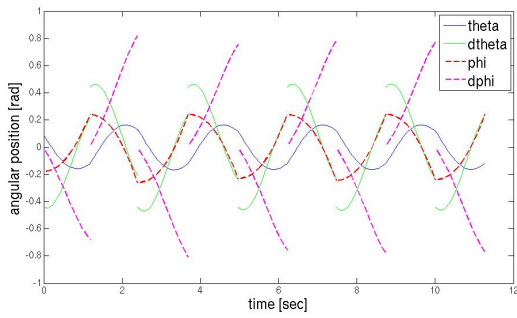
(a) Angular position
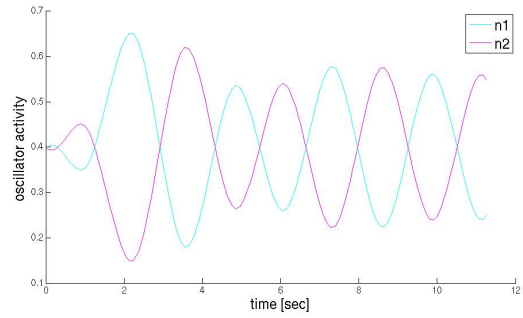
(b) Oscillator activation
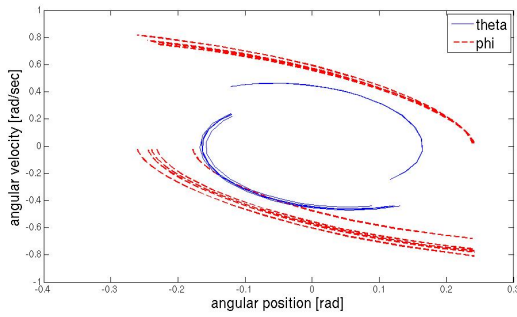
(c) Phase plot
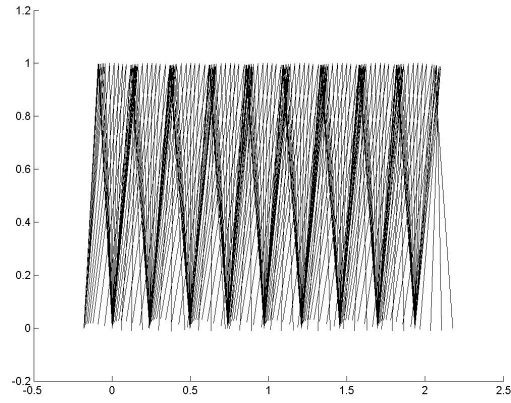
(d) Movement

Figure 3.18: Variation of neuron parameter $s = 2$ results in a lower step frequency. Stable 1-periodic walking movement with parameter $f_{dv} = 3.5, T_b = 1.5$.
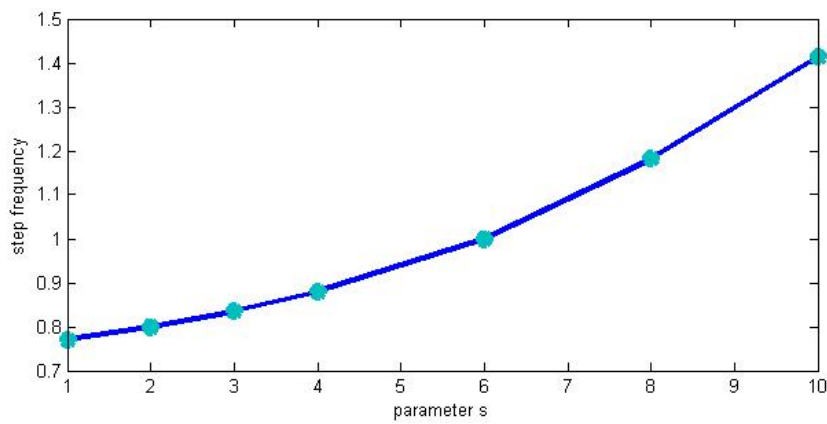
Figure 3.19: Dependency of step frequency on variations in parameter s from 1 to 10.

3.8 Simulated Stepping Movements in the Frontal Plane

In the following a selection of simulation results is presented to demonstrate the abilities and possibilities of the proposed actuated model for stepping movements in the frontal plane. The complete model used for simulation, consists of the mechanics presented in section 2.3 and is actuated by the oscillator networks P_i producing joint torques and using proprioceptive muscular feedback as explained in section 3.4.2 and 3.4.1. This is visualized in figure 3.14. With the instantaneous ground contact of section 2.3.2 this becomes a hybrid system with the states double support phase and single support phase (swing phase) which is shown in figure 2.6. The ground contact will be modeled with slight variations as the ground contact for e.g. stepping in place or stepping up has to be varied according to the ground level, ground reaction forces and direction of initial velocities according to the movement direction. So below in section 3.8.1 three different movement patterns are presented to show the variability in movement types of the model. Next, in section 3.8.2 the influence of the variation of single parameters is shown which imply the possibility of extending this model with external control and input. In section 3.8.5 there are applied external perturbations to the system. The effect of such perturbations on the movement and its stability are tested. In section 3.8.6 the movement pattern 'stepping in place' is compared to a real movement pattern recorded in an experimental setup with real subjects. This shows that it is possible to simulate movement patterns which are very similar to real stepping movements with the proposed model. Finally, in section 3.10 the possibilities and restrictions of the proposed model are discussed for further extensions of the model.

The proposed model has several parameters which are in the following once explained in the related equations. Here the values for the parametrization of the models are given which are used to simulate the following results. There are the mechanical parameters, body mass M, leg masses m, leg length l, hip width h and gravitational force g. The values of these parameters are for all simulations identical. For the used values see table 3.5 The constant parameters for the oscillator network are the same for all neurons. The

parameter	value	unit
M	49	$[kg]$
m	11	$[kg]$
l	0.5	$[m]$
h	0.1	$[m]$
g	9.8	$[kg * m/sec^2]$

Table 3.5: Parameters of the mechanics.

name of the parameters correlates with equation 3.1 of the Matsuoka oscillator. The parameter values are shown in table 3.6:

parameter	value
a	2.5
b	3.5
c	2
d	2
s	4

Table 3.6: Parameters of the neuronal oscillators.

3.8.1 Simulation of Different Movement Patterns

The proposed model is developed to generate rhythmic stepping movements in the frontal plane. The movements are of a general sort, as the parameter setting of the model was not especially adapted to experimental human data, because this model shall demonstrate general potentials of this relative simple musculoskeletal model. So the first result are the types of stepping movement patterns which can be achieved with this model. In the following four general types of patterns are presented:

- Stepping in place with dropping of hip

- Stepping in place with lifting of hip

- Stepping aside

- Stepping up as e.g. on a ladder

These are four stepping movements which can be done by every human being and which are general movements in the frontal plane. The stepping in place can be done in two different ways, the more natural way is by dropping the hip but it is also possible to lift the hip at the beginning of step and then let it drop again to get ground contact. In figure 3.20 the position, activation and phase plot can be seen for case (1) stepping in place with dropping hip. Here the hip drops so the leg dips into the ground and comes up again till it is level with the ground surface which is detected as the ground contact. As can be seen in the phase plot the stepping movement is a 1-periodic limit cycle movement. So all trajectories are identical and the gait is symmetric and stable.

Another example can be seen in figure 3.21 where the phase plot is not a limit cycle but the movement looks stable for 8 steps. In this case no periodic solution is found and no symmetric one either. This stepping movements can be a n-periodic gait.Or it is an instable configuration that is close to a stable solution but after several more steps the system would collapse or it is really a chaotic attractive solution. If the system is unstable but can though do 8 steps, which is according to the whole body mechanics still a stable physical stepping solution, this kind of instability can be handled by a high-level control that will be proposed in chapter 5.

A third shown possible stepping in place movement pattern is seen in figure 3.22. This is a 'drifting' movement which is surely unstable. This drifting can be seen as the phase plot slowly drifts in one direction. In the position plot a slow increase or decrease of the angles
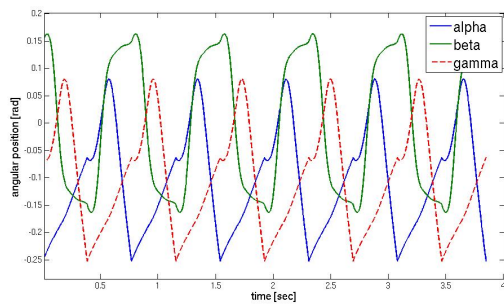
(a) Angular positions
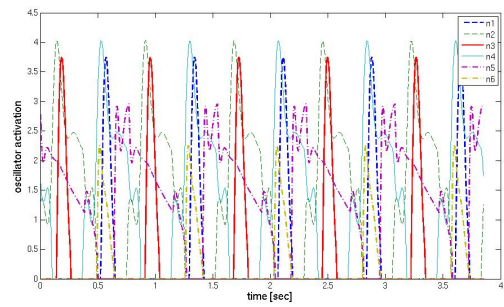
(b) Oscillator network activations
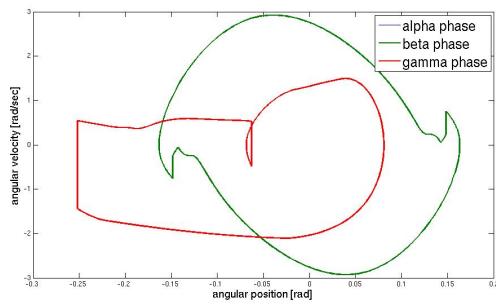
(c) Phase plot
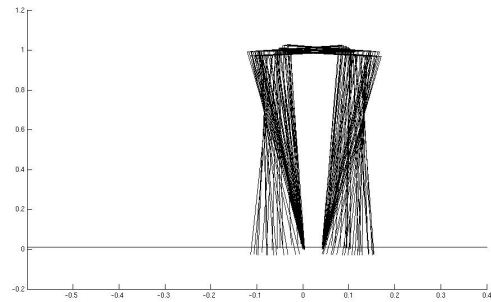
(d) Movement

Figure 3.20: Simulation of stable movement stepping in place with dropping hip: simulated with the parameters $T_a, T_b = 0.05$, $f_d = 0.5$, $f_{dv} = 1$, initial state vector $init_1$ and ankle and hip strategy $F12$.
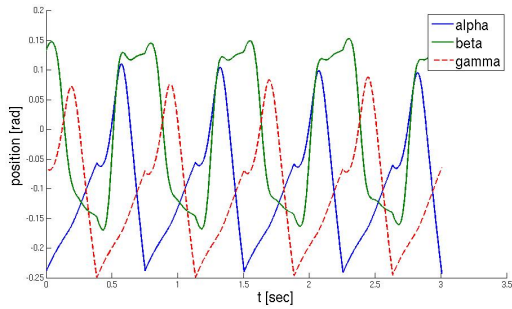
(a) Angular positions
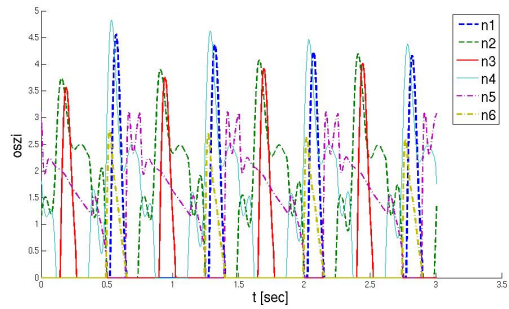
(b) Oscillator network activations
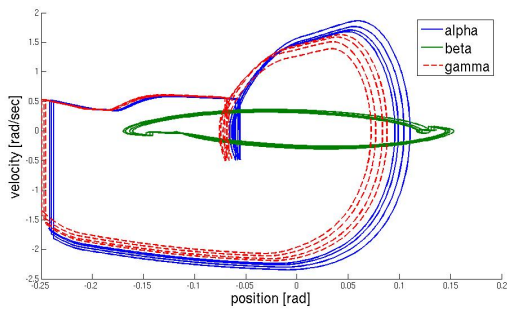
(c) Phase plot
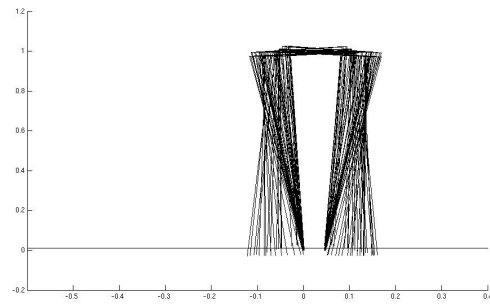
(d) Movement

Figure 3.21: Solution of another stepping in place movement with dropping hip. The solution is not proven to be stable but there is no obvious fall risk either: simulated with the parameters $T_a, T_b = 0.05$, $f_d = 0.5$, $f_{dv} = 1.2$, initial state vector $init_1$ and ankle and hip strategy $F12$.
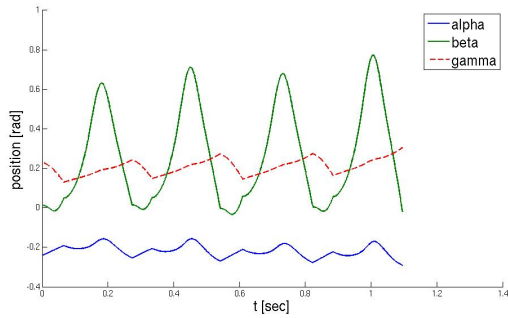
(a) Angular positions
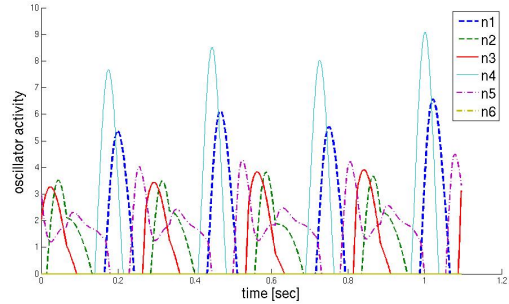
(b) Oscillator network activations
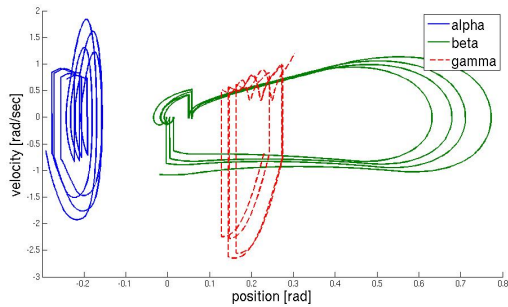
(c) Phase plot
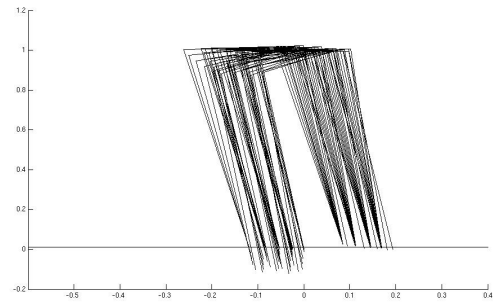
(d) Movement

Figure 3.22: Stepping in place with dropping hip with a drift movement in one direction as the step movement is unsymmetrical between right and left leg. This is like limping: simulated with the parameters $T_a, T_b = 0.05$, $f_d = 0.4$, $f_{dv} = 1.1$, initial state vector $init_1$ and ankle and hip strategy $F10$.

denotes this drift. With this constellation, several steps can be generated, which are still a stable whole body constellation but after several steps the system becomes instable. The resulting movement looks like an asymmetric limping. As mentioned above this drift instability can be prevented with a high-level control that senses the whole body position and movement. In the low-level musculoskeletal model the position of the whole body is not included.

The three examples above of stepping in place movements are generated with the same oscillator network but with different feedback or extern oscillator input ext. The strategy for hip or ankle activation was for all three cases a uniform hip and ankle strategy.

The next example of movement is stepping in place with lifting hip. Stepping in place with lifting the hip starts not with the usual drop of the hip but in contrary a lifting up of the hip against gravitation. This change in movement needs another initial value for the mechanics. The starting hip velocities have to be the contrary direction to lift the hip
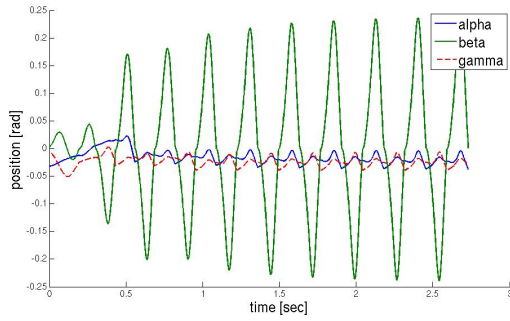
(a) Angular positions
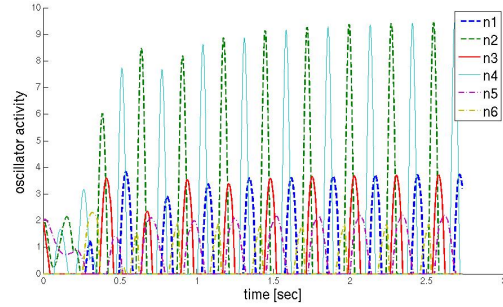
(b) Oscillator network activations
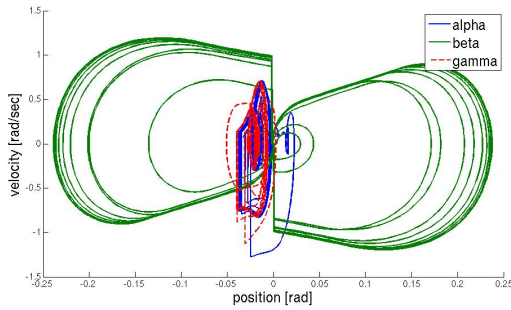
(c) Phase plot
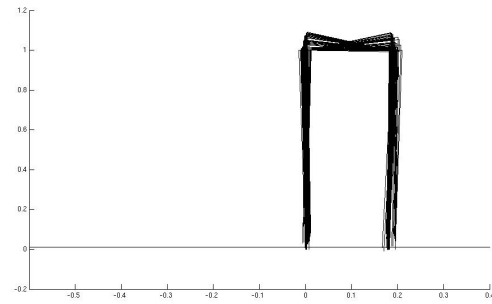
(d) Movement

Figure 3.23: Stable symmetric stepping in place movement with lifting hip: simulated with the parameters $T_a, T_b = 0.1$, $f_d = 1.2$, $f_{dv} = 1.69$, initial state vector $init_1$ and hip extensor strategy $F14$.

and not to drop it which happens according to gravitational forces. As this movement is not so natural, therefore the activation level of the hip joints have to be much higher than in the stepping in place with dropping hip. This higher activation level, which can be clearly seen in figure 3.23, is about 2.5 times magnified related to figure 3.20. The higher hip level enables the system to react against the gravitational forces and lift the hip. Therefore, the energy level at the beginning of a step has to be higher than it is for dropping hip. The amplitude of the hip movement is higher and the amplitude of the leg movement is very low. As can be seen in phase plot 3.23, (c) the presented solution is also a stable solution where all periodic trajectories are attracted to the limit cycle. The gait is symmetric, so, the limit cycle for α and γ are congruent. Another characteristic of this hip lift up stepping in place is that the hip velocity is highly discontinuous in the ground contact. This means if the leg touches ground with a velocity $\vec{v}$, the leg leaves ground with a velocity in the other direction $-\vec{v}$. This can be best seen in the phase plot 3.23 (c) where the green phase space line is highly discontinuous for the hip.

The third stepping mode is stepping to the side. This intention to step to the side has to be clear at the beginning so the initial values can be adapted to stepping to the side and the ground contact model is adapted. The model for the ground contact was presented in section 2.3.2, here the initial velocity values for the next step are calculated by equation 2.20 and though by equation 2.21. In the case of stepping aside the force applied to the mechanics when ground contact occurs has another direction than in the case of stepping in case without moving the body in the frontal plane. This movement to the side is like a steering command of an upper control center which says 'go to the left or right'. It is an intentional signal. This leads to a ground reaction force which is not in a more or less vertical direction but the tangential component of this force is higher. So the initial movement of the new stance leg has a direction also horizontal so that the whole body moves to the side. This is realized by a joint torque of the new and old stance ankle α and γ, which have an initial value that has the same direction and keeps this horizontal movement vector for each step. So the general movement direction is determined by the initial value and the horizontal vector direction of the ground contact initial movement. This is determined in the equation for the energy preservation detailed in 2.3.3. The equation for this is according to equation 2.22:

$$E(step_i(1)) - E_{pot}(step_{i+1}(1)) = E_{kin}(step_{i+1}(-\dot{\alpha}(1), \dot{\beta}(1), -\dot{\gamma}(1))$$

where the velocities of α and γ have the same direction but opposite to the direction of the last step. This configuration of the ground contact leads to a stepping to the side movements shown in figure 3.24. This movement is also simulated with dropping hip steps alike figure 3.20.

Another possible walking pattern to the side is with small short steps that are more controlled by the ankles than the hip. As the ankles are not such a strong actuator as the hip the steps are smaller. This stepping movement to the side with smaller steps and ankle strategy $F11$ is seen in figure 3.25.

The forth and last stepping type is the stepping up. This is a stepping in place but here the hip is lifted as e.g. for stepping up a ladder. Furthermore, the ground contact is different compared to stepping in place. If the whole body steps upwards, the ground contact has to be adapted to a structure, e.g. like a ladder which can be stepped up. For this movement the ground contact was modified as follows: For each step the ground contact condition is moved by a delta upwards. So, for the first step the ground level is zero for the next it is delta higher and so on. The condition according to equation 2.15 is adapted by the additional term delta Δ, which means a higher ground level then before. The equation for this is:

$$l * cos(\alpha) - h * sin(\beta) - l * cos(\gamma) = \Delta \tag{3.15}$$

 The four types of stepping movements can be varied mainly by the initial values and the ground contact which defines the new initial condition for the next step and the strategy of actuation as ankle or hip strategy. For a limit cycle stability of those stepping movements, the feedback parameters are essential. So in the next section 3.8.2 some parameters are
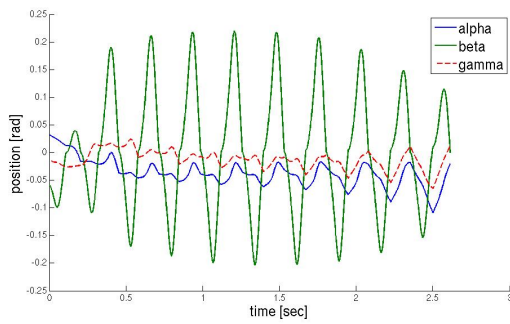
(a) Angular positions
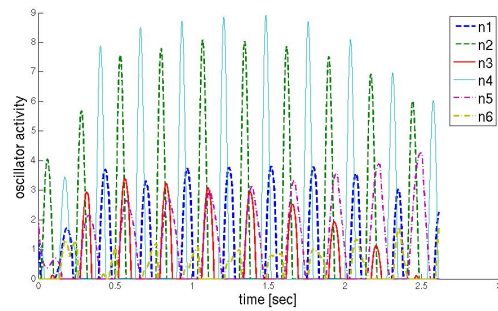
(b) Oscillator network activations
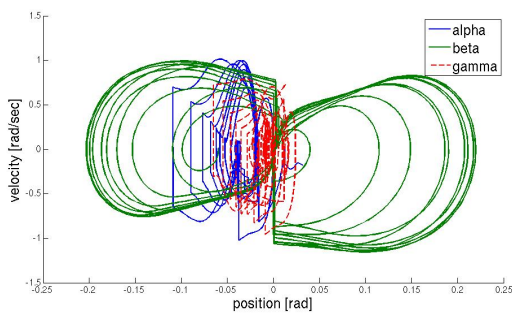
(c) Phase plot
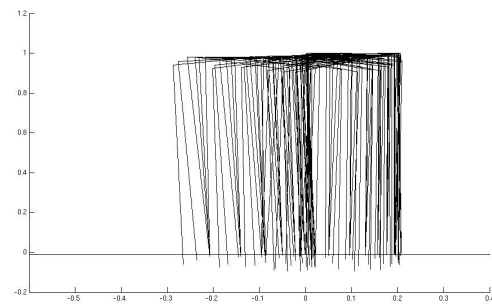
(d) Movement

Figure 3.24: Stepping to the side with dropping hip, simulated with the parameters $T_a = 0.1, T_b = 0.3, f_d = 0.6, f_{dv} = 3.5$, initial state vector $init_8$ and hip strategy $F10$.
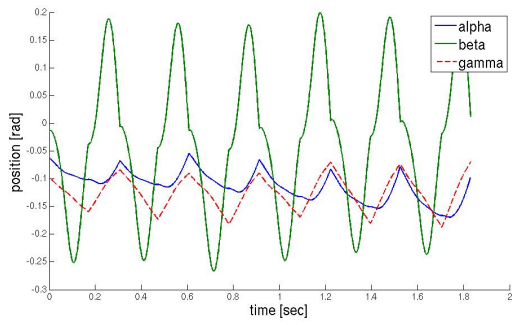
(a) Angular positions
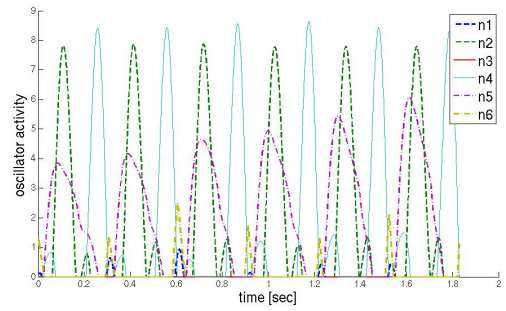
(b) Oscillator network activations
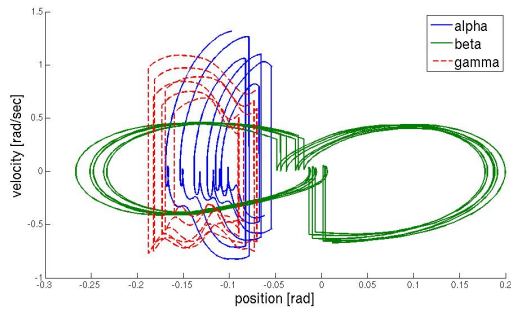
(c) Phase plot
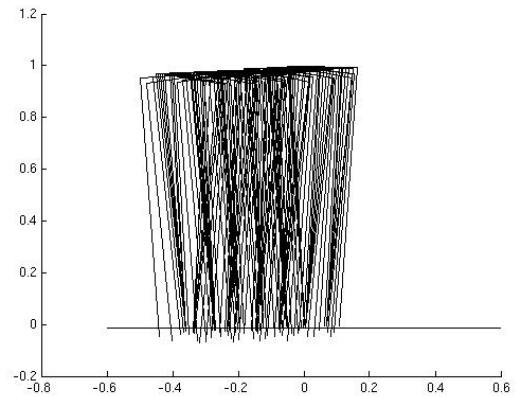
(d) Movement

Figure 3.25: Another stepping to the side movement with dropping hip has more hip actuation which results in smaller steps: simulated with the parameters $T_a = 0.3, T_b = 0.1$, $f_d = 0.6$, $f_{dv} = 4.5$, initial state vector $init_8$ and ankle strategy $F11$.
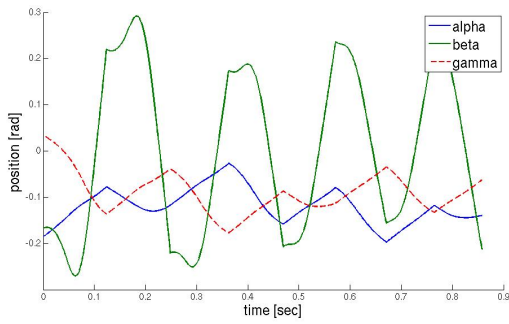
(a) Angular positions
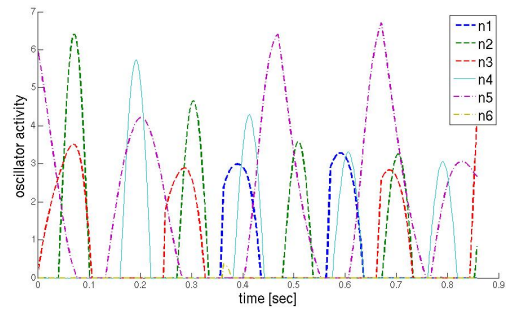
(b) Oscillator network activations
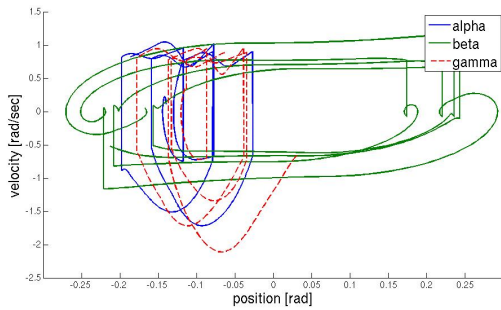
(c) Phase plot
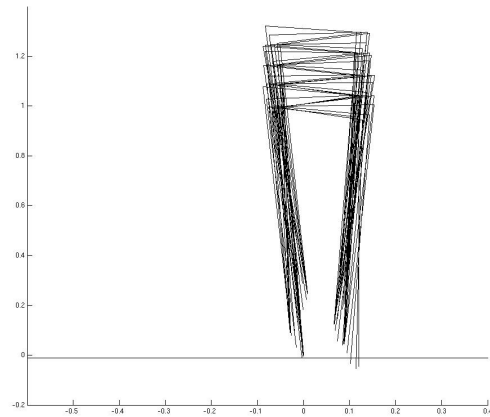
(d) Movement

Figure 3.26: Stepping upwards with rising hip which is like going up a ladder and is related to the ground level condition: simulated with the parameters $T_a = 0.3, T_b = 0.1, f_d = 0.85, f_{dv} = 3.8$, initial state vector $init_8$ and hip strategy $F10$.
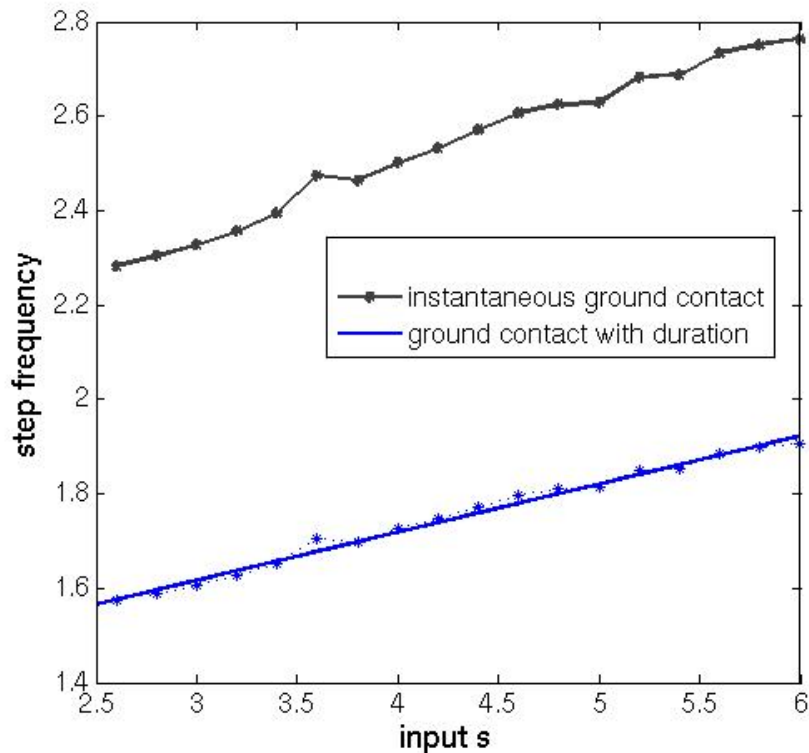
Figure 3.27: Influence of oscillator input s on step frequency with duration of one third of the step cycle (lower curve) or duration zero (upper curve) of the double support phase.

varied systematically to analyze the influence of those parameters on the system.

3.8.2 Influence of Parameter Changes on Movement Patterns

External Oscillator Input

A very interesting parameter of the oscillator network is the input s which can be a control input from higher levels as the brain and sensors. In the following the variation of parameter s and its influence on the stepping movement is shown. In figure 3.27 a rising of s for the same model parametrization results in a varying of step frequency. There is a direct linear interconnection between the oscillator input s and the step frequency.

An additional factor which influences the step frequency is the ground contact. The ground contact presented in this work is an instantaneous contact so the length of time of the contact is zero. If this contact duration would vary between zero and about one third of time of the step cycle, which is a normal value for slow walking, the step frequency is influenced. It is a linear indirect proportion which describes an increasing duration of ground contact which leads to a decrease in step frequency. This is shown in figure

3.27 with the second line, which is the result of varying the parameter s with a longer ground contact duration of about one third of the swing time instead of zero. This shall only demonstrate that the absolute value of step frequency depends largely on the ground contact time but the frequency change by parameter variation is valid independent of the ground contact time.

Actuation Strategies

The joint torque generation transfer function that produces the torques for each joint out of the oscillator activation levels are varied. The variation is motivated by experimentally found hip and ankle strategies in humans [66, 59, 60]. The ankle strategy means that the ankle muscles are activated primarily and the hip strategy that the hip muscles are used primarily. So different muscle groups are prevalently used for the same movement dependent on the strategy a person uses. This means that different strategies lead to a similar result. What strategy is used by a person depends on different factors, e.g. training and age. In the experiments of [66, 59, 60] the muscle activation was measured by EMG to prove the two strategies and their mixture. Training effects have also been found to influence the posture control strategy [60]. In [66, 59], the hip and ankle strategies are studied for stance and posture control and not for stepping, but it can be assumed that similar neuronal pattern changes occur in stepping and that there are different strategies how to perform a special movement. For the sagittal walking movement there are some analysis of walking strategies in [194, 133], which show that there are different strategies for hip and ankle actuation during gait. As in stance and sagittal gait those strategies are found for the frontal-plane movement similar strategies can be expected.

For this reason, in the following 8 different actuation strategies are evaluated to study the influence of actuation weight changes and strategies on the low-level stepping model. The equation to change the applied torques for the hinges was introduced with equation 3.4. The produced torques for the single hinges are shown in table 3.4.1. The weighting values w of this equation and table are varied according to different strategies of hip and ankle actuation.

	F10	F11	F12	F13	F14	F15	F16	F17
w_{12}	60	30	30	60	5	20	130	30
w_{22}	60	30	30	60	30	50	160	30
w_{33}	20	30	30	60	5	20	5	30
w_{43}	20	30	30	60	5	20	5	30
w_{51}	20	90	30	60	10	40	140	70
w_{61}	20	90	30	60	20	50	150	60
strategy	**h**	**a**	**a & h**	**a & h**	**a&h&ext&ns**	**a&h&ext**	**a&h&ns**	**a&ext**

Table 3.7: The weighting factors for the joint torque generation according to equation 3.4 for different strategies.

The abbreviations are **a**: ankle strategy, **h**: hip strategy, **ext**: the extensors gain is higher

than the flexor gain and **ns**: very low swing leg activation.

The 8 actuation weighting patterns are hip strategy $F10$, ankle strategy $F11$ and $F17$ and the rest is combined hip and ankle strategy. The combined strategy is divided into equal activation with higher $F13$ and lower activation level $F12$. For the combined strategy there exists also a low activation but nearly no swing leg activation $F14$ and high activation with no swing leg activation $F16$ where the extensors are enforced. Finally, $F15$ is a combination with less swing leg activation and higher ankle activation and more hip extensor activation. The hip joint $k = 2$ has always two equal values for extensor and flexor or a higher extensor value. This higher value w is like an initial tension of the joint according to expected loads like the gravitational forces. The named strategies are listed in the table 3.4.1 with the weighting factors w according to equation 3.4. Weights w which are not shown are all zero.
An example of a torque transfer function variation for a stepping in place movement is shown in figures 3.28 and 3.29.

In figure 3.28(g-i) the stepping in place movement with a hip and ankle strategy, which was already presented in figure 3.20, is shown. The same configuration of all parameters was taken for all shown plots in 3.28 and 3.29. The only variation is the torque generation function which are combinations of hip and ankle strategies represented by $F10 \ldots F17$. Naturally, the shown configurations are not all stable because for this also other parameters have to be adapted e.g. the feedback gains or the oscillator time and gain parameters. The same actuation strategy but with higher gains as there are the pairs low gain $F12$ and higher gain $F13$ or $F14$ and $F16$. This higher or lower gain needs an adaption of parameters as the feedback. All torque generation functions are compared to the reference function $F12$. The lines of plot 3.28 and 3.29, with each three plots, show the following:

$F10$**:** The hip joint is mainly actuated which leads to an asymmetric movement that has a higher hip amplitude but the nearly unactuated ankle and swing leg joint show smaller amplitudes. The initial tilted ankle position and the ankle position by the first hip transient is not corrected but is kept during the whole movement.

$F11$**:** The ankle joint is mainly actuated. This determines a symmetric movement because the initial ankle position can be adapted to the hip movement. The amplitude of the ankle movement is smaller as the ankles are more actuated. The difference to the combined hip, ankle and swing leg actuation of $F12$ is not very strong.

$F13$**:** The same actuation as in $F12$ with a higher gain is used so the movement is not stable with the same parameter setting. But it can be seen that the general amplitude of the hip and ankle movement is much smaller.

$F14$**:** This is a combined hip and ankle strategy with more actuation of the extensors and nearly no swing leg actuation. This movement is likewise not stable but the stance and swing leg amplitude is more centered which means it is more like a natural pendulum swinging around the zero point.

*F*15**:** Actuates hip and ankle with emphasis on the extensor but on a higher level and the swing leg is also actuated a bit. This leads to an asymmetric stepping movement with a larger hip movement on the side to which the body is tilted. As in *F*10 the initial ankle position can not be straightened because the ankle extensor actuation is too weak compared to the flexor actuation.

*F*16**:** Here the ankle and hip are actuated but with a much larger gain and the swing leg is nearly not actuated. This leads to a symmetric stepping movement. The higher gain leads to smaller amplitudes and therefore also a higher step frequency so the swing leg has not much time to swing free.

*F*17**:** More ankle activation than hip but swing leg is actuated the same as the hip. This leads to a result in between *F*11 and *F*12.

3.8.3 Different Feedback Gains

As mentioned above, the feedback gain factors for position and velocity feedback of equation 3.5 can be varied. This variation mainly influences the stability of the resulting movement. So if the feedback gain is only slightly changed, the attractive basin of the periodic stepping solution is not left, so the trajectories are attracted to the limit cycle after several periods. This can be seen in a solution which needs some steps for the transient effect after the trajectory is attracted to the limit cycle.

This change of the feedback gain can be interpreted as if there occurs a change to the system, like a load added to the system or the geometry of the system is changed by something or simply the strategy of reaction is changed by training or better benefits. These changes result in an adaption of the system to the new constellation. Another important point is that for most of the stable movements a little variation of the feedback does neither result in a great change of the movement nor in an instant instability. This means that the system acts robust to small changes in the feedback. This can be seen in figure 3.31 where the phase plots are shown and in figure 3.30 where the angular pattern of the movements is visualized. It was varied the feedback gain $f_d v$ and f_d. The feedback gain f_{dv} was varied by steps of 0.1 in the vertical series of plots and for f_d by a stepsize of 0.1 in the horizontal series of plots. The intervals of variation are: $f_d = [0.3, 0.4, 0.5, 0.6]$ and $f_{dv} = [0.6 \ldots 1.2]$. This was always done for the same system constellation with the parameters: $F12, P_1, s = 4 \; T_a, T_b = 0.05$.

In the phase plots it can be seen that there are several connected stable solutions for the variation of the feedback gains. The movement pattern changes slightly in appearance but not profoundly in characteristics. So, a varied feedback in the same basin of attraction does not influence the movement fundamental until it leaves the basin of attraction of a limit cycle and is therefore instable.
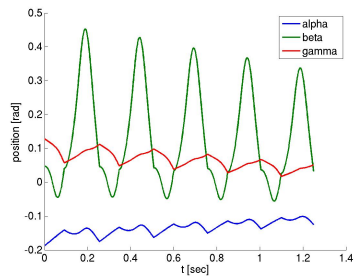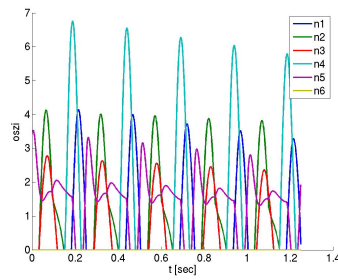
(a) Angular positions $F10$ (b) Oscillator activity $F10$ (c) Phase plot $F10$
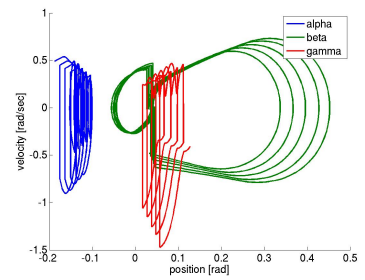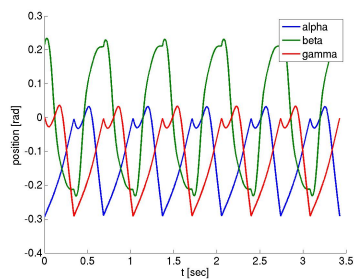
(d) Angular positions $F11$ (e) Oscillator activity $F11$ (f) Phase plot $F11$
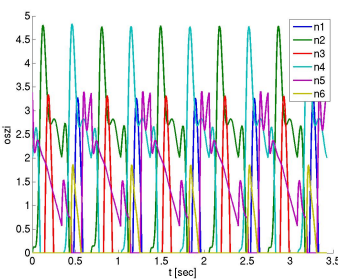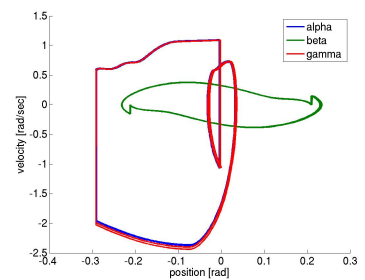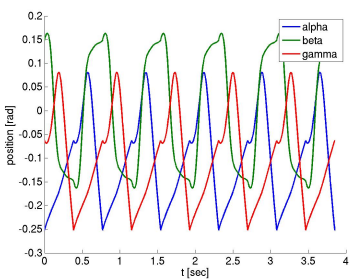
(g) Angular positions $F12$ (h) Oscillator activity $F12$ (i) Phase plot $F12$
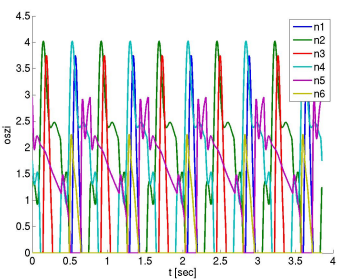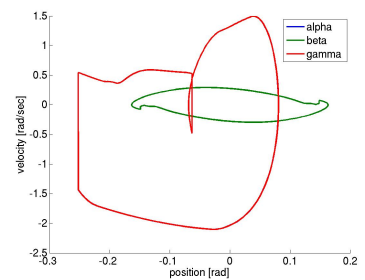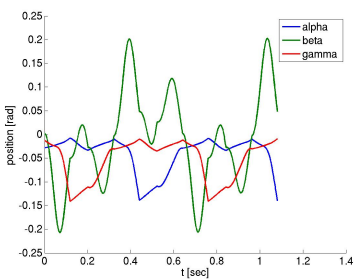
(j) Angular positions $F13$ (k) Oscillator activity $F13$ (l) Phase plot $F13$
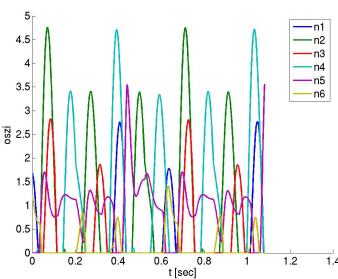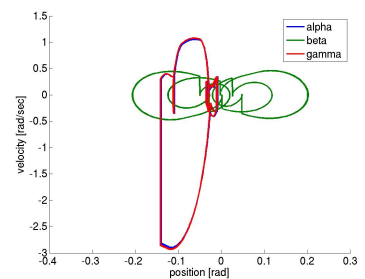
Figure 3.28: Influence of joint torque variation according to different torque transfer strategies $F10 \ldots F13$. Here the strategies are according to table 3.8.2: hip, ankle, ankle and hip with low actuation, and ankle and hip with higher actuation levels.

71
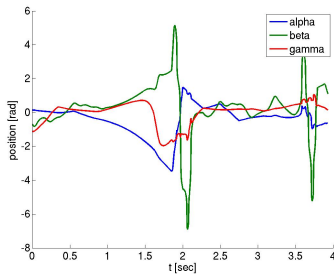
(a) Angular positions $F14$
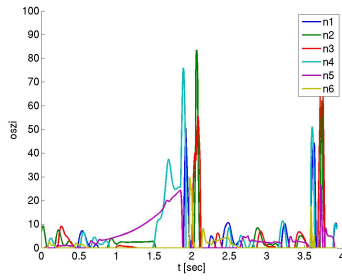
(b) Oscillator activity $F14$
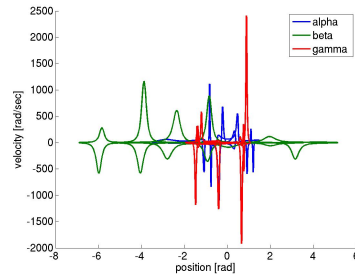
(c) Phase plot $F14$
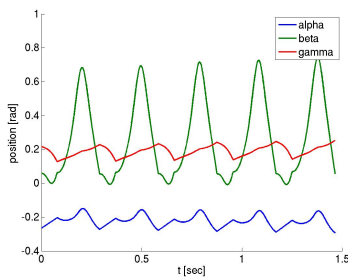
(d) Angular positions $F15$
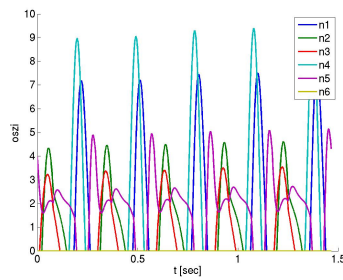
(e) Oscillator activity $F15$
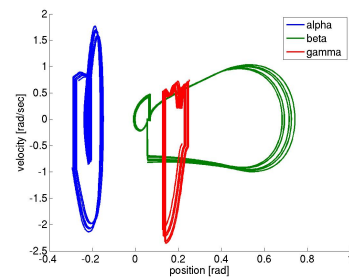
(f) Phase plot $F15$
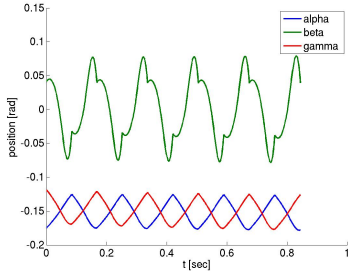
(g) Angular positions $F16$
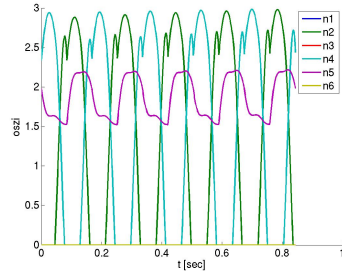
(h) Oscillator activity $F16$
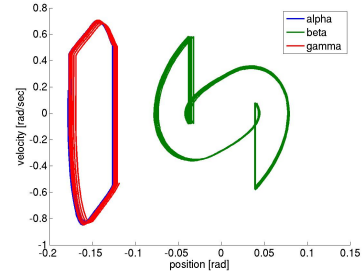
(i) Phase plot $F16$
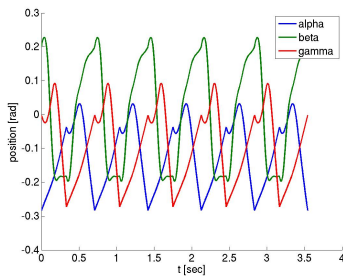
(j) Angular positions $F17$
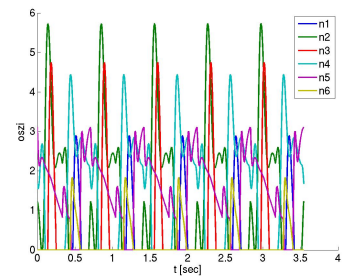
(k) Oscillator activity $F17$
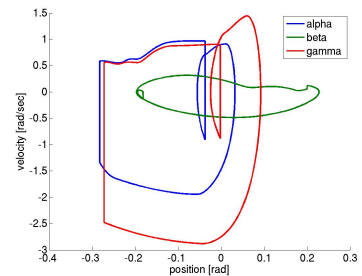
(l) Phase plot $F17$

Figure 3.29: Influence of joint torque variation according to different torque transfer strategies $F14\ldots F17$. Here the strategies are according to table 3.8.2: mixture of ankle and hip strategy with different swing leg actuation and hip extensor activation and the last example is ankle strategy with higher extensor than flexor levels.
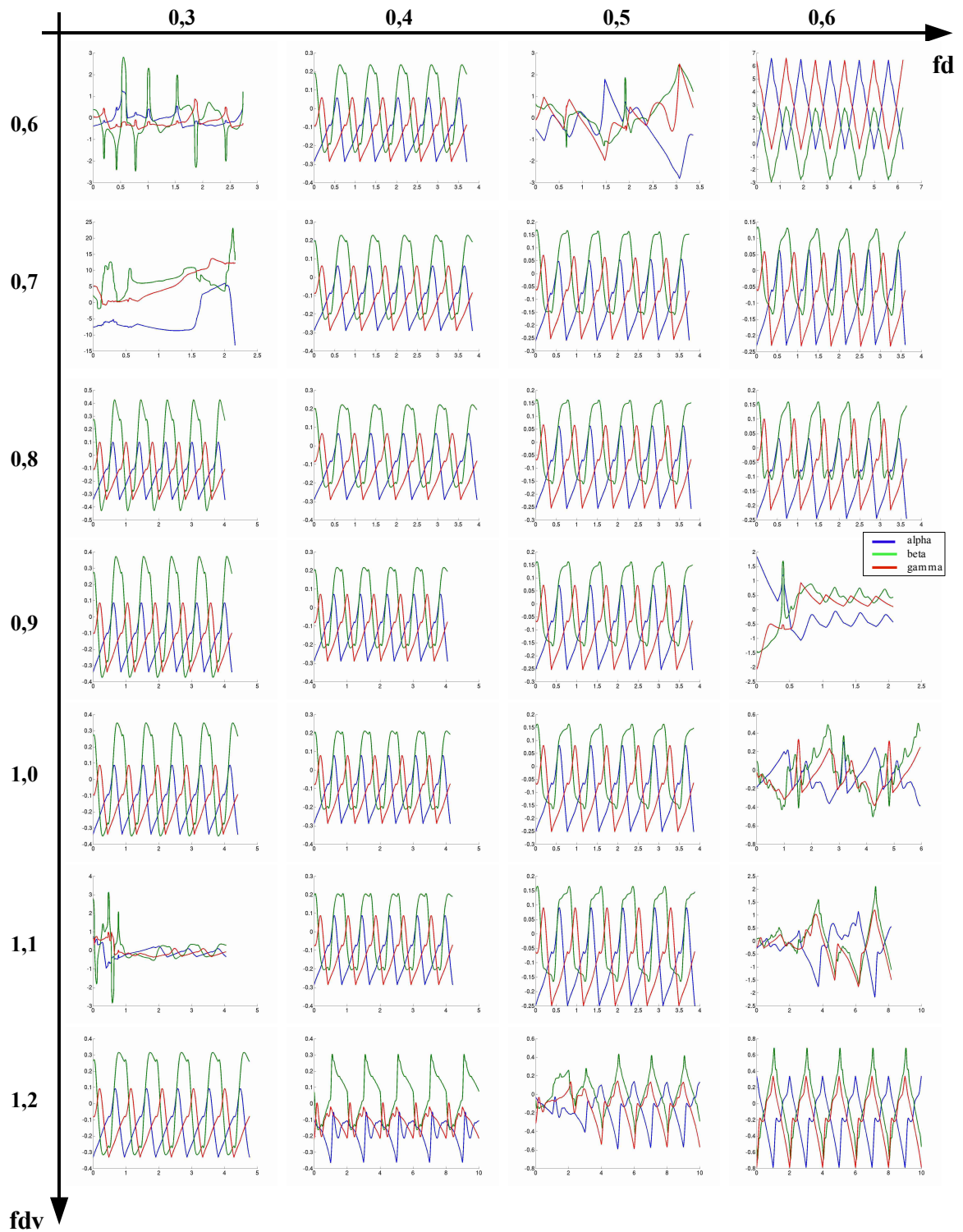
Figure 3.30: Plots of the stepping movement angles for variation of the proprioceptive feedback of position f_d from 0.3 to 0.6 and velocity f_{dv} from 0.6 to 1.2.
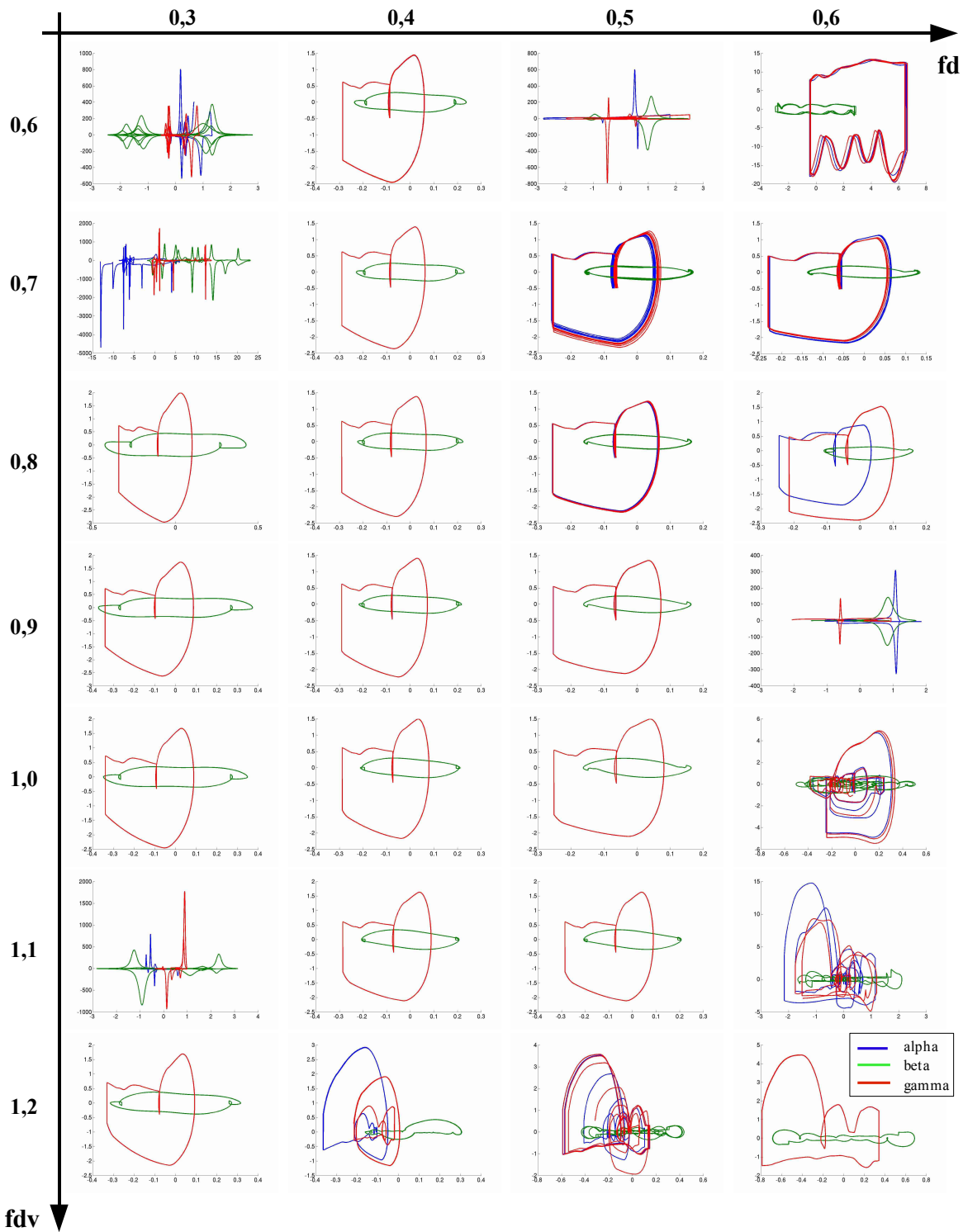
Figure 3.31: Phase plot for the same movements for variation of proprioceptive feedback of position f_d from 0.3 to 0.6 and velocity f_{dv} from 0.6 to 1.2. Stability is achieved for limit cycle solutions.

3.8.4 Different Oscillator Patterns

In section 3.3, four different oscillator network types are proposed. Different networks have different properties but those differences do not automatically lead to different movement patterns because a movement is a complex combination of all the parametrized influences. In the following a selection of movements produced by different oscillator network $P_1 \ldots P_4$ are exemplary explained and analyzed to show characteristics.

In the figures 3.32, 3.33, 3.34 and 3.35 four stepping solutions are shown for the four different oscillation patterns.

It can be seen that a crosswise neuron interaction pattern as P_2 leads to a more symmetric phase between hip and leg angular movement. This is because the neuron activation of the two legs is symmetric synchronous and the hip neuron activation is shifted. Another result of this is that the hip amplitude is larger.

	$init_0$	$init_1$	$init_2$	$init_3$	$init_4$	$init_5$	$init_6$	$init_7$	$init_8$
α	0.0257	0	0	0	0	0	0.0257	0	0
β	0.0002	0	0	0	0	0	0.0002	0	0
γ	0.0238	0	0	0	0	0	0.0238	0	0
$\dot{\alpha}$	0.0354	0.0238	0.1	0.1	0.238	-0.1	0.354	0.1	0.1
$\dot{\beta}$	-0.0145	0.0354	0	0	0.0354	0	0.0145	0.01	0.01
$\dot{\gamma}$	-0.0602	-0.0145	0	0	0.145	-0.1	0.102	0.1	0.1
n_1	1.7869	1.7869	1.98	-1.99	1.7869	-1.98	-1.7869	-2	2
n_2	-6.0811	-6.0811	-1.98	1.99	-6.0811	-1.98	6.0811	2	-2
f_1	0.7525	0.7525	0.7	0.7	0.7525	0.7	-7525	0.7	0.7
f_2	0.379	0.379	0.7	0.7	0.379	0.7	0.379	0.7	0.7
n_3	-12.8904	2.8904	2	-2	2.8904	2	-12.8904	2	-2
n_4	0.6977	-0.6977	-2	2	-0.6977	-2	0.6077	-2	2
f_3	0.1272	0.1272	0.7	0.7	0.1272	0.7	-0.1272	0.7	0.7
f_4	5.1681	5.1681	0.7	0.7	5.1681	0.7	5.1681	0.7	0.7
n_5	-0.4533	-0.4533	-2	-2	-0.4533	-2	4.533	2	-2
n_6	0.1893	0.1893	2	-2	0.1893	2	-1.893	2	-2
f_5	0.6659	0.6659	0.7	0.7	0.6659	0.7	0.6659	0.7	0.7
f_6	0.0105	0.0105	0.7	0.7	0.0105	0.7	-0.0105	0.7	0.7
n_7	4.6201	-4.6201	-2	-2	-4.6201	-2	4.6201	2	-2
n_8	-15.8628	15.8628	2	2	15.8628	2	-15.8628	2	-2
f_7	2.2592	2.2592	0.7	0.7	2.2592	0.7	2.2592	0.7	0.7
f_8	0.1733	0.1733	0.7	0.7	0.1733	0.7	0.1733	0.7	0.7

Table 3.8: Different initial values for the system.
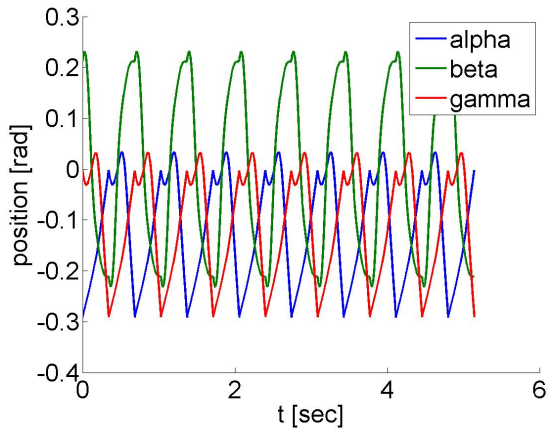
(a) Angular position
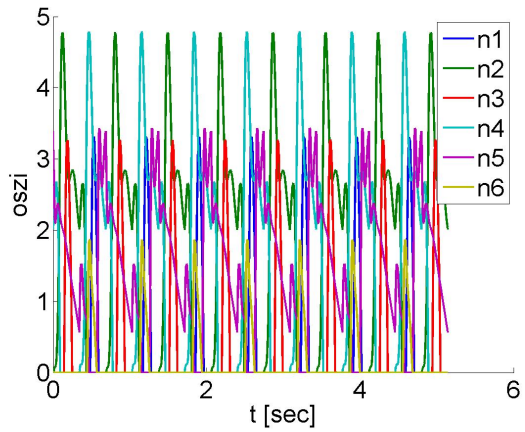
(b) Oscillator network activation
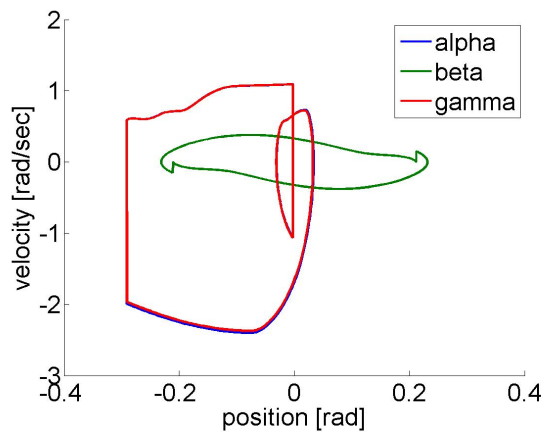
(c) Phase plot
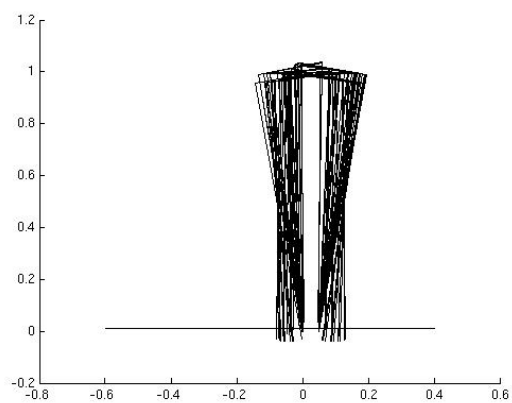
(d) Movement

Figure 3.32: Simulation of pattern P_1 with the parameters $F11$, $s = 4$, $f_d = 0.5$ *and* $f_{dv} = 1$ results in a stable stepping in place movement with dropping hip and larger stance and swing leg amplitude.
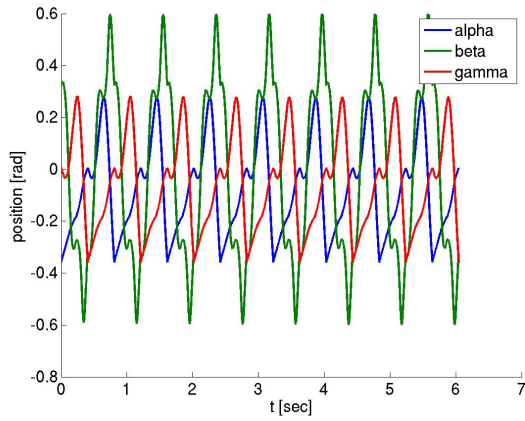
(a) Angular position
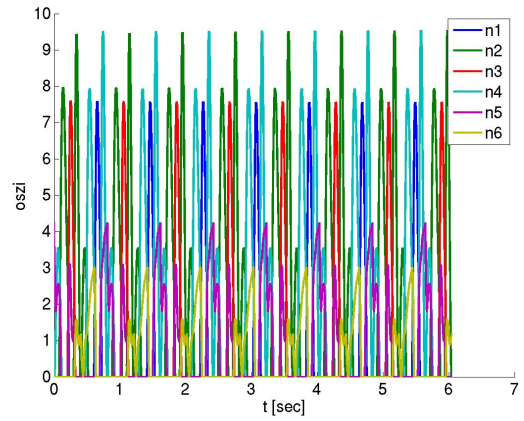
(b) Oscillator network activation
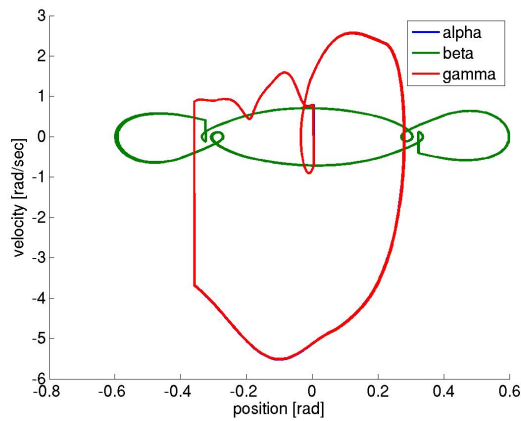
(c) Phase plot
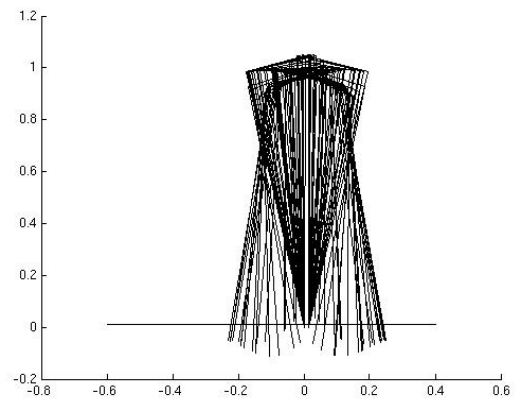
(d) Movement

Figure 3.33: Simulation of pattern P_2 with the parameters $F11$, $s = 4$, $f_d = 0.48$ and $f_{dv} = 1.2$ results in a stable stepping in place movement with dropping hip. It shows a higher activation of the hip with larger amplitude and different velocities during the movement.
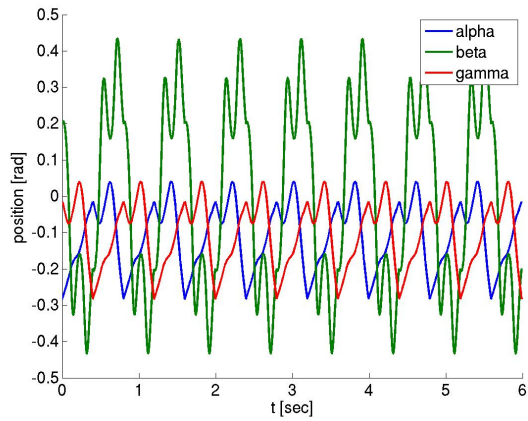
(a) Angular position
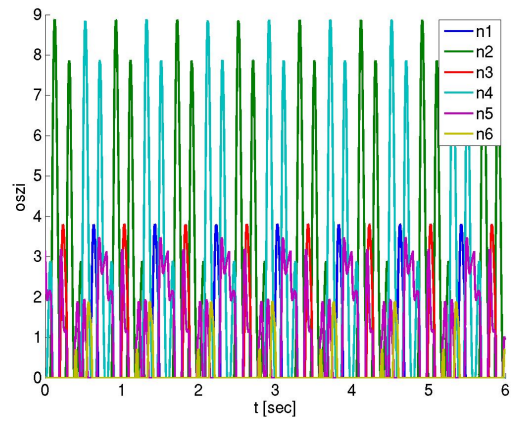
(b) Oscillator network activation
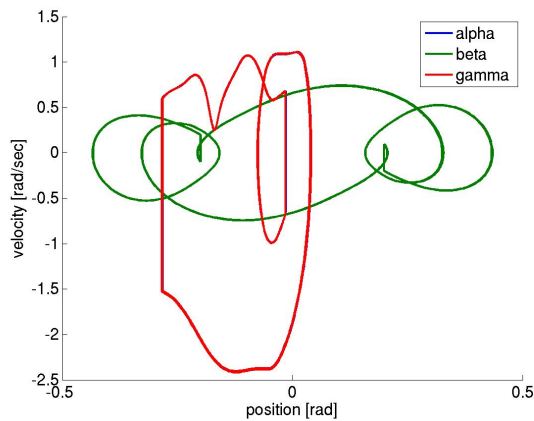
(c) Phase plot
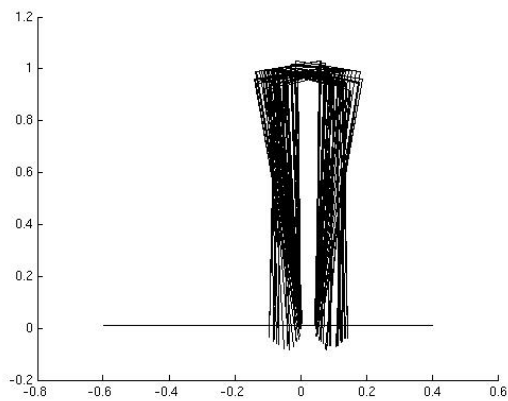
(d) Movement

Figure 3.34: Simulation of pattern P_3 with the parameters $F11$, $s = 4$, $f_d = 0.48$ and $f_{dv} = 1.2$ results in a stable stepping in place movement which is more dynamic. The higher the degree of interaction between the neurons the more the joint movement is influenced. The hip movement depends therefore more on the stance and swing leg movement.
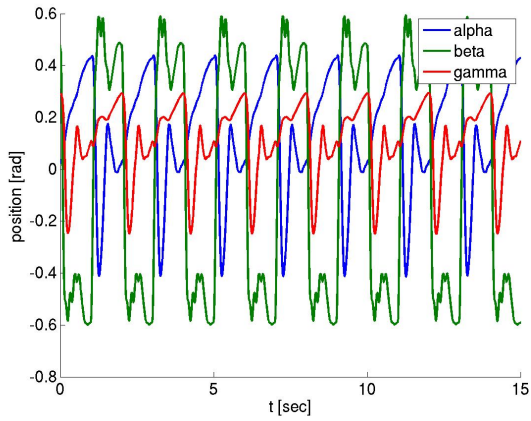
(a) Angular position
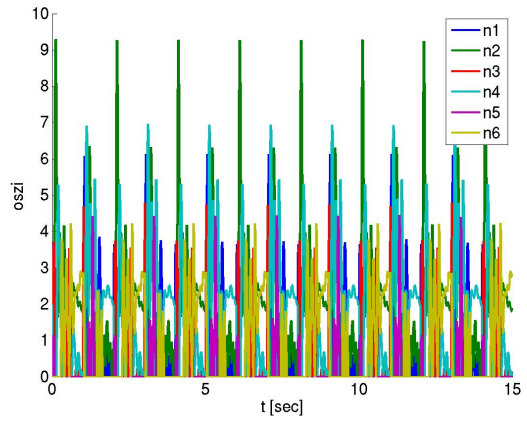
(b) Oscillator network activation
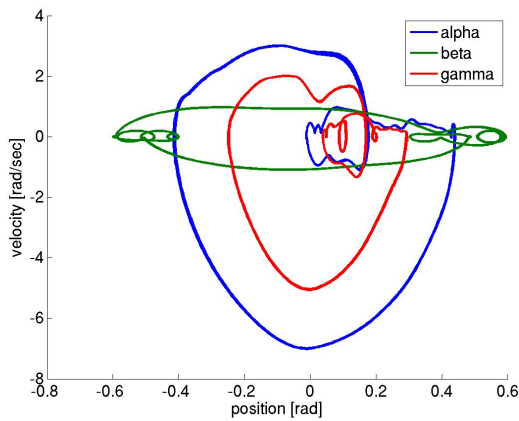
(c) Phase plot
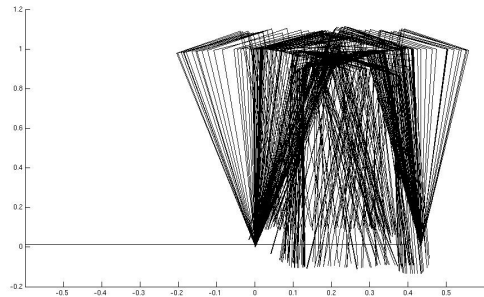
(d) Movement

Figure 3.35: Simulation of pattern P_4 with the parameters $F11$, $s = 4$, $f_d = 0.5$ *and* $f_{dv} = 1.5$ results in a stable stepping in place movement with the highest dynamic. Here even more neuron interconnections lead to faster reaction times and the velocities, especially of the legs, are much higher.

3.8.5 Stability of Movements with External Perturbations

Stability is the most important characteristic of the presented stepping movements. Further it is interesting how robust the movements are regarding to external perturbations, which are applied to the system. In nature these perturbations could be events like uneven ground occurring suddenly and unexpectedly, a slipping of the leg or a blow from an external source, which disturbs the body movement directly. Such external disturbances to the system are common and often in natural walking. There is no preaction to these disturbances as they are not foreseen but only a reaction. It will be shown that an oscillator-driven mechanics is generally able to regain stability after a perturbation if it is not so strong to push the system out of the attractive region. This ability leads to a more robust system for a wide range of movements. In the following three simple perturbations are shown. Each angle α, β and γ is perturbed once by a sudden discrete change.

In figure 3.36 the perturbation of stance angle α is shown. The stance foot e.g. slips away to the side opposite to the induced movement. This perturbation leads to a disturbance of the system which is compensated after short time. The next two steps have to stabilize the system again. The compensation work of the first step is smaller than that of the second. Afterwards the stepping movement is stable again.

In figure 3.37 the stance leg is disturbed at the same instant but the direction of disturbance is opposite. Here the disturbance can be imagined as e.g. again a slipping of the stance leg but now towards the swing leg. This disturbance even leads to less perturbance of the stepping system because it is in the same direction as the natural movement would have been. The stable configuration is regained very quickly. An instant slipping of the stance leg in direction of the movement and in the opposite direction have been applied with the result, if the stance leg slips the direction of the foreseen movement there is not much reaction of the system. The step length and amplitude is enlarged a bit but the successive steps are again as normal. By contrast the perturbation against the movement direction leads to a far bigger disturbance of the system but not in the related step but in the following. The step is shorter because the muscle feedback reacts on the sudden angular change and the successive three steps are needed to compensate this disturbance because the hip movement takes a great part of the compensation part.

In figure 3.38 the swing leg is disturbed at the beginning of the swing phase. This happens for example if the swing leg gets stuck or caught by an obstacle just after the push off phase. This disturbance leads to a real disturbance of the system. The ground contact ahead is reached with completely different angular values. The following step is out of balance and therefore the second following step has to compensate and regulate the stepping movement with a big hip and stance leg counter movement. Thereafter the system has found its stable configuration again and the stepping movement is symmetric and uniform again.

In figure 3.39 the swing leg is disturbed at the ending of the swing phase like if an obstacle just prevents the normal double support phase heavily. This disturbance leads to relatively small disturbances of the system. The ground contact ahead is retarded only

a little bit. The next step shows little influence which comes from the modified ground contact and the whole angle constellation is only very slightly modified. Afterwards the step cycle is back to the original.

In figure 3.40 the hip is disturbed which is a discrete change of the angle β. This disturbance is the most severe one because the hip mass is the biggest and it it not so well-balanced over the stance leg to be quickly stabilized again. But after one big compensation movement of the whole body the system regains stability and returns after one more step to the normal stepping movement.

This demonstration of three different system perturbation shall only demonstrate that the system is robust against perturbations. There is always a compensation movement where the amplitude and duration depends on the type of perturbation. The stepping movement regained after compensation movements is again stable and of the same type as the movement was before the perturbation.
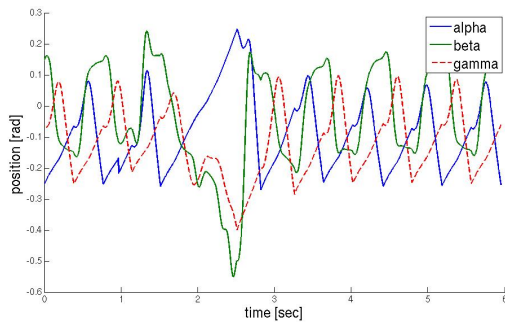
(a) Angular position
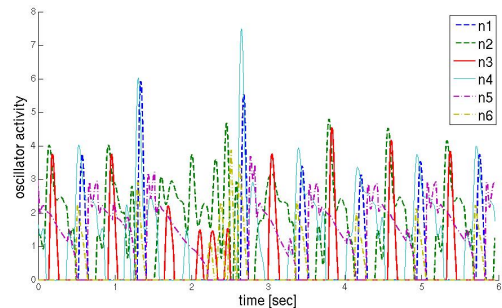
(b) Oscillator network activation
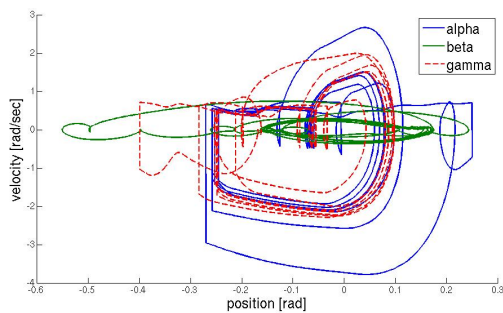
(c) Phase plot

Figure 3.36: Perturbation of angle α of the stance leg which is a slipping to the side. Parameters used for simulation are: pattern $P1$, torque generation strategy $F12$, feedback $f_{dv} = 1$ and $f_d = 0.5$.
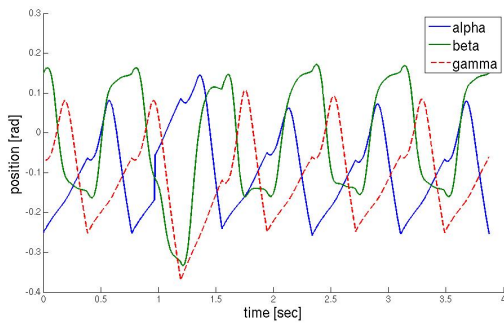
(a) Angular position
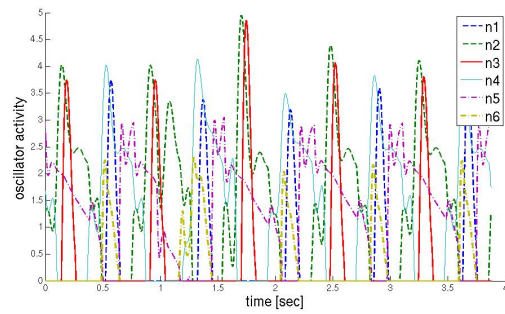
(b) Oscillator network activation
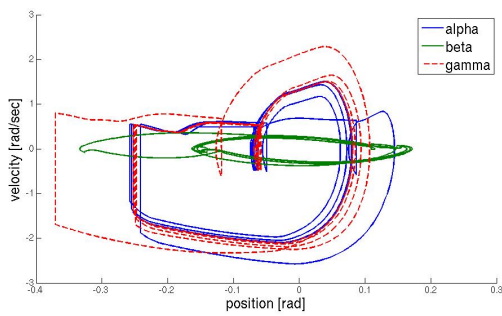
(c) Phase plot

Figure 3.37: Perturbation of angle α of the stance leg, which is a slip towards the other leg. Parameters used for simulation are: pattern $P1$, torque generation strategy $F12$, feedback $f_{dv} = 1$ and $f_d = 0.5$.
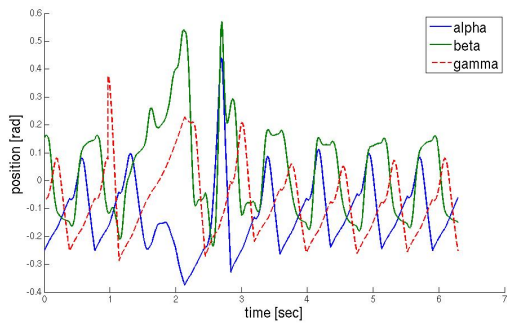
(a) Angular position
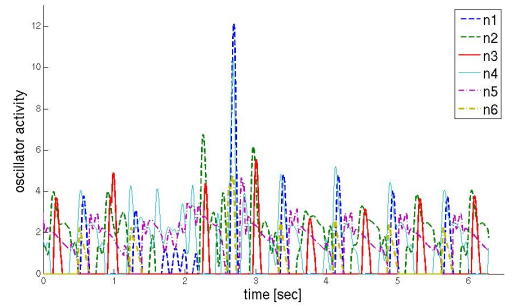
(b) Oscillator network activation
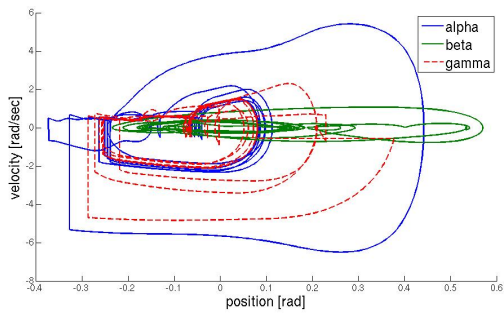
(c) Phase plot

Figure 3.38: Perturbation of angle γ of the swing leg, which is like caused by getting stuck. Parameters used for simulation are: pattern $P1$, torque generation strategy $F12$, feedback $f_{dv} = 1$ and $f_d = 0.5$.
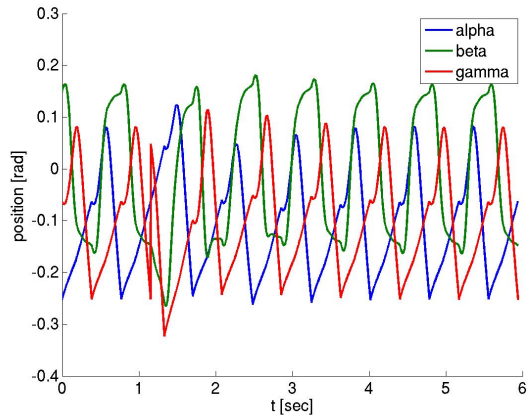
(a) Angular position
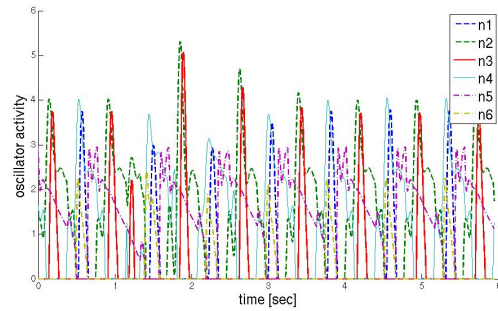
(b) Oscillator network activation
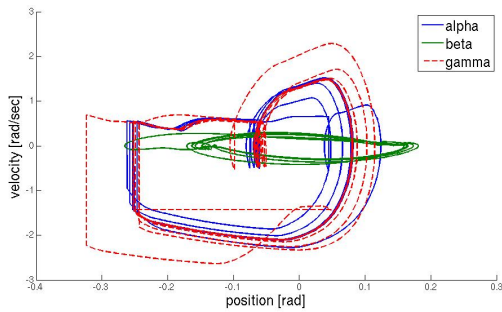
(c) Phase plot

Figure 3.39: Perturbation of angle γ of the swing leg at the very end of the swing phase. Parameters used for simulation are: pattern $P1$, torque generation strategy $F12$, feedback $f_{dv} = 1$ and $f_d = 0.5$.
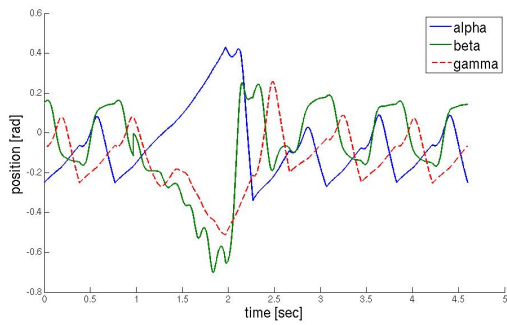
(a) Angular position
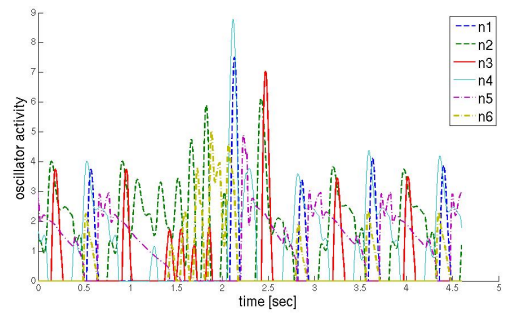
(b) Oscillator network activation
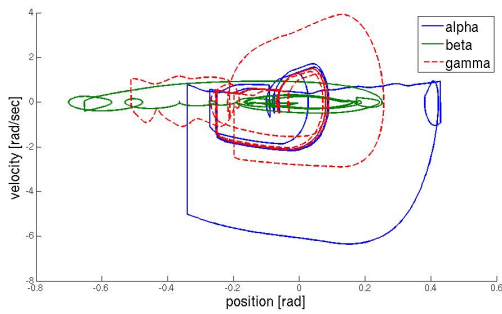
(c) Phase plot

Figure 3.40: Perturbation of angle β of the hip, which is like a direct push to the hip. Parameters used for simulation: pattern $P1$, torque generation strategy $F12$, feedback $f_{dv} = 1$ and $f_d = 0.5$.

(a) Video image   (b) Extracted possible markers
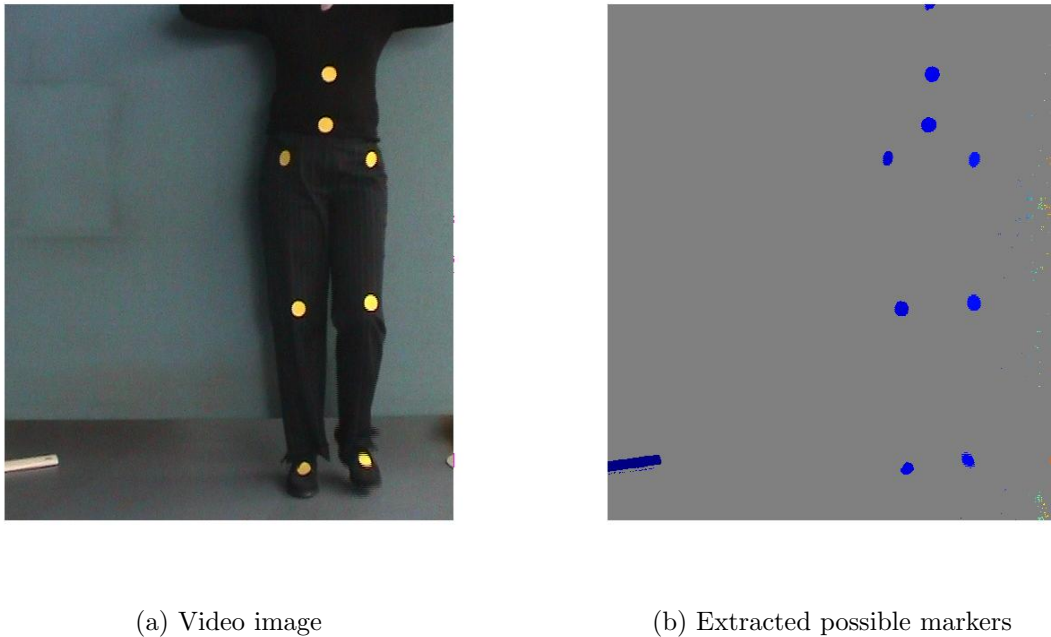
Figure 3.41: The video image is filtered and thresholded to receive image regions for possible markers.

3.8.6 Comparison of Simulation Data with Real Stepping Data

Last but not least this biomechanical model was made to represent characteristics of real stepping movements. Therefore, the model data are compared to real data which are gained from experimentally raised data. The experimental setup to get the data is shortly explained and the resulting movement data are compared qualitatively with the simulation data.

In the experiment movement data was collected via video tracking of markers put on the joints. As this is for a rough comparison of real and simulated data, the markers were put on the clothes where the joints and the interesting hinges are well visible. This can be seen in figure 3.41(a). The feet are just marked around the ankle to see the lifting movement of the lower leg, not to get ankle movements. Then, the markers are put to the knees, the hips and additionally two markers are put above the middle of the pelvis to get the upper body movement. The stepping person is recorded with a camera with a framerate of 25 fps and a resolution of 720x576. Afterwards via image processing in MATLAB these eight markers are extracted and identified and put together to a stick figure which represents the stepping subject. For this see figure 3.42(b).

The image processing in MATLAB consists of the following processing steps: The image seen in figure 3.41(a) is decomposed into its three color channels R, G and B. Afterwards, the Green Channel is transformed into the *'hiv'* color space. This image is simply thresholded to get the possible regions for the yellow markers which is seen in figure 3.41(b).
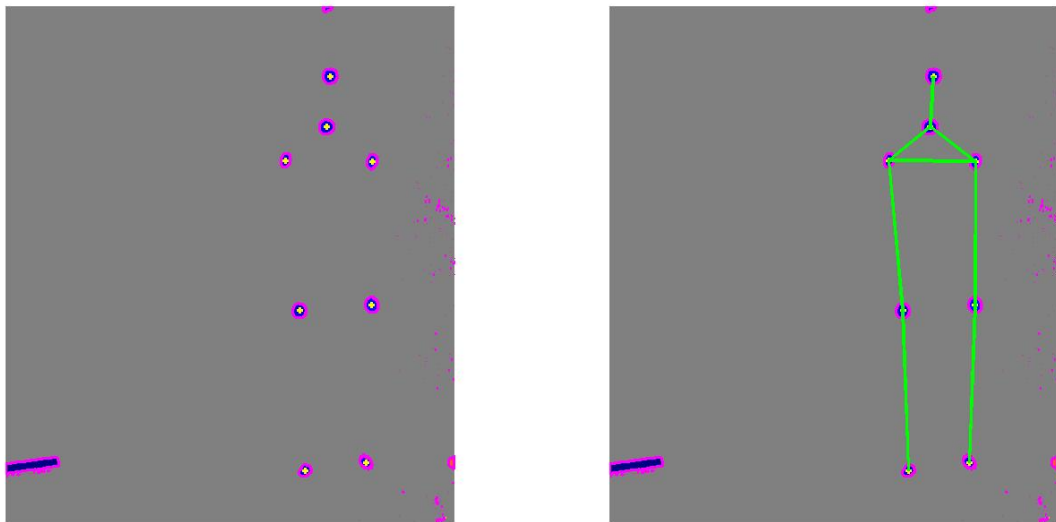
(a) Determination of boundary and centers   (b) Selection of markers for stick figure

Figure 3.42: The extracted regions are classified and observed over several images to match the regions to markers and afterwards connect them as a stick figure.

The single regions are classified according to their size, boundary and centroid. In the following only the searched markers are extracted finally as seen in figure 3.42(a). The found centroids are observed over several subsequent images and matched to them. In the following the centroids are matched to the position on the body and afterwards they are connected to a stickfigure which is presented in figure 3.42(b). From this stickfigure the angles α, β and γ are reconstructed. The angles are defined in the same way as in the mechanics section in figure 2.4. The hip and feet marker are taken to calculate the angles. The knee markers do not change the angles largely as the knee is more or less in line with the hip and feet with a slight deviation according to the joint positioning as knock knees or bow legs of the subjects. The angular velocities can also be reconstructed with the information of the framerate. The received angles are compared in characteristic and phase to the simulated data. The two stepping modes stepping in place with dropping hip and stepping aside have been compared.

(a) Angular positions   (b) Phase plot
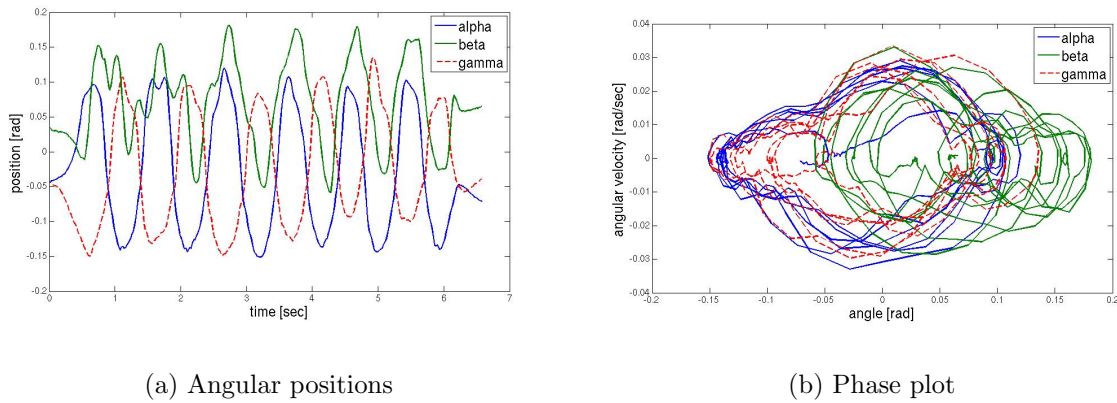
Figure 3.43: Video tracking: angular position and phase plot of experimental data of stepping in place.

(a) Angular positions   (b) Phase plot
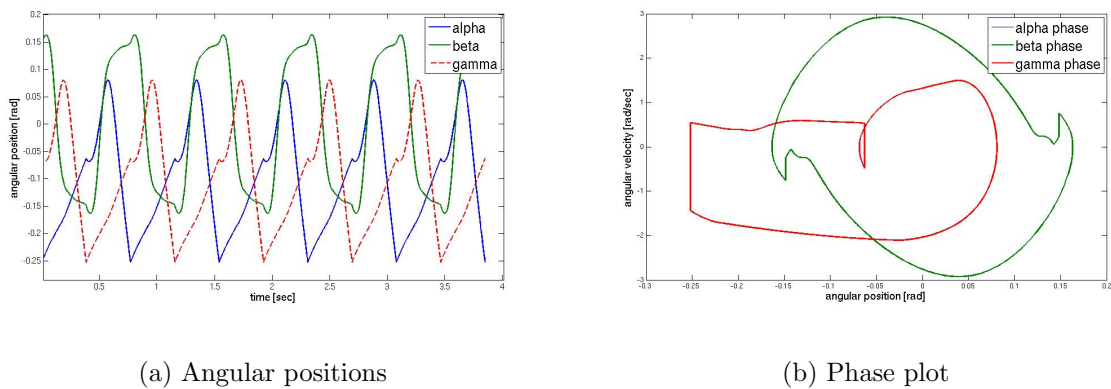
Figure 3.44: Simulation: angular position and phase plot of simulated data of stepping in place.

Stepping in place is a more or less symmetric movement where the legs are moved alternating in a pendulum movement. The movement of the legs is though diametrical time shifted. One leg moves towards the other and back again during one step while the movement of the two legs is opposite. This means that the plot of the stance and swing leg angle is symmetric if the same if the time shift is omitted. This movement is represented by the simulation very appropriately which is seen in figure 3.43 and 3.44. The characteristics of the leg and hip movement is the same and the phases are also a good match where the hip drops before the swing leg swings back again. The stance leg oscillates in the same sequence as the hip drops down. And the two legs do a pendulum movement. The amplitudes of the angles have a good matching relation only the velocity in simulation is higher then in reality. This is because there is no slow down by ground contact and no energy storage in e.g. muscle fibers or joints during the swing phase. This means that a very suitable solution of the model was found to represent stepping in place.

(a) Angular positions
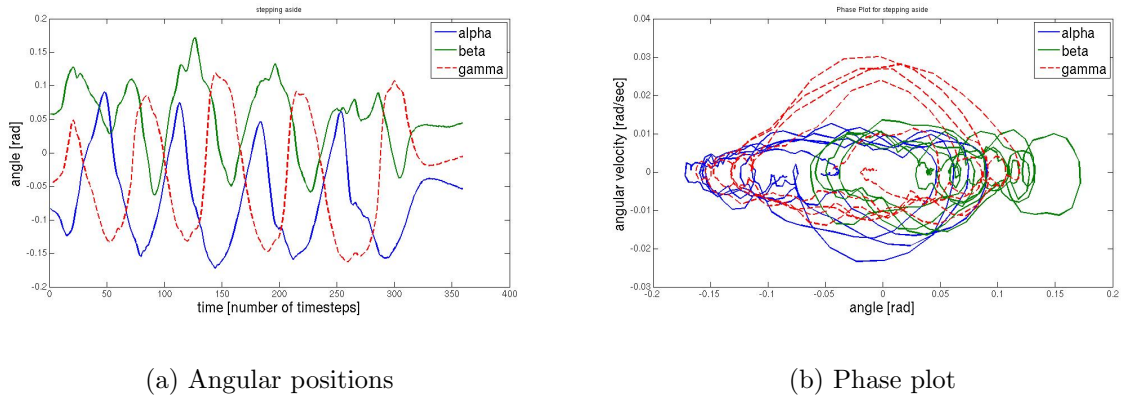
(b) Phase plot

Figure 3.45: Video tracking: angular position and phase plot of experimental data of stepping to the side.

(a) Angular positions
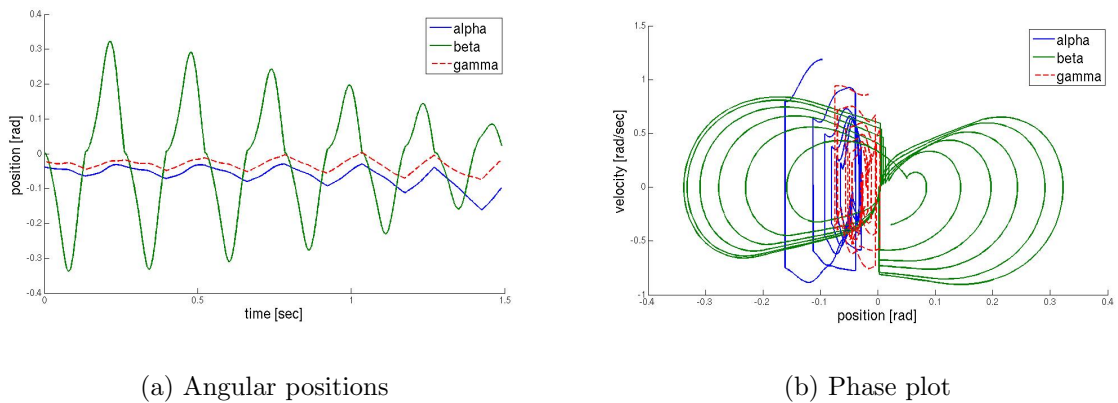
(b) Phase plot

Figure 3.46: Simulation: angular position and phase plot of simulated data of stepping to the side.

Characterizing stepping to the side is a leg movement of the stance leg in the opposite direction of the swing leg (which means the same angular position because the angles are opposite counted as shown in figure 2.4). This movement leads to the sideway movement. The leg movements have some latency to each other and the hip. The simulated data has this leg movement, but the movements are synchronous without any latency. And the hip has a much higher amplitude related to the leg amplitudes than in reality. This refers to the fact that there are no latencies modeled nor are there any structures which delay movements like elastic fiber structures or a ground contact with a determined duration. The only structures in the model which can produce big differences in latencies and shifts between legs and hip are the type of oscillator network as the connections influence the timing relations of activation. And the weighting according to different actuation strategies is also an important factor influencing the latencies and shifts. These two influencing factors were not specially adapted for the sideways movement. In the natural sideways stepping a larger part of the hip shift is done during the double support phase which is not reproduced by the model's instantaneous ground contact. This leads to simulation data which is different to the video-tracking data although both show sideways stepping. The experimental data can be seen in figure 3.45 and the simulated data in figure 3.46.

3.9 Discussion

The proposed model consists of the frontal or sagittal mechanics actuated by an oscillator network of Matsuoka oscillators and antagonistic joint torque generators, plus a muscular feedback mechanism based on position and velocity information. This model already provides on a low level many of the typical stepping movements found in biology. "Low-level" means without the use of any higher control such as the brain and high-level sensors. In contrast to the models of Geng et al. [41, 40, 144], where only the sagittal plane is modeled, the presented research models the frontal plane and analyzes it in detail. Geng models a biologically motivated robot, which means that the neurons do not incorporate adaptation effects but have direct reflexive coupling to the position with the aim of achieving fast reaction times for each step. Another example of neuronally driven mechanics is given by Righetti and Ijspeert [152]. Here Hopf oscillators are used which are coupled in chains with a master oscillator to guarantee phase shifts between the oscillators. However, the stability of the lateral motion is controlled by the sensory output of the gyros representing a vestibular sensor, and not by an autonomous CPG pattern as in the presented model. Also in Miyakoshi et al.[123] lateral stabilization is achieved by a high-level PD-control scheme. None of these other models, in literature, evaluated the possibilities of the neuro-mechanical model for performing lateral stepping movements and the abilities of the model which depend on the parameters of the oscillator system. There is so far no other work known to the author which studies lateral stepping patterns on the basis of the neuronal actuation; these are the four simulated patterns: stepping in place with dropping and lifting hip, stepping sideways and stepping up. For the purpose of validation the actuation concept was also tested successfully with the sagittal model.

Kuo [94] argues that stabilization of the frontal plane and of the sagittal plane movements are largely independent. There are, however, no biological studies about the mechanism of the separation or the interaction. This combination would therefore be a suitable subject for future research.

Three characteristics of stepping movements: stability, frequency (or velocity) and ground contact are analyzed. As stability is the primary characteristic investigated when analyzing stepping patterns and strategies, it is often studied in literature [127, 128, 49, 48, 38, 39]. Stability was proven using the numeric method proposed by Goswami [48]. There were shown stable movements and unstable ones which can do several steps before falling. The three main stepping movements which are possible with the frontal mechanics, *stepping in place* (with lifting and dropping hip), *stepping to the side* and *stepping up*, were realized as autonomous stepping movements of the oscillator-driven mechanics. The three stepping types were realized with different initial conditions or different ground contacts. Thus means that in general there is no difference between stepping with dropping hip or stepping with lifting hip. In addition the known strategies of hip, ankle or mixed actuation were tested according to Horak et al. [59, 60]. Horak postulates that these changing strategies occur as a result of learning and experience. This means that the automated rhythmic movements are not fixed but can be adapted in line with learning effects. This learning has not been implemented in the presented research, but the strategy changes which have been tested here could also be implemented as learned strategies, because the strategy influences performance factors such as efficiency or appearance of the stepping movement. The model developed by Geng et al. [40] shows that learning algorithms can be used to adapt actuation to the environment.

One important model parameter is the external input to the neurons s. This input was proven to change the step frequency together with the duration of the ground contact. By isolating parameter s it is possible to tune the step frequency without greatly influencing other stepping parameters. As Manoonpong [105] mentions, the speed variation, which mainly correlates with the step frequency, could not be easily adapted in earlier neuro-mechanical models as in [171].

In Horak et al.[66] and Müller et al.[133], the hip and ankle strategies used in posture control and sagittal walking are studied. There are no studies known to the author where medio-lateral strategies are analyzed. With the model presented here it was shown that different joint actuation strategies influence the appearance, the phase and the coordination of the stepping movements. These results can be a good starting point for experimental studies of medio-lateral hip and ankle strategies because medio-lateral stabilization is even more dependent on active stabilization than sagittal stabilization [6, 94].

A natural system of walking is often exposed to disturbing influences, some of which can be foreseen but many of which occur unexpectedly and suddenly. Such perturbations of the system were surveyed whether and how the system reacts. The three angles were disturbed in different directions or in different points in time of the step cycle. The system compensates for the perturbation within a few steps and returns to a stable step cycle. This robust behavior is a big advantage of using distributed actuation feedback.

Distributed walking systems as in [171, 105] were also found to display robust behavior.

Last but not least, the simulated movements were compared with real experimental data received from a video tracking analysis. This comparison was carried out in order to check for qualitative similarities and differences. For medio-lateral stepping movements there are no experimental walking patterns known to the author. It can be concluded that there are simulation solutions which resemble the experimental movements quite well as regards phase, periodicity, amplitude and appearance, but there are also many solutions found which are quite different. Human stepping is a very individual movement which adapts to changes and influences of the movement apparatus and shows a wide range of variable movements which are never repeated exactly the same way.

3.10 Conclusion

In this chapter a combination of the passive mechanics of chapter 2 with a neural actuation by antagonistic joint torque application and muscle-type feedback was presented. This model is also called the low-level model because it does not include high-level posture control functions of the brain. Simulation of the low-level model was performed to evaluate the characteristics of neural actuation and to reveal the properties, potential and shortcomings of the model.

The actuation concept was applied effectively both to the frontal-plane mechanics and to the sagittal-plane mechanics. This shows that the concept is general and can be applied to different mechanics and rhythmic movement patterns. A combination of those two planes is possible but is left for future research. This thesis concentrates on studying the medio-lateral stepping movements of the frontal-plane model. In general it was demonstrated that the stability range and the stepping variability were increased by the actuation concept.

Simulation of the frontal plane showed that three typical stepping movements such as stepping in place (dropping and lifting hip), stepping to the side and stepping up (e.g. a ladder) can be produced. In addition the strategies which are used for actuation were tested according to the hip, ankle and mixed strategies found experimentally (in the literature). These strategies can be applied successfully and result in different stepping movements. Consequently, it is possible to influence the low-level model by varying the strategies and stepping patterns used. This can be achieved on a higher level by either adapting or overruling automatic movements to suit conditions which have been experienced and learned, such as efficiency and stability, or to take conscious decisions such as the selection of stepping up because there is an obstacle or stepping to the side because this is an instruction. Analysis of the parameters ascertained three parameters which systematically influence movement characteristics: Firstly, feedback gains directly influence stability. Secondly, initial conditions, as well as the ground contact, which triggers a new initial condition for the next step, influence the direction of movement. Thirdly, parameter s is directly proportional to the stepping frequency. These are parameters which could be integrated in a high-level model to influence precisely those three properties. This is

left to future research because this correlates strongly with the intention of walking, which was not subject of the research performed in this thesis.

It was proven that it is possible to simulate stepping movements which are very similar to the real human stepping movements which have been analyzed.

In conclusion the presented model accounts for several characteristics of human stepping movements, though there are also some limitations. One large limitation that has already been mentioned is the "low-level" aspect. This means that there are no high-level functions integrated in the model presented so far. Therefore the whole body position remains unknown and environmental influences are not taken into account. If inappropriate initial conditions are chosen or the feedback gains are not adapted completely, this leads to unstable movements. After some steps the stepping model will fall over or might even tumble with the first step. In the next chapter 4 a high-level posture control model is developed to stabilize the whole body position and to integrate sensory perception into the model. This model also bases on biologically principles and structures but at the same time aims to keep the high-level posture control relatively simple.

4 High-Level Posture Control

Sensors measure the relation between the environment and the body or the relationship between individual body parts. High-level posture control is a control which bases on the information provided by these sensors and on knowledge of the body, the environment and the relationship between them. This means that there is a knowledge which has been gained by experience and memorized and this is able to relate the sensory information to a context. The brain has to correlate the internal body states with the external world and produces the right reaction of the internal system to internal and external events. This integration task is named high-level here because such functions as sensory information processing or a knowledge base are located higher than the mechanical levels, reflex levels and spinal cord levels and are therefore found in the brain. The objective of this high-level information processing is posture control of the body for standing and stepping.

Posture control in this context always means controlling that the body does not fall or that high-level specifications for the movement are defined, e.g. the direction or speed of movement. In the case of standing, the task is to maintain stable stance and the target position is "standing upright". For stepping movements there is no direct control of each individual leg angle, but information on individual positions is gathered by all sensors and is integrated to stabilize the whole upright body position. The technical equivalents to a general body position such as this are, e.g. the zero moment point (ZMP), the center of pressure (COP) or the center of mass (COM). Those values represent the whole body position which are controlled in order to achieve upright stepping and standing movements.

The measurements registered by the sensory systems are transmitted into body movements in order to coordinate them and to use them for high-level body movement corrections. The sensory systems which are addressed in the following are the visual sense, the vestibular sense, the proprioceptive sense and for state-of-the-art models, the somatosensory sense. The measurements registered by these four sensory systems are: retinal image, head accelerations, relations between body parts such as joints and muscles and finally other sensor measurements such as temperature, haptic feedback etc.
The sensory information used in the following is derived from the four following sensitive systems:

- the vestibular sense, which senses body accelerations in all 3 translations and 3 rotations and which is located in the head in the inner ear.

- the visual sense, which senses light producing the retinal image and subsequently measures the environmental movements in relation to the head and eye movements.

It is situated in the head.

- the proprioceptive sense, which senses the body itself and its relations e.g. in joints and in the muscular feedback as already mentioned in section 3.4.2. It is distributed over the whole body and is not centralized in one organ.

- the somatosensory sense, which includes all skin sensors and measures e.g. pressure, temperature, pain and vibration and proprioception as described in [185].

There are many examples and possibilities for integrating sensory modalities into a high-level posture control. As there is no proof that there is a biological analogy of sensor integration functions for the complex human posture control system, these models are ideas for solutions with a greater or lesser degree of possibility; they need to be verified by experiments step by step to explain characteristics of posture control. Posture or stance control are therefore the subject of intensive study, including experiments and clinical findings as well as model explanations [88, 120, 80, 97, 180]. The model presented in this work consists of the sensory measurement part, which provides information about the body states, environment and the relation between them, and transmitts this to the high-level processing component, the brain. The high-level processing component integrates the sensory information and uses it to determine the way the system reacts to keep the body in balance. For this high-level model new experiments on eye movement and artificial vestibular stimulation are evaluated together with findings from the literature in order to evaluate the posture control model provided. Integration of sensory measurement and processed posture control commands leads to a stance model which maintains balance and is able to demonstrate the influence of sensory inputs on posture. By extending the visual sensory cue by an alternative sensory nonlinearity, according to state-of-the-art models, experimental results are reproduced.

In section 4.1 some ideas for models and related experimental studies are presented to provide insight into the complexity and abstraction of sensor integration posture models. It is also derived why a statistical estimator is chosen as the sensor integration model.

Section 4.2 presents the sensory models which are used in this work and which validate experimental results. These are the transfer functions used to relay the environment and body information perceived by the sensors for internal processing. In section 4.3 the model for the internal estimation is derived. A Kalman filter estimation model is introduced and extended with a nonlinear sensory part. The high-level posture control model is applied and tested using a negative feedback of optimal control as presented in subsection 4.3.4 and also the mechanics of an inverse pendulum. This application is detailed in section 4.3.2. The simulation results of this model are established according to experimental findings regarding posture response to visual and vestibular stimulations. The findings are delivered from the literature and from the author's own experiments. These experimental studies and results are detailed in sections 4.4.2 and 4.4.3. The model is implemented and simulated in MATLAB. Simulation results are compared to experimental results in section 4.5. Finally, in section 4.7 the simulated results are discussed.

4.1 State of the Art of Sensorimotor Posture Models

The ideas for models presented in the following all involve the use of sensory models. These sensory models differ, but the kind of information they provide is similar and often of the same characteristic. No special explanation is given of any of the sensory models used in the state-of-the-art posture control models presented; mention is only made of the type of sensory information integrated in the model.

Very straightforward stance control is provided by models which integrate the sensory signals in a PID-control model. In the research published by Peterka et al. [138, 139, 140] a biologically motivated model is developed which weights the information provided by each sensor individually and integrates the information by summation. This sensory information is time-delayed and then used for PID control of the body position by corrective joint torque input. This control acts parallel to the passive muscle dynamics which are stabilized with positive force feedback in order to investigate their qualitative influence on posture control. The purpose of this model is explained in Peterka [140] (p.6) *"Our relatively simple models allowed us to apply systems identification methods in order to estimate the relative contributions (sensory weights) of various sensory orientation cues in different environmental conditions"*. [61] also proposes a PID model with sensory weighting to explain differences in standing with eyes open and eyes closed. Other examples of reweighted multisensory inputs combined with PID control are given by Mergner et al. [119, 120, 118, 109]. They use the model to introduce a nonlinear relation between sensory inputs and position control. The nonlinearity of the sensory system is modeled by thresholds which lead to nonlinear reactions in the position response. The sensory cues for visual perception are more closely investigated in [120], whereas the sensory cues for proprioception have been studied in Becker et al. [7, 116], always in combination with vestibular sensor cues. The studies conducted by Becker introduce another aspect with regard to sensory combination. The averaged weighting for sensory cue fusion is opposed by a cognitive "eigenmodel" of vestibular perception. This cognitive model is used to explain the discrepancies in gain (ratio of achieved to desired rotation position) between high and low stimulation velocity and duration. It was found that longer and slower stimulus of passive rotation or treadmill stepping on a rotating platform lead to an overestimation of the subject's own rotation position; this stands in contrast to single reweighting and decreasing gain theory outlined above.

Stance stabilization can also be achieved using fuzzy control [74, 106], which is not as clearcut and direct as classic control methods and is therefore also called "soft-computing". In [74] fuzzy control is applied to internal control which only relates to internal values such as proprioceptive sensation. In [106] fuzzy control is applied to a more general task than gait and is therefore extended by a learning ability. But it is also reduced to simple measurements such as length and angle from the proprioceptive sense.

Another group of position control models for human stance and gait are the statistical estimation models. The estimation of system states is used as feedback to stabilize the system. Estimation requires model knowledge of the system and the sensors. This is

represented here as Kalman estimation or in a more general way as Bayes estimation. The Bayes approach for head position estimation with several sensors is detailed in [47, 99]. For both, the statistical idea is that the control of upright stance is absolutely essential for human survival. Frequent falls would have been a serious handicap for escape, defense or other simple daily tasks. It is not important that the individual movement or control task is optimized absolutely but that the statistical procedure is optimized and robust over all control tasks. This solution is therefore an interesting approach for biological models. Wolpert [98] states for cognition models that: *"... Bayesian Decision Theory. This theory defines optimal behaviour in a world characterized by uncertainty, and provides a coherent way of describing sensorimotor processes."* (p.319)

Kalman filters which base on the Bayesian theory are common models for estimation and observation filters applied to technical systems [162]. The linear Kalman filter has been proved to give the optimal estimation for white Gaussian processes [190]. The Kalman filter approach was therefore selected for this thesis in order to develop a high-level control model incorporating multisensory processing and model knowledge. Another reason is that with too simple or static approaches the sensory information fusion does not reproduce the complete spectrum of functionality. For this reason a statistical model based on posture control seemed an appropriate approach here.

Examples of Kalman estimation models for biological stance control with multiple sensors are e.g. those developde by van der Kooij et al. [179, 180], Jeka et al. [136, 14] and Kuo [96, 6, 97]. In [179] the Kalman filter is not linear but extended by a nonlinear noise covariance description. This nonlinearity leads to a decreasing gain of sway response with increasing sensory inputs. In [96, 6, 97] the sensors are state-dependent sensory models which are integrated in the linear posture control model with an estimation for the sagittal plane stance. The optimal feedback control strategy is varied with different control objectives and time delays to establish the differences for different control strategies which are compared with experimental findings. The experimentally found hip and ankle strategies are reproduced by slightly changing one parameter which defines the ratio of COM control objectives to angular position. In [97] the sensory models are developed further. This thesis examines wether the loss of a sensory modality such as vision or the vestibular sense stimulates increased postural response. The change in sensory modalities with increasing age is also modeled and explained by decreasing signal-to-noise-ratios, which lead to less information being gathered by sensory input. In [14] the difference between presence and lack of model-knowledge of the environment are compared. The conclusion is that an unmodeled environment gives simulation results which are closer to experimental data.

Another question relates to the form in which the information from the sensors is processed, especially the information from visual sensors. This is investigated in the control model described by Oie et al. [80]. Velocity seems to be the most effective information type. Freeman et al. [34] also found the velocity information to be the main processing cue in visual motion perception.

4.2 Sensory Models

The sensors named before can be described by different sensory and cognition models which are further integrated into the high-level posture control concept.

There are three main types of sensors which influence walking movements and which are detailed further. First, there is the vestibular sense located in the inner ear. The vestibular sense consists of the otoliths which sense the translational accelerations of the head and the semicircular canals which sense the rotational accelerations of the head. Second, there is the visual sense, the eyes. Here a retinal image is produced and processed. And third, there is the complex of somatosensoric and proprioceptive sensors which cannot be named nor located as this complex is not centralized in one organ and the exact mechanisms and interactions are not completely known. In this thesis the somatosensoric perception is based on the definition of [150, 185], perception of influences of the skin e.g. tactile inputs, temperature inputs and not on the body surface but deeper structures like the proprioceptive sensory cues. The proprioception is the sensing of one's own properties. This means sensing of the relative position of two body segments or the applied torques to a joint which are related to the muscle and joint sensors. In chapter 3 the muscular stretch receptors have already been explained in section 3.4.2. This sensory feedback which is directly coupled to the low-level muscular activation loop belongs to the local proprioceptive sensors. The direct joint and muscle feedback used in the low-level model has also a high-level component as the proprioception is certainly an input to high-level decisions and intentions. And there are also other parts of the proprioceptive perception which are more high-level and therefore integrated with other sensory cues. This means that there are determined commands for a whole body position and balance control.

In this thesis only the proprioception is considered according to [150]. Neither the somatosensory cues nor e.g. the auditive sensory cues are modeled and integrated in the model as it is concerned not to be the most important information for posture control.

4.2.1 Vestibular Sense

To explain the components of the vestibular organ in a simple manner it can be said: the vestibular organ consists of a symmetric pair of two organs positioned symmetrically in the head. The exact position can be seen in figure (4.1). Each vestibular organ consists of the three semicircular canals and the otoliths, maculae and sacculae. The semicircular canals serve to measure the rotational accelerations and the otoliths to detect the translatoric and gravitational accelerations. In a standing position the movements of an inverse pendulum are relatively small which leads to the approximation of the vestibular sensation, which is in the following only rotational accelerations. The otoliths are subject of research in literature in e.g. [31, 76, 75]. For the presented model only the semicircular canals are modeled.

The vestibular semicircular canals are a well analyzed sense and there are many examples in literature to name only a few [44, 166, 81].

The semicircular canals according to [62, 192, 13] are ordered in a nearly orthogonal position to each other see figure (4.1). A canal is a tube filled with fluid (endolymphe). A membrane (cupula) which is spanned across the tube cross section is moved by head acceleration. Finally, this movement causes in the afferent nerves an action potential which encodes the head velocity and acceleration. These potentials are transmitted to the brain stem by frequency modulation and relative timing of the action potentials.
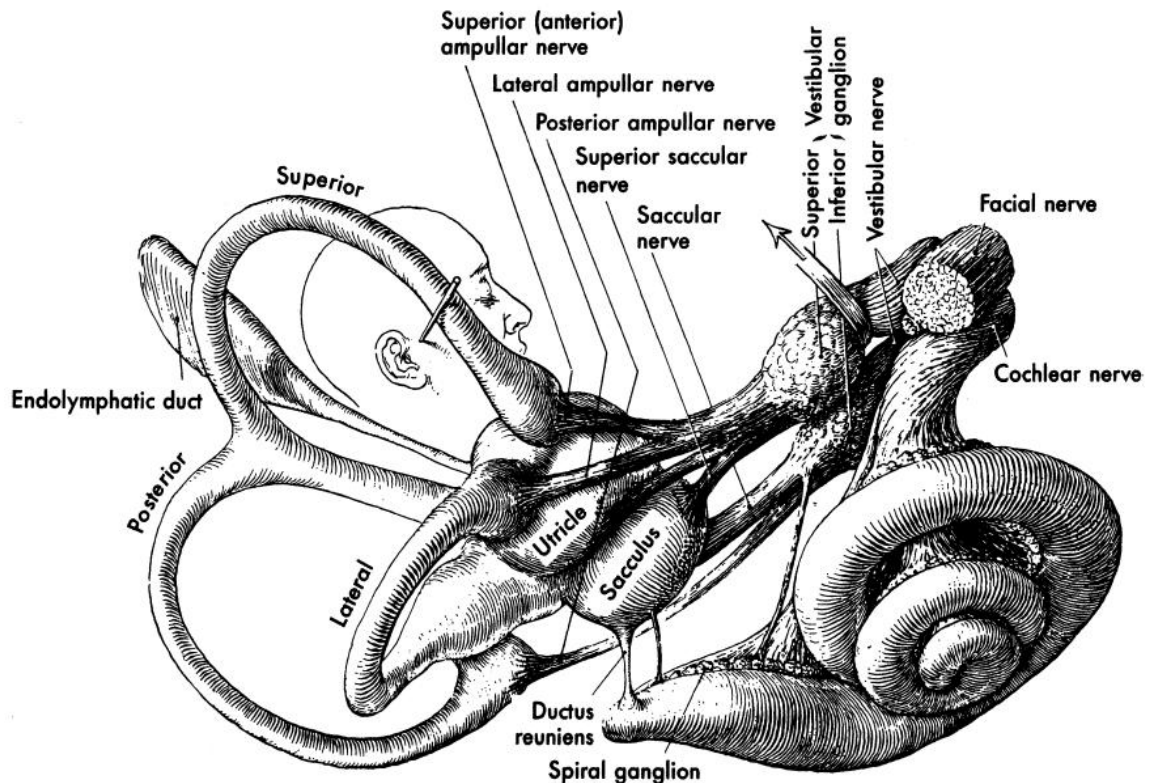
Figure 139-1. The vestibular end organs. (From Brodel M: *Three unpublished drawings of the anatomy of the human ear,* Philadelphia, WB Saunders, 1946.)

Figure 4.1: The vestibular organ [13].

The transfer function for the semicircular canals as found in [192] and in [13] is derived from a fluid-filled torsional pendulum. The angle of cupular deflection x_{scc} is determined by the difference of angular head movement x_{head} which is in an inverse pendulum model identical to the angular system state x subtracted by the movement of endolymphe X_e in the semicircular canal. The sum of torques which is the head acceleration multiplied by the moment of inertia is identical to the sum of the resulting viscous and the elastic torques. The viscous torques are defined according to the fluid mechanics of a laminar flow in a thin tube which results in a torque proportional to the fluid velocity. The elastic torque is defined according to a pendulum model where the torque is proportional to the

angular deflection of the membrane x_{scc}. So the resulting model is given in equation 4.1

$$\ddot{x}_{scc}(t) = \ddot{x}(t) - K_1 * \dot{x}_{scc}(t) - K_2 * x_{scc}(t) \tag{4.1}$$

where K_1 and K_2 are the proportional gains for the viscous and elastic torques in combination with the inertia. A more detailed explanation of this equation is given in [192, 13]. This formula is transformed to Laplacian form and the gains K_1 and K_2 are transformed to the time constants T_{scc1} and T_{scc2}. Where $T_{scc1} * T_{scc2} = \frac{1}{K_2}$ and $T_{scc1} + T_{scc2} = \frac{K_1}{K_2}$. The equation is as follows:

$$\frac{y_{scc}(s)}{\dot{x}(s)} = \frac{T_{scc1} * T_{scc2} * s}{(T_{scc1} * s + 1) * (T_{scc2} * s + 1)} \tag{4.2}$$

Equation 4.2 stands for the transfer function of the semicircular canal, where according to the other sensory models $\dot{x}$ is the system or head velocity and y_{scc} is the sensed membrane (cupula) deflection resulting from head movement. T_{scc} are two time constants which describe the torsional pendulum model. Again this system can be given in state space form and the equation therefore is:

$$\dot{x}_{scc}(t) = A_{scc} * x_{scc}(t) + B_{scc} * u_{scc}(t)$$
$$y_{scc}(t) = C_{scc} * x_{scc}(t) + D_{scc} * u_{scc}(t) \tag{4.3}$$

where x_{scc} is the state of the vestibular organ and the input u_{scc} is the head velocity $\dot{x}$. The matrices $A_{scc}, B_{scc}, C_{scc}, D_{scc}$ are constant matrices. The external applied vestibular stimulation which is added via the skin to the nervous signal is therefore not included in the B_{scc} term but in the following transfer function.The transfer function for the afferent nerves is approximated with a filter with equation which is given according to Goldberg et al. [44]:

$$\frac{y_{vest}(s)}{y_{scc}(s) + GVS(s)} = \frac{y_{vest}(s)}{u_{vest}(s)} = g_{na} \frac{t_a * (t_r * s + 1)}{t_a * s + 1} \tag{4.4}$$

where t_a is the time constant for adaptation and t_r for the high frequency behavior and g_{na} is a gain factor of the vestibular nerve transfer function.

$$\dot{x}_{vest} = A_{vest} * x_{vest}(t) + B_{vest} * u_{vest}(t)$$
$$y_{vest} = C_{vest} * x_{vest}(t) + D_{vest} * u_{vest}(t) \tag{4.5}$$

where x_{vest} is the state of the vestibular nerve and the nerve signal u_{vest} consists of the natural impulse of the semicircular canals and the galvanic stimulation which is directly applied on the nerve over electrodes pinned to the skin.

4.2.2 Proprioception

The proprioception is a sense not located in one organ but distributed over the body and often not exactly traceable. In literature there are many studies for proprioceptive

influence to the body system for balance, orientation and position control [77, 64, 119, 121, 117, 82, 199]. In [180, 97] the proprioceptive cue on high-level is represented by a bandpass transfer function. This bandpass-filter model according to Kuo [97] is used here. The proprioceptive transfer function couples the complete body position e.g. angular position, COM, COP or ZMP position with the sensed position and the sensory outputs. Here the equation in Laplace and state space form is:

$$\frac{y_{prop}(s)}{x(s)} = \frac{(T_{sp} * s + 1)}{(T_{sp} * \alpha * s + 1)} \tag{4.6}$$

which is written in state space form as:

$$
\begin{aligned}
x_{prop}(t) &= A_{prop} * x_{prop}(t) + B_{prop} * u_{prop}(t) \\
y_{prop}(t) &= C_{prop} * x_{prop}(t) + D_{prop} * u_{prop}(t)
\end{aligned}
\tag{4.7}
$$

with the state of the body x and the state of the proprioceptive sensory system x_{prop}. y_{prop} is the measurement output of the proprioceptive cue, T_{sp} is a time constant, α a gain constant. u_{prop} is an input to the proprioceptive system which is the body state x here the angular position of the body center of mass, $A_{prop}, B_{prop}, C_{prop}$ and D_{prop} are constant matrices.

Another proprioceptive system which needs to be explained, is the sensory system of the eye movements. As the visual system information is a combination of retinal image information, proprioception and vestibular coupling, this is best seen and studied in compensatory eye movements to stabilize the gaze e.g. on a target. These are non-guided movements which are not voluntary but reflex movements according to a internal coupling of eye motor control with the vestibular system e.g. in the vestibulo occular reflex VOR [184]. Smooth eye pursuit with slow eye movements are of interest in this work. So the proprioceptive sense for such movements is modeled. Here the eye movement transfer function is modeled as an estimation of the eye velocity which is given by the efference copy of the motor command.

An idea of [155] of a eye pursuit transfer function is a time-delayed low pass filtered velocity signal with a gain. The earlier idea of a visual model of [154] was also taken by [97] to represent the visual sensory with an integrated model for general visual velocity perception. In this work the interaction between the retinal image and the eye movement is studied which leads to two separate models for representation of human visual and pursuit movement perception which are integrated in the system which represents the visual motion perception.

For a smooth pursuit eye movement the eye consciously follows a target. The eye velocity depends on the head movement and on the target velocity $\dot{u}_t$. If the gaze is always fixed to the target it is assumed:

$$y_{eye} = (\dot{u}_t - \dot{x}_{head}) * const \tag{4.8}$$

with $const = 0.75 \dots 0.95$.

The *const* factor already considers a certain degree of inaccuracy and time delay. As Niemeier et al.[135] mentions, these reasons for the underestimation of the signal y_{eye} may be because of the calculation of this signal which bases on the comparison of an efference copy with the proprioceptive signal. And of course there is always a time delay also in the visual processing cue which is mainly the reason for a delayed and therefore inaccurate pursuit movement [137]. If the eye movement is correlated to the sensed image velocity there is an additional transfer function which represents this velocity sensation. This is studied in Robinson et al.[155] where a simple low pass characteristic with delay is the simplest internal model of the eye velocity signal. Equation 4.8 is expanded by the low pass characteristics which gives the transfer function used in the following work:

$$\frac{y_{eye}}{(\dot{u}_t - \dot{x}_{head})} = const * \frac{1}{T_v * s + 1} \tag{4.9}$$

with T_v is the time constant of the low pass filter. This equation approximates eye pursuit movements which are below a threshold velocity value. If the velocity or acceleration becomes to high a smooth pursuit is no longer guaranteed. The eyes can move with very quick, so called saccadic, eye movements. In this case this model will no longer represent the eye movements. In the experiments it was guaranteed that only smooth eye pursuit movements are tested.

The state space equation for the transfer function above is given with:

$$\begin{aligned} \dot{x}_{eye}(t) &= A_{eye} * x_{eye}(t) + B_{eye} * u_{eye}(t) \\ y_{eye}(t) &= C_{eye} * \dot{x}_{eye}(t) \end{aligned} \tag{4.10}$$

4.2.3 Visual Sense

The visual system, the eyes, sense light, which means that images are projected to the retina which are processed for further properties. If the image moves on the retina this is called retinal slip or retinal velocity. There are many phenomenons of visual sensation. In the following only the sensing of velocity or movement will be considered. Movements of the surroundings in relation to the body is an important information and influences standing and stepping tasks. The movement can be extracted of the retinal slip or the optic flow. As found by [46, 47] it also can be extracted as a combination of the eye movement signal and the retinal signal which together represent the internal measurement of velocity. The detection of motion can be achieved by the retinal slip of the projected image. If the eyes pursue an object the signal to control the eye motion is taken as efference copy and compared reafferently to the retinal image motion to get the difference. The difference represents the sensing of motion. In experiments in [46] it is shown that a stationary retinal image which is produced by pursuing a moving target is perceived as moving target. But a moving retinal image which is produced by eye movements is perceived as stationary [46]. Which leads to the conclusion that subjects can clearly separate the background movement from the object movement.

The classical model to represent and interpret human motion perception during combined

eye movement y_{eye} and retinal image movement y_{ret} is according to Holst and Mittelstaedt [188, 187] a linear combination of those two velocities. This was extended by Freeman and Banks [35] by gain factors to explain certain phenomenons of how eye movement influence the perceived velocities. The velocity measurement is the difference of the amplified retinal y_{ret} and eye velocity y_{eye}. This leads to the equation which interprets visual perceived velocity of motion y_{vis} as a weighted difference:

$$y_{vis} = g_r * y_{ret} - g_e * y_{eye} \qquad (4.11)$$

with gain factors g_r and g_e with $\frac{g_e}{g_r} < 1$. This model does not reflect the motion sensation for higher velocities. For higher velocities the perception becomes clearly nonlinear and there is an effect of saturation [177, 165]. The nonlinear relation of perceived velocity dependent on eye movement and retinal velocity is defined by Turano and Massof [177] which is quasi linear near the zero velocity and asymptotic to a maximum value $R_m/2$ for higher positive or negative velocities. Here the mapping of real eye and retinal velocities to the internal estimated velocities is nonlinear and saturating. The formula derived in [177] to represent this mapping is as follows:

$$y_{vis} = f_r(\dot{x}_{ret}) - f_e(\dot{x}_{eye}) \qquad (4.12)$$

$$y_{vis} = R_m * \left(\frac{1}{1 + exp(-g_r * \dot{x}_{ret})} - \frac{1}{2} \right) \quad - \quad R'_m * \left(\frac{1}{1 + exp(-g_e * \dot{x}_{eye} - g_i * \dot{x}_{ret})} - \frac{1}{2} \right)$$

where the gain g_i describes the influence of the retinal velocity on the eye movement.

Goltz et al. [47] show in experiments that the perception of velocity can not be represented by a summation of retinal and eye velocity but that there is a multiplicative term. This indicates that there is a dependence of spatial structure of the retinal image and the eye velocity signal. In the experiments of [47] the velocity perception of an object in space is represented by a nonlinear combination between the retinal image and the eye velocity for retinal image parts where the illumination gradients $\frac{dI}{dx}$ are unidirectional. The formula is:

$$y_{vis} = \left(\frac{dI}{dx} \right)^+ * \left(\frac{dI}{dt} + \frac{dI}{dx} * y_{eye} \right) \qquad (4.13)$$

where I is the retinal image intensity which has a spatial derivation according to the location on the retina $\frac{dI}{dx}$ which represents the direction of the movement and a time gradient $\frac{dI}{dt}$ with which this image moves along the retina. The y_{eye} is the velocity of the eye movement. If the brain knows the spatial and the time gradient it can compute the image velocity $\frac{dx}{dt} = \left(\frac{dI}{dx} \right)^{-1} * \frac{dI}{dt}$ but the inverse of vector $\frac{dI}{dx}$ is not uniquely defined. The least-square-fitted solution is taken which is a Moore-Penrose pseudoinverse labeled by $()^+$.

The retinal processing is described in Yang et al.[197] as an approximated low pass filter. Yang says that the transfer function from light entering the human eye which is afterwards sampling the continuous spatial variation by several cell types and its resampling can be described by a low pass filtering. The primary processing of retinal information y_{ret} is

therefore described by the following transfer function:

$$\frac{y_{ret}}{u_{ret}} = \frac{1}{1 + t_r * s} \tag{4.14}$$

where u_{ret} is the spatial variation of light on the retina. Here only the velocity component is of interest. Therefore u_{ret} is the velocity of the visual stimuli which is processed on the retina. In the next paragraph it is explained that this stimuli is a combination of eye velocity y_{eye} and external inputs to the eye as e.g. movements of the environment which are represented by u_b and which has already been presented in the classical equation 4.11 to represent velocity perception. The time constant of the retinal filtering is t_r.

In state space notation this transfer function is:

$$\begin{aligned}
\dot{x}_{ret}(t) &= A_{ret} * x_{ret}(t) + B_{ret} * u_{ret}(t) \\
y_{ret}(t) &= C_{ret} * x_{ret}(t) + D_{ret} * u_{ret}(t)
\end{aligned} \tag{4.15}$$

The characteristics of visual velocity perception found in [167] are that the standard deviation of the visual perception likelihood is proportional to a logarithmic velocity function. The prior probability decreases with a velocity power law which brings about saturation effects for high velocities.

This leads to the following model, representing the sensing of visual motion, which was developed for the postural model in this thesis. The measured visual motion is the velocity y_{vis} which is in general a sum of an estimation of the retinal velocity y_{ret} and the eye velocity y_{eye}. The proportionality to the real velocity is a logarithmic function which is derived the Weber-Fechner law. This correlates to the finding of [167, 197] that the likelihood has logarithmic characteristics and the function of [177] has a similar characteristic. The Weber-Fechner law is explained below in the next subsection in more detail. The measured motion by the visual sensory system is calculated as follows:

$$\begin{aligned}
y_{vis} = c_{vis}(y_{ret}, y_{eye}) = \\
= (sign(y_{ret}) * ln(|y_{ret}| / x_{r0} + 1) - (sign(y_{eye}) * ln(|y_{eye}| / x_{e0} + 1)
\end{aligned} \tag{4.16}$$

where the representation of eye and retinal movement is each correlated to a threshold x_{r0}, x_{e0}. Those thresholds stand for the movements which can just not be measured because they are too small. In [167] for retinal movement this value was given with $0.3[deg/sec]$. For larger velocities the perceived velocity does not raise linearly but logarithmic which leads to a saturation effect. The faster the movements the lesser is the gain of the perceived movement which also means that the influence of a perceived movement does increase first nearly linearly and then less an lesser with increasing velocity. The final model representing perceived visual velocity y_{vis} is therefore determined by the difference of the eye velocity and the retinal image velocity y_{ret} which is influenced by the external visual scene which will be represented as a visual background with defined velocity u_b. The measurement scale of the model is a logarithmic one.

Weber-Fechner Law

The Weber-Fechner law was introduced by Ernst Heinrich Weber and Gustav Theodor Fechner to describe the relation between the objective physical and subjective perceived stimuli. The law consists of the Weber law which says that the just noticable change of a stimulus in relation to the actual stimulus is constant:

$$dx_p = k * \frac{dx_s}{x_s}$$

where dx_p is the just noticable differences perceived, x_s is the actual stimulus, and dx_s is the change of the stimulus. This means that the relation of the stimulus change related to the actual stimulus value at that instant, multiplied by a constant factor k, is proportional to the just noticable difference. Fechner found that this relation is logarithmic. The Fechner law extends this law by integration, under the assumption that the constant relation factor k is independent of the actual stimulus x_s this leads to the Weber-Fechner law:

$$x_p = k * \ln x_s + c = k * \ln x_s - k * \ln x_{s0} = k * \ln \frac{x_s}{x_{s0}} \qquad (4.17)$$

where c is the integration constant which also can be represented by a logarithmic x_{s0} multiplied by a constant factor, x_{s0} is the minimal threshold of perception.

The Weber-Fechner law is applied to many senses as the haptic sense, the taste sense or very commonly for the sensing of light intensity. This describes the intensity of the sensation which is proportional to the logarithm of the stimulus. In this thesis the Weber-Fechner law is applied to represent visual velocity perception. The sensed visual movement y_{vis} has a logarithmic characteristic which means that the measurement is logarithmic. The sensor has the logarithmic property that for lower sensor value the transfer function is nearly linear but for higher sensor values the transferfunction becomes clearly nonlinear. For very high velocities this is not applicable but the velocity range applied in this thesis refers to normal everyday visual motions of moving objects which do not exceed these ranges.

Simoncelli et al. [167] propose an optimal observer construct to represent the visual speed perception. The precise noise characteristics are unknown. Also Rao et al. [148] found good behavior of optimal estimation approaches for representing the visual perception. The statistical observer is named as a 'best guess' of the world for the actual sensory information and the model or prior knowledge which is cited by [167] from [186]. In this thesis the visual sensory cue as the other sensory cues are integrated in an optimal estimator the Kalman filter which is proposed in the next section 4.3.1. The Kalman filter is a linear estimator and has to be extended to represent such nonlinear visual perception cues which is detailed in the Kalman description in section 4.3.3.

4.3 Estimation for Posture Control

The statistical estimation, the Kalman filter, is detailed in the following and applied to the posture control. This demonstrates the integration of sensory information into posture control. The sensor integration is shown for linear visual sensory models and nonlinear which lead to an extension of the Kalman filter. A negative feedback loop for posture control is derived supporting and complementing the properties of the Kalman state estimation. The sum of all this is the posture control model, developed to simulate sensorimotor dependencies for the task of keeping the body in balance.

4.3.1 The Kalman-Filter Theory

To sum up the functioning of the Kalman filter shortly it can be said: the Kalman filter estimates the next system states by using a priori knowledge. The estimated state depends on the conditional probability density function. This a priori knowledge is completed by using the measurements of the system states as innovative information. Additionally the innovation is compared by subtraction to the a priori expected measurements. The resulting difference is called residual. The residual is weighted by the Kalman gain and added to the a priori knowledge about the system to receive the final estimate. The needed a priori information is the system and sensory dynamics, the noise statistics of model and measurements, the initial values for system states and error statistics. All Kalman Filter equations can be applied to continuous time-variant signals (Kalman Bucy Filter) or also to discrete signals. In the following the discrete Kalman filter is introduced. The quantization is done in steps k. So it is determined: $t(\tau) = t_k$ and the next quantization step is $t(\tau + \delta) = t_{k+1}$ with δ is the quantization step size. The continuous-time matrices have to be discretized with an appropriate method e.g. an Euler method. The biological system is more a continuous time system but the implementation is discrete.

The Kalman estimation filter bases on a linear model representation of the system:

$$x_{k+1} = A * x_k + B * u_k + W * w_k \tag{4.18}$$

x_k	:	vector of system states of the model at time k
A	:	interaction between the last state x_k and the next step x_{k+1}
u_k	:	vector of external inputs to the system
B	:	filter matrix to represent the interaction of external influences e.g. from the environment on the system
w_k	:	vector of stochastic noise which is white Gaussian noise with a mean of zero
W	:	Noise gain matrix which filters the noise effects on the system states

Table 4.1: Kalman vectors and matrices for the state model

The output of the system in form of measurements is represented by a linear relation. It

consists of the measurements and the external inputs and noise at time step k by:

$$y_k = C * x_k + D * u_k + v_k \tag{4.19}$$

y_k	:	vector of measurements at time k
C	:	filter matrix which relates system states with measurement output
u_k	:	vector of external inputs to the measurement system
D	:	filter matrix which represents the interaction of external influences with the measurements
v_k	:	vector of stochastic noise which is white Gaussian noise with a median of zero

Table 4.2: Kalman vectors and matrices for the sensory measurements

The statistical error sources as noise are modeled and the error between estimation and real measured values is updated with a time varying gain, the Kalman gain, to receive the next estimation. The characteristics of the noise models are always white, Gaussian and zero mean. The covariances of the noise is described with:

$$E\{w_k\} = E\{v_k\} = 0 \tag{4.20}$$

$$E\{w_k w_j{}^T\} = Q \quad E\{v_k v_j{}^T\} = R \tag{4.21}$$

$$E\{v_k w_k{}^T\} = 0 \tag{4.22}$$

with E is the expectation and $E\{x\}$ is the expected value of x, j is as k a index of time. Q and R are the noise covariance matrices of the system and the measurement noise. In equation 4.20 the zero-mean of the noise process is presented. Equation 4.21 determines the covariances of noise and in equation 4.22 it is shown that the noise processes of system and measurements are uncorrelated. The error covariance matrices Q and R have to be determined for the model to determine the reliability of e.g. a measurement. The bigger a single R value is, the less a single measurement is weighted for the innovation of new estimation, because the reliability is low and vice versa. The Kalman filter minimizes the expected error between estimation and real state by minimizing the error covariance matrix P. To minimize this error covariance P, the Riccati equation is used. The discrete Riccati equation is:

$$P_k = A * P_{k-1} * A^T + W * Q * W^T - P_{k-1} * C^T * (C * P_{k-1} * C^T + R)^{-1} \tag{4.23}$$

This calculation of the error covariance matrix P is realized in two steps, the prediction (equation 4.24) and the correction (equation 4.25) as it was called by [190] which is one a priori estimation and afterward the a posteriori update.

$$P_k^- = A * P_{k-1} * A^T + W * Q * W^T \tag{4.24}$$
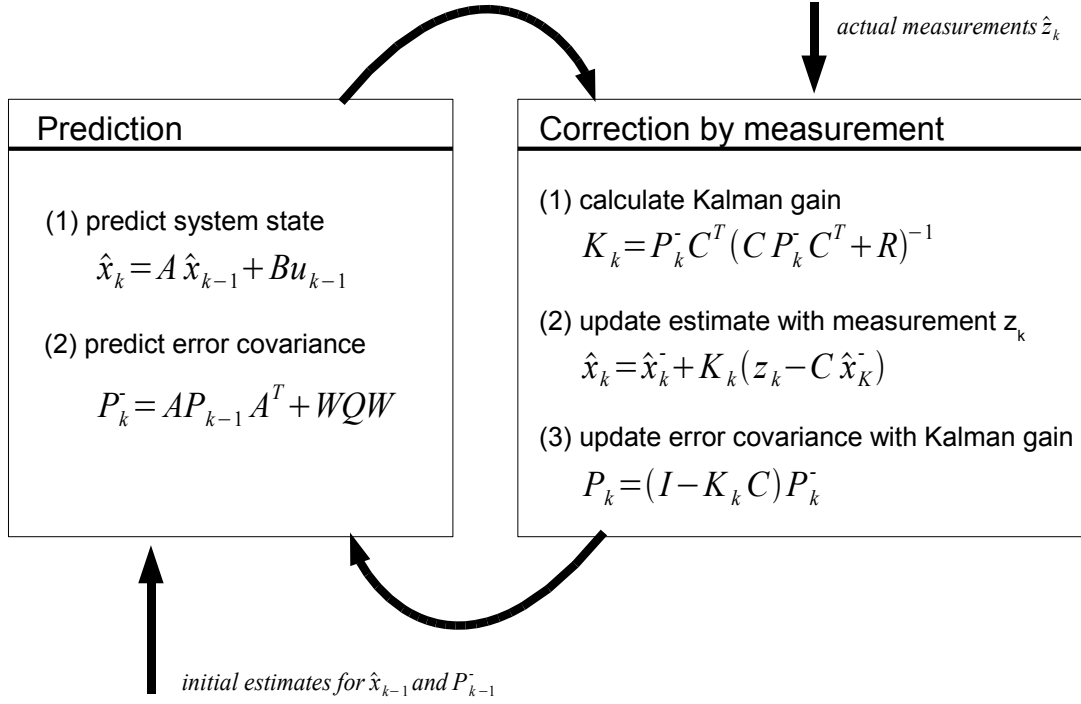
Figure 4.2: The two phases of a Kalman filter: the prediction according to the internal model and the updating and correction by the input of actual sensory data.

and

$$P_k^+ = (I - K_k * C) * P_k^-$$ (4.25)

This minimization is transferred to the optimal Kalman gain which amplifies the measurement residual to update the estimation. This optimal Kalman gain K is calculated by the multiplication of the error covariance with the measurement and the measurement noise covariance matrix. The Kalman gain minimizes the a posteriori error covariance P_k^+ with:

$$P_k^+ = E\{(x_k - \hat{x}_k)(x_k - \hat{x}_k)^T)\}$$ (4.26)

So the Kalman gain has the following formula:

$$K_k = P_k^- * C^T * (C * P_k^- * C^T + R)^{-1}$$ (4.27)

The estimation of the next system state $\hat{x}$ is therefore:

$$\hat{x}_k = \hat{x}_{k-1} + K_k * (y_k - C * \hat{x}_{k-1}) \quad with \quad \hat{x}_{k-1} = A * x_{k-1} + B * u_{k-1}$$ (4.28)

The schematic of the Kalman equations can be seen in figure 4.3.1. The Kalman filter predicts a system with an underlying stochastic process which is case for systems where only noise measurements of the real states of the system are available. The discrete Kalman filter is a recursive statistic estimation method which minimizes an optimization criterion the error covariance matrix P. The a priori estimation $\hat{x}$ depend on all a priori known measurements. The recursion only takes the preceding estimation value which is already a mean value over all past estimation values. This is a Markov process as only the last value is directly used for the calculations. The Kalman gain is related to the covariances of the measurement model C, the expected error covariances P and the measurement noise covariances R. This can be seen in equation 4.27. If the system and measurement models do not model the reality, the measured states diverge from the real states. This is interpreted as measurement noise. The estimation procedure only slowly converges in this case because the system noise covariance matrix Q is small. If Q is increased the convergence is faster but the system is more sensitive to system noise. So, the estimation quality becomes less and system errors are less likely to be detected. If the measurement noise covariances are modeled this represents the reliability of the measurements, if R gets smaller the measurements are taken to be more reliable. Therefore the Kalman gain weights the measurements more.

4.3.2 Application of the Kalman Filter to the Stance Model

The presented sensory models can now be integrated in a posture control model. The posture which shall be controlled is the upright stance. The mechanics of stance can be represented by an inverted pendulum. This representation of a standing position is often used in literature as e.g. in [86, 138, 120, 136, 179]. In this thesis the frontal-plane mechanics are analyzed in detail. The inverse pendulum mechanics can be used for both stance models in sagittal and in frontal plane. The characteristics of the pendulum model will always depend on the special stance position constraints for the feet. So there is of course a difference if stance is analyzed with feet side by side in a narrow position or in a wide position or if the stance position is even a tandem foot position (one foot is placed in front of the other standing on one line). In the following the stance position is a very narrow position feet side by side and the lateral stance sway is analyzed. So the inverse pendulum model is identical to the mechanics of the frontal-plane model of section 2.3 if the phase is double support and the feet position is identical which means one point. For the stepping movements the double support phase was always modeled as a discrete event which occurs instantaneously between two swing phases. Now the double support phase last for the whole stance. The equation for the inverted pendulum mechanics is explained in section 2.2.1 in equation 2.2.

The movement of the mechanics is measured by the sensors. The proprioception sensors measure the sway angle Φ, the vestibular sensor measures the change of the angular velocity $\dot{\Phi}$ and for the eye movement, the visual sensor measures the velocity difference between the visual world and the self motion. This information measured by the sensors is now integrated by the brain using a statistical estimation using model knowledge ac-
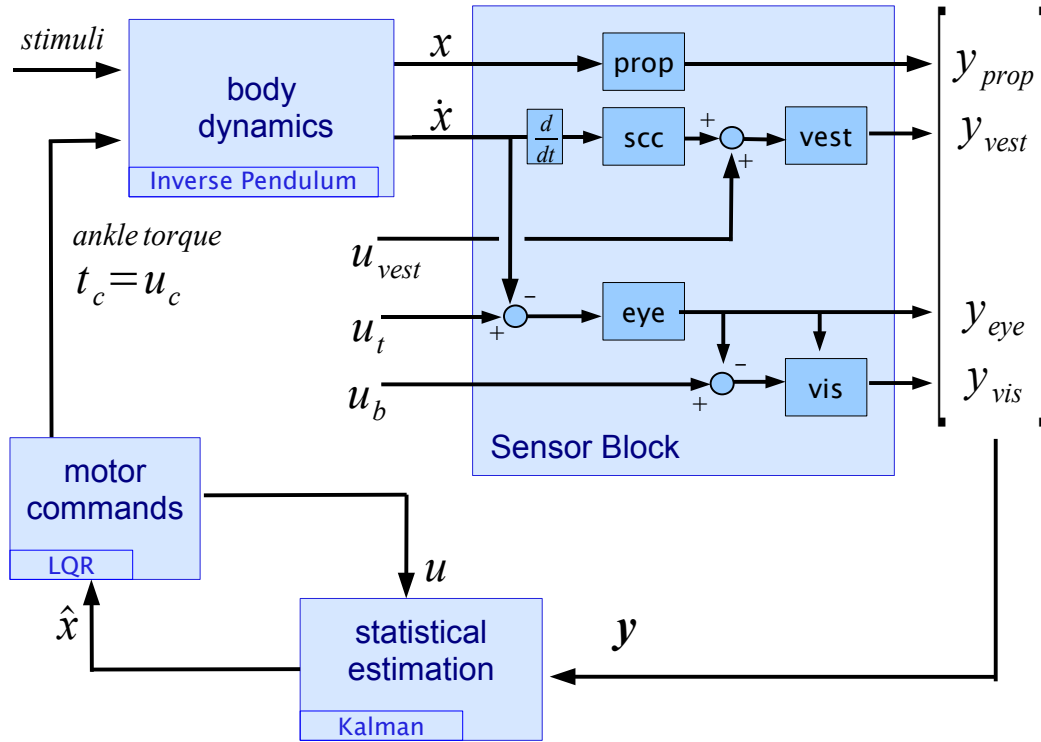
Figure 4.3: An overview of the posture control system with mechanics, sensors, statistical estimation and integration and the feedback controller.

cording to experiences and these actual measurements. The integration results in motor commands, here represented as ankle torques, that stabilize the standing body. This system of mechanics, measurements, integration and command generation is shown in figure 4.3.

The part of the integration is a complex task of the brain and only little is known about the internal processes. For reasons already named in the introduction of this chapter and because it is well known in literature the integration in this thesis is implemented as an estimation filter with model knowledge. The estimation is realized by a Kalman filter. Therefore the model knowledge of the system which is represented by an inverse pendulum and the sensors which are described and modeled as in 4.2 according to their physical and cognitive properties. This model knowledge is used together with the sensory measurements in a Kalman filter to estimate the system and sensory states a priori. This estimation is like an expectation and a priori knowledge of not yet received and processed system information on base of statistical knowledge. The continuous sensory models are transformed in a state space representation as required for the Kalman filter and discretized by the Forward Euler Method with the following equation:

$$A = I + \delta * F \quad and \quad B = \delta * \Xi \tag{4.29}$$

where I is the identity matrix and δ is the time step between $t(\tau) = t_k$ and $t(\tau + \delta) = t_{k+1}$. The state space transformation was simulated in MATLAB with the **tf2ss** function. The sensory measurements are not only influenced by the system states and the external influences but by the last internal state as they have integrating or derivating properties. This leads to the representation of the Kalman system states which includes the mechanical states as well as the sensory states. The state vector of the Kalman filter to estimate the system is $\mathbf{x} = (x, \quad \dot{x}, \quad x_{prop}, \quad x_{scc}, \quad \dot{x}_{scc}, \quad x_{vest}, \quad x_{eye}, \quad x_{vis})$ which is x the mechanical angular state of the body, $\dot{x}$ its velocity, x_{prop} the state of the proprioceptive sensor, $x_{scc}, \quad \dot{x}_{scc}, \quad x_{vest}$ the vestibular states to sense angular accelerations, x_{eye} the proprioceptive state of the eye movement and x_{vis} the visual sensory state of the retinal velocity. The measured values by the four sensory models are the vector $y = (y_{prop}, \quad y_{scc}, \quad y_{eye}, \quad y_{vis})$ which is the proprioceptively measured position, the acceleration of the roll movement sensed by the vestibular semicircular canals, the sensed eye velocity and the measured retinal velocity which gives a retinal signal and is processed for visual velocity measurement. As external inputs to the system from the environment the vector is $u = (u_c, \quad u_t, \quad u_b, \quad u_{vest})$ which are the corrective torque applied to the joints of the mechanics, the target velocity of the target which is fixated by the eyes, the background velocity which is visually sensed and the galvanic stimuli which is applied to the vestibular nerve.

For the inverse pendulum model the upright stance is controlled by the corrective torque applied to the ankle joint which can be seen in figure 2.2 with $u_c = \tau_a$. The eyes and the vestibular organ are situated in the head and are therefore modeled at the top of the inverse pendulum. The angle and angular velocity of the pendulum are therefore the same as measured by the sensors. As stimulations to the system different signals are applied. The visual fixation target is a moving point which is fixated with the eyes so a pursuit movement is the result. The equation for this relation was given in 4.9. Where the input u_t is the velocity of the pursued target and the output is the eye velocity y_{eye}. The retinal image is the combination of the different visible object movements. In this work there is used a stationary or moving background and a pursued target which was also moved or stationary. The model for sensory information processing for vision was derived in section 4.2. The input is the background movement u_b and the eye movement y_{eye} which are combined to the output y_{vis}. In the linear case the visual sensory cue is determined by equation 4.11 in the nonlinear case by equation 4.16. Finally, the vestibular sense can be stimulated artificially by an externally applied stimulus to the vestibular system u_{vest}. This externally applied stimulus is summed up to the vestibular signal of the rotational acceleration. This was explained in equation 4.3 and 4.5.

The system model and sensory models are integrated in the Kalman filter in the following. All the states are integrated in the state vector x, the system inputs are the vector u and the measurements of a single sensory system are represented by vector y. The general system equation for the Kalman filter is therefore:

$$x_{k+1} = A * x_k + B * u_k \tag{4.30}$$

and the measurement system is:

$$y_k = C * x_k + D * u_k \tag{4.31}$$

The single matrices of equation 4.30 and 4.31 are as follows. The state matrix A of all states is:

$$A = \begin{pmatrix} A_{mech} & 0 & 0 & 0 & 0 & 0 \\ B_{prop} & A_{prop} & 0 & 0 & 0 & 0 \\ B_{scc} & 0 & A_{scc} & 0 & 0 & 0 \\ B_{vest} * D_{scc} & 0 & B_{vest} * Cvest & A_{vest} & 0 & 0 \\ -B_{eye} & 0 & 0 & 0 & A_{eye} & 0 \\ 0 & 0 & 0 & 0 & 0 & A_{vis} \end{pmatrix} \tag{4.32}$$

The matrix to apply the external inputs to the mechanical system and the sensors is matrix B with:

$$B = \begin{pmatrix} B_{mech} & 0 & 0 & 0 \\ 0 & 0 & 0 & 0 \\ 0 & 0 & 0 & B_{vest} \\ 0 & B_{eye} & 0 & 0 \\ 0 & -B_{vis} & B_{vis} & 0 \end{pmatrix} \tag{4.33}$$

For the measurement matrix C the measurement terms of all sensors are integrated in one matrix which is:

$$C = \begin{pmatrix} D_{prop} & C_{prop} & 0 & 0 & 0 \\ D_{vest} & 0 & C_{vest} & 0 & 0 \\ -D_{eye} & 0 & 0 & C_{eye} & 0 \\ 0 & 0 & 0 & 0 & C_{vis} \end{pmatrix} \tag{4.34}$$

The external input to the measurement system is mapped by matrix D:

$$D = \begin{pmatrix} 0 & 0 & 0 & 0 \\ 0 & 0 & 0 & D_{vest} \\ 0 & D_{eye} & 0 & 0 \\ 0 & -D_{vis} & D_{vis} & 0 \end{pmatrix} \tag{4.35}$$

This state space model of the system and its sensors describes the influence of the external inputs to the system and its measurements. With this system model the following results are simulated and compared to experimentally found causalities. An overview of the system and Kalman filter combination can be seen in figure 4.4. This figure shows that the sensory system measures the system states which is the input for the Kalman filter innovation, the residual. The output of the Kalman filter is the estimation of the system states $\hat{x}$.
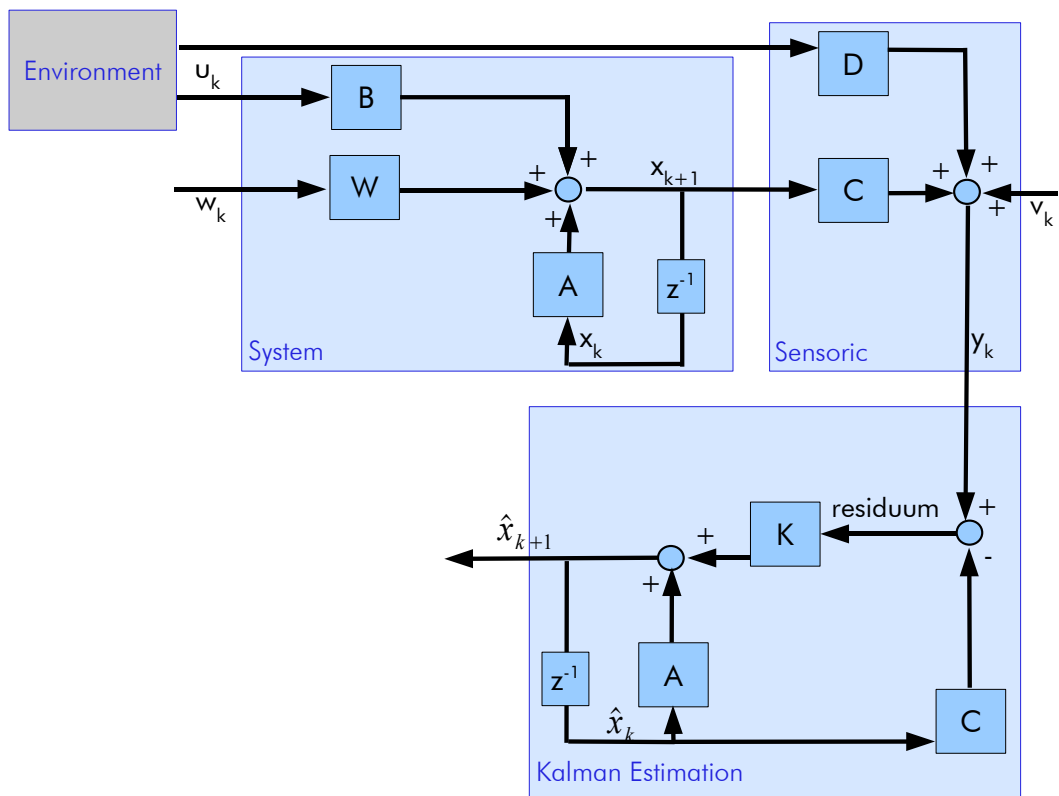
Figure 4.4: A schematic overview of the Kalman filter components in combination with system and sensors. The discrete estimation of the state x with measurement correction by the sensory output.

4.3.3 Extended Kalman for Nonlinear Sensory Models

As was already mentioned in section 4.2 the visual sensory cue is modeled nonlinearly, here logarithmically. This leads to the nonlinear measurement function 4.16 for the visual perception of velocity. In the linear case the state space representation of the visual cue is described by the low pass retinal processing of equation 4.14 or 4.15 and the linear summation of the eye movement with the environmental movement given by equation 4.11 which leads to the matrices $A_{vis}, B_{vis}, C_{vis}$ and D_{vis} mentioned above. For the nonlinear sensory cues the Kalman filter is extended in the measurement matrix. The general procedure for an extended Kalman filter is the linearization around a working point. This is the linearization around the a priori state estimation. It is done by calculating the Jacobian at the a priori state estimation. For a nonlinear measurement function C this is:

$$\left.\frac{\partial C}{\partial x}\right|_{\hat{x}} = \left.\begin{pmatrix} \frac{\partial c_1}{\partial x_1} & \frac{\partial c_1}{\partial x_2} & \cdots & \frac{\partial c_1}{\partial x_n} \\ \vdots & & & \vdots \\ \frac{\partial c_m}{\partial x_1} & \frac{\partial c_m}{\partial x_2} & \cdots & \frac{\partial c_m}{\partial x_n} \end{pmatrix}\right|_{\hat{x}} \tag{4.36}$$

This linearized measurement results in the Jacobian matrix $\frac{\partial C}{\partial x}$ which can be used to calculate the usual Kalman equations for Kalman error covariance, gain and estimation as described above. All functions are further modeled linearly except the visual velocity measurement. Therefore the velocity perception is linearized around the estimated velocity value. In case of the visual logarithmic function $c_{vis}(y_{ret}, y_{eye})$ the Jacobian matrix C_{vis} is calculated as follows:

$$\left.\frac{\partial c_{vis}}{\partial x}\right|_{\hat{x}} = \left.\begin{pmatrix} \frac{\partial c_{vis}}{\partial x_{eye}} & \frac{\partial c_{vis}}{\partial x_{ret}} \end{pmatrix}\right|_{\hat{x}} = \begin{pmatrix} \frac{sign(\hat{x}_{eye})*C_{eye}}{C_{eye}*\hat{x}_{eye}+x_{e0}} & \frac{sign(\hat{x}_{ret})*C_{ret}}{C_{ret}*\hat{x}_{ret}+x_{r0}} \end{pmatrix} = \begin{pmatrix} c_{1vis} & c_{2vis} \end{pmatrix} \tag{4.37}$$

This equation leads to a modified measurement matrix C of the sensory model with:

$$C = \begin{pmatrix} D_{prop} & C_{prop} & 0 & 0 & 0 \\ D_{vest} & 0 & C_{vest} & 0 & 0 \\ -D_{eye} & 0 & 0 & C_{eye} & 0 \\ 0 & 0 & 0 & c_{1vis} & c_{2vis} \end{pmatrix} \tag{4.38}$$

In the following the nonlinear posture control model is generated with this sensor measurement matrix whereas the linear posture control model uses the matrix given in equation 4.34.

Influence of Noise

The Kalman estimation model defines noise covariances σ_q and σ_r and the error covariance matrices Q and R which are defined in equation 4.21. They define the reliability of the system and measurements. Especially the measurement covariances can be adapted to show different sensory weightings. Oie et al. argue in [136] that if two or more sensors measure the same system state this redundancy leads to a weighting of all of these sensory

outputs. A weighting could be a mean value of all measurements of the same state. This mean value would be less noisy than the single sensory outputs. The covariances are reduced related to the number of measurements. This brings about that the measurements are given a higher reliability and so the measurements are weighted more in the model and influence it more. Kiemel [136] also defines the values of the covariances in his model to best resemble his experimentally found transfer functions. A consequence of this resemblance is that the covariances of the velocity measurements is smaller than those of the position measurements.

For the proposed model the measurement noise covariance matrix is chosen as follows. The general measurement covariance σ_R is weighted differently to the single measurement. The sum of over all weights is always one:

$$R = \begin{bmatrix} \sigma_R/n_c & 0 & 0 & 0 \\ 0 & \sigma_R/n_c & 0 & 0 \\ 0 & 0 & w_c * \sigma_R/n_c & 0 \\ 0 & 0 & 0 & \sigma_R/(n_c * w_c) \end{bmatrix} \tag{4.39}$$

with n_c = number of available sensory cues and w_c is the abstraction of amount of information delivered by the retinal system which can be the same as the eye movement or conflicting. So, if there is much retinal information available this causes a decrease of the error covariance and therefore the visual sensory cue is more relevant for the estimation process. On the contrary if the eye movement and the retinal image have opposing information the use of the visual sensory cue is less reliable so the error covariance increases and for the estimation this cue has less influence. This is especially important if the sensory cues of eye movement and retinal image have to be integrated to get a good estimation for the self-motion.

4.3.4 Optimal Linear Quadratic Regulator

The feedback of the estimated values to the corrective torque applied to the mechanics is realized by a feedback loop. This feedback is a simple PD-feedback controller which bases on an optimality criterion.
The system of a pendulum can be approximated by a linear system model for small angles. The Kalman estimator estimates all the system states of the system. This is the basis for an optimal controller. The optimal controller is a feedback controller which feeds back all the system states which are optimally weighted. This optimality is defined due to an optimality criterion or performance criterion which can be (1) the minimization of energy, (2) regulation of the system output with minimization of the distance to a desired output value, (3) time-based minimization of transitions or some more general criteria as (4) the Lagrangian criterion or the (5) Mayersches criterion according to [36]. For the linear quadratic regulator LQR this criterion J minimizes the quadratic performance criterion

which is calculated with the following equation:

$$J = \frac{1}{2} * x(T)^T * S * x(T) + \frac{1}{2} \int_{t_0}^{T} [x(t)^T * Q(t) * x(t) + u(t)^T * R(t) * u(t)]dt \quad (4.40)$$

with $x = x - x_e$ which is the deviation of the stance state x from the desired state in position and velocity. For the inverse pendulum stance model the system state $x = (\Phi).u$ is the corrective torque applied to the inverse pendulum which shall also be minimized. In the present model according to [36] the energy defined by the input to the system and the system state deviation according to an intended position are optimized. The weighting matrix Q is a symmetric positive semidefinite matrix and the matrix R is symmetric positive definite. S for the weighting of the terminal penalty cost is a positive semidefinite matrix. The final state which shall be reached is normally never achieved because of inaccuracy of the sensors, the model etc.. Therefore in the performance criterion the final state is weighted by S to receive a minimal deviation. Where the matrices can be, but do not have to be, time-dependent. To minimize J the Ricatti equation is used. This usage of the Ricatti equation resembles the optimization in the Kalman Filter. Optimal feedback control is often combined with the Kalman filter [86, 96, 179, 162, 36]. And the Kalman filter provides all states of the system in an estimation which in a natural system are normally not completely measured by sensors and therefore not available for an optimal control. A feedback of the full state vector of the system is required for optimal control. The Ricatti equation is given by equation 4.23 which is the term:

$$\dot{U} = U * B + R^{-1} * B^T * U - U * A - A * U - Q$$

which is solved for U. But to solve the equation the initial condition has to be defined $U(t_0) = S$ [36]. The resulting feedback gain is given by the term:

$$u = -K * \begin{pmatrix} x \\ \dot{x} \end{pmatrix} \qquad with \qquad K = R^{-1} * B^T * U \qquad (4.41)$$

The feedback of the optimal linear regulator is the weighted angular position vector of system states x in a negative feedback loop. The gain K is optimized according to the performance criterion which is minimized by the Ricatti equation. The choice of the matrix $R = B * I$ as the application of the torque to the system is defined by B and the further application is due to linear factors represented by the identity matrix I [96]. The matrix Q defines the regulation performance and R the control effort. The matrix Q is weighted relatively to R by a weighting factor. The single matrix elements of Q are reduced to the element of the origin as proposed in Kuo [96, 97]. The cost functions which are derived are three functions. The first is the minimization of the angular positions from the zero position the vertical position. This leads to:

$$c1 = (x * x^T)^2 \qquad Q1 = \begin{pmatrix} I & 0 \\ 0 & 0 \end{pmatrix} \qquad (4.42)$$

where I is the identity matrix and x angular states of the system. Second, the angular velocity should be minimized:

$$c2 = (\dot{x} * \dot{x}^T)^2 \qquad Q2 = \begin{pmatrix} 0 & 0 \\ 0 & I \end{pmatrix} \tag{4.43}$$

where $\dot{x}$ are the angular velocity states of the system. And third the position of the center of mass should be in a horizontal position which is within the support area sa plus a small adjacent extra area δa which stands for the non-critical sway area. This support area is for the inverted pendulum just $-\delta a < sa < \delta a$. For the frontal-plane model this is defined as the area between the stance leg and the swing hip joint in the direction of the x-axis plus the adjacent area. This leads to the cost function:

$$c3 = (x_{com} * x)^2 \qquad Q3 = \begin{pmatrix} x_{com}^2 & 0 \\ 0 & 0 \end{pmatrix} \tag{4.44}$$

where x_{com}^T is a vector of the influence on the COM of the single mechanical position states. This depends on the mechanical model.

This control problem is applied to the inverse pendulum as well as later to the mechanical frontal-plane model with three links. The inverse pendulum model as defined in 2.2 and figure 2.2 has the same COM position as the position of the single mass of the pendulum. So, a deviation from the angular position and the COM is the same. This means that an additional COM penalty cost function is like doubling the angular deviation penalty function. This leads to the following matrix Q:

$$Q = w_{QR} * (\mu_1 * Q1 + \mu_2 * Q2 + \mu_3 * Q3) \tag{4.45}$$

with w_{QR} is a positive weighting factor of the matrix Q in relation to matrix R and the factors μ are the weighting factors of the single cost functions to each other. As defined in Kuo [96] the sum of these weighting factors shall be $\mu_1 + \mu_2 + \mu_3 = 1$ to guarantee not to influence the inter matrix weighting w_{QR} with this factor. For the inverse pendulum model the matrix is defined as: $Q = w_{RQ} * \begin{pmatrix} 2/3 & 0 \\ 0 & 1/3 \end{pmatrix}$ because all three cost functions have been weighted equally.

4.4 Experimentally Found Influences of Sensory Cues on Posture Control

Posture control models which use the Kalman filter represent integration mechanisms of sensory information. The trueness and accuracy of this mechanism can only be validated by stance and perception experiments with subjects. There is a wide range of perception and posture response experiments which concern visual, somatosensoric and/or vestibular
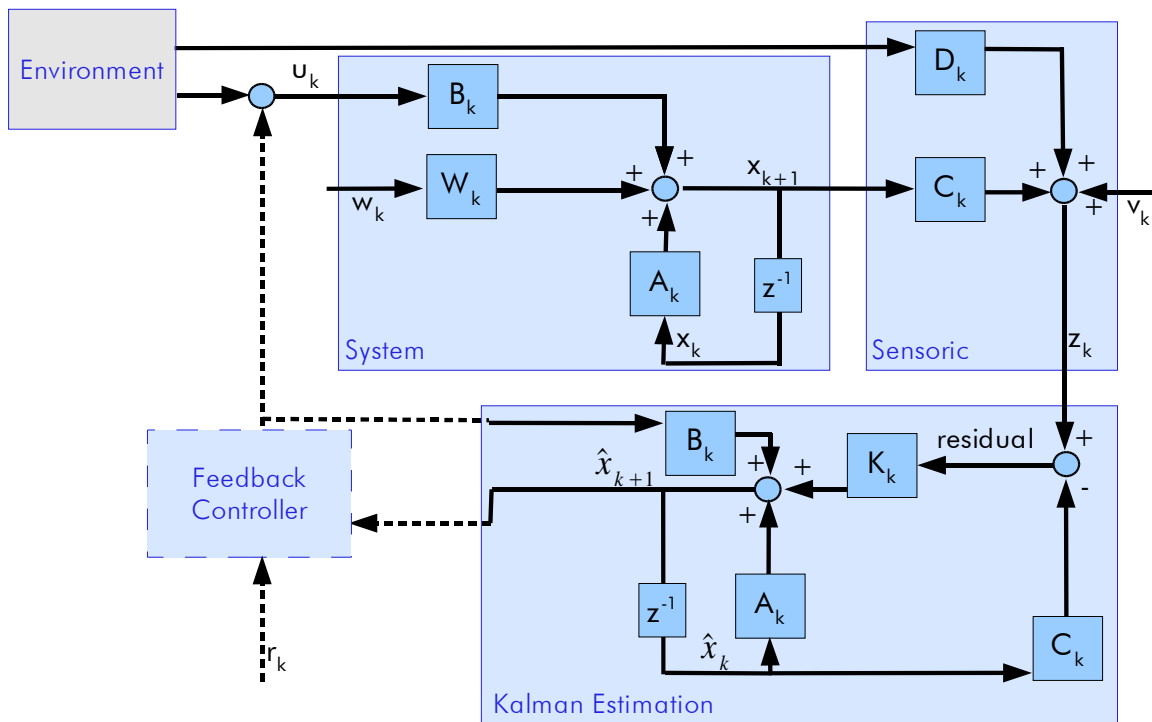
Figure 4.5: The Kalman estimator in combination with a controller in the feedback loop to control the system via corrective input u.

information processing. Those perception cues have of course a delay in time between the real sensory impression and the use of the information for a motor command. This delay is given in literature with varying values e.g. by [180] with about 100 ms and e.g. by [142] with up to 200 ms. In the following especially the visual cue including proprioceptive eye movement information in section 4.4.2 and the vestibular processing cue are in section 4.4.3 are regarded. The influence of the stimulation of those two cues and the combination is evaluated in clinical and other experimental studies.

4.4.1 Plots and Presentations

Interesting properties of the model are presented by four different plot types:

(a) The posture response of individual stimulations are analyzed by signal over time plots which show sway response, estimated states and sensory output over time.

(b) The frequency response is presented by amplitude or also called gain and phase of the transfer function H. The transfer function is defined as follows:

$$H(jw) = \frac{S_o(jw)}{S_i(jw)} \tag{4.46}$$

where S_o is the output signal which is here the angular signal of the sway. And this angular signal is FFT-transformed into the frequency range, so it results in $S_o(jw)$. The same applies for the input signal S_i which is here the stimulus applied to the system giving $S_i(jw)$. For the presented results the MATLAB function *'fft'* was used. The amplitude (gain) and phase of the transfer function $H(jw)$ was calculated with the MATLAB functions *'abs'* and *'phase'*. Which use the following computation:

$$gain(H) = abs(H) = |H| = sqrt(real(H(jw))^2 + imag(H(jw))^2) \tag{4.47}$$

$$phase(H) = angle(H) = arctan\left(\frac{imag(H)}{real(H)}\right) \tag{4.48}$$

(c) The stimulus over response amplitude plot shows the amplitude relation between the stimulus and the posture response. Especially nonlinear effects like the saturation with increasing stimulus amplitude can be seen in this visualization. The sway amplitude is directly correlated to the sway angle of the body or pendulum and the increasing factor is the stimulus amplitude.

(d) For the sway response, the **R**oot **M**ean **S**quare **RMS** of the sway angle is used to detect statistical relevant differences between single stimulation modes. For each trial an RMS is determined and the single conditions can be compared by the

quantitative value of the conditions' RMS. For Root Mean Square measurement the following formula is used:

$$RMS_x = \sqrt{\frac{\sum_{k=1...n}(x_k)^2}{n}} \qquad (4.49)$$

where x is a state varying over time with the time steps $k = 1 \ldots n$.

4.4.2 Influence of Visual Perception with Eye Movements on Posture Control

State of the Art

The visual perception is an important factor of stabilization and orientation of posture especially in relation to the surroundings. As well the combination of visual retinal information with eye and head movements influences the sway response. In [72] the influence of head and eye in head position on stance is studied. It was found that head rotation and eye orientation influence the sway of the body which is aligned in the same direction. The gaze direction had a significant influence on the sway direction. And gaze and head direction are significantly correlated which was also found in [77]. But [72] did not find an influence of gaze direction in the neutral head position what was explained with the 'neutral or most natural' configuration. Probably, this correlates with the result found in [77] of less influence of isolated gaze manipulation as in contrast to a highly significant head orientation influence and influence of the combined head and eye orientations.

Another characteristic can be the sway amplitude and frequency response of stance experiments. Different amplitudes and frequencies of visual stimulations have an influence on the stance sway [170, 149, 136, 139]. In [149, 136] the visual stimulation is a field of triangles moving with a sinusoidal oscillation plus a transversal velocity component. The increase of translational velocity changes the COM sway, analyzed in the frontal plane, in a nonlinear manner. With increasing stimulus velocity the COM sway response decreased at the stimulus frequency of the oscillation. This relation indicates that the higher the velocity the less is the weighting of the sensory input. Another interesting finding of [149, 43] is that even a visual input with high velocity or large movement amplitude provides information which can be used for the stance stabilization. The results show that the closed eye condition has the highest sway amplitude and variability. It is even higher than stimulation situations with fast moving or high amplitude visual stimulations.

A detailed analysis of the influence of stimulus frequency and amplitude on anterior-posterior sway frequency response is found in Peterka et al.[139, 141]. The two stimuli support surface and visual surrounding are applied to normal subjects. The visual and proprioceptive stimulus attain similar characteristics. So, with increasing stimulus amplitude the sway response saturates. For frequency variation of visual stimulus, the Fast Fourier DFT transformed stimulus response was evaluated for gain and phase. Gain first increases slightly and than decreases rapidly. Phase is leading (> 0) at the beginning and

for higher frequencies lagging (< 0). A perfect response of the system to the stimulus would be a sway-response with gain 1 and phase 0 as is also mentioned by [139].

Experiments with visual stimulus which induces eye pursuit and combine therefore eye movement with visual retinal perception have been made by Glasauer et al. [43]. Here the sinusoidal moving visual target is followed with the eyes by a smooth pursuit. The eye pursuit movement matched the target movement very closely. The additionally added background which produces retinal image gives the indication that the eye movement does influence the medio-lateral body sway significantly. This leads to assumptions that there is as well retinal image information which provides a reference of the relation body to environment as additional the eye movement which is often coupled to everydays life tasks which also indicates a reference between body and environment. Not only the retinal motion but also the eye movement influences the postural sway as was found by Ivanenko et al. [72]. The sway response always diverges in direction of gaze. This influence was tested in combination with head trunk rotation. The eye movement influence on posture happens also if no relation between body and environment is given like in [78] with a head-fixed visual pursuit stimulus. Vestibular neuritis patients could be stabilized by fixating a head fixed stimulus [78]. With moving eyes during pursuit movements, the postural sway increases again even more than sway in darkness which is shown in Glasauer et al. [43] with healthy subjects. The interaction of retinal and eye movement information is not clear. A subject is able to distinguish self-motion and environmental motion [27]. Though, how much of the used eye movement information and retinal flow information is used and how this information is integrated are still subject to actual research. Relations between background movement and a moving target which is fixated are studied in [43]. The fixation of a space fixed target results in the lowest postural sway answer where the eye pursuit with no space reference or moving space reference showed the highest sway response. In cases where the eye movement (fix/pursuit) was contradictory to the reference movement (moving/fix) the sway response was in between the two cases named before and similar to the condition darkness where there is neither retinal input nor eye movement. This could support the theory that even with contradictory information there is still information that can be used to stabilize stance or that the visual information is not used such as in the case darkness. The single conditions of pursuit and background information are shown in figure 4.6 from [43].

A contrary finding of Stoffregen et al. [169, 168] is that the eye pursuit frequency is not coupled to the sway frequency and that sway variability was reduced when subjects pursuit a target. The frequency range of Stoffregen is (0.5, 0.8 and 1.1 [Hz]) for an amplitude of 11 [deg]. This range as was already mentioned by Stoffregen [168] could be too small to receive representative results.

Implemented Own Experiments

To get a comparing and extended knowledge of posture sway correlation to eye movement frequency additional experiments have been made for this thesis. Therefore, the experi-
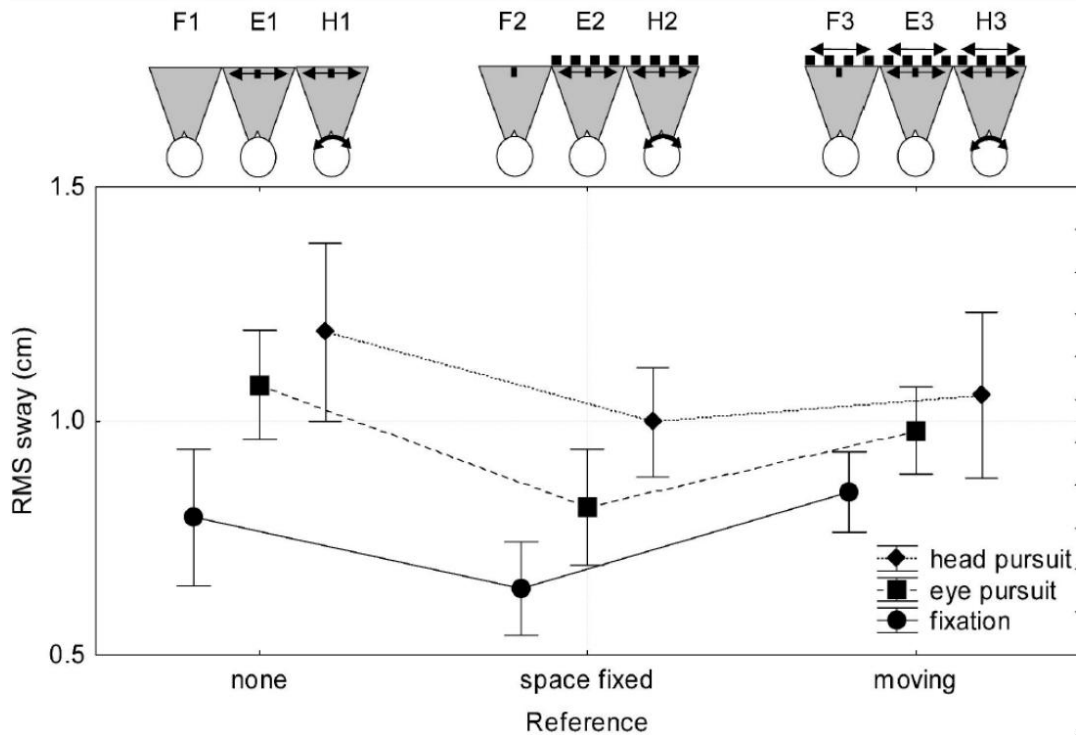
Figure 4.6: Nine conditions E1-E3 and F1-F3 and H1-H3 with eye pursuit with or without background and additional head rotation are shown. The graphics are taken from [43].

ments of Glasauer et al. [43] have been extended to find out if frequency and amplitude variation of eye pursuit movements have an influence on the posture response related to the movement variation. Especially the eye movements are studied in more detail for lower frequencies and different amplitudes. Lower frequencies in comparison to those Stoffregen evaluated are motivated because smooth pursuit movements can only be guaranteed for low frequencies. In [1] the horizontal eye pursuit for frequencies in the range of 0.07 ...0.42 [Hz] with an amplitude of 22.5 [deg] have been studied. For the highest frequencies with normal subjects the pursuit was interrupted by saccadic movements. Therefore the frequencies and amplitudes have been chosen lower for the pursuit experiments made for this work.

The experiment setup is as follows: Healthy subjects standing in complete darkness on a Kistler posturographie platform (Model 9286AA) and pursuing a sinusoidal moving light point on a translucent screen. The distance of the screen to the subject was 0.7 m. The posture response was measured by measuring the COP via the Kistler platform and the head position via an optical 3D tracking system (from Intersense Model IS-600) for a head fixed marker. Sway is the sway in medio-lateral direction. The task was always to fixate with the eyes the stationary or moving target point which is equivalent to the condition "E1" in Glasauer et. all [43]. All subjects got the same instructions how to achieve the standing position and to pursuit the visual target. There are three series of experiments. First, a short series with 6 subjects and 5 conditions for evaluation of the design. Second,
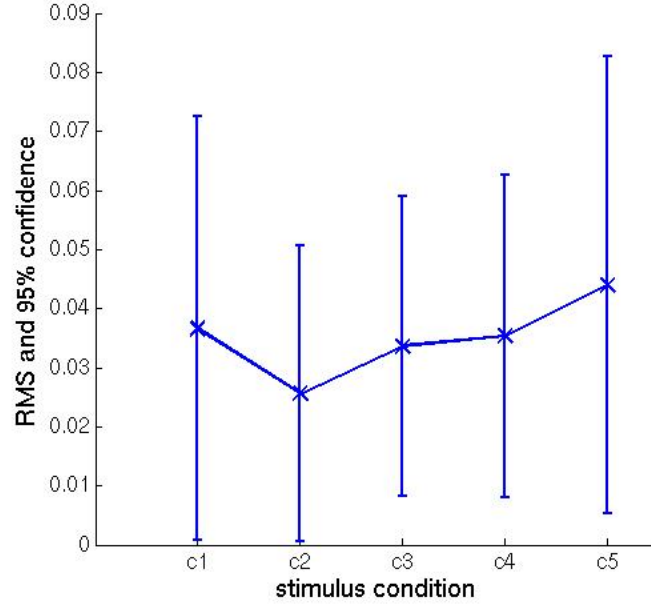
Figure 4.7: Mean RMS of the COP for all 5 conditions with 95% confidence interval shown by the bars.

a longer series with 13 subjects and 10 conditions. Third, the same as second but with different stance condition and 8 subjects. The conditions are always the control condition standing in complete darkness and fixation of a target light point which is not moving. The other conditions are combinations of amplitude and frequency variation of the target movement. The progression of one trial was 5 seconds of darkness afterwards 5 seconds of the fixation point and thereafter a 25 seconds duration of the stimulus according to the different conditions; with a 5 second pause between each condition. The condition order is randomized for all subjects. The conditions of the first experiment series are as follows:

condition	c1	c2	c3	c4	c5
	dark	fixation	a1 f1	a2 f1	a2 f2

Table 4.3: Conditions **c1 ... c5** of the experiments with control condition darkness and different amplitude and frequency conditions

with a1=2.5[deg] and a2=12[deg] angle of the maximum medio-lateral visual target point amplitude and the stimulus frequencies with f1=0.33[Hz] and f2=0.0833[Hz]. Results of the root mean square **RMS** of the center of pressure **COP** can be seen for the 5 conditions in figure 4.7 with the 95% confidence interval shown as bars around the mean RMS value. Calculation of the 95% confidence interval over n samples x_i:

$$\frac{1}{n}\sum_{i=1}^{n} x_i \pm icdf(1-\frac{q}{2},\mu,\sigma)*\frac{std(x)}{\sqrt{n}} \quad with \quad std(x)=\sqrt{\frac{1}{n-1}\sum(x_i-\bar{x})^2} \quad (4.50)$$

123

where *icdf* is the inverse cumulative distribution function which signifies the $1 - \frac{q}{2}$-quantile of the normal distribution with mean μ and variance σ.

Calculation of the Mean Squared Error of a sample mean over n samples x_i:

$$MSE(\overline{X}) = E\{\overline{X} - \mu)^2\} = \sigma^2/n \quad with \quad \overline{X} = \frac{1}{n}\sum_{i=1}^{n} x_i \qquad (4.51)$$

The eye movement stimulated sway responses **c3, c4, c5** have a higher RMS than the fixation condition $(F(3, 15) = 4.884, p = 0.0145)$. This was also found in other studies [43, 146]. One result of the stimulation conditions was that an amplitude of a1=2.5[deg] produced a COP sway response which did not show a peak at the stimulus frequency. This could be due to the fact that this small amplitude was very close to the signal to noise ratio so no response is visible. This can be seen in figure 4.8. For a higher amplitude and both frequencies a correlation in the frequency could be found.
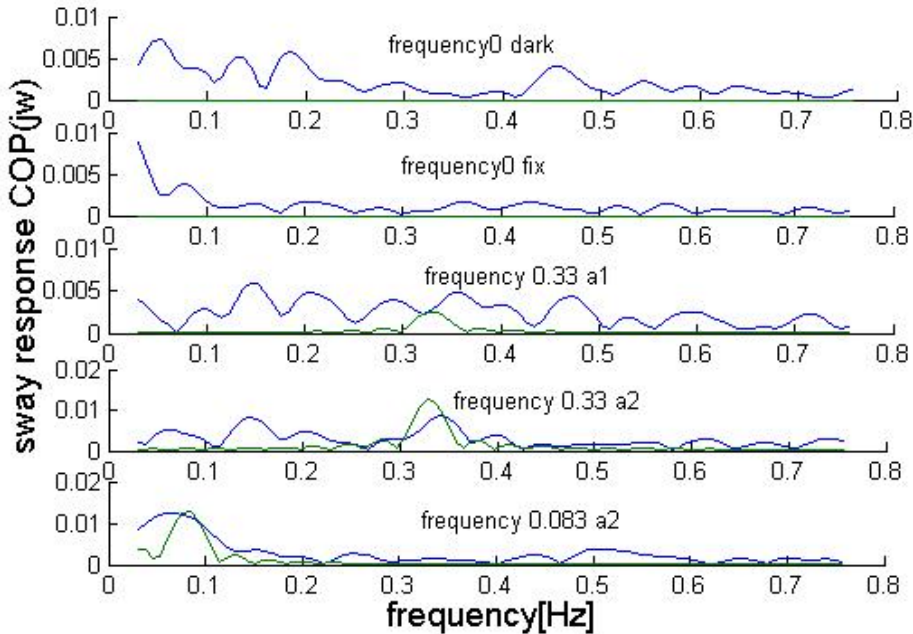
Figure 4.8: Frequency sway response of the COP and the frequency transfered by the stimulus.

Starting from this little study the following experiment for amplitude and frequency variation of the eye pursuit stimulus was evaluated. The second experiment consists of 10 conditions with different frequency and amplitude variations which are shown in the following table: with the stimulus amplitudes a1=6[deg] and a2=12[deg] angle of the maximum

condition	c1	c2	c3	c4	c5	c6	c7	c8	c9	c10
	dark	fix	a1 f1	a1 f2	a1 f3	a1 f4	a2 f1	a2 f2	a2 f3	a2 f4

Table 4.4: 10 conditions of the second experiments.
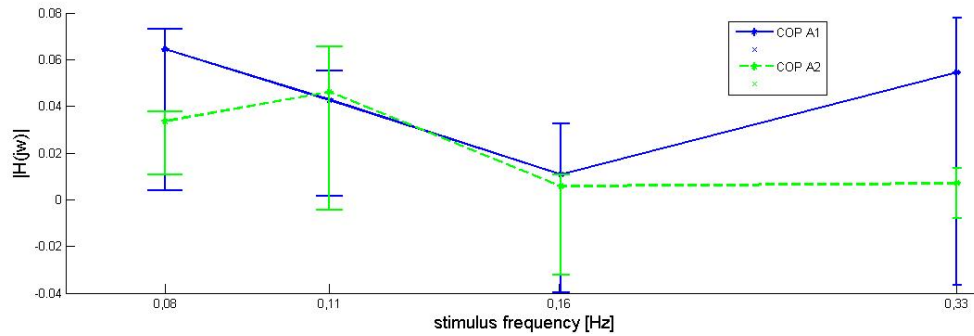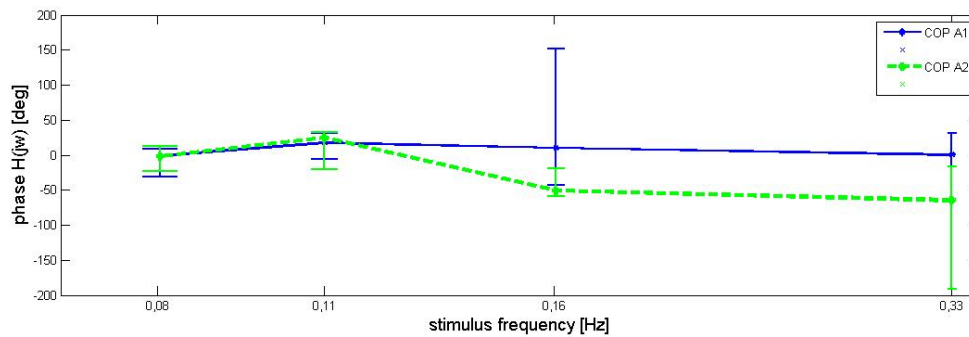
(a) Amplitude

(b) Phase

Figure 4.9: Transfer function amplitude and phase for four different stimulus frequencies and two amplitudes.

medio-lateral visual target point and the stimulus frequencies with $f1 = \frac{1}{12} = 0.0833[Hz]$, $f2 = \frac{1}{9} = 0.111[Hz]$, $f3 = \frac{1}{6} = 0.1667[Hz]$, $f4 = \frac{1}{3} = 0.33[Hz]$. In this experiment 13 normal subjects participated. In figure 4.9 the transfer function of postural response to visual stimuli in the frequency range is shown. The transfer function with its gain $|H(jw)|$ and phase $< H(jw)$ is defined as in section 4.4.1. It is shown the postural response of the COP and the head position at four different stimulation frequencies $f_1 \ldots f_4$ for two different amplitudes a_1, a_2. The values signify the mean transfer function over all subjects and the bars show the 95% confidence interval.

The amplitude of the transfer function looks similar and frequency appears to have a decreasing effect. For the phase plot for the two higher frequencies with bigger amplitude a2 the phase is decreasing which signifies a lag of the response. If the frequency transposed signal of each trial and condition is evaluated at the according stimulus frequency which means the amplitude of the function $H(jw)$, a significant difference between the single conditions c3 ... c10 can be found. For the gain function the overall effect is significant with $(F(7, 84) = 2.917, p = 0.0088)$. For the phase function of the frequency response
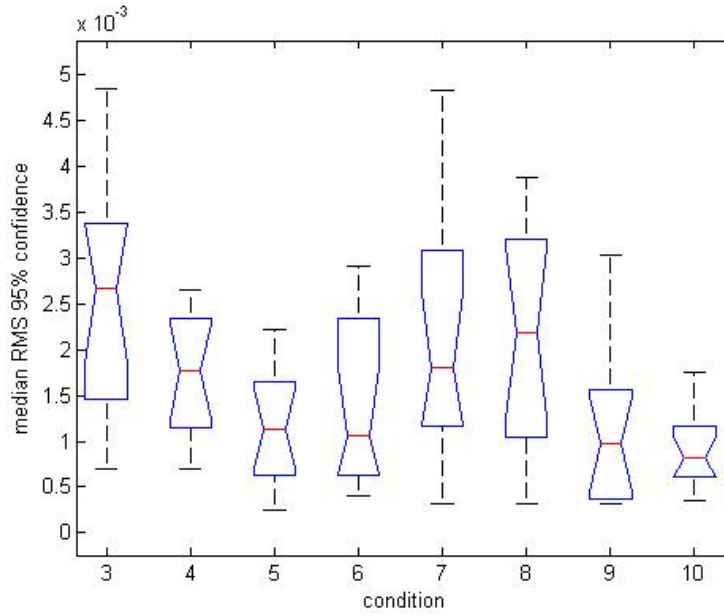
Figure 4.10: The median values of $|S_o(jw_{stim})|$ with 95% confidence interval bars.

it is significant with $(F(7, 84) = 4.513, p = 0.0003)$. If the same evaluation is done for the conditions c7 ... c10 which have the higher amplitude a2. The overall effect for the gain function is significant with $(F(3, 36) = 3.804, p = 0.0182)$, and the phase function with $(F(3, 36) = 4.829, p = 0.0063)$. Further, with a 2-factor repeated measurement ANOVA, in the gain function the frequency factor is also significant with $(F(3, 36) = 3.80, p = 0.018)$ without interaction. In the phase function the frequency is significant with $(F(3, 36) = 4.096, p = 0.0134)$. The amplitude factor shows no significant effect in the gain function. In the phase function the amplitude effect is significant with $(F(1, 12) = 14.56, p = 0.0025)$. The post-hoc Scheffe Test shows a significant difference for the phase function between the two amplitude levels and between frequency level 1 and 3. The four levels f1: $(mean \pm MSE = 0.0024 \pm 0.0571 * 10^{-5})$, f2: $(mean \pm MSE = 0.0024 \pm 0.527 * 10^{-5})$, f3: $(mean \pm MSE = 0.0013 \pm 0.102 * 10^{-5})$, f4:$(mean \pm MSE = 0.0016 \pm 0.320 * 10^{-5})$. For this see figure 4.10.

In Glasauer et al. [43] the RMS of the lateral COP sway value is evaluated. So, in the following the RMS values are shown for the 10 conditions with 95% confidence interval bars. The RMS values are evaluated by repeated measurement variance analysis. The overall effect is significant with $(F(9, 108) = 3.390, p = 0.0011)$. Further the dark condition is significantly different from the visual stimulation condition$(F(8, 108) = 3.405, p < 0.0017)$.

The next figure 4.11 shows the RMS over all conditions. There is no significant effect for the frequency or amplitude factor found but an unexpected difference is visible. The RMS sway response is not lowest for the fixation condition but all stimulation conditions have a lower sway response. The darkness condition has the highest sway response. The difference between the conditions c1 $(mean \pm MSE = 0.0199 \pm 0.00193 * 10^{-5})$ and c2-c10
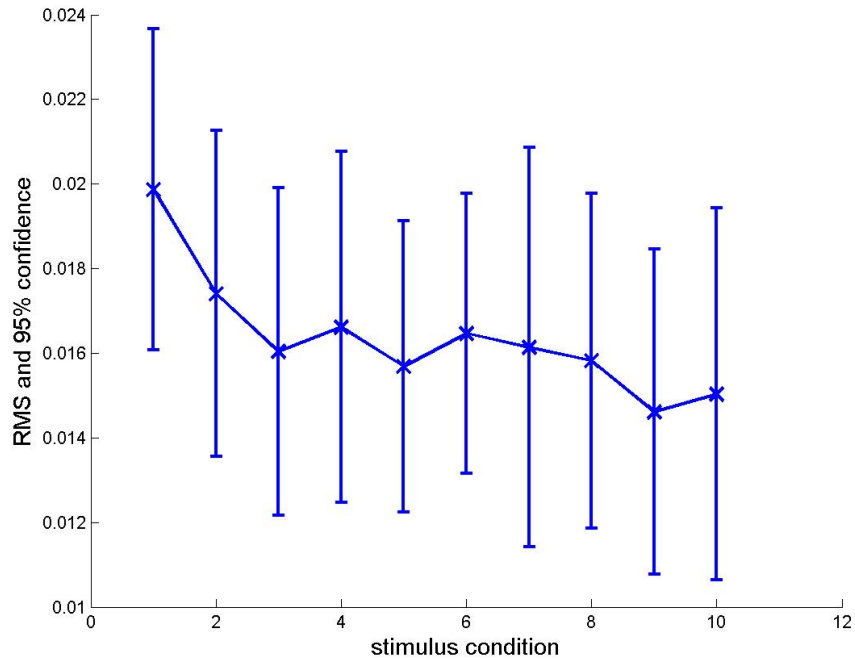
Figure 4.11: Mean RMS sway response for all conditions c1 to c10 with 95% confidence interval. There is a decreasing tendency with higher frequencies.

$(mean \pm MSE = 0.016 \pm 0.717 * 10^{-5})$ is a reduction of sway. For frequency variation for both amplitudes no significant response variation could be found. As well for the two different amplitudes there is no different sway response found over all stimulus frequencies. In plot 4.12 it can be seen that the tendency for both amplitudes over all frequencies is decreasing and that the higher amplitude decreases even more, but not significantly. To see the two amplitudes in comparison the plot 4.12 shows the two amplitudes over all frequencies beside each other. The higher amplitude leads to a smaller RMS sway. Till now it was assumed that the two factors amplitude and frequency have an independent influence on the sway response. If now everything is recalculated as actual visual target velocity it can be seen that an increasing velocity leads to a decreasing RMS response. The maximum velocities are determined in the zero target position for all conditions which leads to 6 different velocities. The conditions c5 and c7 result in the same velocity and the conditions c6 and c9. In figure 4.13 the RMS sway response to the 6 velocities is shown.

The stance condition may influence the sway response significantly. Therefore, a third experiment with the same 10 conditions, 8 normal subjects and a different stance condition was evaluated to see eventual differences according to the stance condition. Now stance is a normal narrow stance with the feet close side by side on a rubber foam of 20 cm thickness. The rest of the experimental setting is identical. As before the gain does not vary much with frequency and the amplitude has a slightly decreasing effect. In the phase plot it can be seen that the phase lag has become bigger because the damping effect of the rubber foam is seen. But the phase decreases as before with the frequency. No overall effect is
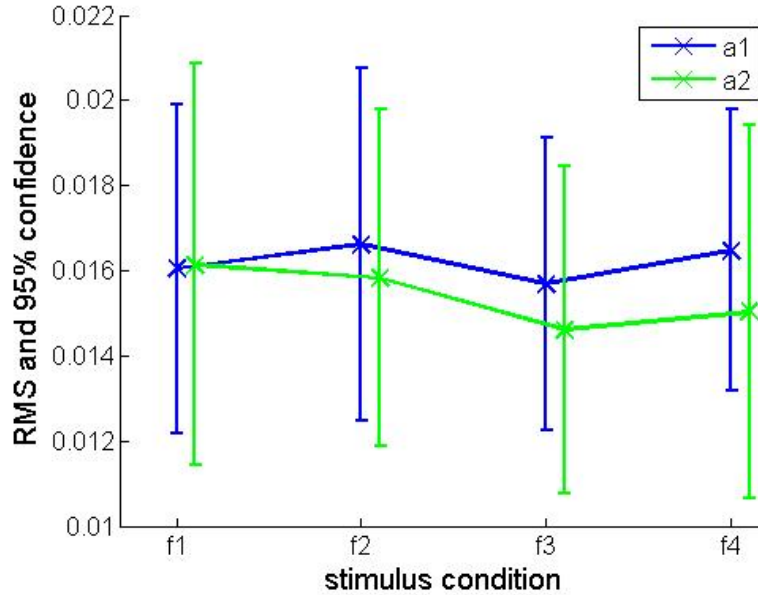
Figure 4.12: Mean RMS sway for both amplitudes a1 and a2, varied with the four frequencies f1 ... f4. For the higher amplitude a decreasing effect with rising frequency is visible.
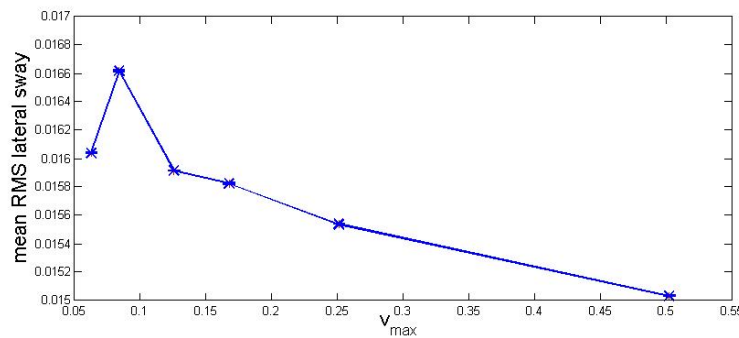
Figure 4.13: Mean RMS sway response for the 6 velocities of the pursuit target.
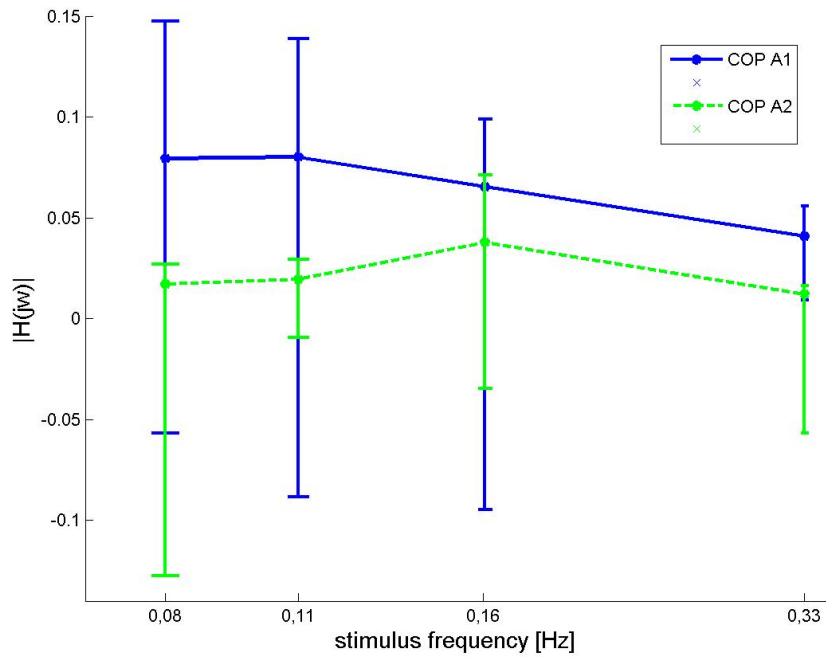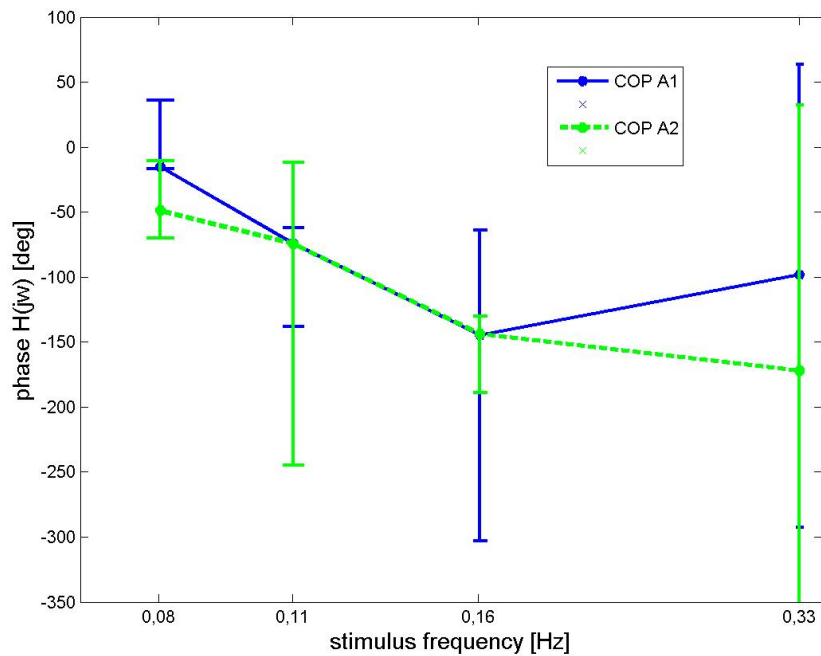
(a) amplitude

(b) phase

Figure 4.14: Transfer function amplitude and phase for four different stimulus frequencies and two amplitudes a1 and a2. The amplitude shows a decreasing effect for the gain. The frequency has a decreasing effect on the phase and for a1 on the gain.
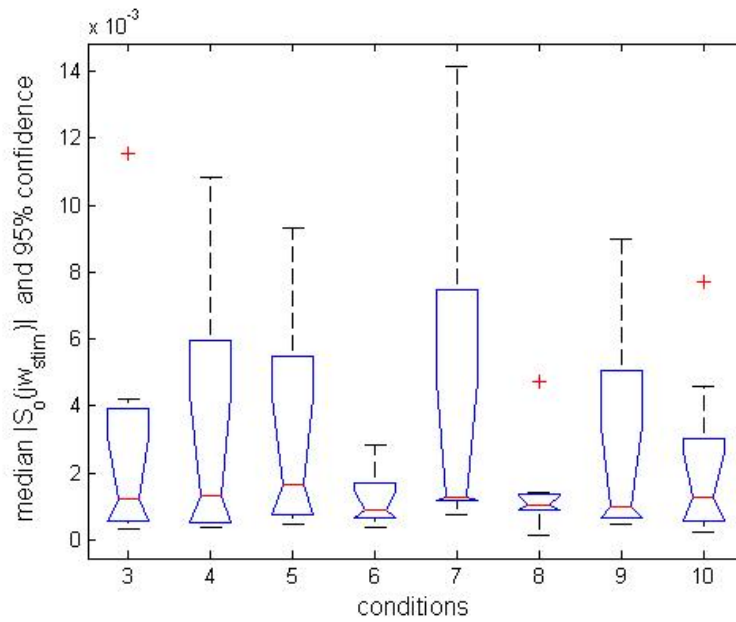
Figure 4.15: The median values of $|S_o(jw_{stim})|$ with 95% confidence interval bars.

found for the frequency gain and phase function as well as for the RMS function. This is the case because the sway response is much less in this more stable stance condition. The overall effect for the frequency gain is with $(F(7,49) = 2.09, p = 0.0617)$ just not significant. This is the same for the 2 factor variance analysis which has similar close results to significance for both factors but no interaction. In figure 4.15 it can be seen that the variance within a condition is much higher and so the differences are not so clear.

In figure 4.17 there is no effect of the amplitude seen. Though, within one amplitude especially for a2 a tendency of decreasing RMS sway with increasing frequency can be seen. This stance condition is generally more stable, but with the foam rubber underground the variance of the measurements increases which is seen in all plots compared to the tandem stance condition of experiment E2. The effect is that there are no significant differences between the conditions but the characteristics are very similar to the results seen in experiment E2. This makes clear that the stance condition is a very important condition which can reduce or enforce effects and which can be very noisy.

Concluding it can be said, that no significant influence of frequency or amplitude value could be proven on the RMS value but on the frequency sway response a significant influence of the frequency value is determined. The tendency found is decreasing sway response with rising frequency in all conditions. The stance condition change has an influence on the absolute values but not on the tendency of decrease. The darkness condition is significantly different of all visual stimulated conditions, the sway response RMS is significantly higher.
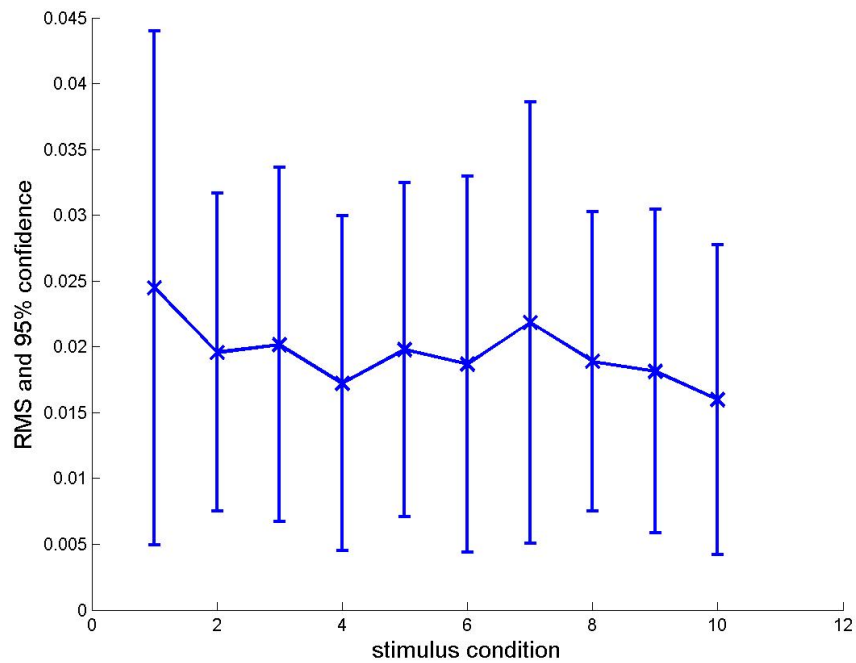
Figure 4.16: Mean RMS sway response for all conditions with mean RMS values and 95% confidence interval.
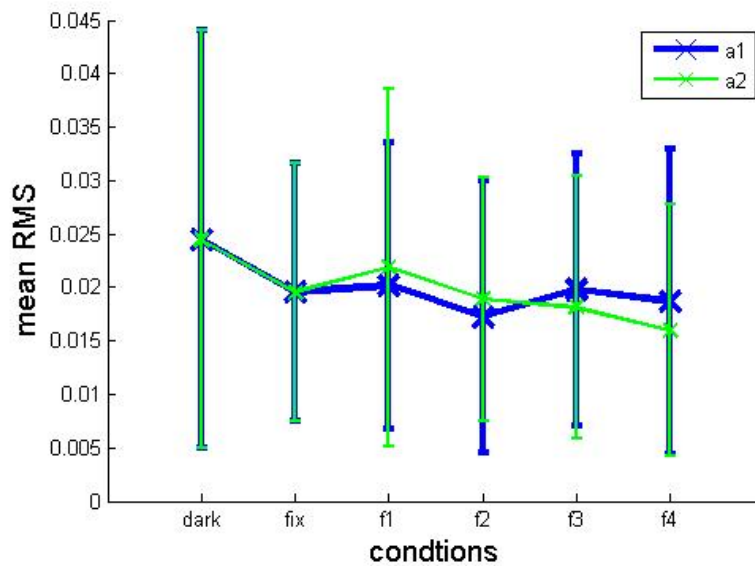
Figure 4.17: Mean RMS sway response for the two different amplitudes a1 and a2 in comparison. A decreasing sway response effect is registered as the frequency of the amplitude a2 rises.

4.4.3 Influence of Vestibular Perception on Stance Control

Basics and State of the Art

Vestibular perception is here the perception of angular acceleration acting on the vestibular sensor. Stimulation of this sensor can be achieved by e.g., changes of the support surface, which also result in proprioceptive impressions, or by galvanic vestibular stimulation GVS. The GVS is an artificial electro stimulation which is directly applied to a mastoid under each of the subject's ears. An electric stimulus of about 0.25 - 1 [mA] is usually used. This stimulus induces an electrical stimulus on the skin and therefore the nerve lying below the surface is depolarized. This depolarization leads to a sensational input to the sensory processing system which was not originated by a real sensory input of the vestibular organ but the depolarization of the afferent vestibular nerve [44]. This depolarization means that a positive anode increases the afferent firing rate. This increased firing rate leads to a sensation which is artificial because this movement perception could not be reproduced with natural physical stimulation. The single perception vectors of each semicircular canal of the vestibular organ and the resulting sum of these vectors which is the perceived movement was analyzed in detail by Fitzpatrick et al. [32]. The vectorial sensation which is produced by a bilateral bipolar GVS stimulus is shown in figure 4.18.
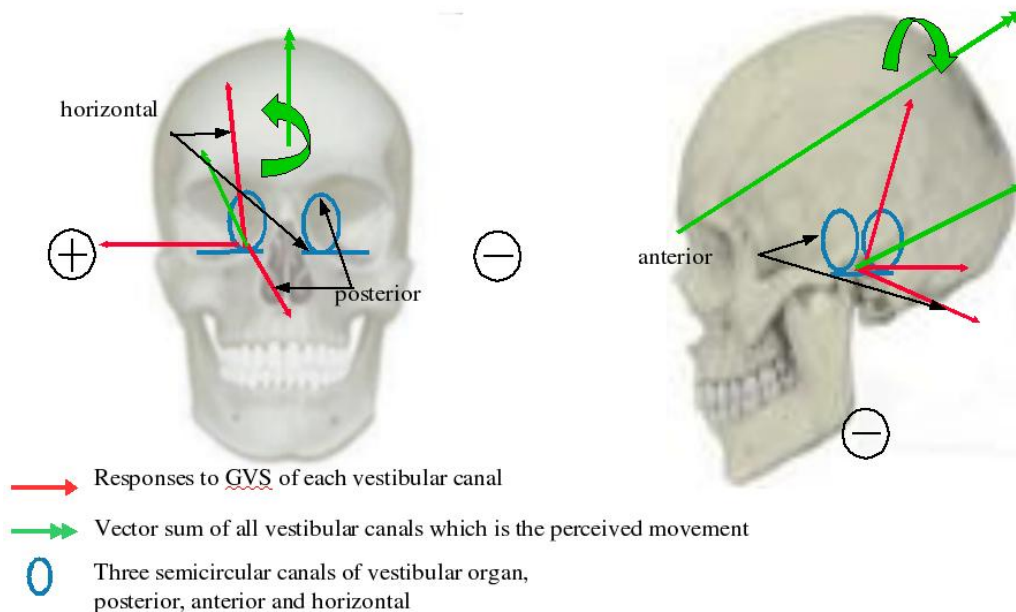
Figure 4.18: The electrical stimulation produces different movement perception vectors in the different vestibular organ parts. The vectors combine to produce the movement finally perceived.

The produced impression resembles a rolling movement in the frontal plane with its main vector and a rotational movement in the horizontal plane. The main movement, the roll

in the frontal plane will be the stimulation factor for this chapter. The decomposition of this vector is detailed in [189]. The polarity which means that the right side is the anode and the left the cathode or vice versa influences the direction of sensory input. This direction indicates if the roll movement is to the right side or the left. The stimulus induces a roll movement to the cathodal side. The mechanism of galvanic stimulation and its effect on the organism is explained in detail in Fitzpatrick et al. [33, 189, 32].

In Bent et al. [8] the GVS stimulus applied in stance induces a body sway response which was a roll of the body segments head, trunk and pelvis. The unexpected finding was that the condition eyes closed or eyes open did not influence the sway response very much which is opposed to former findings of Day and Bonato [25] which found a reducing influence of vision input on the sway response.
The vestibular response to GVS with different amplitudes was studied in [65]. An increasing amplitude showed an increasing sway response of the COP. Additionally, somatosensory loss subjects have been tested beside normal subjects and they showed an even larger sway response to the stimuli. The increase found was in both cases a linear relation with the slope depending on the grade of somatosensory loss. A further study of Hlavacka [64, 63] showed that the COP sway response to a stimulus has a large delay of about one second. The combination of proprioceptive feedback from the legs and the vestibular information are linearly combined [64].
According to Day et al. [26, 32] the continuous time sway response of head, trunk and pelvis is a lateral sidewards movement starting with some latency 120 ms. Then after a short time of sidewards tilting the position stays constant and after the stimulus ceased the body returns to its original position.

Implementation of Own Experiments

This could also be verified in the stance and stepping experiments made for this thesis. The stimulus duration was chosen to be 1 [sec] which is about the time the body sway response needs to reach the maximum tilt position. The resulting sway response is therefore an increasing and afterwards decreasing tilt movement. The stimulus amplitude was 1 [mA]. This is shown in figure 4.19. The data shown are a mean response for each condition over all trials. There have been tested 6 healthy subjects with 2 trials for each condition. The 6 conditions are, stance, walking in place and jogging in place each in combination with GVS with the anodal electrode once on the left and once on the right side. The measurement of the body sway was attained by measuring the trunk movement by a stereo vision tracked marker. This measurement delivers 3D data of the tracked marker with 0.30 [Hz].The galvanic stimulus for stepping conditions was always started in the moment when the heel-strike of the right foot occurred. The subjects where all blindfolded. The characteristic trunk sway response over time of one subject is given in figure 4.20. In all cases a clear body sway in medio-lateral direction can be seen. It also can be seen that when the body returns to the original position a slight overswinging of the system appears. An explanation for this could be the following. When the body reacts to the GVS stimulus with some delay the corrective movement also controlled by
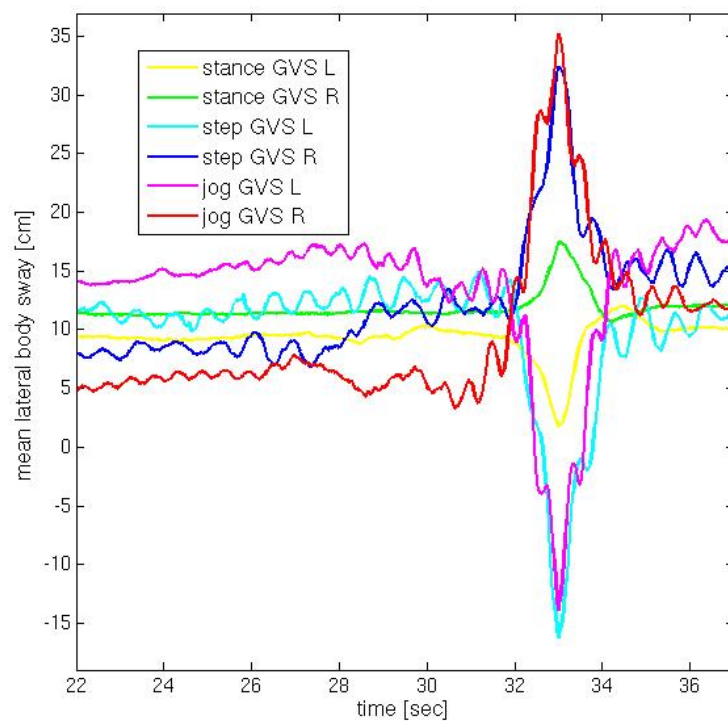
Figure 4.19: Mean continuous body sway over time for anodal stimulation sides left and right, shown for stance, stepping and jogging in place.
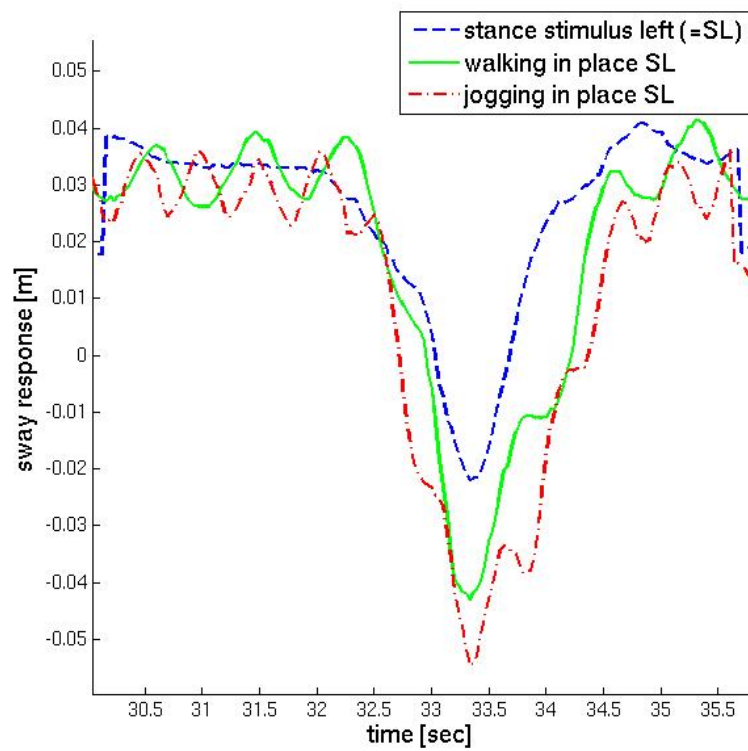
Figure 4.20: Continuous body sway over time for one anodal stimulation side, shown for stance, stepping and jogging in place for one single subject.

the other sensory cues (especially proprioception) produces a counter movement to prevent the body from falling. If the stimulus is stopped this counter movement is adapted again with some delay so there is a small overswing of the system in the other direction. This would also explain the reduced effect of GVS with additional visual sensory cues. The sway response lasts about two seconds which is the double of the stimulus duration. The body sway goes on for about one second and then decreases with the cease of the stimulus for a bit more than a second. The difference between stance and stepping or jogging in place is that the sway amplitude is increased. In the case of stepping or jogging the body sway is enlarged because of the swaying of the trunk with each step and if the GVS stimulus acts of the system in the moment of heel-strike the system is clearly more instable as in case of stance with both feet. The dynamic of the system for stepping is also higher than for stance. So, this can explain the higher GVS induced sway amplitude. In the context of the presented GVS stimulus experiments different moments of time for the stimulus start have been tested. And one result was, that it makes a difference what point in the step cycle for the stimulus start is chosen. E.g. if for jogging movements the stimulus was started in the flight phase which means after the foot leaves the ground the stimulus results had a lot of variance. This is explained by the fact that the possibilities of active balance control during the flight phase are not bound to ground reaction forces and therefore very different to the normal stance control torques. Between stepping and jogging in place the GVS stimulus produces very similar sway responses. This might indicate that the balance control for medio-lateral is not different during those two movement patterns.

It can be summed up that the lateral body sway response is according to the GVS stimulus to the cathodal side. The sway response is lower for stance than for stepping or jogging in place but equal in characteristic. The duration of body sway to the 1 second stimulus is about one second for increase of body sway and about the same time for the decrease sway movement before returning to the original position which ends with a little overswinging.

In the following section the stance and posture control model was stimulated by GVS and visual stimuli to simulate the model posture responses and compare them to the responses found experimentally.

4.5 Simulated Sway Responses for Visual and Vestibular Stimulation

The model consists of (1) the body dynamics of an inverse pendulum equation 2.4, (2) the equations describing the sensory modalities 4.5, 4.7, 4.10 and 4.11 or 4.16, (3) the processing and predictive part of the Kalman filter with equations 4.30 to 4.35 and (4) the feedback controller with equation 4.41. This model which is presented in figure 4.3 is calculated with the general parameters given in section 4.5.1. Interesting properties of the model are presented by four different plot types:(a) the signal in the time range, (b) the transfer function in the frequency range or also called frequency responses, (c) relational

plot stimulus over sway response amplitude and (d) the Root Mean Square plot. Those plots have already been used and explained in the section of experiments 4.4.1.

In the following four different simulations are presented. First, the vestibular stimulation with GVS in comparison to the experiments of 4.4.3. Second, the visual processing of retinal image velocity for the linear and nonlinear visual system model. Third, the sensor integration is shown by the combination of different stimuli for eye movement and visual background movement according to the experiments by Glasauer et al. [43]. Fourth, the eye movement is simulated for different frequencies and velocities in comparison to the experiments in 4.4.2. Before the simulation results are presented, the parametrization of the model is addressed in the next section.

4.5.1 Parameters of the Posture Control Model

The posture control model used here consists of the inverse pendulum model and the linear Kalman estimator in combination with the feedback control related to the optimality criterion J which is defined in equation 4.42 and 4.43. The model simulation is presented by the frequency response amplitude, phase and a sway response over time and the stimulus influence of different stimuli on the sway response. The results presented here have been simulated in MATLAB. The state-space equations used are equations 2.2, 4.41, 4.32, 4.33, 4.34 and 4.35 of the mechanics as well as of the Kalman estimation; they are in discrete form. The sampling rate of the mechanics and the whole system is realized with timesteps of 0.001 [sec]. The Kalman estimation process is sampled with timesteps of 0.1 [sec] which leads to a time delay of 100 [msec]. This difference in sampling rates stands for the time delay produced by sensory and neuronal processing which is given with values about 100 [msec] [180]. The parameters which are fix and used for simulation are the parameters for the equations given above and the sensor transfer functions which are given in the according subsections of 4.2. Further parameters are those of the mechanical system, the pendulum, and the error covariances for the estimation.

If there is no further explanation, the given results are mean results calculated from 5 independent trials for each condition or stimulus. If the model is referred to as linear or nonlinear, this stands for the linear modeling or nonlinear modeling of the visual velocity sensory cue. All other models are the same over all simulation results.

To show the behavior of the linear estimation the single signals produced in the model are shown for one example. The system was stimulated with a visual background movements of $0.2[Hz]$ and an amplitude of $2[deg]$. The Kalman filter estimation was calculated with the noise covariances $Q_{cov} = 0.005$ and $R_{cov} = 0.05$. The system states are measured by the sensors. The sensory signals with system states and external stimuli input are shown in figure 4.3. The estimated Kalman filter values of the system position and velocity is plotted in figure 4.21.

In the left plot (a) it can be seen the real system states and their estimations. The position estimation resembles the real position very closely with a little delay. In the estimated velocity signal more deviation can be seen and especially small noisy signal

(a) System state and estimation
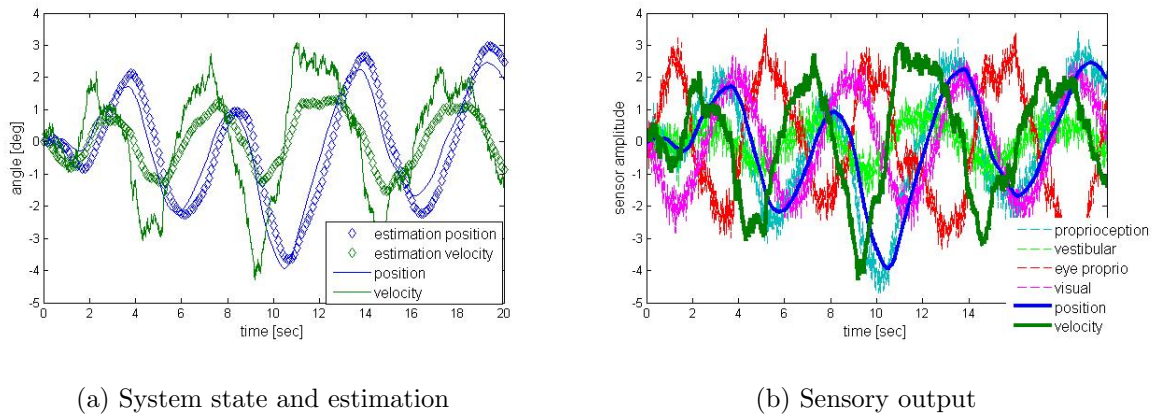
(b) Sensory output

Figure 4.21: System states are estimated by the Kalman filter and measured by the sensory modalities. The graphs show the real and estimated body position, velocity and the four sensory outputs. Sensors and system are noisy.

parts are smoothed by the estimation because of the quantization effect and the modeled inaccuracies. In the left plot (b) the sensory states can be seen for a visual stimulation. Here the state of proprioception which stands for position measurement, the vestibular state which is proportional to the velocity measurement, the eye velocity state which is a combination of body and stimulus velocity and finally the visual measurement state which performs nonlinearly, are shown together with their actual position, velocity and external stimuli.

4.5.2 Vestibular Stimulation

In the following the results for model simulations for different sensory input modalities are shown. First, the system response is shown for the case that all system sensors are available and provide correct information. The results shown are always averaged results. For 10 trials the same situation has been simulated and then calculated the mean over those 10 trials. This is done to reduce the seen influence of noise in the sway responses.

The vestibular sense was stimulated by a GVS of 1 second duration. The experimental results have been given in section 4.4.3. The simulation was calculated for the case that there is no visual input to the system like in the condition eyes closed. The GVS stimulus starts at second 7. The noise covariances put to the system are $\sigma_Q = 0.005$ and $\sigma_R = 0.05$. In figure 4.22 it can be seen that the COM angular response reacts to the stimulus with delay. The response is a sway to one side coming back to the zero position. Then there is an overswinging of the system which results in a sway to the other side before going back to the zero position. Compared to the experimentally found sway response it can be said that the delayed response is very similar. The delay is as found by [65] about one
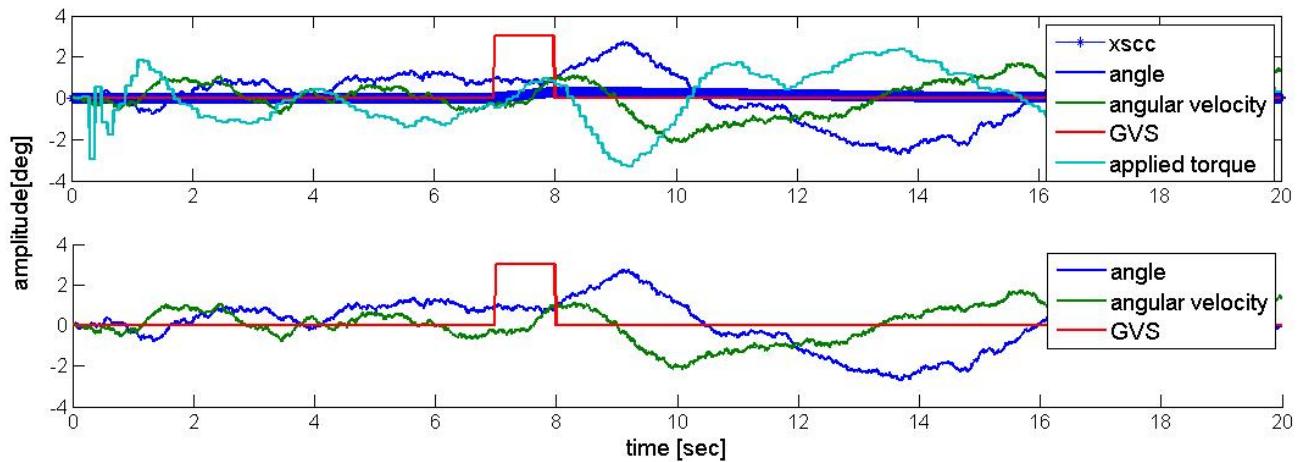
Figure 4.22: Simulated sway response of COM for a galvanic stimulation for one second. The graphs show the vestibular sensory signal and the corrective torque determined (above) in relation to the resulting body movement (below).

second. And there is often also an overswing to the other side as the stimulation side. The duration for a one second stimulus is about one second for the first deviation and then another second to come back to the zero position followed by an overswing. This is the same as found in my experiments.

Also a longer stimulus is simulated in figure 4.23. Here the sway response is also delayed and of longer duration. After a delay of about one second the sway increases till it stays at a level with a slight decrease. This fact correlates with the findings of [26, 32]. When the GVS stimulus is stopped the body returns to the normal body position with delay and a very similar rate as the decrease of body sway.

In figure 4.24 the stimulus of 7 seconds is applied with doubled stimulus amplitude. This leads also to a higher sway amplitude and less effects of noisy disturbances. The increase of the body sway response to increasing stimulus amplitude was also found in Hlavacka [65]. The characteristic of the sway response is the same as for lower stimulus amplitude as shown before in figure 4.23.

An interesting finding in the simulations for longer GVS stimuli is that with the stopping of the stimulus a first small sway of the body in direction of the stimulus is seen before the sway goes back to the zero position. This was a finding during my GVS experiments that the sudden stop of the GVS increases the sway before decreasing it. This could be the case if the change of the stimulus also innervates an information which is processed for further posture control.
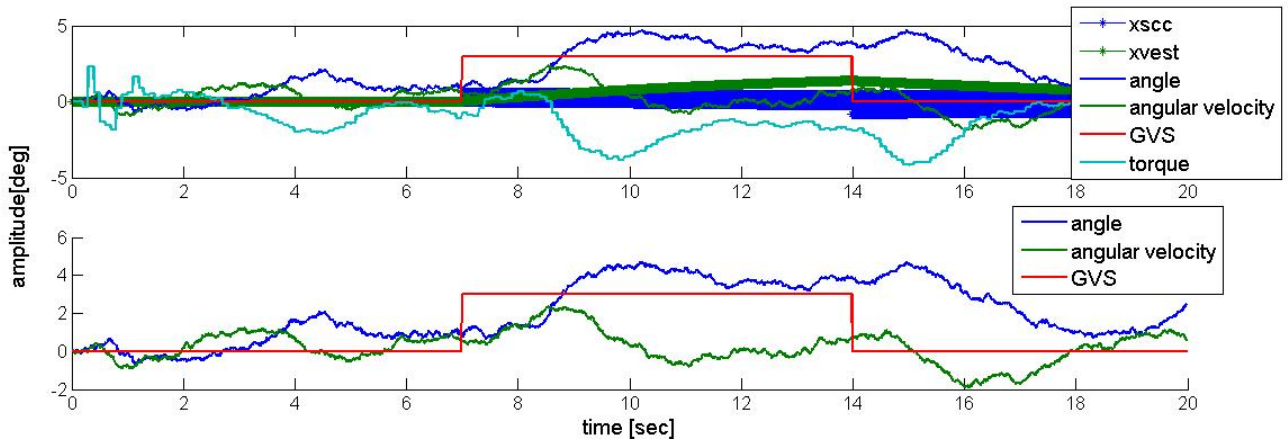
Figure 4.23: Simulated sway response of COM for a longer galvanic stimulation of 7 seconds. The graphs show the vestibular sensory signal and the corrective torque determined (above) in relation to the resulting body movement as long as the stimulus takes (below).
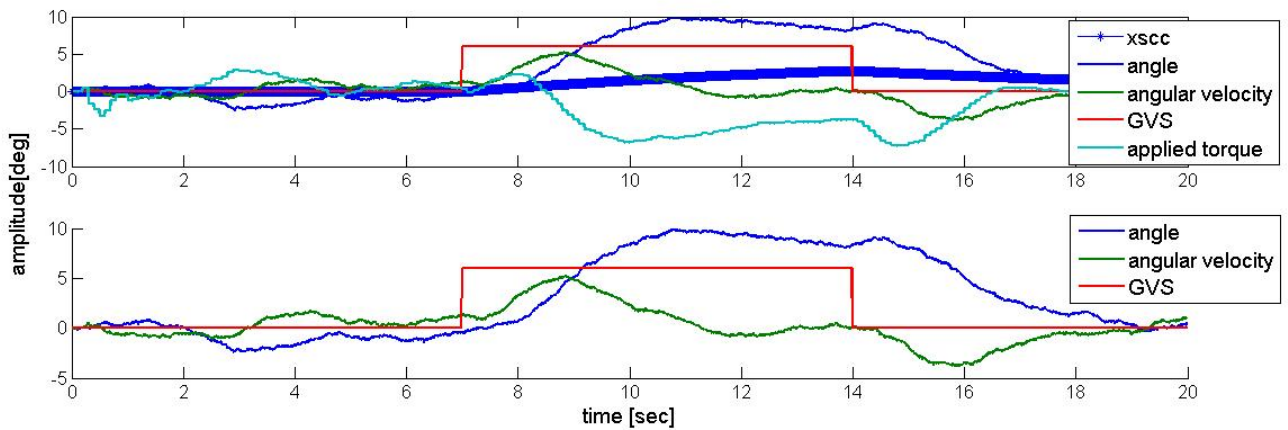
Figure 4.24: Simulated sway response of COM for a galvanic stimulation of 7 seconds with higher amplitude. The graphs show the vestibular sensory signal and the corrective torque determined (above) in relation to the resulting body movement (below), which is larger because of the higher amplitude.

(a) Gain
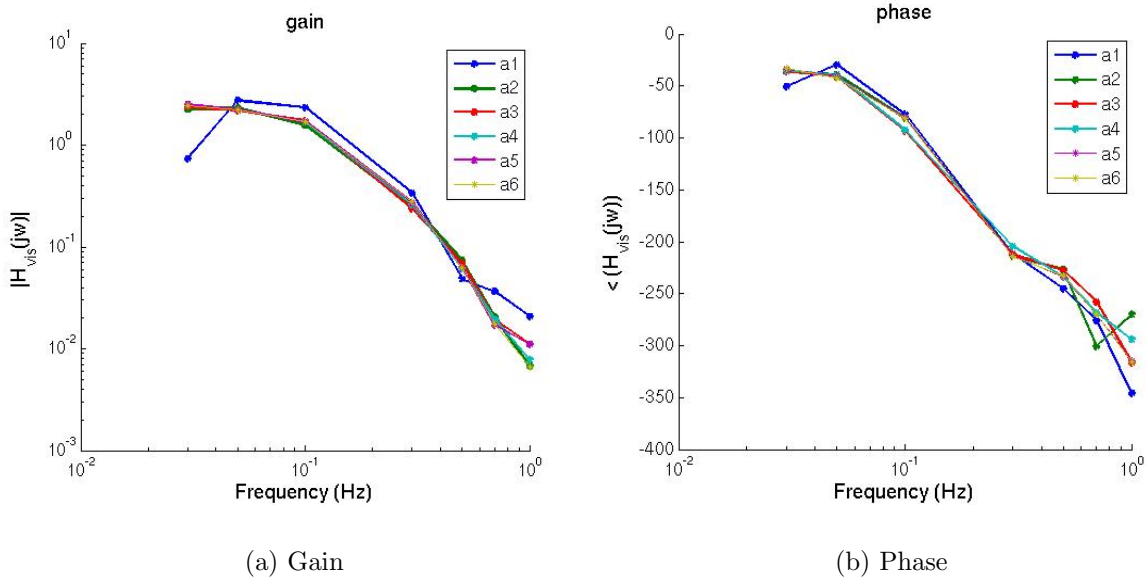
(b) Phase

Figure 4.25: Linear model: Frequency sway response of the body to a sinusoidal stimulus with different frequencies and amplitudes. This is presented as gain and phase function of the transfer functions in the frequency domain.

4.5.3 Retinal Stimulation

Second, another simulated stimulation is visual stimulation which stands for the retinal perceived movement. In the following two stimuli are distinguished. First, eye pursuit stimulus u_t, a visual target point which is fixated with the eyes and followed when moving. And second, a visual background which produces a different retinal image than the target. The processed visual information is always the visually measured movement velocity.

The simulation of the system is stimulated by a visual horizontal background stimulus which is a sinusoidal movement of the background. This produces a retinal moving image. The frequency of the stimulus was varied. The values are $0.03, 0.05, 0.12, 0.3, 0.5, 0.7, 1 [Hz]$. The amplitude was also varied from a1 to a6. The model is simulated with the amplitudes $1, 3, 5, 8, 12, 18$ [deg]. In the following the frequency response with margin and phase is shown. This plot was chosen in resemblance to Peterka [139] but with a horizontal visual stimulus for the sway response in the frontal plane. It can be seen in figure 4.25 the linear model response and the non-linear model response in figure 4.26. For both cases a rising frequency causes a rapid decrease of amplitude of the transfer function. In figure 4.25 the frequency response shows a decreasing gain function with a successive plateau. For the nonlinear model this is very similar and with increasing amplitude the gain decreases slightly.

The phase of the transfer function shows a first slowly, then faster dropping function. This signifies that there is a phase lag of the response to the stimulus, meeting the expectations of theory. The phase starts already in the negative because the model includes a delay

(a) Gain   (b) Phase
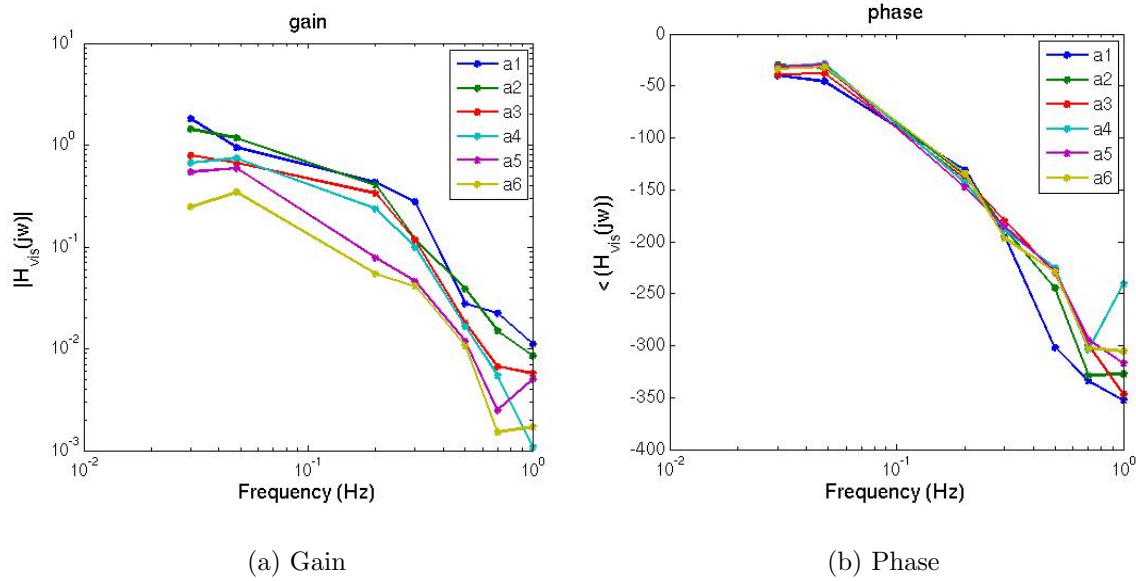
Figure 4.26: Nonlinear model: Frequency sway response of the body to a sinusoidal stimulus with different frequencies and amplitudes. This is presented as gain and phase function of the transfer function in the frequency domain. Now the gain is amplitude dependent.

of 0.1 seconds which is always presented in the prediction. This leads to a delay in the processing of the posture command which therefore produces the corrective torque always delayed. Another possibility where the delay is generated is the sensory processing. Then the estimation could also be more prediction and brings a phase lead for very slow stimuli because the expectation of a stimulus would already produce a reaction to prevent the destabilization by this input. This hypothesis was not tested in this thesis and is left to future research. In the nonlinear model the lower amplitudes and frequencies lead to an increase in phase but as the sway response contains a high level of noise, due to the great amplification of the nonlinear function, this raise is also due to noise.

Very low frequencies could not be reasonably simulated because the quantization error lies by 0.01 Hz. Lower frequencies than 0.03 [Hz] are therefore not simulated. Second, according to the properties of a linear system, the COM sway amplitude for different stimuli amplitudes is a linear relation with different gradients for different frequencies which is seen in figure 4.27.

If the visual velocity processing is modeled nonlinearly this influences the sway response nonlinearly. In figure 4.28 the nonlinear system response can be seen for different amplitudes. For low amplitudes the response increases but for higher amplitudes the response saturates. The saturation is due to the nonlinear logarithmic correlation of the visual processing to the visual stimulus which was described earlier in 4.2. The tested stimuli here had an amplitude of $(1, 3, 5, 8, 12, 18 \quad [deg])$ of angular maximum. The frequency is simulated with 0.2 [Hz]. A saturation effect is also documented in literature [139, 136].
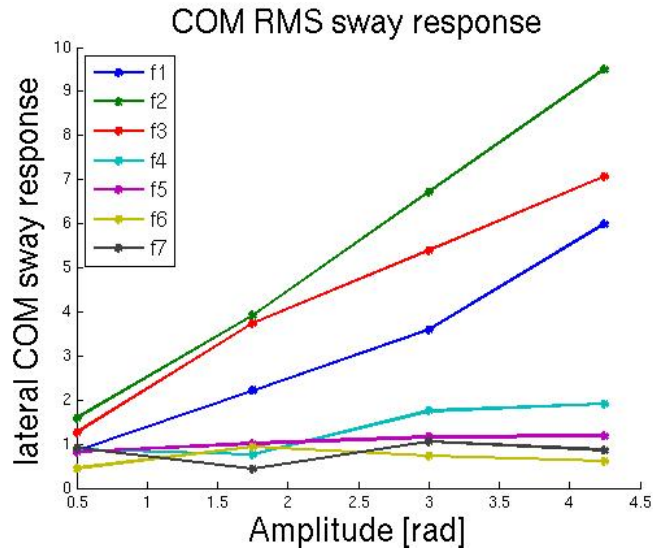
Figure 4.27: Linear model: Angular COM sway response is linear over varying stimulus amplitudes with different gradients for different frequencies.
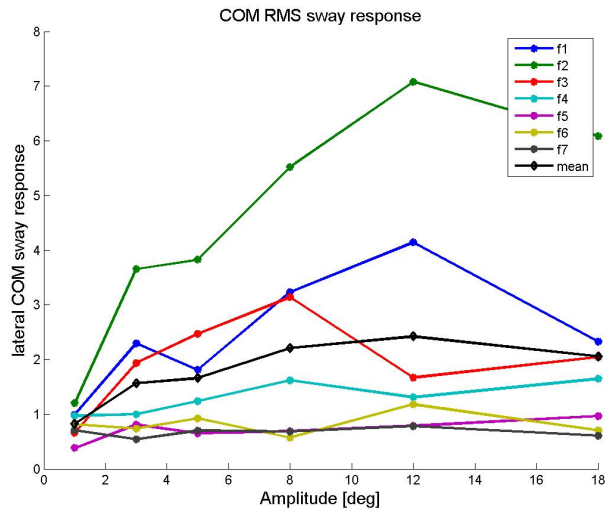
Figure 4.28: Nonlinear model: Angular COM sway response over varying stimulus amplitudes for all frequencies.
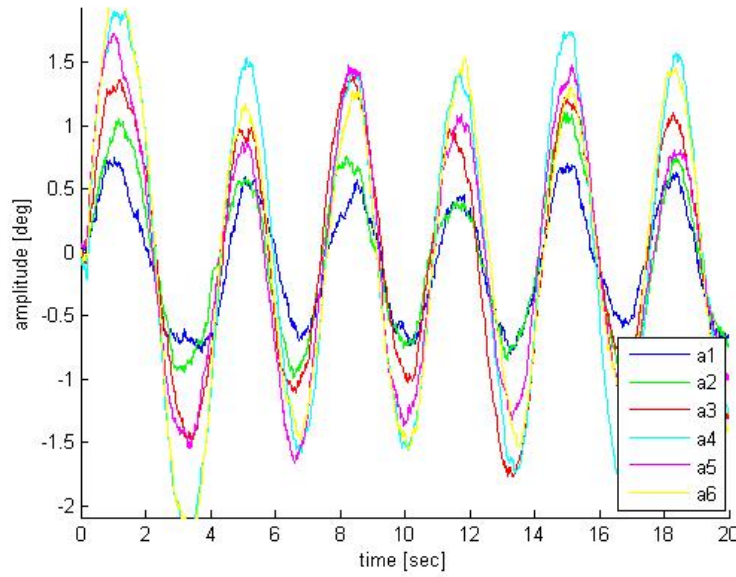
Figure 4.29: Nonlinear model: Body sway response to visual stimuli with different amplitudes with low noise covariances $Q_{cov} = 0.0005$ and $R_{cov} = 0.005$.

One example of actual sway response positions is shown in figure 4.29. The nonlinearity of the visual sensory cue leads to the decreasing effect of sway amplitude raise for increasing stimulus amplitudes $a1$ to $a6$. A saturation of sway response is performed with increasing stimulus amplitude. The visual sensation of movement decreases with increasing movement. This phenomenon is also found in many intensity-based visual perception tasks and in this research adapted as explained in section 4.2.3.

4.5.4 Eye Movement Stimulation

Third, the eye movement is simulated according to the own eye movement experiments presented in 4.4.2. The eye stimulus produces a smooth pursuit movement of the eye which follows a moving target. The target movement is sinusoidal. Related to the experiments the amplitude and frequency of the target movement is varied. The simulated position frequencies are f1=0.08 [Hz], f2=0.11 [Hz], f3=0.17 [Hz], f4=0.33 [Hz] and the position amplitudes are a1=6 [deg] and a2=12 [deg]. The noise covariances are modeled with $Q_{cov} = 0.05$ and $R_{cov} = 0.1$. The simulation results are represented in the amplitude and phase of frequency response and the RMS of COM position. The COM position is the angular position of the inverse pendulum. In figure 4.30 the frequency response is seen.

It can be seen that the gain decreases with increasing frequency. This relates also to the findings of the experiment which indicate a decrease of gain. Though the decreasing gain effect in the model is much clearer than in the experiment. The gradient in the

(a) Gain   (b) Phase
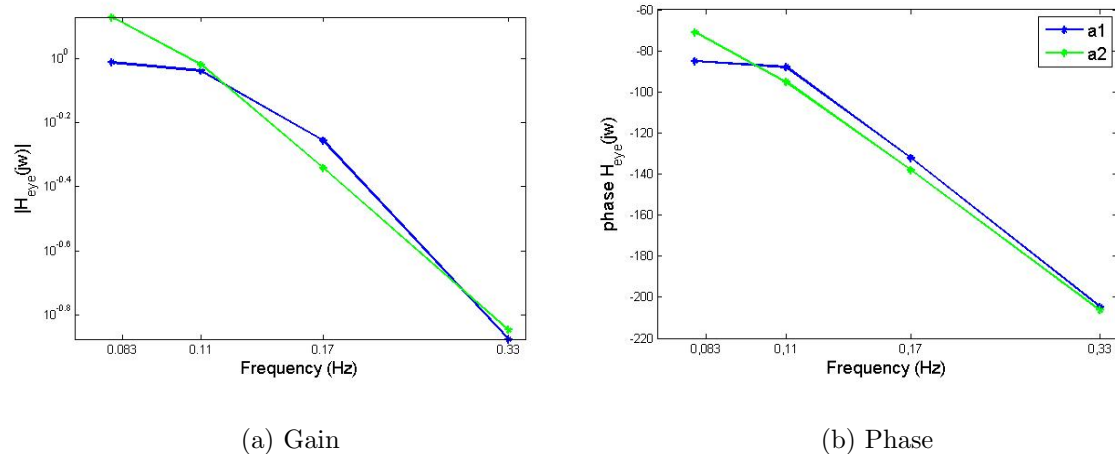
Figure 4.30: Frequency sway response of the body to a sinusoidal stimulus of the eye pursuit for different frequencies and amplitudes. The gain and phase decreases with increasing frequency. The postion amplitude does not make any difference.

simulation depends on the eye movement gain of the processing which could be damped or integrated with further information before used for the posture control. Here in the model the eye movement information is directly used for the sensor integration which can be a reason for a more direct and enforced influence of the eye movement compared to the experiment. Another reason can be that the experiment measures are influenced by more than only the eye pursuit and produce therefore a noisy diminished response. The amplitude variation does make little difference in the simulated gain or phase. This indicates that the proportion of stimulus to sway response is linear over the amplitudes. If the frequency is close to the cutoff frequency of the low pass filter the amplitude makes a difference because the transfer function is no longer linear. The phase function also shows a decrease which means more lagging with increasing frequency which is also expected. This phase decrease is more variable in experimental data. But in the experiments with higher amplitude $a2$ a steady decrease down to -175 [deg] shows the same effect. For the low amplitude the sway response is not so closely correlated and therefore the phase lag is much more variable. The phase decrease of the simulation for amplitude a2 is about the same in simulation. A lower amplitude a1 leads to a slower phase decrease which is due to the lower velocity of the stimulus.

In the next figure 4.31 the simulated mean RMS values of the COM can be seen. In figure 4.31 it can be seen that the RMS value decreases with increasing frequency and with decreasing amplitude. The decrease has a bend near the cutoff frequency of the eye movement low pass filter. This low pass filter is a simplification of reality, this bend would be expected not so clear and sharp in reality. In the experiments also a tendency of decrease is seen especially for the condition with higher amplitude $a2$. The best correlation is with higher amplitude and the normal stance condition on foam rubber which is also
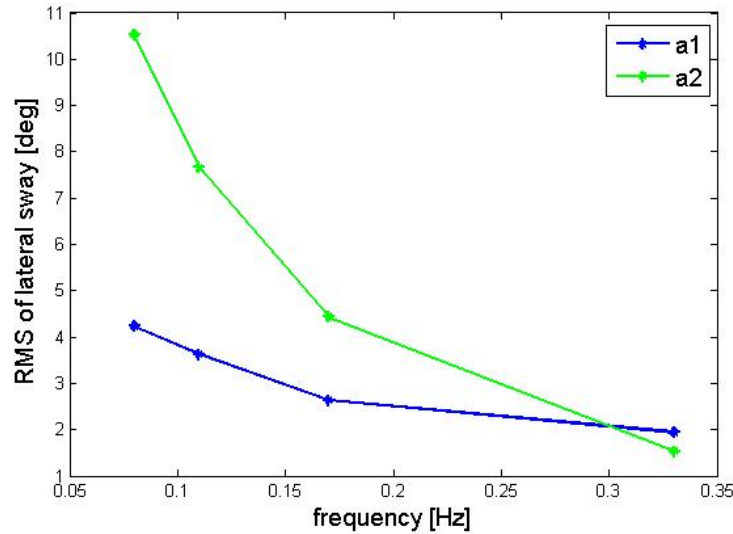
Figure 4.31: Body sway response (displayed by the mean RMS of COM angular values) for the four stimulus frequencies and two amplitudes of the eye pursuit experiments. The sway decreases with increasing frequency and an increase in amplitude triggers a rise in the sway response for low frequencies.

closest to the simulated model. In general the higher amplitude produces a higher RMS sway response but this effect decreases with rising frequency. Why the results are like this can best be seen for 4 examples of the real mean time signals of body response to input signal u_t. For this see the following plots 4.32. One can see, that the target velocity is directly proportional to the sway amplitude but indirectly proportional to the sway frequency according to the low pass characteristic. In the model the decrease with increasing amplitude could only be achieved by the nonlinear logarithmic visual sensory cue. In this eye pursuit experiment the visual input is small and the effect of this nonlinear visual perception is therefore not visible for high gains of the transfer function.

The experiment of Stoffregen et al. [169] uses higher frequencies $f1 = 0.5$, $f2 = 0.8$, $f3 = 1.1$ $[Hz]$, those frequency conditions have also been tested with the model. The frequency transfer function results are similar to the results above but the RMS values differ. This is seen in figure 4.33. In the figure it can be seen that there is no increasing or decreasing tendency recognizable. This happens because the low pass characteristics applied to the eye movement sensation reduce these higher frequencies to a similar response gain and thus the effect is not different. Further, it can be seen that the fixation condition has a higher variability which would also correspond to the findings of Stoffregen et al.[168].
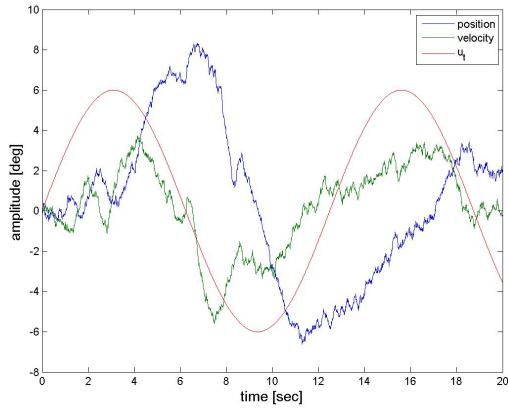
(a) a1 f1
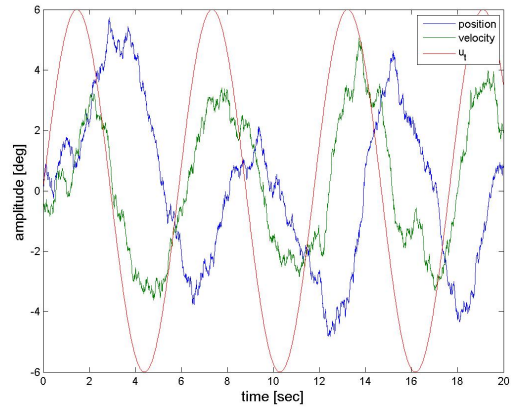
(b) a1 f3
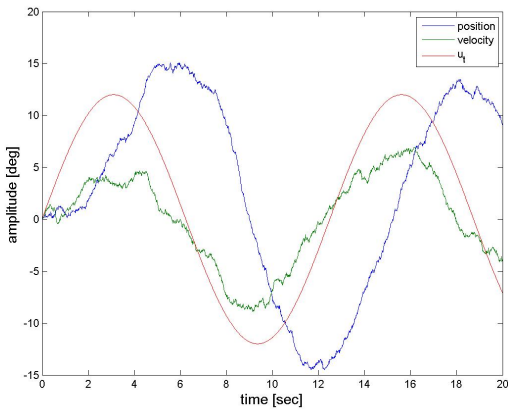
(c) a2 f1
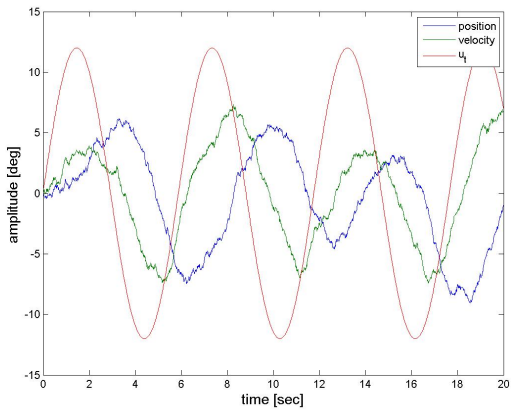
(d) a2 f3

Figure 4.32: Simulated signals of angular sway position and velocity in relation to the visual input u_t of target movement for eye pursuit.
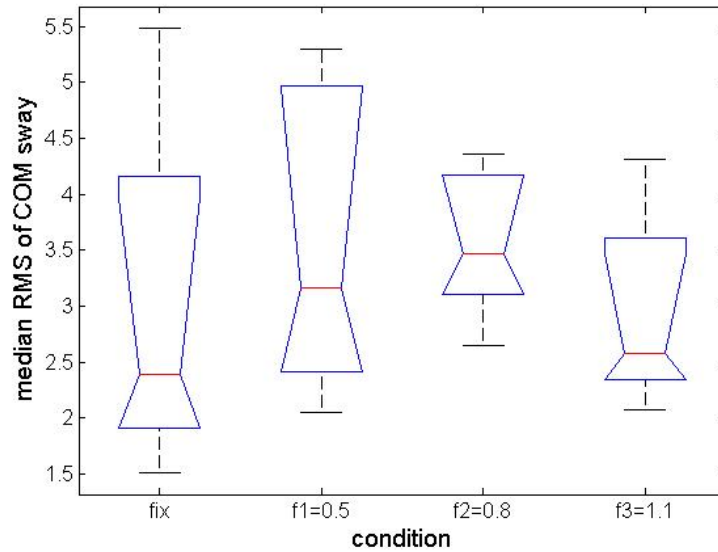
Figure 4.33: Body sway response median RMS for the experiments of [169] with higher frequencies in relation to the fixation condition.

4.5.5 Combined Retinal and Eye Movement Stimulation

Fourth, the dependence on the stimulus is simulated according to the experiments of Glasauer [43]. The visual stimulus consists of a sinusoidal moving point, as mentioned above, which is pursued by the eyes, and a background which is off or on and moving together with the point or stable. The conditions therefore are as set down in Glasauer et al. [43].

(a) The sway response of eyes closed condition is simulated. Then (b), the sway response to eyes open and fixation of a stable or sinusoidally moving point is presented. And (c), the sway response of a stable or sinusoidally moving point with a background is shown.

The simulations have been run with linear and nonlinear visual and eye proprioception sensory parts. The six visual conditions $F1, F2, F3, E1, E2$ and $E3$ (dark,fixation,fixed target with moving background, moving target without background, moving target with fixed background, moving target and background) explained in figure 4.6 of [43] have been simulated with the following parameters: $Q_cov = 0.0005; R_cov = 0.005$, stimulus amplitude 3[deg], stimulus frequency 0.2[Hz]. The noise and noise covariances have been chosen to be very small to avoid the influence of noise on the response and to see the characteristics more clearly. Five trials have been averaged to show the results. In figure 4.34 the six conditions can be seen with mean sway response and the applied stimulus. The mean response is calculated from 5 trials. The RMS was also calculated and the median RMS of sway angle with 95% confidence is shown in figure 4.35. The conditions F2, F3 are clearly different to the conditions E. This is because the influence of visual influence is none in F1 and constant in F2 which means zero velocity. The background movement of F3 is diminished by the eye movement which is fix and linear. In conditions E1 to E3 the
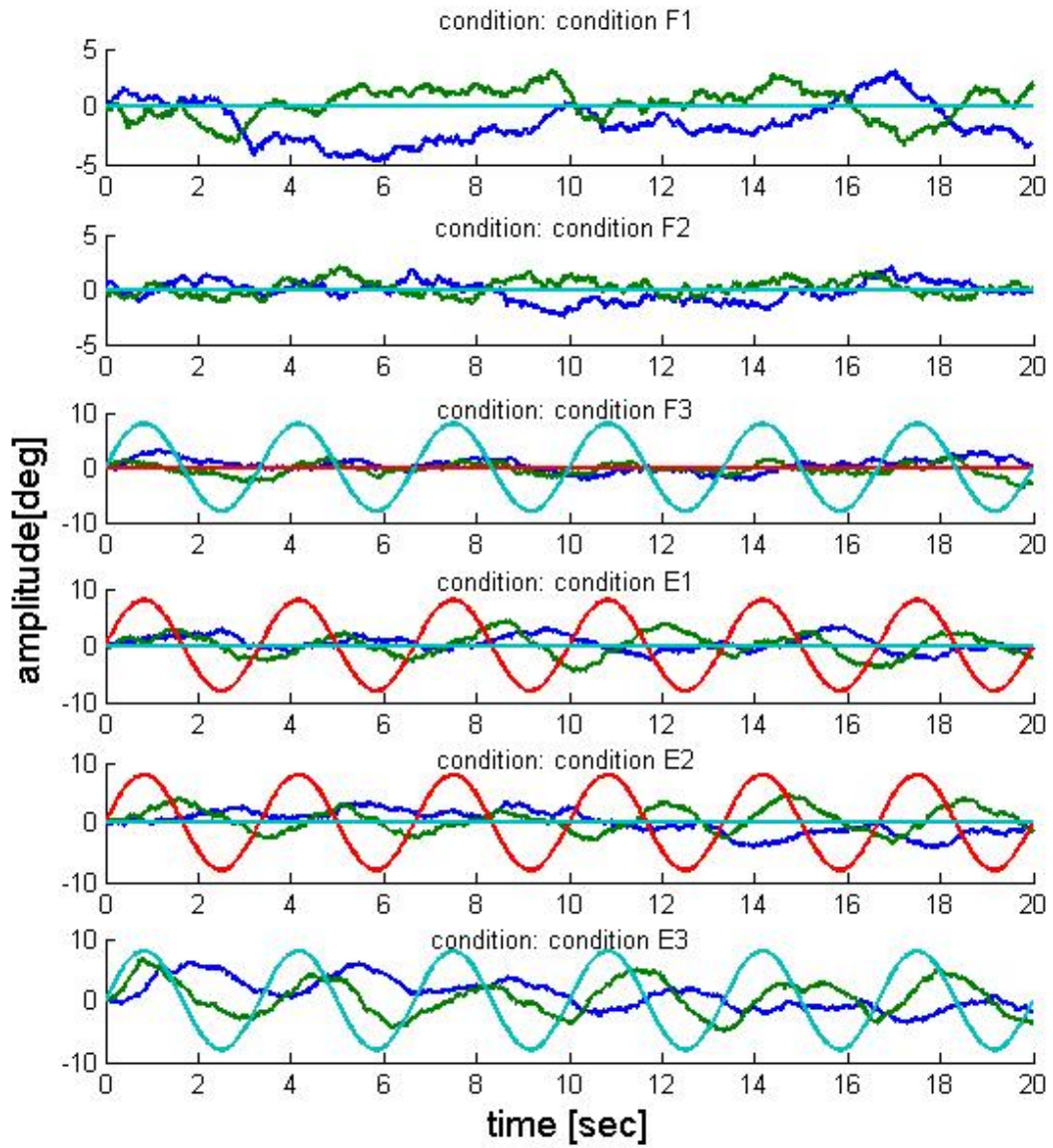
Figure 4.34: The conditions with varying stimulation combinations E1 to E3 and F1 to
F3 (red) with resulting angular body position (blue) and velocity (green).
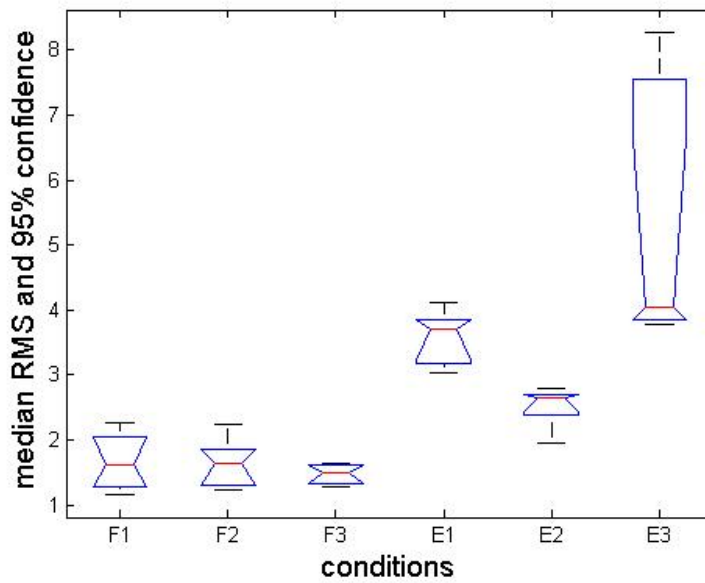
Figure 4.35: Median RMS sway values for all 6 visual stimulation conditions E3 and F1 to F3 with higher relative visual gain.
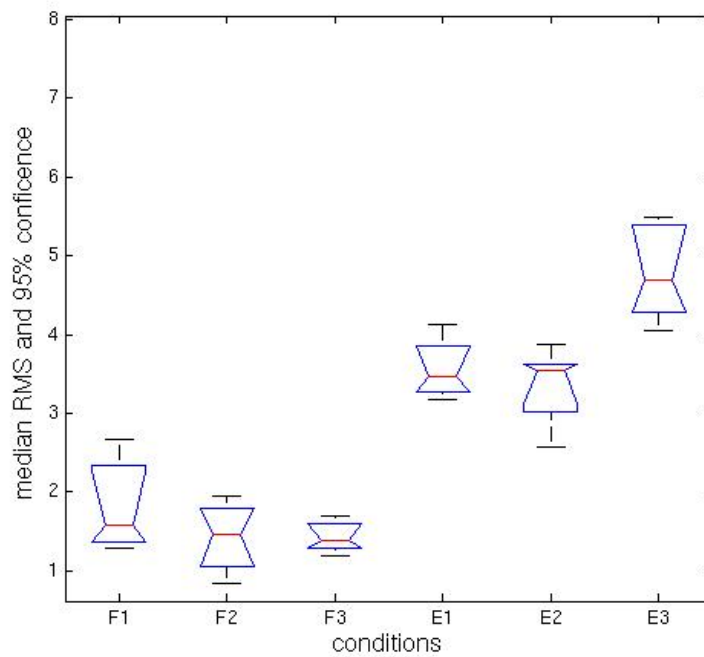
Figure 4.36: Median RMS sway values for all 6 visual stimulation conditions E3 and F1 to F3 with lower relative visual gain.

amount of visual information differs but in condition E1 and E3 the information of the eye movement and the visual background are equal and therefore the effect is reinforced. The effect of E3 is higher than in E1 because the amount of visual information is in E1 reduced to one moving point but in E3 it is a point and the whole background moving together. The condition E5 shows the moving point with stable background here the information of the eye movement conflict the retinal measured movement of the background. The influence of eye pursuit on posture control is therefore not so strong if it is measured as conflict, or even the cue with the right information, here the background, is favored. This can be seen in the difference between the two plots 4.35 and 4.36 here the general fixed weight of the visual velocity measurement was decreased. Therefore the visual influence decreases and the eye movement gets more weight. If the visual information gives correct information to stabilize the body like in F2 and E2 the body sway increases, else it stays or decreases. In other words there is more information available which is correct, related to the environment and body relation and which can be used to stabilize the body more effectively. The effect that F3 stabilizes the body better than condition E2 could be attributed to the influence of eye movement on the posture control. If the eye movement is very important for the postural stabilization this will lead to a stronger influence of the sensory input of eye movement than of the visual measured movement, because in this case no additional visual or learned context information could be used to enforce one cue.

4.6 Discussion

Vestibular, visual and eye movement stimulations were tested in the author's own experiments and examined in literature and were evaluated in simulation using the posture control model presented. The general characteristics of the stance model are described as sensor integration in the Kalman estimation process with a delay in processing, and negative feedback control with optimization criteria.

Galvanic stimulation leads to very good sway response similarities comparing simulation with experiments. The timing and characteristics of the sway response correlate highly with the experimental findings and theory.

Eye movements and visual processing are more complex sensory cues. Nevertheless, in many conditions the simulation results show the same characteristics as those found in experiments and in the literature. Retinal velocity stimulation leads to similar frequency response functions. Only the phase is different, and this is explained by the fact that the estimation processing incorporates only one delay, which is a rough simplification of reality.

The same phase as that found by e.g., Peterka [139], cannot be reproduced. This could be due to the simple delay modeling or due to the fact that it is the frontal sway response which is evaluated rather than the sagittal sway. This is sufficient, however, for the later balance control function of the stepping movement and the phase function represents reality qualitatively, but not quantitatively.

The simulation of various eye movement stimulations finds that the sway response gain decreases as stimulus frequency increases. This is the same finding as in the experimental results. In the literature there are two contrary hypotheses about the correlation between eye movement and postural sway. Glasauer et al. [43, 146] postulates that they correlate and Stoffregen et al. [169] says that this is not the case. In the model developed here the decreasing effect of the eye movements on the sway response can be explained by the low pass filtering of the eye movements. This explains the finding of [169] as well as the results of the experiments presented here; the explanation is not that there is a lack of correlation between the eye movements and postural sway but that there is low-pass correlation. Eye movements were tested on the model used in the present study but at higher frequencies of 0.5 0.8 and 1.1 [Hz] used in Stoffregen et al. [169] in relation to a fixed stimulus with a frequency of zero. In this case, as the frequencies are already high and the body sway response is therefore very low, the RMS values do not differ much; in particular there is no evidence of sway response tending to decrease with increasing frequency. This is a probable explanation of why no difference was established between the frequencies in the studies published by Stoffregen et al. [169].

Then there is still the question of whether eye stimulation leads to an increase or decrease in body sway response. As was shown in the 3 different experiments both are possible, which means the studies in [43], which ascertain increasing body sway, as well as in [169], which find decreasing body sway have to be considered. The explanation for these contradictory findings, according to the model proposed here, is that the sway response depends on both the frequency and amplitude. The higher the frequency and the smaller the amplitude, the lower the RMS of the sway response. But if the amplitude is very low, it is also very close to the signal-to-noise ratio. This can also be seen in figure 4.8 in condition $c3$ where the amplitude is too small. As is seen in the simulation results in figure 4.33, where the condition fixed is compared to the others, and 4.36, with conditions F2 and E1, the mean RMS value of the sway for fixation and eye movement is not always equal. The model proposed here makes it clear that sway response as a result of eye movement conditions depends on the frequency and amplitude of the stimulus and also that the fixation varies because of the noise variances. This is one possible reason for the contradicting results of the experiments but there are also other factors which explain this effect. For example the type of visual stimulus e.g., size, contrast, information, and the influence from other sources such as level of attention to a task or the stance condition. This cannot be tested with the model presented, because those factors are not modeled; a larger eye movement study which takes such factors into account would be of further use. As noted e.g. in Peterka [141], an additional fixation of the body itself reduces the noise in the sway data, and this helps to isolate the body sway response.

The combined eye movement and retinal velocity processing was represented by a nonlinear model related to the logarithmic perception law of Weber-Fechner. This extension of the model reproduced nonlinear saturation effects which are explained by other models, such as [180] where state noise covariances are adapted, or in [136] where sensory weights are adjusted to minimize the mean square of the control or in [118] where threshold func-

tions are reweighted. In the presented research the visual velocity processing is modeled nonlinearly according to the Weber-Fechner law. The eye movement sensory cue model is linear according to the amplitude behavior. However for stimuli which already lead to highly nonlinear responses, the eye movement cue automatically has a greater influence on posture control because of the saturation effects. This is an explanation for the differences established for conditions F3 and E2 of [43]. The saturation effects in posture response of visual stimuli amplitude can also be reproduced by this nonlinearity. The evaluation of this hypothesis needs to be studied in further experiments for eye vision combinations and combinations with other sensory cues.

4.7 Conclusion

Using the chosen sensors, high-level processing for state estimation (Kalman) and LQR feedback control, the model presented here provides a solution for balancing in the upright stance using high-level integrated sensory information. In other words this model enables the environment to influence posture control and in addition a holistic posture is determined for the stabilization of the whole body.

According to the simulation results it can be said that the model takes into account several vestibular and visual sensory stimulations at the same time stabilizing the posture for upright stance. These simulations were compared with real experiments and experimental findings in the literature to show that the behavior is very similar.

The model is therefore able to take different environmental conditions into account. It can adapt to different sensation situations such as: missing sensory cues (eyes closed), disturbed sensory cues (galvanic vestibular stimulation), sensory cues being influenced by a task (eye pursuit influences vision), or stimuli situations such as a visual background and eye movements conveying the same or different information about the environment, leading to conflicting measurements. These situations can happen in real life and they are used here to evaluate the posture control system. Extending visual sensory cue by a logarithmic nonlinearity accounts for the stimulation effects and explains the nonlinearity by a common perception law (Weber-Fechner).

Although the model presented here was tested and evaluated for balance in stance, the maintaining of equilibrium generally represents the same task during stepping movements. The sensory information is needed for the present study, although the special influence of sensory cue stimulus inputs on stepping posture is not examined extra in this work. In the present research the stimulus effect on balance was evaluated in order to guarantee that the posture model explains typical stimulated postural responses; these constitute a suitable basis for further perception experiments as well as for extended posture control tasks. The model developed here for posture control is able to determine the whole body position, a feature which the low-level neuro-mechanical model lacks. In the following chapter, the same model is applied to the stepping task.

5 Integration of High-Level and Low-Level Models

The high-level posture control model uses high-level sensory information to stabilize the whole body. In contrast to this the low-level model autonomously generates stepping movements without taking the overall position into account. The objective of the integration in this chapter is to improve the stability of the low-level model by integrating high-level sensory information and knowledge. In the following, those two models are integrated to achieve enlarged moving range by incorporating sensory cues, and thus enabling perception of the body in relation to the environment. The concept of integration is a superposition of high-level and low-level actuation which depends on the overall body balance. Only if the balance is considered to be at risk or consciously influenced, the high-level control influences the stepping task.

In the following the integration of high-level and low-level models represents a possibility to expand the working range of the stepping model. The performance of the integration is examined by looking at the following four exemplary problems of the low-level model:

1. First, the stability depends on the initial values as the limit cycle approximation is an initial value problem; in contrast to this a human being can start a stable stepping movement with any normal initial leg position.

2. Second, an asymmetric stepping pattern is not corrected in the low-level model but repeats itself which leads to a drift in the movement.

3. Third, unsuitable feedback tuning can lead to instability.

4. Fourth, the sideward movement tends to drift because the direction of movement is not determined.

Section 5.1 presents a number of state-of-the-art models which combine stepping movements with body stabilization. Here a special mention is made of the correlation between the model and the most common principles of robotics, as robotics is the field with the largest variety of low-level and high-level control principles. In section 5.2 the superposition control concept used for the integration is derived. In section 5.3 the integrated model composed of the individual components is introduced, adapted to the stance-control concept and extended to include the possibility of additional hip control. The results of the simulation of the four cases proposed above is detailed in section 5.4. And, last but not least, in sections 5.5 and 5.6 the control concept is discussed and summed up on basis of these four representative stabilization cases .

5.1 State of the Art of Integration Models

In robotics there are many integration concepts as these are essential for building a stable walking robot. There are some impressive examples of walking robots such as the Honda's ASIMO [173], robots JOHNNY and its successor LOLA developed by the Technische Universität München [42] or the biologically motivated RunBot [41]. In robotic systems no differentiation is necessarily made between high level and low level, but e.g. the exact position, velocity or acceleration, are used in the same way as overall information in a central control unit or a centrally mastered distributed control system.

Control and generation of actuation is often divided into pattern generation, e.g. by trajectory generation and overall balance control. There are various examples of this division, e.g. trajectory planning and control [173, 42, 104] which is used in ASIMO and JOHNNY to control the movements of all links. In RunBot sensory perception is directly integrated in the neuronal actor to control the link movement directly and locally [105]. The overall behavior is trained by a high-level learning algorithm for the neuronal system.

One difference between theoretical models and the robotic systems named above is the ground contact. In theory the ground contact is often modeled instantaneously, as in this study, but in a real robot the double support phase has a defined duration. This duration is very important for step control and the smoothness of stepping [160] because this phase includes the slow-down of the last step and the speed-up with the next step. In real systems this phase is not as abrupt as with an instantaneous model and is dependent on several ground contact constraints to control step parameters [103].

A large group of robots are based on trajectories which are either precalculated [83, 164] or calculated online on basis of models [84, 191]. Those trajectory calculations depend on the model and require accurate state information e.g. the inertia of the links, acceleration of body parts etc. In Sobotka et al. [164, 196] the precalculated gait trajectories are modified online by a Jacobi compensation. With this method trajectories are adapted in the case of unexpected deviations from the precalculated situations. This is achieved by adding to the precalculated value a joint space transformation which corrects the movement to follow one direction.

The overall balance controllers are a group which Kajita [84] termes ZMP (Zero Moment Point) controllers because the ZMP is often used to control the balance. This means to maintain balance the ZMP is controlled which means it is kept in the allowed range for example the support foot area or a desired position. Many similar but different explanations have been given for the ZMP. One practical explanation is that published by Arakawa and Fukuda [2], who state that the ZMP is the point on the ground where all moments generated by reaction forces and reaction torques are in balance, the point at which their sum is zero. This ZMP control requires either an exact knowledge of the dynamics of the body mechanics and their states, or a model-based approach including prediction. The latter group of systems which use rough knowledge in the form of a model of the body dynamics, e.g. the ZMP, are mainly dependent on feedback information. In this context an inverted pendulum model is often used to represent simplified body

mechanics [84].

If a system is generally unstable or has an internal dynamic according to the theory of non-minimal-phase systems, such as an inverted pendulum with unstable pole-zero compensation, a static state feedback is not sufficient to stabilize the system [71]. As invariant control feedback is not sufficient to stabilize such zero-dynamic systems [71] the direct relation between control torques and ZMP dynamics in a loop has to be broken by predictions or substitutions. There are therefor several control approaches in robotics which combine ZMP feedback control with an additional approach. In robot JOHNNY [104] the ZMP control is substituted by direct contact force control, once it has left a permitted range for the ZMP area. Another example is found in Sobotka [163], where a nominal ZMP control is substituted by precalculated trajectories. This substitution occurs when the ZMP leaves the allowed ZMP area. The balance control is then determined by invariant control of degree-one ZMP feedback linearization. A multi-control approach is used by Kim et al. [90], where the nominal trajectory planning is complemented by three additional controllers to achieve balance control. One controller is the ZMP compensator, which compensates the instability on the bais of the poles of zero-dynamic system.

Another class of control strategies which are applied to generate walking movements are the models which use predictive control, often in combination with optimal control, to achieve e.g energy efficient gait patterns or to enforce periodicity of the trajectory for a periodic gait. An example is given in Morimoto and Atkeson [130], where optimization is achieved by applying a modified criterion of low torques and periodicity which includes disturbances, and therefore results in robust stable walking. In [176] the body dynamics are modeled by linearized pendulum dynamics and the movement is predicted in order to control joint impedance. Kajita et al. [84] uses a combination of model-based ZMP control with predictive movement control to generate stable stepping movements. In Wieber [191], too, a method is proposed for generating walking movements by prediction of the ZMP movement and optimization of maintaining the COM (Center of Mass) at a constant height.

The biologist Cruse [24] once said that a characteristic behavior of the biological system is the autonomy of the movement parts. This means that not only the brain but all parts like e.g. muscles, neurons have their own rules and plans to follow to achieve a final successive movement.

Therefore in the model of this thesis the low-level component for stepping is left autonomous as presented in chapter 3. Therefore the low-level stepping control itself is not directly influenced but indirectly because the two levels are superposed. The superposition of high and low level actuation is dependent on the overall body balance. Only if the balance is considered at risk the additional high-level actuation is applied. Further, the model of the body dynamics in the brain is simplified very much to the abstract inverted pendulum model of the COM. The high-level sensor integration part of chapter 4 is used to predict and control the COM to stay in a normal range. With normal a range is considered to be stable with high probability and the fall risk is low. The control is achieved by superposition of low-level actuation with high-level corrective torques if the normal range of the COM is left. The interaction of these two parts is shown in principle to give

and idea about the possible influences and dependencies and not to give a full analysis of the control problem.

5.2 Control Strategy for the Stepping Model

The four scenarios described in the introduction of this chapter, (1) initial conditions correction, (2) prevention of drifting movements (3) improper feedback gains and (4) stepping to the side are presented to show the application of the high-level control model to the low-level stepping model. This application needs a slightly extended control concept than the linear quadratic feedback controller of the stance control. This is because now not only the stance leg but also hip and swing leg movements are parts of the system which have to be considered. In the following it is not the objective to control the general rhythmic stepping movement but the global stability and balance. As before the stepping is generated by the low-level neuronal level. If one imagines a stepping body it is obvious that the high-level sensors only perceive movements of the whole body which in turn leads to the brain generated corrective commands. This whole body is represented by the center of mass (COM). Biologically this can be interpreted as the balance point of a body according to gravity. This is selected because the vestibular or proprioceptive sensors perceive the whole body sway acceleration or position and the visual sense perceives the relation between the whole body movement and the movement of surroundings. This is a simplification of the body. The brain does not have an accurate model of all body parts which leads to the fact that the posture control Kalman estimation bases on an inverse pendulum model representing the COM movement according to the stance leg. This simplification comes up for inaccuracies and not well experienced movements and inadequacies of the brain computations. Additionally the hip movement which results in an up and down movement is sensed by actual sensory data and COM prediction values to control the vertical hip movement in relation to the COM.

The general feedback control concept applied to the low level is divided in two: no additional control if the system works in the normal range and an additional high-level control if the system leaves this normal range and is at a risk to become instable. So, when everything is 'normal' the stepping is an automatic autonomous movement. But if stability is threatened or something is consciously intended an additional corrective control signal is applied as superposition of the actual movement. In the following the concept of the 'normal' range and the according control is introduced.

5.2.1 Feedback Linearization Theory

A negative feedback linearization for a time invariant control system for an input output SISO or MIMO system is derived in the following. With the nonlinear system is written

with input vector u and output vector y as:

$$\dot{q} = f(q) + g(q) * u \qquad (5.1)$$

$$y = h(q) \qquad (5.2)$$

where q is the vector of system states and f is a function of the dynamics of these states, g is the mapping of the states and the inputs on the states and h the output function. Now the output y is differentiated till the output is any function f of the input $\partial y / \partial q = f(u)$. The differentiation is:

$$\dot{y} = \frac{dh(q)}{dq}\dot{q} = \frac{dh(q)}{dq}f(q) + \frac{dh(q)}{dq}g(q) * u \qquad (5.3)$$

If now the equation of the n-th differentiation is set to $\partial y^n / \partial q^n = f(u) = a(q) + b(q) * u = v(q)$ where a and b are matrices and b is called the invertible matrix for MIMO systems. Therefrom the value of u can be determined analytically by:

$$u = b^{-1} * (-a + v) \qquad (5.4)$$

A common term to describe the differentiation is the Lie derivative. The derivative in equation 5.3 is computed using the chain rule. The Lie derivative of h(q) is defined with respect to f(q) as:

$$L_f h(q) = \frac{dh(q)}{dq}f(q) \qquad (5.5)$$

And similarly, the Lie derivative of h(q) is defined with respect to g(q) as:

$$L_g h(q) = \frac{dh(q)}{dq}g(q) \qquad (5.6)$$

This notation leads to the expression of $\dot{y}$:

$$\dot{y} = L_f h(q) + L_g h(q) * u = v(q) \qquad (5.7)$$

n times differentiation of the output y leads to:

$$
\begin{aligned}
y &= h(q) = z_1 \\
\dot{y} &= L_f h(q) = \dot{z}_1 = z_2 \\
\ddot{y} &= L_f^2 h(q) = \dot{z}_2 = z_3 \\
&\quad\vdots \\
y^{(n)} &= L_f^n h(q) + L_g L_f^{n-1} h(q) * u = \dot{z}_n = v(q)
\end{aligned}
\qquad (5.8)
$$

The control input u can be derived as before in equation 5.4 with:

$$u = \frac{1}{L_g L_f^{n-1} h(q)}(-L_f^n h(q) + v)$$

To design v a linear term can be used e.g. a term of the form:

$$v(q) = -k_0 * y - k_1 * \dot{y} - k_2 * \ddot{y} \ldots$$

With this design the objective is that the values run to their desired values: $y \rightarrow y_d$. If there are internal dynamics (zero-dynamics), so that the system requires a perfect model to achieve a robust control, then the order of the control term has to be raised. A possibility is an additional robustness term added to the control according to [58] e.g. a dynamic extension which considers the zero-dynamics.

5.2.2 Applied Feedback Linearization for Hip Movements

As the model does not contain a trunk model, a representative movement of the whole body is given by the center of mass COM. The modeled angular positions and velocities are the COM position and velocities in medio-lateral direction. Additionally, there is a model of the vertical movement of the COM as bigger hip movements result in a vertical movement which can not be achieved by an inverse pendulum model. It is a vertical movement according to gravitation.

The vertical part of the COM com_y which is also perceived by the sensory cues is determined by:

$$y = com_y = f(\alpha, \beta) = 1/M_G*((2*M*l+3*m*l)*cos(\alpha)+(M*h+2*m*h)*sin(\beta) \quad (5.9)$$

where the angles and masses are as introduced in the mechanics section 2.3 in figure 2.4 and 2.5. The derivative of com_y after the vertical position and velocity of the COM is built to get a direct relation between the com_y and the external input u_b to the hip joint. This is the feedback linearization, according to equation 5.3. The up-and-down COM movement for big hip movements can be described as a movement originated by gravitation and external input u_b. The hip movement originates from gravity and applied joint torques which interact to stabilize the hip which lead to the following simplified equation:

$$\begin{pmatrix} \dot{x}_1 \\ \dot{x}_2 \end{pmatrix} = \begin{pmatrix} 0 & 1 \\ 0 & 0 \end{pmatrix} * \begin{pmatrix} x_1 \\ x_2 \end{pmatrix} + \begin{pmatrix} 0 \\ u_b - g \end{pmatrix} \quad (5.10)$$

where the vector x are the vertical hip position and velocity. The $y = com_y$ is differentiated according to $\dot{y} = \dot{com}_y = \frac{\partial com_y}{\partial x_1} * \dot{x}_1 + \frac{\partial com_y}{\partial x_2} * \dot{x}_2$ two times until the input u is part of the

equation according to equation 5.8 which leads to:

$$z_1 = y$$
$$z_2 = \frac{\partial y}{\partial x} = M_v * cos(x_1) * \dot{x}_1 = M_v * cos(x1) * x_2 = L_f^1 \qquad (5.11)$$
$$z_3 = -M_v * sin(x_1) * x_2^2 - M * cos(x_1) * \dot{x}_2 = L_f^2 + L_g(L_f^1) * u$$

with $M_v = M*h+2*m*h$. By insertion of equation 5.10 into equation 5.11 the following equation is obtained:

$$L_f^2 + L_g(L_f^1) * u = M_v * sin(x_1) * x_2^2 - M_v * cos(x_1) * g + M * cos(x_1) * u_b = v \quad (5.12)$$

Now $v = k_0 * (com_y - com_{y0}) = k_0 * (y - y_d)$ is a linear controller with y_d is the desired and normal position of the COM com_{y0}. This leads to the equation of control input u_b:

$$u_b = \frac{v}{M_v * cos(x_1)} + tan(x_1) * x_2^2 + g = \frac{-k_0 * (y - y_d)}{M_v * cos(x_1)} + tan(x_1) * \dot{x}_1^2 + g \qquad (5.13)$$

This calculates the corrective input for the hip movement where x_1 is the hip position derived from the angular hip movement which is derived as $x_1 = h * sin(\beta)$ (for this see figure 2.5). This is proportional to the actual COM position minus the com_{y0} value which depends mainly on the actual stance leg angle. x_2 is the vertical velocity of the hip which is approximated by the velocity of the vertical COM movement which is valid if the hip movement gets larger. This is exactly the case when the additional control is used.

5.2.3 Applied Preview Control and Optimization Criteria

First, the preview control is used for the COM position. The COM is modeled as an inverse pendulum movement according to equation 2.4 with the state vector $q = \begin{bmatrix} \Phi_{com} & \dot{\Phi}_{com} \end{bmatrix}$. In the Kalman estimation the COM movement is previewed to be controlled by an optimization criterion like in section 4.3.4. The COM movement is perceived by the sensory system and thus integrated in the posture control.
The real COM of the frontal plane mechanical body is calculated as follows:

$$\Phi_{com} = tan(\frac{com_x}{com_y}) = \frac{M_c * sin(\alpha) + M_v * cos(\beta) + m * l * sin(\gamma)}{M_c * cos(\alpha) + M_v * sin(\beta) - m * l * cos(\gamma)} \qquad (5.14)$$

with $M_c = 3 * m * l + 2 * M * l$ and $M_v = 2 * m * h + M * h$. The COM position determined in equation 5.14 is the sensed body COM motion by proprioceptive, vestibular and visual senses. This body motion is representative for one single step from double support phase to the next double support phase and is approximated by an inverted pendulum motion. The modeled COM is represented by the inverse pendulum with angle and angular velocity with the foot of the COM pendulum in the stance foot. The modeled COM mass is represented by one single mass which is determined by the sum of all real body masses which is $M_G = 2 * m + M$. The modeled COM angle relates mainly to the

stance leg angle as the hip mass only contributes to the sinus of the hip angle which is a small value. The desired COM angle is Φ_d and the desired angular COM velocity is zero. The principles of the optimal control according to quadratic minimization criteria was explained in section 4.3.4 of chapter 4 high-level balance control. The criterion to minimize the angular deviation of position and velocity can be directly applied to the COM inverse pendulum position and velocity. The performance is specified by the optimization index derived from equation 4.40. The first J_a is for the pendulum COM movement and the second J_b for the vertical hip movement:

$$J_a = \sum_{i=k}^{\infty} q_i^T * Q_x * q_i + u_a^T * R * u_a$$

$$J_b = \sum_{i=k}^{\infty} e_i^T * Q_e * e_i + u_b^T * R * u_{b0}$$

The two criteria to optimize the COM movement by J_a are therefore:

$$c1, c2 = q * q^T \quad with \quad q = [\Phi_{com}, \dot{\Phi}_{com}] \quad with \quad Q_x = w_{RQ} * \begin{pmatrix} 0.5 & 0 \\ 0 & 0.5 \end{pmatrix} \tag{5.15}$$

with w_{QR} is a positive weighting factor of the matrix Q_x in relation to matrix R. And R is the unity matrix. The third criterion $c3$ to minimize J_b is the optimization of the vertical motion of the COM value, because this is not adequately modeled with the pendulum equation. The vertical hip movement according to the hip angle which is $h * sin(\beta)$ is not modeled. So the com_y goes up and down during a step. If something unexpected happens the com_y is destabilized more than during a normal step and therefore has to be stabilized independently of the pendulum COM movement. Therefore the com_y is feedback linearized with the input u_b to get the relation between input and output. The value of the control factor k_0 is determined by the optimization criterion. The vertical COM position com_y is added as a third criterion which depends on the value of the vertical hip position x_1 and becomes minimal by the hip angle going to be zero:

$$c_e = (x_1)^2 \qquad Q_e = \begin{pmatrix} 1 & 0 \\ 0 & 0 \end{pmatrix} \tag{5.16}$$

u_{b0} is calculated for the boundary condition com_{y0} of the vertical COM movement. If equation 5.13 is calculated with this value, this gives the estimation of the factor k_0 for the feedback linearized vertical COM control by once solving the equation for k_0.

5.3 Applied Integration Model

The control is split up into two parts: the low-level control which is already realized by the muscular position velocity feedback function and an additional corrective control which is applied if the range of normal movements is left. This range of normal movements

is defined according to the inverse pendulum model for the stance leg and a normal dropping and lifting of the hip which is common for stepping movements. For each of the movement directions a range with upper and lower bounds is defined wherein the movement is 'normal' and though not controlled additionally with corrective control u_c. The superposition is:

$$u = u_{act} + u_c = \begin{pmatrix} u_1 \\ u_2 \\ u_3 \end{pmatrix} + \begin{pmatrix} u_a \\ u_b \\ 0 \end{pmatrix} \tag{5.17}$$

The superposed torques are according to the normal range as follows:

$$u = \begin{cases} u_c(1) = 0, & if \quad \Phi_{com}{}^{low} < \hat{x} < \Phi_{com}{}^{high} \quad or \\ & if \quad \dot{\Phi}_{com}^{low} < \hat{x} < \dot{\Phi}_{com}^{high} \\ u_c(1) = u_a & else \\ \\ u_c(2) = 0, & if \quad com_y{}^{low} < x_{esti}(com_y) < com_y{}^{high} \\ u_c(2) = u_b & else \\ \\ u_c(3) = 0 \end{cases} \tag{5.18}$$

with $u_a = K * \hat{x}$ according to the minimization of J_a using method and equation 4.41 given in section 4.3.4. Here $\hat{x}$ is the estimation of the COM states $\begin{bmatrix} \Phi_{com} & \dot{\Phi}_{com} \end{bmatrix}$. u_b is calculated with equation 5.13 by using k_0 calculated with equation 5.16 and $x_{esti}(com_y)$ is the estimation of the vertical COM displacement according to the estimation model of the COM. The values Φ_{com}^{low}, Φ_{com}^{high}, $\dot{\Phi}_{com}^{low}$, $\dot{\Phi}_{com}^{high}$ $com_y{}^{low}$ and $com_y{}^{high}$ are the upper and lower boundaries for the range of the COM movement which is considered to be 'normal' and therefore stable. If the vertical COM movement is larger than the normal range it is certainly due to hip movement. So, the difference between the desired vertical COM position and the actual position is related to the sinus of the hip angle β. The desired value of the the absolute vertical body COM depends also on the stance leg, because the more vertical the stance leg is the higher is desired value $y_d = com_{y0}$. The com_y depends on the input torque of the hip u_b as described in equation 5.13. The value com_{y0} is not static and changes the control condition therefore. The values of $u_c(1)$ are derived from the predictive control of the optimization criteria very similar to the posture control in stance before. The value $u_c(2)$ is derived from the feedback linearized control of equation 5.13.

The complete system is shown in figure 5.1 where the high-level (blue) and low-level (orange) parts are integrated. The torque generation is the superposition of low-level oscillator originated torques u_{act} and high-level torques $u_c = \begin{bmatrix} u_a, & u_b, & 0 \end{bmatrix}$ which are added if the COM position leaves the normal and as stable considered region. On low-level the body states are perceived via the muscular feedback function on high-level they are perceived via the sensors. The high-level statistical estimation estimates the COM position and velocity as angles and angular velocities $\Phi, \dot{\Phi}$ and its estimated vertical

component $\hat{com}_{y0}$ which is compared with the real sensed value com_y to determine the corrective control torques. In the following three examples of superimposed corrective control are shown to demonstrate the effect on stepping stability and sidewards stepping movement.
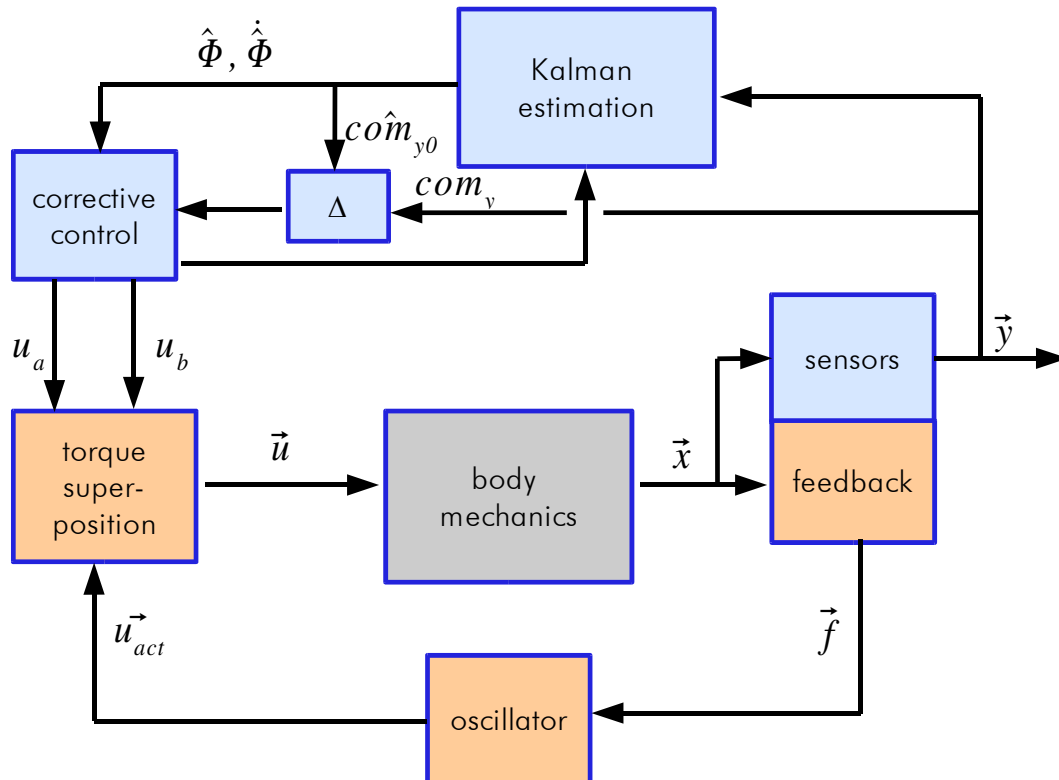
Figure 5.1: Integration of low- (orange) and high-level (blue) systems. The sensors are divided into low-level feedback for direct muscular feedback and high-level feedback for other sensory cues processed in higher levels. Here the high level estimation is abstracted to the COM position and velocity $\Phi, \dot{\Phi}, com_y$. The high-level control is applied by superposition to the low-level joint torques u_{act}.

5.4 Simulation of Low-Level Stepping Movements with High-Level Posture Control

The four examples which are stabilized or improved with the integration of high-level information via sensors and posture control processing are:

(1) bad initial conditions,

(2) asymmetric stepping patterns which lead to a drift,

(4) improper feedback gains which lead to a destabilization and

(3) stepping to the side.

For more convenience the original low-level simulations are always repeatedly shown below the improved new simulations in smaller size. The referenced figures include both figures, the original figures and the small repeated figures with two different reference numbers.

In figure 5.2 case (1) with bad initial conditions can be seen with additional high-level control. It shows the original low-level movement in figure 5.3 which is related to the case seen in figure 3.29. If unsuitable initial conditions are chosen, which are though still realistic angular starting positions, no correction of the initial inadequacy can be achieved. This happens because the autonomous low-level stepping model only continues or reproduces the initial conditions with the provided local feedback and no correction of the global position. In this study, the high-level posture control is used to compensate initially unsuitable values by correcting them. Thereafter, the movement is pushed back to the attractive basin of the low-level stepping movement and is maintains stable without any additional high-level control. The values are all in the normal range again and are not evaluated as a risk to fall, due to unsafe COM positions. The additional control at the beginning drives the system into a stable movement.

In figure 5.4 case (2) with an asymmetric leg movement leads to a drift, which results in increasing leg and hip angles. This would be like a limping with a slow increase of the limping leg angle due to the asymmetry. After several more steps this would lead to a fall down. The original figure for this movement can be seen in figure 5.5 which is related to figure 3.22. The resulting COM movement is a drift and especially an increase of the lateral COM movement. With the additional control this movement can be adapted to a stepping movement with symmetric steps; after a larger first reaction in order to correct the initial asymmetric movement. The following symmetric steps are stable because they are attracted to a stable limit cycle movement after a few steps.

Stepping is unstable if the feedback is not modeled correctly as in case (3) or if the feedback is not correct because of e.g., a longer injury. Figures 3.30 and 3.31 and the repeatedly shown figure 5.7 visualize the original movement with unsuitable feedback (in figure 3.31 it is the first plot in the second line with $f_{dv} = 0.7$, $f_d = 0.3$). The instability occurs because the feedback is not appropriate for the movement and actuation pattern. With a superposition of the high-level control a stable solution of stepping is achieved. In
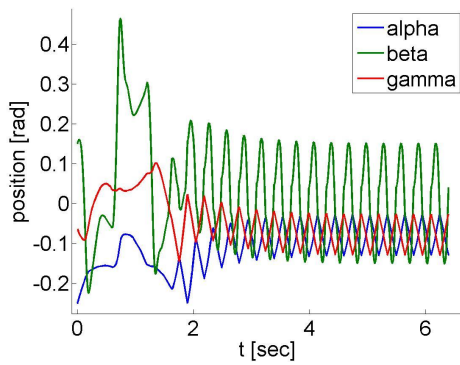
(a) Angular positions

(b) Oscillator activation $F14$

(c) Phase plot

(d) Movement of three steps with initial overshooting

Figure 5.2: Stepping in place with bad initial conditions is converged to a stable stepping in place movement by pushing the solution back to the attractive basin of the limit cycle with the additional high-level COM control.
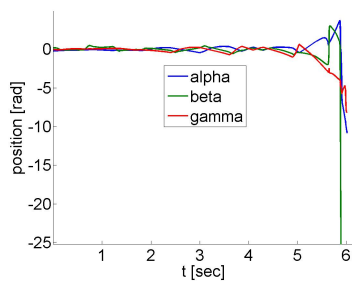
(a) Angular positions
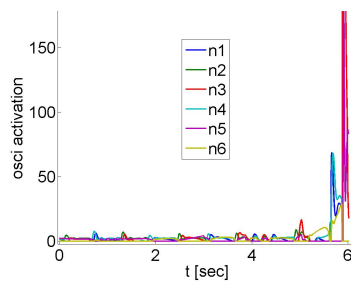
(b) Oscillator activation $F14$
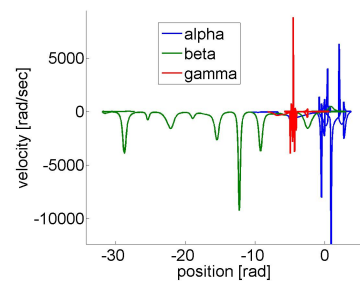
(c) Phase plot

Figure 5.3: The original stepping in place movement with bad initial conditions is unstable.

(a) Angular positions

(b) Oscillator activation

(c) Phase plot

(d) Movement of two steps after settling as stable solution
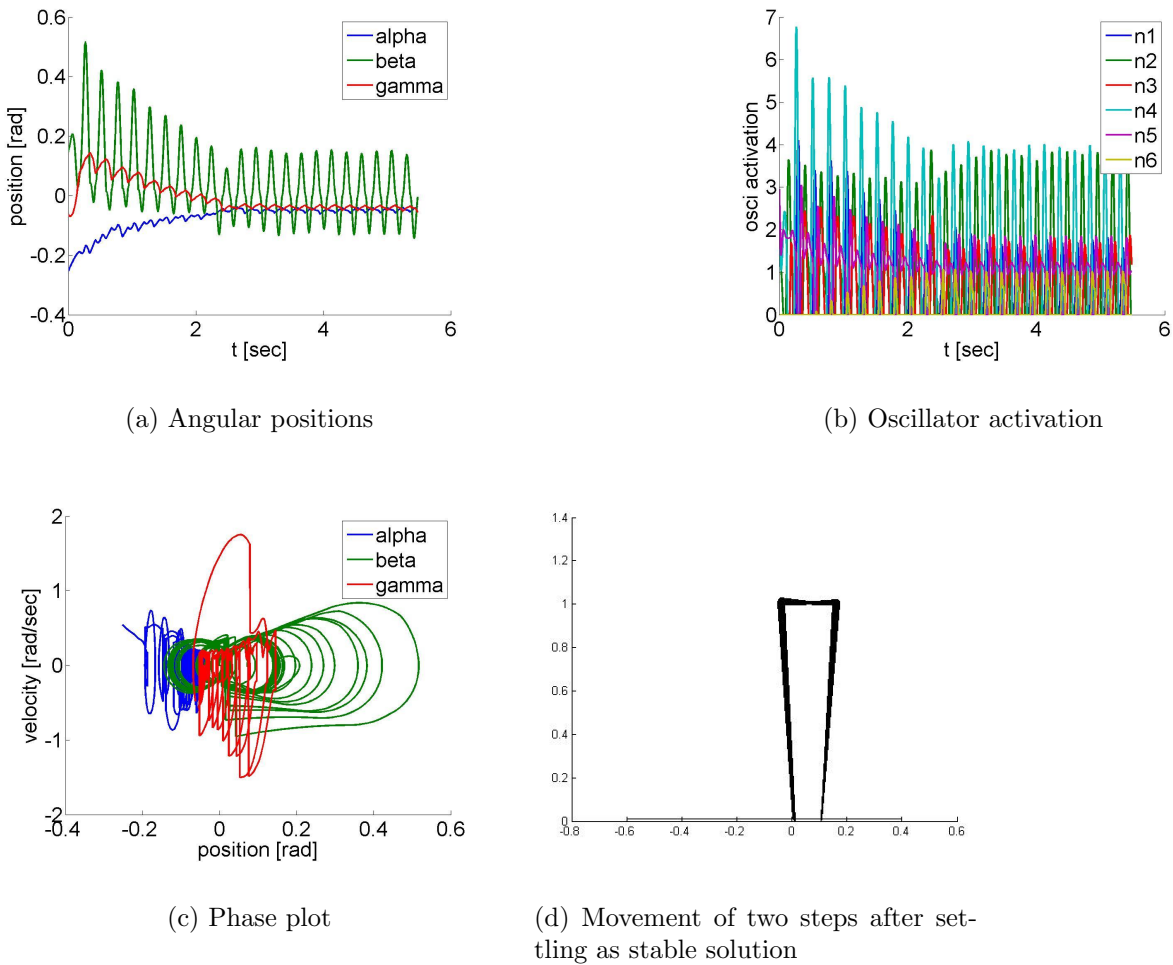
Figure 5.4: Stepping movement which is unsymmetrical and therefore drifts and moves to the side. With additional COM control initial stepping to the side is converted to periodic and symmetric stepping in place.

the first step when the normal movement range is left, the superposed control stabilizes the movement. This can be seen in the following figure 5.6.

The stabilization is very quick because the model is too ideal. During an injury the actuation would be weakened and not acting with full strength and the local muscular structures and mechanics would be slightly changed. This is not modeled, and the control is also optimal. The superposed control leads therefore to an instant adjustment of the deficits.

In figure 5.8 the case (4) is shown, a sidewards stepping movement. Here, the original movement is shown in figure 5.9. The sidewards movement is not stable because the single angles have a drift. The legs together movement is not exactly the opposite of the legs apart movement which leads to the sidewards movement. With the high-level control several steps to the side can be achieved without a fall or tendency to instability. The

(a) Angular positions   (b) Oscillator activations   (c) Phase plot
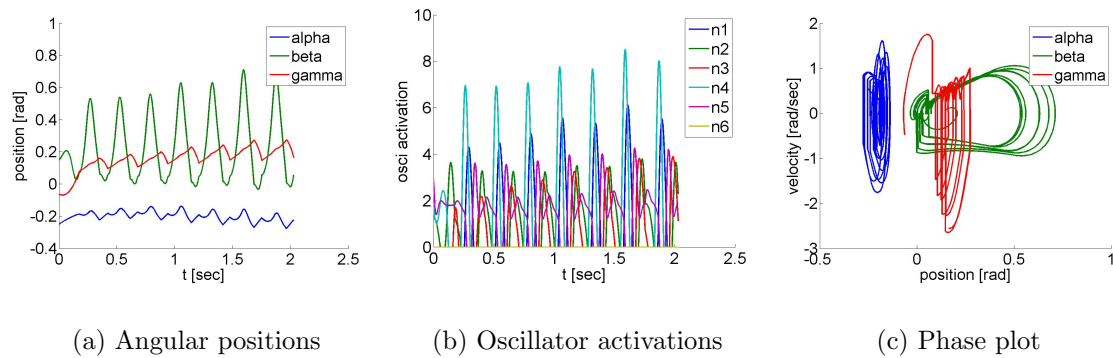
Figure 5.5: Original stepping in place movement with a drift movement in one direction as the step movement is unsymmetrical.

graphics show 20 steps to the side.

5.5 Discussion

The high-level posture control defines a control for the overall body position which is supposed to be as stable as possible. The integration between high and low level was achieved by a superposition principle. If the body leaves the normal movement range and is at risk to fall or become instable, additional torque was applied to bring the system back to normal range. There are no given values for the trajectories because they are determined online in the low level and they are not predefined but variable and dynamic. This is different to the classic robotic systems as e.g. in [143, 173, 29, 11]. Or, as Lydoire et al. said "Biped robot control techniques are usually based on the tracking of pre-computed reference trajectories. Therefore, to achieve autonomy in locomotion, it is necessary to store a set of trajectories handling all the possible situations and events..." [103] (p. 749). So, the additional control can not generate a control input which is close to the planned trajectory control [163] or substituted by a direct control [104] but it is additional. It is superposed with the low-level but does not influence it directly. To say it in other words the two actuations are superposed like an emphasizing of something or to overrule the lower control but never to replace it.

The necessity of exact state data (e.g positions) and of course the exchange of all data between control and location of data generation leads to a high complexity in robotics which was mentioned by Kajita et al. [84]. With the relatively simple additional control concept proposed in this work, it is possible that the system does all the stepping movements while enlarging its stability range with low complexity and low data exchange rate. This is achieved by using a simple model to approximate and estimate the whole body COM to determine the high-level control. Therefore the amount of exchanged data is reduced, which are the COM sensed position and velocity.

(a) Angular positions

(b) Oscillator activation

(c) Phase plot
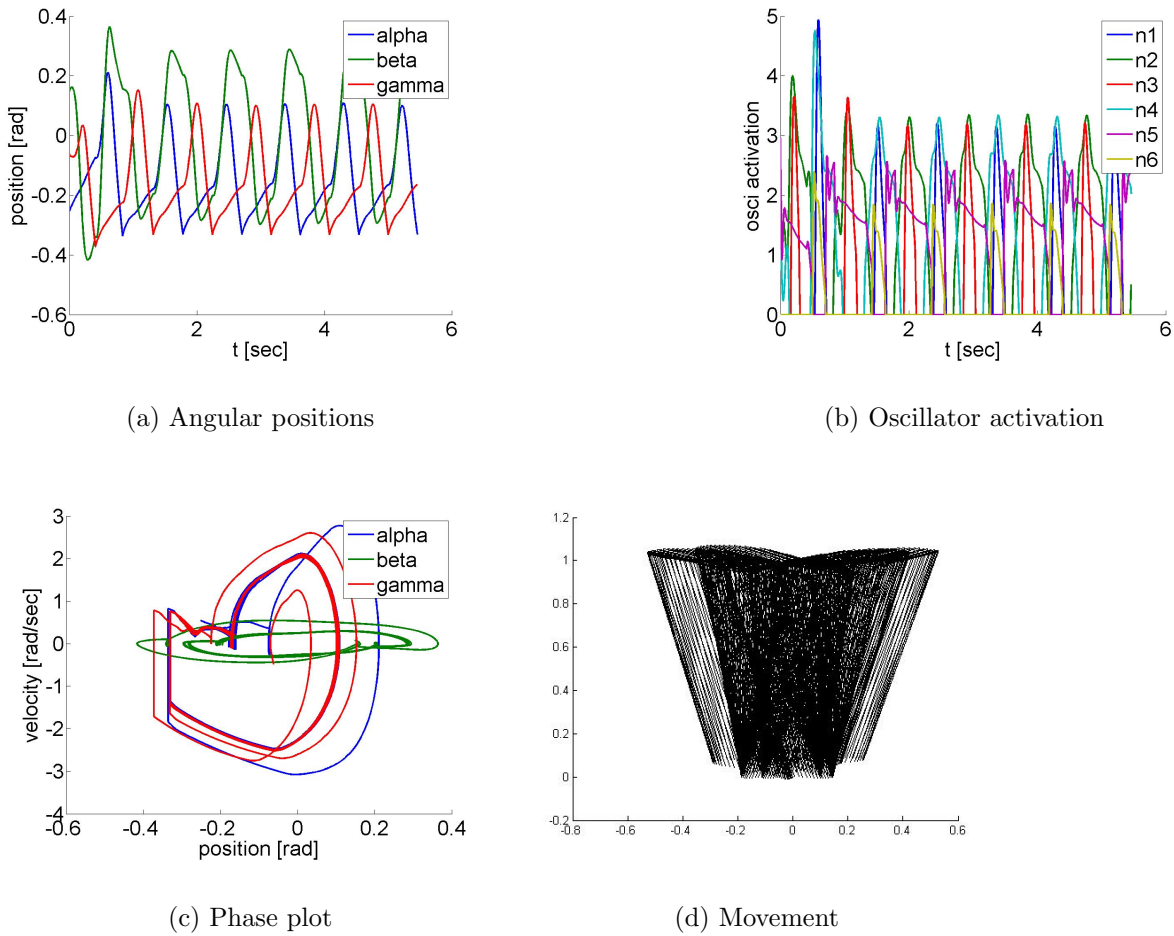
(d) Movement

Figure 5.6: Stepping in place with slightly unsuitable muscular feedback gains with $f_{dv} = 0.7$ and $f_d = 0.3$. The superposed high-level control leads to a stable stepping pattern.

(a) Angular position

(b) Oscillator activation
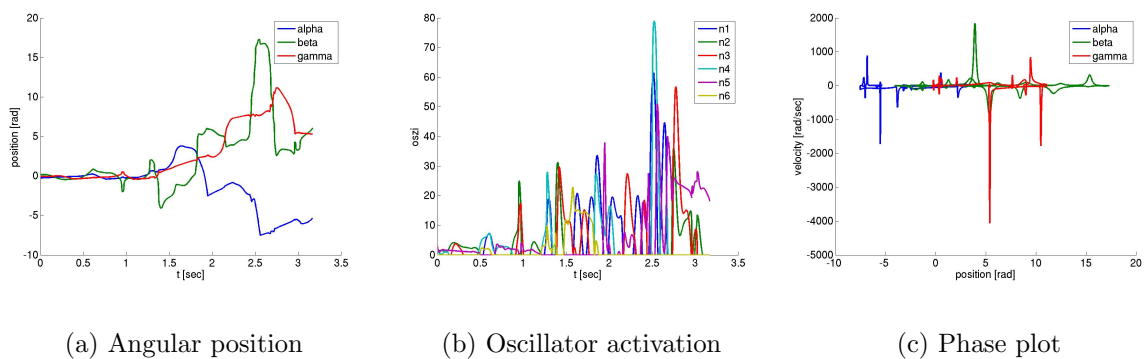
(c) Phase plot

Figure 5.7: Original stepping in place movement with slightly unsuitable muscular feedback gains with $f_{dv} = 0.7$ and $f_d = 0.3$, which lead to instability.
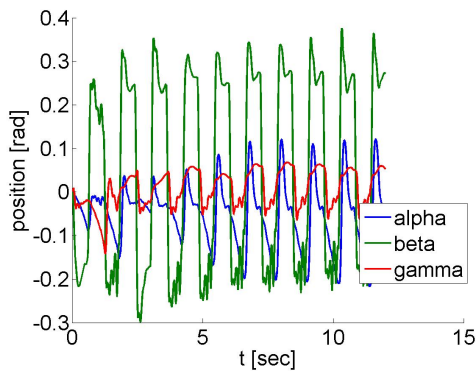
(a) Angular positions
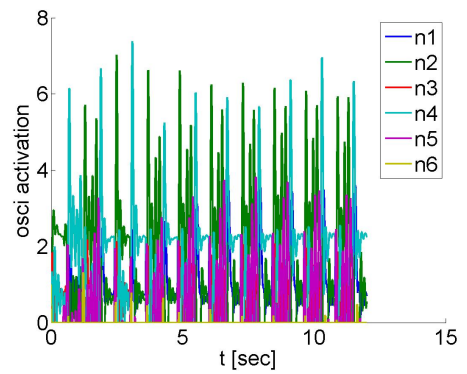
(b) Oscillator activation
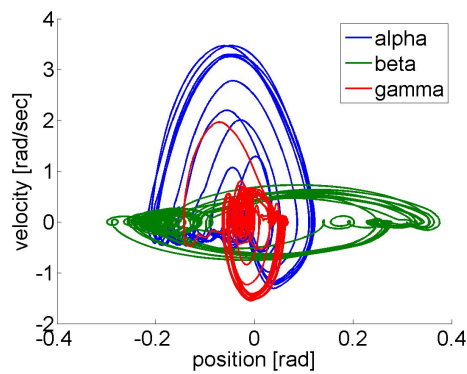
(c) Phase plot
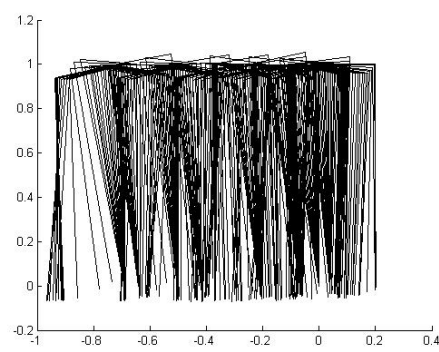
(d) Movement of the first 11 steps to the side

Figure 5.8: The graphs show stepping to the side which originally had drifting leg angles. With superposed high-level hip and COM control the movement stays within the normal region.
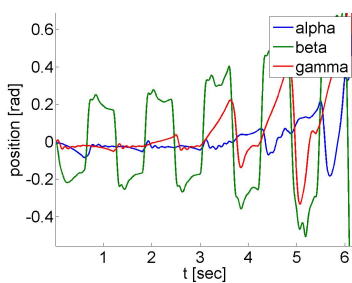
(a) Angular positions
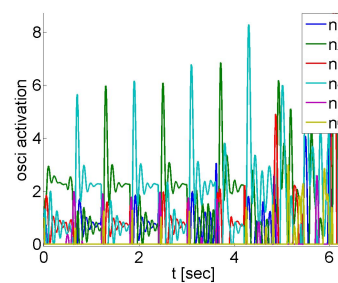
(b) Oscillator activation
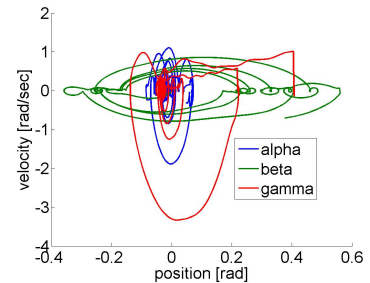
(c) Phase plot

Figure 5.9: Original stepping to the side movement with drifting leg angles.

The simulation results show that inappropriate conditions as initial conditions, affected feedback, unusual actuation strategies and asymmetric positions are successfully stabilized. When the movement instability reaches too risky and extreme values the low-level control is support by high-level control. In all simulated cases the movement could be brought back to the stable attractive region of the limit cycle or to a normal range of movement. This leads to a prevention of abnormal positions. It is not due to fix constraints as e.g. in [103] (initial foot position and distance, relation of COM to stance) but with a simple superposition principle.

In comparison to [17] no precise position of a leg or a contact point is calculated only too extreme positions are considered. The proposed high-level control strategy is not to guarantee a stable range for all position ranges and as it is exactly defined and modeled in the robotics with e.g analytic solutions of inverse kinematics [191] but it pushes the system back into normal range and the system goes back to a low-level stable movement if there exists a low-level stable movement.

5.6 Conclusion

Concluding it can be said, that many shortcomings of the low-level actuated stepping model as critical initial values, accurate feedback gains, change of actuation strategy and stepping to the side can be achieved with a superposed high-level posture control. For all simulations it is characteristic that the additional control is mainly applied to stabilize the stance leg which is the most critical parameter of keeping balance. Also the hip movements are high-level controlled but this is mainly to prevent an unnatural dynamic range of the hip and to smooth the movements. The original unstable stepping patterns are all stabilized by bringing the system back to the attraction basin of the limit cycle solution.

The low level oscillators are not directly influenced by the high-level posture control, only the varied positions of legs and hip influence the oscillator actuation via the muscular feedback. If the oscillator actuation is not supposed to be so low-level but is influenced by the high level more directly, like an additional control input, this would lead to a mechanism which relates the two levels. Especially, for influences which change the stepping movement for longer like injuries or training a direct interaction of both mechanisms constitutes an interesting enhancement.

The high-level control proposed in this work considers the stability of whole body posture which leads to improved stability of stepping patterns. However, a control of the stepping movement which is consciously influenced as the increase of stepping frequency, the change of stepping strategy or the direction of movement is not yet considered. Though, there have been shown the interface parameters to influence the stepping pattern. And the variations of those interesting parameters have been analyzed to show the possibilities but the implementation of such parameter variations on a high-level is left to future research.

6 Summary and Final Conclusion

In this thesis a new model for frontal-plane stepping movements was developed in order to evaluate medio-lateral movements during gait, and investigate influences exerted by systematic parameter changes on the model, its stability and its movement abilities. The modeling was carried out on the basis of biological principles and using a bottom-up approach, which means that the starting point for the introduced model is as simple as possible, and the model is enhanced consistently throughout the work to extend its abilities and performance. This approach stands in contrast to conventional robotic solutions. The principal extensions to the model were also applied to a sagittal-plane walking model to show that the model presented is also applicable to other movement planes, and to show that the foundations have already been laid for the planned integration of the two planes to a 3D model in future.

Due to the bottom-up approach the model was split into a low-level and a high-level model component in line with biological processes where low-level tasks are the more automatic tasks and high-level tasks are primarily directive. For the low-level model ballistic mechanical dynamics are applied. The disadvantages such as a small stability range, dependency on initial values and gravitational input have been improved by actuating the mechanics. The transition from a passive to an active model was achieved by creating a neuronal oscillator structure with muscular feedback and joint torque generation working on an antagonistic principle. The parameters of the model were varied to identify characteristic parameters for special functions. In this way, parameters for varying actuation strategy, step frequency, stepping patterns and stepping stability have been identified. The most critical factor with the low-level stepping model was found to be the stability of the stepping solutions i.e. ensuring that no fall occurs. In this work various possibilities for achieving stable stepping in place with dropping or lifting hip, stepping aside, and stepping upwards were proposed. The movements were compared with video tracking data of real stepping movements and found to be very similar, especially for the stepping in place movement. The movements were also tested under disturbing influences such as slipping, getting stuck or sustaining an external push; the model is found to have robust reactions and to return to a stable solution if the disturbance is not too strong. Stability and performance were much better than with the passive model but there stayed still some limitations which result from lacking perception of the overall context of the stepping movement. Due to the principle 'keep it simple' the addition of another model level leaded to a further extension and improvement of the low-level model and not like in many other research the elaboration of the low-level mechanics and actuation. This was realized in the high-level model.

The high-level model was developed to represent a sensor-driven perception of the whole body position and to establish a relationship between the environment and the body to accomplish posture control tasks. The basis for this model is model knowledge in the form of statistical estimation and sensor models derived from biological examples. The combination of body movements and environmental influences perceived by the senses with a statistical estimation, based on experiences, in a feedback control loop was proposed as the high-level posture control model. The extension of the visual cue by a nonlinearity derived from the Weber-Fechner law takes the nonlinear sway response effects into account. To evaluate the performance of the sensor-driven posture control model, two experiments with real subjects have been performed, one for vestibular stimulation and another for visual pursuit stimulation. The experimental data for posture response during stimulation were reproduced and verified by the high-level posture model simulation.

To improve the performance and enhance the abilities of the low-level model, the two models were integrated by a superposition control concept. The control influences mainly the stance leg, which is the most critical parameter for maintaining balance, and the hip movement. The superposition concept does not influence the low-level actuation, but the two levels are superimposed. This means that in case the stability is at risk an additional high-level control is superimposed. This superposition is comparable with an overruling of the low-level autonomous movement generation by a high-level command. It was shown that this integration leads to improved stability of the stepping movements. Stability of movements is no longer mainly dependent on the initial values and this leads to an increased range of stable solutions and the possibility of influencing posture by sensory cues.

In conclusion it can be said that this relatively simple model of the frontal plane can provide a wide spectrum of movements, producing stable, realistic, flexible and robust medio-lateral stepping solutions. Movements are not predefined but determined online according to dynamic constraints such as mechanics, external influences, general optimization criteria (e.g. staying upright), acting with a movement strategy (e.g. selecting ankle or hip strategy), or choosing a general movement pattern (e.g. stepping in place or to the side).

The influence of perception and high-level control on the task of posture control requires an additional model for an additional task. The basis of the high-level model is not as obvious as the mechanics and is even more complex than the low-level neuronal structures. This means that it can only be evaluated by e.g. conducting experiments with real subjects. The integration by statistical estimation combined with optimal control reproduces the author's own experiments and also experimental results from the literature. Nonlinearities in the sway response can be reproduced by extension to nonlinear perception rules. This abstraction of high-level processing to a statistical estimation is a general approach which leaves further scope for developing environmental or model characteristics and other probability distributions.

Stability is a key factor for stepping movements which can be enlarged by bringing solutions to the attractive basin of a stable solution in the form of high-level posture control implemented as superposition of low-level control and additional corrective control. This

all means that finding stable solutions is not a critical initial value problem any longer but is much softer because of the wider stability range.

6.1 Outlook

Although the models developed in this thesis provide stable and variable solutions for stepping movements, there is still scope for further enhancements of the abilities and performance of the models. This thesis presents a general model for studying the influence of sensory cues on medio-lateral stepping and this can now be applied to further experiments of stimulations influencing lateral stepping stability. The superposition principle showed the desired behavior, but further conclusions about a high-level control concept should be tested and expanded; special sensory inputs in particular would be a suitable subject for future research. One important factor affecting abilities and performance is without a doubt the mechanics. The ground contact and the energy storage in the joints during the double support phase due to elastic properties are key factors for generation of efficient walking movements. The mechanical dynamics as elaborated in chapter 2 have a large influence on the movement. Many research groups study exclusively the mechanics and the special properties connected with these, so the extension of mechanics would certainly improve characteristics like natural appearance, energy efficiency and in some cases stability. Another possibility for further development, for which the foundation has already been laid, because the two mechanical planes are modeled and actuated by the same principle, is the combination of the two 2D models to a 3D mechanical model. This mechanical combination would increase the complexity of the model immensely and the overlying biological strategies for combining the two movement planes are not yet known. Some starting points have been proposed by Kuo [6, 94] for finding the relation between the actuation of lateral and sagittal movements in order to stabilize them. Experiments into metabolic costs are valuable for gaining an insight into the amount of actuation, but the type of actuation needs to be studied in further experiments and models.

The perception experiments should be extended to include further visual and vestibular stimulations, because the influence of these, especially on the sideward movement during stepping, can be studied in more detail on the basis of the model which has been developed. One difficulty with such experiments is the high sway variability which occurs during stepping movements due to the step dynamics. This means that any additional body sway in this connection is difficult to extract but as in the case of the GVS experiments, the additional sway is short and big enough to measure. Other measures such as COP or raised muscular activation levels could also be chosen to measure medio-lateral sway response. One general application which is very appropriate for neuronally actuated mechanical models are learning algorithms. These learning algorithms can be used to find more and better or fitter solutions for stepping movements; these could for example be an adaption of neuron frequency to frequencies suitable for stepping dynamics or neuron activation levels. As the whole body position in the present thesis is controlled on both a low level and a high level, the learning could also be used to adapt the low-level model

to longer-lasting high-level destabilization cases which are predictable. This knowledge could be used, for example to increase the actuation level if a counterforce is expected due to environmental influences.

Bibliography

[1] D. Anastasopoulos, T. H. M. Fetter, and J. Dichgans. Smooth pursuit eye movements and otolith-ocular responses are differently impaired in cerebellar ataxia. *Brain*, 121, 1998.   122

[2] T. Arakawa and T. Fukuda. Natural motion generation of biped locomotion robot using hierarchical trajectory generation method consisting of GA, EP. layers. In *Proceedings of the IEEE International Conference on Robotics and Automation*, pages 211–216, Albuquerque, April 1997.   155

[3] S. A. Bailey. *Biomimetic Control With a Feedback Coupled Nonlinear Oscillator. Insect Experiments, Design Tools, and Hexapedal Robot Adaptation Results.* PhD thesis, Stanford University, 2004.   34

[4] G. L. Baker and J. A. Blackburn. *The Pendulum A Case Study in Physics.* Oxford University Press, 2005.   8

[5] G. L. Baker and J. P. Gollub. *Chaotic Dynamics: An Introduction.* Cambridge University Press; 2nd ed., 1996.   46

[6] C. E. Bauby and A. D. Kuo. Active control of lateral balance in human walking. *Journal of Biomechanics*, 33:1433–1440, 2000.   3, 91, 97, 173

[7] W. Becker, G. Nasios, S. Raab, and R. Jürgens. Fusion of vestibular and podokinesthetic information during self-turning towards instructed targets. *Experimental Brain Research*, 144:458–474, 2002.   96

[8] L. R. Bent, B. J. McFadyen, and J. T. Inglis. Visual-vestibular interactions in postural control during the execution of a dynamic task. *Experimental Brain Research*, 146:490–500, 2002.   133

[9] M. D. Binder and D. G. Stuart. Motor unit - muscle receptors interactions: Design features of the neuromuscular control system. *Progress in Clinical Neurophysiology*, 8:72–98, 1980.   45

[10] J. Buchli, L. Righetti, and A. J. Ijspeert. Adaptive frequency oscillators applied to dynamic walking II. Adapting to resonant body dynamics. In *Proceedings of Dynamic Walking*, 2006.   3

Bibliography

[11] M. Buss, M. Hardt, J. Kiener, M. Sobotka, M. Stelzer, O. von Stryk, and D. Wollherr. Towards an autonomous, humanoid, and dynamically walking robot: Modeling, optimal trajectory planning, hardware architecture, and experiments. In *Proceedings of the third International Conference on Humanoid Robots*, Karlsruhe, 2003. 2, 30, 51, 167

[12] J. Camp. Powered "passive" dynamic walking. Master's thesis, Human Power, Biomechanics and Robotics Lab, Cornell University, 1997. 51

[13] J. Carey and C. D. Santina. *Cummings Otolaryngology Head and Neck Surgery.* Elsevier, 2004. 99, 100

[14] S. Carver, T. Kiemel, H. van der Kooij, and J. J. Jeka. Comparing internal models of the dynamics of the visual environment. *Biological Cybernetics*, 92:147–163, 2005. 97

[15] M. Cenciarini and R. J. Peterka. Stimulus-dependent changes in the vestibular contribution to human posture control. *Journal of Neurophysiology*, 95:2733–2750, 2006. 3

[16] J. Chestnutt, M. Lau, G. Cheung, J. Kuffner, J. Hodgins, and T. Kanade. Footstep planning for the Honda ASIMO humanoid. In *Proceedings of the 2005 IEEE International Conference on Robotics and Automation, ICRA*, pages 629– 634, 18-22 April 2005. 2

[17] C. Chevallereau, A. Formal'sky, and B. Perrin. Control of a walking robot with feet following a reference trajectory derived from ballistic motion. In *Proceedings of the IEEE International Conference on Robotics and Automation,ICRA*, pages 1094–1099, Albuquerque, New Mexico, April 1997. 2, 30, 170

[18] M. Coleman. *A Stability Study of a Three-Dimensional Passive-Dynamic Model of Human Gait.* PhD thesis, Cornell University, 1998. 6, 11, 48, 51

[19] M. Coleman and A. Ruina. An uncontrolled toy that can walk but cannot stand still (tinkertoy walker). *Physical Review Letters*, 80(16):3658–3661, April 1998. 6

[20] S. Collins, A. Ruina, R. Tedrake, and M. Wisse. Efficient bipedal robots based on passive-dynamic walkers. *Science*, 307:1082–1085, 2005. 2

[21] S. Collins, M. Wisse, and A. Ruina. A three-dimensional passive dynamic walking robot with two legs and knees. *International Journal of Robotics Research*, 20(2):607–615, 2001. 3

[22] S. H. Collins. Walking robots. http://www-personal.umich.edu/ shc/robots.html, 2005. 2, 3

[23] S. H. Collins and A. Ruina. A bipedal walking robot with efficient and human-like gait. In *Proceedings of the IEEE International Conference on Robotics and Automation*, pages 1983–1988, 2005. 2, 30

[24] H. Cruse. Die Gelenke sind frei. *Die Zeit*, (29), 10. July 2003. 156

[25] B. L. Day and C. Bonato. Modification of the galvanic sway response by visual conditions. In F. H. T. Mergner, editor, *Multisensory Control of Posture*, pages 169–172. Plenum Press New York. 133

[26] B. L. Day, A. S. Cauquil, L. Bartolomei, and I. N. L. M. A. Pastor. Human body-segment tilts induced by galvanic stimulation- a vestibularly driven balance protection mechanism. *Journal of Physiology*, 1997. 133, 139

[27] J. Dichgans and T. Brandt. Visual-vestibular interaction: effects on self-motion perception and postural control. *Handbook of Sensory Physiology, Springer*, 1978. 121

[28] M. Donelan, R. Kram, and A. Kuo. Mechanical work for step-to-step transitions is a major determinant of metabolic cost of human walking. *Journal of Experimental Biology*, 205:3717–3727, 2002. 39

[29] E. Dunn and R. Howe. Foot placement and velocity control in smooth bipedal walking. *IEEE International Conference on Robotics and Automation*, pages 578–583, June 1996. 7, 22, 30, 167

[30] C. Eliasmith and C. H. Anderson. Rethinking central pattern generators: A general framework. *Neurocomputing*, 32-33:735–740, 2000. 30

[31] C. Fernandez and J. Goldberg. Physiology of peripheral neurons innervating otolith organs of the squirrel monkey. (i) response to static tilts and to long-duration centrifugal force. *Journal of Neurophysiology*, 39(5):970–984, September 1976. 98

[32] R. Fitzpatrick and L. Day. Probing the human vestibular system with galvanic stimulation. *Journal of Applied Physiology*, 96(6):2301–2316, 2004. 132, 133, 139

[33] R. Fitzpatrick, D. Wardman, and J. Taylor. Effects of galvanic vestibular stimulation during human walking. *Journal of Physiology*, 517(3):931–939, 1999. 133

[34] T. C. Freeman and J. H. Sumnall. Motion versus position in the perception of head-centered movement. *Perception*, 31:603–615, 2002. 97

[35] T. C. A. Freeman and M. Banks. Perceived head-centric speed is affected by both extra-retinal and retinal errors. *Vision Research*, 38:941–945(5), April 1998. 103

[36] O. Föllinger and G. Roppenecker. *Optimale Regelung und Steuerung*. Oldenburg Verlag München Wien, 1994. 115, 116

[37] M. Garcia. *Stability, Scaling, and Chaos in Passive-Dynamic Gait Models*. PhD thesis, Cornell University, 1999. 6, 7, 48

[38] M. Garcia, A. Chatterjee, and M. Coleman. The simplest walking model: Stability, complexity and scaling. *ASME Journal of Biomechanical Engineering*, 120(2):281–288, 1998. 5, 6, 9, 10, 11, 24, 50, 51, 91

[39] M. Garcia, A. Ruina, and A. Chatterjee. Efficiency, speed and scaling of passive

dynamic bipedal walking. *Dynamics and Stability of Systems*, 15(2):75–99, 2000. 6, 91

[40] T. Geng, B. Porr, and F. Wörgötter. Fast biped walking with a sensor-driven neuronal controller and real-time online learning. *International Journal of Robotics Research*, 25(3):243–259, 2006. 30, 90, 91

[41] T. Geng, B. Porr, and F. Wörgötter. A reflexive neural network for dynamic biped walking control. *Neural Computation*, 18(5):1156–1196, 2006. 29, 90, 155

[42] M. Gienger, K. Löffler, and F. Pfeiffer. Design and control of a biped walking and jogging robot. In *Proceedings of the 2nd International Conference on Climbing and Walking Robots (CLAWAR)*, pages 49–58, Portsmouth, UK, 1999. 155

[43] S. Glasauer, E. Schneider, K. Jahn, M. Strupp, and T. Brandt. How the eyes move the body. *Neurology*, 2005. 120, 121, 122, 124, 126, 137, 148, 152, 153

[44] J. M. Goldberg and C. Fernandez. Physiology of peripheral neurons innervating semicircular canals of the squirrel monkey. i. resting discharge and response to constant angular accelerations. *Journal of Neurophysiology*, 34(4):635–660, July 1971. 98, 100, 132

[45] M. Goldberger and M. Murray. Locomotor recovery after deafferentation of one side of the cat's trunk. *Experimental Neurology*, 67:103–117, 1980. 32

[46] E. Goldstein. *Wahrnehmungspsychologie*. Spektrum Akademischer Verlag, 2002. 102

[47] H. Goltz, J. DeSouza, R. Menon, D. Tweed, and T. Vilis. Interaction of retinal image and eye velocity in motion perception. *Neuron*, 39:569–576, July 2003. 97, 102, 103

[48] A. Goswami, B. Espiau, and A. Keramane. Limit cycles in a passive compass gait biped and passivity-mimicking control laws. *Autonomous Robots*, 4:273–286, 1997. 6, 22, 24, 48, 50, 51, 91

[49] A. Goswami, B. Thuilot, and B. Espiau. Compass-like biped robot, part i: Stability and bifurcation of passive gaits. Technical report, INRIA Rapport de recherche, October 1996. 6, 9, 10, 22, 50, 51, 91

[50] A. Goswami, B. Thuilot, and B. Espiau. A study of the passive gait of a compass-like biped robot: Symmetry and chaos. *International Journal of Robotics Research*, 17(15), 1998. 6, 22

[51] S. Grillner. Locomotion in vertebrates: Central mechanisms and reflex interactions. *Physiological Reviews*, 55:247–304, 1975. 30, 31, 32

[52] S. Grillner. Control in locomotion in bipeds, tetrapods and fish. *In Brooks VB: Handbook of physiology*, Waverly Press:1179–1236, 1981. 45

[53] S. Grillner, P. Wallen, and I. Brodin. Neuronal network generating locomotor behavior in lamprey: Circuitry, transmitters, membrane properties, and stimulation. *Annual Review of Neuroscience*, 14:169–199, 1991.   30, 31, 32

[54] W. J. Grizzle, G. Abba, and F. Plestan. Asymptotically stable walking for biped robots: Analysis via systems with impulse effects. *IEEE Transactions on Automatic Control*, 46:51–64, January 2001.   6, 10, 18, 19

[55] B. I. R. Group. Lecture 3, biai. http://birg2.epfl.ch/biai-material/lecture3.pdf.   31

[56] J. M. Hausdorff. Gait variability: methods, modeling and meaning. *Journal of Neuroengineering Rehabilitation*, 2:19, 2005.   2

[57] H. He, H. Jiping, R. Herman, and M. Carhart. Modulation effects of epidural spinal cord stimulation on muscle activities during walking. *IEEE Transactions on Neural Systems and Rehabilitation Engineering*, 14(1):14–23, March 2006.   3

[58] J. Hedrick and A. Girard. Control of nonlinear systems: Theory and applications, 2005.   159

[59] S. M. Henry, J. Fung, and F. B. Horak. Control of stance during lateral and anterior/posterior surface translations. *IEEE Transactions on Rehabilitation Engineering*, 6(1):32–42, March 1998.   68, 91

[60] S. M. Henry, J. Fung, and F. B. Horak. EMG responses to maintain stance during multidirectional surface translations. *Journal of Physiology*, 6(1):1939–1950, 1998.   68, 91

[61] K. Hidenori and Y. Jiang. A PID model of human balance keeping. *IEEE Control Systems Magazine*, December 2006.   96

[62] S. Highstein, R. Rabbitt, G. Holstein, and R. Boyle. Determinants of spatial and temporal coding by simicircular canal afferents. *Journal of Neurophysiology*, 93:2359–2370, May 2004.   99

[63] F. Hlavacka. Human postural responses to sensory stimulations: Measurements and model. *Measurement Science Review*, 3(2):21–24, 2003.   133

[64] F. Hlavacka, T. Mergner, and M. Krizkova. Control of the body vertical by vestibular and proprioceptive inputs. *Brain Research Bulletin*, 40(5/6):431–435, 1996.   101, 133

[65] F. B. Horak and F. Hlavacka. Somatosensory loss increases vestibulospinal sensitivity. *Journal of Neurophysiology*, 86:575–585, 2001.   3, 133, 138, 139

[66] F. B. Horak and L. Nashner. Central programming of postural movements: Adaptation to altered support-surface configurations. *Journal of Neurophysiology*, 55(6):1369–1381, June 1986.   68, 91

[67] Y. Hurmuzlu. Dynamics of bipedal gait part ii: Stability analysis of a planar five-link biped. *Journal of Applied Mechanics,*, 60:337–343, 1993.   48, 51

Bibliography

[68] Y. Hurmuzlu and D. Marghitu. Rigid body collisions of planar kinematic chains with multiple contact points. *International Journal of Robotic Research*, 13(1):82–92, 1994. 19

[69] Y. Hurmuzlu and Moskowitz. The role of impact in the stability of bipedal locomotion. *Dynamics and Stabilities of Systems*, 1(3):217–234, 1986. 48

[70] H. Inada and K. Ishii. A bipedal walk using central pattern generator CPG. *Brain IT*, 2004. 30

[71] A. Isidori. *Nonlinear Control Systems*. Springer, 1989. 156

[72] Y. P. Ivanenko, R. Grasso, and F. Lacquaniti. Effect of gaze on postural responses to neck proprioceptive and vestibular stimulation in humans. *The Journal of Physiology*, 519(1):301–314, 1999. 120, 121

[73] D. Ivashko, B. Prilustsky, S. Markin, J. Chapin, and I. Rybak. Modeling the spinal cord neural circuitry controlling cat hindlimb movement during locomotion. *Neurocomputing*, pages pp. 621–629, 2003. 3, 32

[74] R. Jacobs. Control model of human stance using fuzzy logic. *Biological Cybernetics*, 77:63–70, 1997. 96

[75] R. Jaeger and T. Haslwanter. Otolith responses to dynamical stimuli: Results of a numerical investigation. *Biological Cybernetics*, 90:165–175, 2004. 98

[76] R. Jaeger, A. Takagi, and T. Haslwanter. Modeling the relation between head orientations and otolith responses in humans. *Hearing Research*, 173:29–42, 2002. 98

[77] K. Jahn, R. Kalla, S. Karg, M. Strupp, and T. Brandt. Eccentric eye and head positions in darkness induce deviation from the intended path. *Experimental Brain Research*, 174(1):152–157, 2006. 3, 101, 120

[78] K. Jahn, M. Strupp, S. Krafczyk, O. Schüler, S. Glasauer, and T. Brandt. Suppression of eye movements improves balance. *Brain*, 125:2005–2011, 2002. 121

[79] J. Jeka, L. Allison, M. Saffer, Y. Zhang, S. Carver, and T. Kiemel. Sensory reweighting with translational visual stimuli in young and elderly adults: the role of state-dependent noise. *Experimental Brain Research*, 174:517–527, 2006. 3

[80] J. Jeka, T. Kiemel, R. Creath, F. Horak, and R. Peterka. Controlling human upright stance: Velocity information is more accurate than position or acceleration. *Journal of Neurophysiology*, 2004. 95, 97

[81] R. Jäger and T. Haslwanter. Otolith responses to dynamical stimuli: results of a numerical investigation. *Journal of Biological Cybernetics*, 90:165–175, March 2004. 98

[82] R. Jürgens, T. Boß, and W. Becker. Estimation of self-turning in the dark: compari-

son between active and passive rotation. *Experimental Brain Research*, 128:491–504, 1999.   101

[83] S. Kagami, T. Kitagawa, K. Nishiwaki, T. Sugihara, M. Inaba, and H. Inoue. A fast dynamically equilibrated walking trajectory generation method of humanoid robot. *Autonomous Robots*, 12(1), January, 2002.   155

[84] S. Kajita, F. Kanehiro, K. Kaneko, K. Fujiwara, K. Harada, K. Yokoi, and H. Hirukawa. Biped walking pattern generation by using preview control of zero-moment point. In *Proceedings of the 2003 IEEE International Conference on Robotics and Automation, ICRA*, pages 1620–1626, Taipei, Taiwan, September 14-19, 2003.   155, 156, 167

[85] S. Karg. Stability of stepping movements in the frontal plane - a biomechanical model. In *Proceedings, ASME Bioengineering Conference, Keystone, USA*, 2007.   29, 37

[86] S. Karg, K. Jahn, and S. Glasauer. Sensory integration model for human postural control with visually induced sway. In *Proceedings, 4th International Posture Symposium, Smolenice,Slovakia*, 2006.   109, 116

[87] S. Karg, S. Zhang, K. Jahn, and S. Glasauer. Lateral stabilization of neurally controlled bipedal walking. In *Proceedings, 5. World Congress of Biomechanics, Munich, Germany*, 2006.   29

[88] S. A. Karg. Analyse der menschlichen Stand- und Gangregulation. In *VDI Verein Deutscher Ingenieure, FIB Kongress*, 2005.   95

[89] S. A. Karg. Biologische Vorbilder in der Robotik. In *Ferienakademie Tutzing, Forum: Evolutionäre Algorithmen und Robotik*, 2005.   3

[90] J.-Y. Kim, I.-W. Park, and J.-H. Oh. Experimental realization of dynamic walking of biped humanoid robot khr-2 using ZMP feedback and inertial measurement. *Advanced Robotics*, 20(6):707 – 736, June 2006.   156

[91] W. Koon. Poincaré map, floquet theory, and stability of periodic orbits. Technical report, Control and Dynamical Systems: California Institute of Technology, 2006.   46, 47

[92] A. Kuo. Stabilization of lateral motion in passive dynamic walking. *International Journal of Robotics Research*, 18(9):917–930, 1999.   6, 12, 22, 29

[93] A. Kuo. Energetics of actively powered locomotion using the simplest walking model. *ASME Journal of Biomechanical Engineering*, 124:113–120, 2002.   6, 10, 51

[94] A. Kuo. Mechanical and metabolic requirements for active lateral stabilization in human walking. *Journal of Biomechanics*, 37(6):827–835, June 2004.   5, 6, 12, 28, 91, 173

[95] A. Kuo, M. Donelan, and A. Ruina. Energetic consequences of walking like an

inverted pendulum: Step-to-step transition. *Exercise and Sport Science Review*, 33(2):88–97, 2005. 39

[96] A. D. Kuo. An optimal control model for analyzing human postural balance. *IEEE Transactions on Biomedical Engineering*, 42(1):87–101, 1995. 97, 116, 117

[97] A. D. Kuo. An optimal state estimation model of sensory integration in human postural balance. *Journal of Neural Engineering*, 2:235–249, 2005. 95, 97, 101, 116

[98] K. Körding and D. Wolpert. Bayesian decision theory in sensorimotor control. *Trends in Cognitive Sciences, Special Issue: Probabilistic models in cognition*, 10(7):319–326, 2006. 97

[99] J. Laurens and J. Droulez. Bayesian processing of vestibular information. *Biological Cybernetics*, 2006. (Published online: 5th December 2006). 97

[100] L. Liu, A. B. Wright, and G. T. Anderson. Trajectory planning and control for a human-like robot leg with coupled neural-oscillators. In *The 7th Mechatronics Forum International Conference*, 2000. 30

[101] L. Liu, M. Zhao, D. Lin, J. Wang, and K. Chen. Gait designing of biped robot according to human walking based on six-axis force sensors. *Computational Intelligence in Robotics and Automation, 2003. Proceedings. 2003 IEEE International Symposium on*, 1:360–365, 16-20 July 2003. 3

[102] S. Lohmeier, K. L. M. Gienger, and H. Ulbrich. Sensor system and trajectory control of a biped robot. In *Proceedings of the International Workshop on Advanced Motion Control*. 2, 30

[103] F. Lydoire, C. Azevedo, B. Espiau, and P. Poignet. 3d parameterized gaits for biped walking. In *International Conference on Climbing and Walking Robots (CLAWAR)*, pages 749–757, Paris, France, 2002. 3, 155, 167, 170

[104] K. Löffler, M. Gienger, and F. Pfeiffer. Sensor and control design of a dynamically stable biped robot. In *IEEE International Conference on Robotics and Automation, ICRA*, pages 484–490. IEEE, 2003. 155, 156, 167

[105] P. Manoonpong, T. Geng, B. Porr, and F. Wörgötter. The runbot architecture for adaptive, fast, dynamic walking. In *IEEE International Symposium on Circuits and Systems, ISCAS*, pages 1181–1184. IEEE, 2007. 91, 92, 155

[106] D. Marhefka and D. Orin. Fuzzy control of quadrupedal running. In *IEEE International Conference on Robotics and Automation, ICRA*, volume 3, pages 3063–3069, 2000. 96

[107] K. Matsuoka. Sustained oscillations generated by mutually inhibiting neurons with adaptation. *Biological Cybernetics*, pages 367–376, 1985. 34, 35, 36, 37

[108] K. Matsuoka. Mechanisms of frequency and pattern control in the neural rhythm generator. *Biological Cybernetics*, pages 345–353, 1987. 34, 35

[109] C. Maurer, T. Mergner, and R. Peterka. Multisensory control of human upright stance. *Experimental Brain Research*, 171:231–250, 2006.   96

[110] D. A. McCrea. Topical review - spinal circuitry of sensorimotor control of locomotion. *Journal of Physiology*, 533(1):41–50, 2001.   3, 32

[111] T. McGeer. Passive dynamic walking. *International Journal on Robotic Research*, 9(2):62–82, 1990.   5, 6, 9, 10, 18, 22, 51

[112] T. McGeer. Passive walking with knees. In *Proceedings of the IEEE Conference on Robotics and Automation*, pages 1640–1645, 1990.   6, 22, 51

[113] T. McGeer. Passive dynamic biped catalog. *In Proceedings 2nd International Symposium Experimental Robotics*, pages 465–490, 1991.   3, 6, 51

[114] T. McMahon and J. Bonner. *Form und Leben*. Spektrum der Wissenschaft, Heidelberg, 1984.   5, 39

[115] T. A. McMahon. *Muscle, Reflexes and Locomotion*. Princeton University Press, 1984.   5

[116] T. Mergner and W. Becker. A modeling approach to the human spatial orientation system. *New York Academy of Science*, 1004:303–315, 2003.   96

[117] T. Mergner, W. Huber, and W. Becker. Vestibular-neck interaction and transformations of sensory coordinates. *coordinates. Journal of Vestibular Research*, pages 119–135, 1997.   101

[118] T. Mergner, C. Maurer, and R. Peterka. A multisensory posture control model of human upright stance. *Progress in Brain Research*, 142:189–201, 2003.   96, 152

[119] T. Mergner and T. Rosemeier. Interaction of vestibular, somatosensory and visual signals for postural control and motion perception under terrestrial and microgravity conditions - a conceptual model. *Brain Research Reviews*, 1998.   96, 101

[120] T. Mergner, G. Schweigart, C. Maurer, and A. Blümle. Human postural responses to motion of real and virtual visual environments under different support base conditions. *Experimental Brain Research*, 167:535–556, 2005.   95, 96, 109

[121] T. Mergner, C. Siebold, G. Schweigart, and W. Becker. Human perception of horizontal head and trunk rotation in space during vestibular and neck stimulation. *Experimental Brain Research*, 85:389–404, 1991.   101

[122] H. Miura and I. Shimoyama. Dynamic walk of a biped. *International Journal on Robotics Research*, 3(2):60–74, 1984.   8

[123] S. Miyakoshi, G. Taga, Y. Kuiyoshi, and A. Nagakubo. Three-dimensional bipedal stepping motion using neural oscillators: Towards humanoid motion in the real world. *Journal of Biomechanical Engineering, Proceedings of the IEEE/RSI International Conference on Intelligent Robots and Systems*, pages 84–89, October 1998.   29, 90

Bibliography

[124] S. Mochon and T. McMahon. Ballistic walking. *Journal of Biomechanics*, 13:49–57, 1980. 5

[125] S. Mochon and T. McMahon. Ballistic walking: an improvement. *Mathematical Biosciences*, 52:241–260, 1980. 3

[126] K. Mombaur. *Stability Optimization of Open-Loop Controlled Walking Robots*. PhD thesis, Rupprecht-Karls Universität Heidelberg, 2001. 22, 48, 51

[127] K. Mombaur, H. Bock, and J. Schlöder. Human-like actuated walking that is asymptotically stable without feedback. *Proceedings of the IEEE International Conference on Robotics and Automation, ICRA*, May 2001. 51, 91

[128] K. Mombaur, R. Longman, H. Bock, and J. Schlöder. Open-loop stable running. *Robotica*, 23:21–33, 2005. 91

[129] T. Mori, Y. Nakamura, M. aki Sato, and S. Ishii. Reinforcement learning for a CPG-driven biped robot. *Proceedings of the Conference on Artificial Intelligence, AAAI*, pages 623–630, 2004. 30

[130] J. Morimoto and C. Atkeson. Robust low torque biped walking using differential dynamic programming with a minimax criterion. In *Proceedings of the Fifth International Conference on Climbing and Walking Robots and their Supporting Technologies (CLAWAR 2002), September, 2002.* 156

[131] I. Morishita and A. Yajima. Analysis and simulation of networks of mutually inhibiting neurons. *Kybernetik*, 11:154–165, 1972. 34

[132] S. Morita, H. Fujii, T. Kobiki, S. Minami, and T. Ohtsuka. Gait generation method for a compass type walking machine using dynamical symmetry. In *Proceedings of IEEE International Conference on Intelligent Robots and Systems*, pages 2825–2830, October 2004. 7

[133] M. Mueller, D. Sinacore, S. Hoogstrate, and L. Daly. Hip and ankle walking strategies: effect on peak plantar pressures and implications for neuropathic ulceration. *Archives of Physical Medicine and Rehabilitation*, 1994. 68, 91

[134] R. Neptune and K. S. S. Kautz. The effect of walking speed on muscle function and mechanical energetics. *Gait & Posture*, 2007 Dec 22. 3

[135] M. Niemeier, D. Crawford, and D. Tweed. Optimal transsaccadic integration explains distorted spatial perception. *Letters to Nature*, 422:76–80, 6 March 2003. 102

[136] K. S. Oie, T. Kiemel, and J. J.Jeka. Multisensory fusion: simultaneous re-weighting of vision and touch for the control of human posture. *Cognitive Brain Research*, 2002. 97, 109, 114, 115, 120, 142, 152

[137] C. Pack, S. Grossberg, and E. Mingolla. A neural model of smooth pursuit control and motion perception by cortical area MST. *Journal of Cognitive Neuroscience*, 13(1):102–120, 2001. 102

[138] R. J. Peterka. Postural control model interpretation of stabilogram diffusion analysis. *Biological Cybernetics*, 82:335–343, 2000.   96, 109

[139] R. J. Peterka. Sensorimotor integration in human postural control. *Journal of Neurophysiology*, 88:1097–1118, 2002.   96, 120, 121, 141, 142, 151

[140] R. J. Peterka. Simplifying the complexities of maintaining balance. *IEEE Engineering in Medicine and Biology Magazine*, pages 63–68, March 2003.   96

[141] R. J. Peterka and M. S. Benolken. Role of somatosensory and vestibular cues in attenuating visually induced human postural sway. *Experimental Brain Research*, 105:101–110, 1995.   120, 152

[142] R. J. Peterka and P. J. Loughlin. Dynamic regulation of sensorimotor integration in human postural control. *Journal of Neurophysiology*, 91:410–423, 2004.   119

[143] F. Pfeiffer and H. Cruse. *Autonomes Laufen*. Springer, 2005.   167

[144] T. G. B. Porr and F. Wörgötter. Fast biped walking with a reflexive controller and real-time policy searching. *International Journal of Robotics Research*, 25(3):243 – 259, 2006.   90

[145] M. Powell. A hybrid method for nonlinear equations. *Numerical Methods for Nonlinear Algebraic Equations*, pages 87–144, 1970.   22

[146] T. Probst, S. Krafczyk, T. Brandt, and E. Wist. Interaction between perceived self-motion and object-motion impairs vehicle guidance. *Science*, 225(4661):536–538, 1984.   124, 152

[147] A. Prochazka and Yakovenco. Locomotor control: from spring-like reactions of muscles to neural prediction. *The Somatosensory System: Deciphering The Brain's Own Body Image, CRC Press*, pages 141–181, 2001.   32

[148] R. P. Rao. An optimal estimation approach to visual perception and learning. *Vision Research*, 39(11), 1999.   105

[149] E. Ravaioli, K. Oie, T. Kiemel, L. Chiari, and J. Jeka. Nonlinear postural control in response to visual translation. *Experimental Brain Research*, 160:450–459, 2005.   120

[150] P. Reuter. *Springer Taschenwörterbuch Medizin*. Springer, 2001.   98

[151] L. Righetti, J. Buchli, and A. J. Ijspeert. Adaptive frequency oscillators applied to dynamic walking I. Programmable pattern generators. In *Proceedings of Dynamic Walking*, 2006.   3

[152] L. Righetti and A. J. Ijspeert. Programmable central pattern generators: an application to biped locomotion control. In *Proceedings of the IEEE International Conference on Robotics and Automation, ICRA*, May 2006.   30, 90

[153] M. Robertson and K. Pearson. Neural circuits in the flight system of the locust. *Journal of Neuralphysiology*, 53(1):110–128, 1985.   30

Bibliography

[154] A. Robinson. *The Nervous System II, Control of Eye Movements*, chapter 28, pages 1275–1320. Handbook of Physiology. American Physiological Society, 1981. 101

[155] D. Robinson, J. Gordon, and S. Gordon. A model of the smooth pursuit eye movement system. *Biological Cybernetics*, 55:43–57, 1986. 101, 102

[156] S. Rossignol. *12. Exercise: Regulation and Integration of Multiple Systems - Neural control of stereotypic limb movements*, pages 173–216. Handbook of Physiology. American Physiology Society, 1996. 30

[157] V. Sangwan and S. K. Agrawal. Generation of leg-like motion and limit cycles with an underactuated two DOF linkage. In *Proceedings of the first IEEE / RAS-EMBS International Conference on Biomedical Robotics and Biomechatronics*, 2006. 51

[158] V. Sangwan and S. K. Agrawal. Leg-like motion with an under-actuated two DOF linkage using differential flatness. In *Proceedings of the American Control Conference*, pages 1790–1795, 2006. 51

[159] R. Shadmehr and S. Wise. The computational neurobiology of reaching and pointing: a foundation for motor learning. *Cambridge, MA: MIT Press*, 2005. 45

[160] C.-L. Shih and W. Gruver. Control of a biped robot in the double-support phase. *Systems, Man and Cybernetics, IEEE Transactions on*, 22(4):729–735, Jul/Aug 1992. 155

[161] M. L. Shik and G. N. Orlovsky. Neurophysiology of locomotor automatism. *Physiological Reviews*, 1976. 32

[162] G. M. Siouris. *Optimal Control and Estimation Theory*. John Wiley and Sons, 1996. 97, 116

[163] M. Sobotka. *Hybrid Dynamical System Methods for Legged Robot Locomotion with Variable Ground Contact*. PhD thesis, Technische Universität München, 2007. 156, 167

[164] M. Sobotka, D. Wollherr, and M. Buss. A Jacobian method for online modification of precalculated gait trajectories. 155

[165] J. L. Souman, I. T. Hoge, and A. H. Wertheim. Frame of reference transformations in motion perception during smooth pursuit eye movements. *Journal of Computational Neuroscience*, 20:61–76, 2006. 103

[166] W. Steinhausen. Über den Nachweis der Bewegung der Cupula in der intakten Bogengangsampulle des Labyrinthes bei der natürlichen rotatorischen und calorischen Reizung. *Pflügers Archiv ges. Phyiologie*, 228:322–328, 1931. 98

[167] A. A. Stocker and E. P. Simoncelli. Noise characteristics and prior expectations in human visual speed perception. *Nature Neuroscience*, 9:578–585, 2006. 104, 105

[168] T. A. Stoffregen, B. G. Bardy, C. T. Bonnet, P. Hove, and O. Oullier. Postural

sway and the frequency of horizontal eye movements. *Motor Control*, (11):86–102, 2007.   121, 146

[169] T. A. Stoffregen, B. G. Bardy, C. T. Bonnet, and R. Pagulayan. Postural stabilization of visually guided eye movements. *Ecological Psychology*, 18:191–222, 2006.   121, 146, 148, 152

[170] M. Strupp, S. Glasauer, K. Jahn, E. Schneider, S. Krafczyk, and T. Brandt. Eye movements and balance. *Annals of the New York Academy of Science*, 1004:352–358, 2003.   3, 120

[171] G. Taga. A model of the neuro-musculo-skeletal system for human locomotion. *Biological Cybernetics*, 73:113–121, 1995.   91, 92

[172] G. Taga, Y. Yamaguchi, and H. Shimizu. Self-organized control of bipedal locomotion by neural oscillators in unpredictable environment. *Biological Cybernetics*, 65:147–159, April 1991.   30, 45

[173] T. Takenaka. The control system for the Honda humanoid robot. 35-S2, 2006.   155, 167

[174] R. Tedrake, T. Zhang, and M. Fong. Actuating a simple 3d passive dynamic walker. In *Proceedings of the IEEE International Conference on Robotics and Automation, ICRA*, volume 5, pages 4656–4661, April 2004.   51

[175] P. Terrier and Y. Schutz. Variability of gait patterns during unconstrained walking assessed by satellite positioning (gps). *European Journal of Applied Physiology*, 90(5-6):554–561, Nov. 2003.   2

[176] F. Towhidkhah, R. Gander, and H. Wood. Model predictive impedance control: application to human walking model. *Engineering in Medicine and Biology Society, 1995., IEEE 17th Annual Conference*, 2:1263–1264 vol.2, 20-23 Sep 1995.   156

[177] K. A. Turano and R. W. Massof. Nonlinear contribution of eye velocity to motion perception. *Vision Research*, 41:385–395, 2001.   103, 104

[178] F. van der Helm and L. Rozendaal. Musculoskeletal systems with intrinsic and proprioceptive feedback. In C. P. Winters JM., editor, *Neural control of posture and movement*, pages 164–174. Springer Verlag, 2000.   45

[179] H. van der Kooij, R. Jacobs, B. Koopman, and H. Grootenboer. A multisensory integration model of human stance control. *Biological Cybernetics*, 80:299–308, 1999.   97, 109, 116

[180] H. van der Kooij, R. Jacobs, B. Koopman, and F. van der Helm. An adaptive model of sensory integration in a dynamic environment applied to human stance control. *Biological Cybernetics*, 84:103–115, 2001.   95, 97, 101, 119, 137, 152

[181] R. Q. van der Linde. Actively controlled ballistic walking. In *Proceedings of the IASTED International Conference Robotics and Application*, 2000.   6

Bibliography

[182] B. Vanderborght. *Dynamic stabilization of the biped Lucy powered actuators with controllable stiffness.* PhD thesis, Vrije Universiteit Brüssel, 2007. 2

[183] E. Vaughan, E. Di Paolo, and I. Harvey. The evolution of control and adaptation in a 3d powered passive dynamic walker. In J. Pollack, M. Bedau, P. Husbands, T. Ikegami, and R. Watson, editors, *Artificial Life IX: Proceedings of the Ninth International Conference on the Simulation and Synthesis of Life*, pages 139–145. MIT Press, 2004. 30

[184] T. Vilis. *The Physiology of the Senses.* University of Ontario, Canada, 2007. 101

[185] M. von der Heyde. *A Distributed Virtual Reality System for Spatial Updating - Concepts, Implementation, and Experiments.* PhD thesis, Technische Fakultät der Universität Bielefeld, 2000. 95, 98

[186] H. von Helmholtz. Treatise on physiological optics. *Thoemmes Press*, 2000. Original publication from 1866. 105

[187] E. von Holst. Relations between the central nervous system and the peripheral organs. *British Journal of Animal Behaviour*, 1954. 103

[188] E. von Holst and H. Mittelstaedt. Das Reafferenzprinzip. *Naturwissenschaften*, 37:464–476, 1950. 103

[189] D. Wardman and R. Fitzpatrick. What does galvanic vestibular stimulation stimulate? *Advances in Experimental Medicine and Biology*, 508:119–128, 2002. 133

[190] G. Welch and G. Bishop. An introduction to the Kalman filter. Technical report, Chapel Hill, NC, USA, 1995. 97, 107

[191] P.-B. Wieber. Trajectory free linear model predictive control for stable walking in the presence of strong perturbations. *Humanoid Robots, 2006 6th IEEE-RAS International Conference on*, pages 137–142, 4-6 Dec. 2006. 155, 156, 170

[192] V. J. Wilson and G. M. Jones. *Mammalian Vestibular Physiology.* Plenum Press, New York, 1979. 99, 100

[193] D. Winter. Human balance and posture control during standing and walking. *Gait & Posture*, 3:193–214, December 1995. 3, 39

[194] D. Winter and H. Yack. EMG profiles during normal human walking: stride-to-stride and inter-subject variability. *Electroencephalographic Clinical Neurophysiology*, 67(5), Nov 1987. 3, 30, 68

[195] M. Wisse, A. Schwab, R. Q. van der Linde, and F. van der Helm. How to keep from falling forward elementary swing leg action for passive dynamic walkers. *IEEE Transactions on Robotics*, 21(3):393–401, June 2005. 30

[196] D. Wollherr and M. Buss. Posture modification for biped humanoid robots based on Jacobian method. Proceedings of the IEEE/RSJ International Conference on Intelligent Robots and Systems, IROS, pages 124–129, Sendai, Japan, 2004. 155

[197] J. Yang. Modeling modelfest data and luminance dependent CSFs based on implicit masking. *Journal of Vision*, 6(13):66–66, 12 2006. 103, 104

[198] F. E. Zajac. Muscle coordination of movement — a perspective. *Journal of Biomechanics*, 26:109–124, 1993. 3

[199] R. B. N. Zibi. Simulation der menschlichen Wahrnehmung von Rotationsbewegungen. Master's thesis, Technische Universität München, Lehrstuhl für Realzeit-Computersysteme, 2006. 101